

**Architectural and Non-architectural Effects of
Salinity on Canopy Structure, Light Interception
and Dry Mass Production in Greenhouse Cucumber
and Tomato**

Von der Naturwissenschaftlichen Fakultät der
Gottfried Wilhelm Leibniz Universität Hannover

zur Erlangung des Grades

Doktor der Gartenbauwissenschaften (Dr. rer. hort.)

genehmigte Dissertation

von

M.Sc. Tsu-Wei Chen

Geboren am 18.10.1983 in Taipeh, Taiwan

2015

Referent: Prof. Dr. sc. agr. Hartmut Stützel

Korreferentin: PD Dr. rer. nat. Katrin Kahlen

Korreferent: Prof. Dr. rer. nat. Winfried Kurth

Tag der Promotion: 15.10.2015

Dedicated to my grandfathers

Abstract

Knowledge about the mechanisms of salt tolerance of crop species is necessary for designing new cultivars or strategies to improve crop performance under salinity, a widespread abiotic stress. Cucumber and tomato belong to the most important greenhouse vegetable crops and are often cultivated in regions exposed to salinity or in hydroponic systems, where the presence of salt in the irrigation water may result in salt accumulation. Using these two crop species, this work aims at quantifying the impacts of architectural and physiological limitations (L_a and L_p , respectively) resulting from salinity on canopy light interception (LI), photosynthesis and dry mass production (DMP) under different light and temperature conditions. To achieve this, two frameworks of functional-structural plant models (FSPM), where the 3D architecture of plants is explicitly described, were constructed, parameterized and evaluated. The first framework was a static architecture model of the cucumber canopy, coupled with a biochemical model of photosynthesis and quantitative limitation analysis of photosynthesis, for scaling up the impacts of physiological processes on limiting photosynthesis from leaf to the whole plant level. Using this framework, the influences of salinity, instantaneous light conditions and their interactions on L_a and L_p in cucumber were systematically and quantitatively analyzed. The second framework, a dynamic FSPM of tomato growth, was used to investigate the impacts of architectural traits on whole plant DMP and their interactions with temperature and salinity. In cucumber, L_a was stronger than L_p , especially under high salinity. L_p was mainly due to the toxic effects of Na^+ accumulation in leaves on stomatal regulation. Complex interactions between light, severity of salinity and L_p were found at both, the leaf and the canopy levels. For example, the relative importance of diffusional limitations depended on LI. In tomato, DMP was affected by architectural traits by as much as 20%. DMP and LI of a canopy with higher leaf density (e.g. under low temperature or non-stressed conditions) were more sensitive to changes in architectural traits. High temperature enhanced L_a but reduced L_p of salinity on DMP. The stronger L_a of salinity under high temperature could not be counterbalanced by the smaller L_p . Therefore, long-term influences of high temperature on DMP under salinity were negative. These results highlight the importance of plant architecture at canopy level in studying the plant responses to the environment and show the merits of FSPM as a heuristic tool. Further analyses of these frameworks could improve the breeding strategies and horticultural practices.

Keywords: Cucumber, tomato, functional-structural plant model, salinity stress, light interception, photosynthesis, light use efficiency, quantitative limitation analysis

Kurzfassung

Kenntnisse über Mechanismen der Salztoleranz von Kulturpflanzen sind wichtig für die Entwicklung neuer Sorten oder von Strategien zur Verbesserung des Ertrags von Pflanzen unter Salzstress, einem weitverbreiteten abiotischen Stress. Gewächshausgurken und –tomaten gehören zu den wichtigsten Gemüsepflanzen in Gewächshauskultur und werden häufig in einer von Versalzung betroffenen Region oder einem hydroponischen Anbausystem, wo ionenreiches Bewässerungswasser zur Salzzakkumulation führen kann, kultiviert. Diese zwei Kulturen wurden als Beispielkultur in der vorliegenden Arbeit verwendet, um die Auswirkungen der von Salzstress verursachten strukturellen und physiologischen Limitierungen (bzw. L_s und L_p) auf Bestandlichtaufnahme (BLA), Bestandphotosynthese und Trockenmassenproduktion (TMP) unter verschiedenen Licht- und Temperaturbedingungen zu quantifizieren. Zur Erreichung dieses Ziels wurden zwei funktionell-strukturelle Pflanzenmodelle (FSPM), in denen die 3D-Architektur der Pflanzen explizit dargestellt ist, aufgebaut, parametrisiert und evaluiert. Der erste Modellierungsansatz verknüpfte ein statisches Architekturmodell des Gurkenbestandes mit einem biochemischen Modell für Photosynthese und einer Limitierungsanalyse, um L_p vom Blatt- bis zur Bestandebene hoch zu skalieren und um die komplexen Wechselwirkungen zwischen Salzstress, Lichtintensität und L_p systematisch und quantitativ zu analysieren. Mit dem zweiten Modellierungsansatz, einem dynamischen FSPM, bei dem die Temperatur- und Salzeffekte auf das Tomatenwachstum dargestellt sind, wurden die Auswirkungen der Architekturmerkmale der Tomatenpflanzen auf die TMP quantifiziert. Bei Gurken waren L_s höher als L_p , insbesondere unter hohem Salzstress. Die toxische Wirkung der Natriumakkumulation im Blatt auf die Stomataregulation trug am stärksten zu L_p bei. Komplexe Wechselwirkungen zwischen Salzstress, Licht und L_p wurden sowohl auf Blattebene als auch auf der Bestandebene gefunden. So war z.B. die relative Wichtigkeit der Diffusionslimitierungen abhängig von der BLA. Architekturmerkmale der Tomatenpflanzen beeinflussten TMP bis zu 20%. TMP und BLA eines Bestandes mit hoher Blattdichte (z.B. unter niedriger Temperatur oder nicht-gestressten Bedingungen) waren sensibler für Änderungen in den Architekturmerkmalen. Hohe Temperatur verschlechterte die von Salzstress verursachten L_s aber verbesserte die L_p . Die stärkeren L_s unter hoher Temperatur waren nicht durch die geringere L_p auszugleichen. Daher waren die längerfristigen Einflüsse von hoher Temperatur auf TMP unter Salzstress negativ. Diese Ergebnisse zeigen die Bedeutung der Pflanzenarchitektur auf der Bestandebene, besonders bei der Untersuchung der Reaktion von Pflanzen auf Umweltfaktoren, sowie die Vorteile von FSPM als ein heuristisches Werkzeug. Auf der Basis dieser Modellierungsansätze könnten mithilfe weiterer Analysen neue Strategien für die Züchtung als auch zur Verbesserung pflanzenbaulicher Maßnahmen entwickelt werden.

Schlagworte: Gurke, Tomate, funktionell-strukturelles Pflanzenmodell, Salzstress, Lichtaufnahme, Photosynthese, Lichtnutzungseffizient, quantitative Limitierungsanalyse

Content

Abstract	ii
Kurzfassung	iii
List of Tables	vi
List of Figures.....	viii
Chapter 1	1
Introduction	1
Salinity effects on dry mass production	1
Quantitative assessment of limitations to dry mass production under salinity	2
Using functional-structural plant models	2
Objectives	3
Chapter 2	4
What is the most prominent factor limiting photosynthesis in different layers of a greenhouse cucumber canopy?	4
Abstract.....	4
Introduction.....	6
Materials and Methods	9
Results	15
Discussion.....	21
Chapter 3	27
Disentangling the contributions of osmotic and ionic effects of salinity on stomatal, mesophyll, biochemical and light limitations to photosynthesis	27
Abstract.....	27
Introduction.....	28
Materials and Methods	30
Results	37
Discussion.....	44
Chapter 4	50
Architectural and functional limitations of whole-plant cucumber photosynthesis under salinity	50
Abstract.....	50
Introduction.....	51
Materials and Methods	53
Results	61
Discussion.....	66

Chapter 5	70
Quantification of the effects of architectural traits on dry mass production and light interception of tomato canopy under different temperature regimes using a dynamic functional-structural plant model	70
Abstract.....	70
Introduction.....	71
Materials and Methods	73
Results	80
Discussion.....	88
Chapter 6	92
High temperatures aggravate architectural effects but ameliorate non-architectural effects of salinity on dry mass production of tomato	92
Abstract.....	92
Introduction.....	93
Materials and Methods	95
Results	101
Discussion.....	108
Chapter 7	114
Discussion.....	114
Future research needs	116
Supplementary Materials	119
Reference	143
Acknowledgement	158
Curriculum vitae	159
List of publications	160

List of tables

Table 2-1	Characteristics of the leaves at different leaf ranks. Leaf age (day after leaf appearance) is calculated by assuming a constant leaf appearance rate (0.625 day leaf ⁻¹). Canopy layer leaf area is the sum of the leaf area in the part of the canopy	10
Table 2-2	Reference values of photosynthesis rate (A_j^{ref}), maximum electron transport rate ($J_{\text{max}}^{\text{ref}}$), electron transport rate at PAR = 1300 $\mu\text{mol m}^{-1} \text{s}^{-1}$ (J_s^{ref}), stomatal ($g_{\text{sc}}^{\text{ref}}$) and mesophyll ($g_{\text{m}}^{\text{ref}}$) conductance for the quantitative limitation analysis at non-saturated light conditions	12
Table 2-3	Canopy layers and whole plant photosynthesis and compositions of photosynthetic limitations at four PAR levels above the canopy. S_{Lp} , M_{Lp} , B_{Lp} , and L_{Lp} are stomatal, mesophyll, biochemical, and light limitation, respectively. Leaf area of different canopy layers is shown in Table 2-1.	19
Table 2-4	Values of parameters for the dependence of canopy photosynthesis (A_{C} , $\mu\text{mol CO}_2 \text{ plant}^{-1} \text{ s}^{-1}$) and light use efficiency (LUE_{C} , $\mu\text{mol CO}_2 \mu\text{mol}^{-1}$ photon) on light interception (I_{C} , $\mu\text{mol photon plant}^{-1} \text{ s}^{-1}$) at different canopy layers and whole plant level	20
Table 3-1	Photosynthetic parameters for the quantitative limitation analysis at saturated and non-saturated light conditions and parameters of osmotic and ionic effects.	38
Table 4-1	Parameter list of the photosynthesis model.	58
Table 4-2	Measured whole plant leaf area (LA, m ²) and simulated light interception efficiency (ϵ_i , unit-less).	61
Table 4-3	Statistical analyses for the comparison between simulated and measured data for photosynthesis rate (A_{net} , $\mu\text{mol m}^{-2} \text{ s}^{-1}$) and stomatal conductance to CO ₂ (g_{sc} , $\text{mol m}^{-2} \text{ s}^{-1}$).	62
Table 4-4	Whole plant light use efficiency ($\epsilon_{\text{u},x}$, $\mu\text{mol CO}_2 \text{ mmol}^{-1}$ photon), architectural effect ($E_{\text{a},x}$, %, Eqn. 12a) and functional effects ($E_{\text{f},x}$, %, Eqn. 12b) of salinity on reducing whole plant photosynthesis under x mM NaCl. Data represented simulations under 600 $\mu\text{mol m}^{-2} \text{ s}^{-1}$ PAR above the canopy.	66

Table 5-1	Statistical analysis for the comparison between simulated and measured data for organ and canopy levels over the whole duration of leaf and plant growth at 22/18°C (LT) and 32/28°C (HT) day/night temperatures (L_l , leaf length; L_i , internode length; RMSD: root mean square deviation in Eqn 5-14a).	83
Table 5-2	Influence of leaf angle and internode length on light transmission through the simulated tomato canopy (Q/Q_0), light extinction coefficient (k), and on different days expressed in days after appearance of the first true leaf (DAFLA) at 22/18°C (LT, black bar) and 32/28°C (HT, grey bar) day/night temperature conditions. Numbers are means with standard error in parentheses.	87
Table 6-1	Statistical analysis for the comparison between simulated and measured data for organ level and canopy level for the whole duration of leaf and plant growth at 22/18°C (LT) and 32/28°C (HT) day/night temperature conditions (L_l , leaf length of rank 8; L_i , internode length of rank 8; A_s and $W_{sh,a}$ are, respectively, total leaf area and shoot dry weight(Eqn 6-6a); RMSD: root mean square deviation)	103
Table 6-2	Relative canopy light use efficiency, $k_{T,x}$ (Eqn 6-6a) and effects of high temperature (k_{HT} , Eqn 6-6b) and x mM NaCl salinity (k_x , Eqn 6-6b) on canopy light use efficiency under 22/18°C (LT) and 32/28°C (HT) day/night temperature conditions	106
Table 6-3	Architectural ($R_{a,x}$, Eqn 6-7a) and non-architectural effects ($R_{n,x}$, Eqn 6-7b) on reducing dry mass production under x mM NaCl at 22/18°C (LT) and 32/28°C (HT) day/night temperature conditions	106
Table 6-4	Relative shoot dry mass ($W_{sh,x}$) and total leaf area (A_s , % of the reference canopy architecture), and light transmittance through the canopy (Q/Q_0). Values are simulated data on day 77 after the appearance of the first leaf to different architectural traits under 22/18°C (LT) and 32/28°C (HT) day/night temperature. In all cases, standard errors were smaller than 3%. The magnitudes of change in architectural traits are similar to the reported magnitude reported in the literature (Table 6-S1).	107

List of figures

- Fig. 2-1** The virtual 2-meter cucumber canopy with 18 plants, constructed using digitized data in *GroIMP*, in top view (a) and side view (b). The black arrows show the north. The simulated results were from the plants indicated by red arrows. **9**
- Fig. 2-2** Simulated intercepted PAR of leaves on all ranks with sun position in Hannover, Germany, lat. 52°23'N, long. 9°37'E, on 1 July at 1200h. (a) Light interception of leaves at four light conditions (PAR above the canopy = 100 (closed circle), 500 (open triangle down), 900 (closed square) and 1300 (open diamond) $\mu\text{mol photon m}^{-2} \text{s}^{-1}$, 79% direct light and 21% diffuse light. (b) Light interception of leaves under 100% direct light or 100% diffuse light. PAR above the canopy was assumed to be 1000 $\mu\text{mol photon m}^{-2} \text{s}^{-1}$. Means of 10 simulations with slightly rotated ($\leq \pm 30^\circ$) plants, bars represent standard deviation. **15**
- Fig. 2-3** Evaluation of the photosynthesis model. (a) Simulated and measured photosynthesis; each point represents mean values of simulated and measured photosynthesis rates (for measurement and simulation, $n = 4$ and 10, respectively) Bars represent standard deviations. (b) Difference between measured and simulated data at different PAR levels ($R^2 = 0.006$, $p = 0.50$, 95% confidence intervals of the slope and the intercept were -0.002-0.001 and 0.39-1.43). (c) Difference between measured and simulated data at different leaf ranks ($R^2 = 0.002$, $p = 0.79$, 95% confidence intervals of the slope and the intercept were -0.06-0.05 and 0.20-1.50). The solid line is 1:1 line in (a), and $y = 0$ in (b) and (c). The dashed lines are the regression lines. **16**
- Fig. 2-4** Changes of (a) stomatal, (b) mesophyll, (c) diffusional (stomatal + mesophyll), (d) biochemical, (e) light and (f) total (diffusional + biochemical + light) limitation with leaf rank and light conditions above the canopy (100, 500, 900 and 1300 $\mu\text{mol photon m}^{-2} \text{s}^{-1}$). Symbols are described in Fig. 2-2a ($n = 10$). **18**
- Fig. 2-5** Sensitivity of stomatal limitation to (a) water vapour deficit and (b) parameter g_1 (in Eqn 2-4). Simulations were run for leaves on days 15 (solid line), 25 (dotted line) and 35 (dashed line) after leaf appearance. The vertical solid lines indicate the default parameter values used for analysing the canopy photosynthetic limitation. **19**
- Fig. 2-6** Dependence of (a) canopy photosynthesis rate and (b) light use efficiency on light interception of different canopy layers. **20**
- Fig. 2-7** Simulated leaf photosynthesis rate under 100% direct light (closed circle) and 100% diffuse light (open circle, $n = 10$). PAR above the canopy was assumed to be 1000 $\mu\text{mol m}^{-2} \text{s}^{-1}$. The grey triangles indicate the increases in photosynthesis under 100% diffuse light condition (% of value at 100% direct light). **21**

- Fig. 3-1** Influence of incident light intensity on (a) absolute stomatal limitation, L_{Sj} in Eqn 3-9; (b) relative stomatal limitation, l_{sj} in Eqn 3-10a; (c) absolute mesophyll limitation, L_{Mj} in Eqn 3-9; (d) relative mesophyll limitation, l_{mj} in Eqn 3-10b; (e) absolute light limitation, L_{Lj} in Eqn 3-9; and (f) relative limitation of electron transport rate (ETR), l_j in Eqn 3-10c. Data were obtained from cucumber leaves on days 12 (closed circles) and 21 (open circles) after leaf appearance. Each point was calculated from the averages of four measurements on a given date, on the fourth leaves under non-stress conditions. 37
- Fig. 3-2** Stacked graphs describing the effects of ontogeny and salinity levels on the components of photosynthetic limitation at saturated light conditions (PPFD = 1300 $\mu\text{mol m}^{-2}\text{s}^{-1}$ and $C_a = 380 \mu\text{mol mol}^{-1}$). (a) - (d) represent 0, 20, 40 and 60 mM NaCl in the solution, respectively. The black, dark grey and grey areas represent the stomatal, mesophyll and biochemical limitations, respectively. Limitations are expressed as percentages of the reference values at saturated light conditions given in Table 3-1. Each value was calculated from four measurements on the given dates and salt treatments. 39
- Fig. 3-3** Stacked graphs describing the effects of ontogeny and salinity levels on the components of photosynthetic limitation at non-saturated light conditions (PPFD = 600 $\mu\text{mol m}^{-2}\text{s}^{-1}$ and $C_a = 380 \mu\text{mol mol}^{-1}$). (a) - (d) represent 0, 20, 40 and 60 mM NaCl in the solution, respectively. The black, dark grey, grey and white areas represent the stomatal, mesophyll, biochemical and light limitations, respectively. Limitations are expressed as percentages of the reference values at non-saturated light conditions given in Table 3-1. Each value was calculated from four measurements on the given dates and salt treatments. 40
- Fig. 3-4** Effects of osmotic stress on photosynthetic limitations at saturating (PPFD = 1300 $\mu\text{mol m}^{-2}\text{s}^{-1}$, close circle) and non-saturating (600 $\mu\text{mol m}^{-2}\text{s}^{-1}$, reversed triangle) light conditions. (a) The stomatal limitation increased linearly with the salinity level in the nutrient solution. The solid line represents the regression line of the pooled data because the slopes between saturating and non-saturating light conditions were not different; $y = 0.24x + 0.89$, $R^2 = 0.92$, $p < 0.001$; standard errors of intercept and slope were 1.39 and 0.02 $\% \text{mM}^{-1}$, respectively. (b) The mesophyll limitation increased linearly with the salinity level. Dotted and dashed lines are regression lines under saturating ($y = 0.044x + 0.531$, $R^2 = 0.90$, $p = 0.054$; standard errors of intercept and slope were 0.399 and 0.011, respectively) and non-saturating ($y = 0.019x + 0.368$, $R^2 = 0.95$, $p = 0.025$; standard errors of intercept and slope were 0.114 and 0.003, respectively) light conditions, respectively. Each value was calculated from four measurements under the given light conditions and salt treatments. Measurements were taken on day 2 (non-saturating light) and day 3 (saturating light) after start of salinity treatment. 41

- Fig. 3-5** Effects of ionic stress on stomatal (a, b) and biochemical limitation (c, d) at saturated (PPFD = 1300 $\mu\text{mol m}^{-2}\text{s}^{-1}$, a, c) and non-saturated (600 $\mu\text{mol m}^{-2}\text{s}^{-1}$, b, d) light conditions. Circles, reverse triangles, squares and rhombi represent data collected from plants subjected to 0, 20, 40 and 60 mM NaCl in the nutrient solution, respectively. The solid, dotted and dashed lines represent the regression lines of the data collected from plants subjected to 20, 40 and 60 mM NaCl in the nutrient solution, respectively. Each point was calculated from four measurements under the given light conditions and salt treatments. Measurements were taken between day 2-11 after start of salinity treatment. 42
- Fig. 3-6** Simulated relationships between Na^+ concentrations in leaves and stomatal (a, b) and biochemical limitations (c, d) under saturating (1300 $\mu\text{mol m}^{-2}\text{s}^{-1}$; a, c) and non-saturation (600 $\mu\text{mol m}^{-2}\text{s}^{-1}$; b, d) light conditions under 20, 40 and 60 mM NaCl in the solution. Parameters listed in Table 3-1 were used for simulations; stomatal conductance, mesophyll conductance, maximum Rubisco-carboxylation rate and maximum electron transport rate at Na^+ concentration in leaves with 0 mM Na^+ were assumed to be 0.3 $\text{mol m}^{-2}\text{s}^{-1}$, 0.8 $\text{mol m}^{-2}\text{s}^{-1}$, 104 $\mu\text{mol CO}_2 \text{ m}^{-2}\text{s}^{-1}$ and 135 $\mu\text{mol e}^- \text{ m}^{-2}\text{s}^{-1}$, respectively, which were similar to the values measured in the middle of the experiment. 43
- Fig. 3-7** Relationships between stomatal limitation and photosynthesis rate (a, b), stomatal conductance to water vapor (c, d) and intrinsic water use efficiency (e, f) at saturating (a, c and e) and non-saturating (b, d and f) light conditions. Each point represents the mean values of 4 measurements. Linear regression was used to describe the relationships between stomatal limitation and intrinsic water use efficiency. 44
- Fig. 4-1** Side view of the 3D virtual cucumber canopies on day 0 (a) and day 14 (b) after exposure to 50 mM NaCl salinity. For a clear visual representation, only six plants in one row are shown, instead of 50 plants in five rows used for the simulations. Plants are reconstructed in *GroIMP* by digitized data. 55
- Fig. 4-2** Relationships between day under salinity and Na^+ concentrations in leaf water under 0 mM (a), 25 mM (b) and 50 mM (c) NaCl. These relationships were used to estimate the Na^+ concentrations in leaves for simulating canopy photosynthesis. Each point and bar represents the average and standard deviation of four leaves. 62
- Fig. 4-3** Measured and simulated simulated photosynthesis rate (A_{net} , a) and stomatal conductance to CO_2 (g_{sc} , b). Each point and bar represents the average and standard deviation of eight point measurements and simulations. The grey lines are 1:1 lines. 62
- Fig. 4-4** Changes of (a) stomatal, (b) mesophyll, (c) biochemical and (d) light limitation with leaf rank and salinity level in the nutrient solution (closed circle, open reverse triangle and closed square represent additional 0, 25 and 50 mM NaCl in the nutrient solution) on day 21 after exposure to salinity. Photosynthetically active radiation above the canopy was assumed to be 600 $\mu\text{mol photons m}^{-2} \text{ s}^{-1}$. The leaves with higher leaf rank were the 63

younger leaves in the canopy.

- Fig. 4-5** Simulated whole plant stomatal (a), mesophyll (b), biochemical (c) and light (d) limitations between days 0-35 after exposure to salinity ($n = 3$, each replication represents the average value of 10 simulations). Photosynthetically active radiation above the canopy was assumed to be $600 \mu\text{mol photons m}^{-2} \text{s}^{-1}$. 64
- Fig. 4-6** Changes of whole plant stomatal (a), mesophyll (b), biochemical (c) and light (d) limitations with light (photosynthetically active radiation) above the canopy and salinity level in the nutrient solution (closed circle, open reverse triangle and closed square represent additional 0, 25 and 50 mM NaCl in the nutrient solution) on day 21 after exposure to salinity. 64
- Fig. 4-7** (a) Simulated whole plant photosynthesis rate ($P_{w,x}$, $\mu\text{mol plant}^{-1}\text{s}^{-1}$, Eqn 12) under different salinity levels. (b) Simulated whole plant photosynthesis rate ($P_{w,ax}$, $\mu\text{mol plant}^{-1}\text{s}^{-1}$, Eqn 12) of plants with x mM NaCl architecture but non-stressed photosynthetic capacity. 65
- Fig. 5-1** Representation of a tomato plant architecture (A) and a tomato leaf architecture with leaf length = l (B). Leaf angle (θ) is the angle between stem and petiole. Leaf curvature is defined as the sum of α_1 , α_2 and α_3 . Reference ratio of $\alpha_1 : \alpha_2 : \alpha_3 = 1:2:2$. Reference area of leaflet 1 : leaflet 2 : leaflet 3 : terminal leaflet = $0.12 : 0.17 : 0.13 : 0.16$. Reference ratio of the length and width of all leaflets is 1.33. Reference values were derived from leaves grown in expt. 1. 74
- Fig. 5-2** Time course of simulated leaf elongation rates of the leaves at rank 8. Solid and dashed lines represent the simulated leaf elongation rates at $22/18^\circ\text{C}$ (LT) and $32/28^\circ\text{C}$ (HT) day/night temperature conditions. 80
- Fig. 5-3** Measured (symbols) and simulated (lines) leaf lengths at rank 8 (A) and rank 13 (B) under $22/18^\circ\text{C}$ (LT, closed symbols) and $32/28^\circ\text{C}$ (HT, open symbols) day/night temperature conditions (Expt. 5, $n = 4$). Bars indicate standard errors. The solid line in (C) is the 1:1 line between simulated and measured data. By plotting all data, $y = 1.00x + 0.04$, $R^2 = 0.97$, $p < 0.001$, intercept was not different from zero and slope was not different from one. 81
- Fig. 5-4** Measured and simulated leaf angles at $22/18^\circ\text{C}$ (LT, closed circle) and $32/28^\circ\text{C}$ (HT, open circle) day/night temperature conditions (Expt. 5, $n = 4$). Data were taken from the plants on 50, 56, 63 and 64 DAFLA Bars are standard errors. The solid line is the 1:1 line between simulations and measurements. 82
- Fig. 5-5** Comparison between simulated and measured leaf number (A), plant height (B), total leaf area (C) and shoot dry mass (D) at $22/18^\circ\text{C}$ (LT, closed circle) and $32/28^\circ\text{C}$ (HT, open circle) day/night temperature conditions (Expt. 5, $n = 4$). Bars are standard errors. Lines represent the averages of simulated data under LT (solid line) and HT conditions. 83

- Fig. 5-6** The predicted influence of the leaf angle (A), leaf curvature (B), leaf length and width ratio (C) and internode length (D) on shoot dry mass on 77 DAFLA at 22/18°C (LT, closed circle) and 32/28°C (HT, open circle) day/night temperature conditions. The reference values for relative leaf angle, leaf curvature and internode length were 1. The reference value for leaf length and width ratio was 1.33. Simulated shoot dry mass on 77 DAFLA with the reference values was set to 100%. 84
- Fig. 5-7** The predicted influence of the leaf curvature angle ratio (A) and leaflet arrangement (B) on total shoot dry mass on 77 DAFLA at 22/18°C (LT, black bar) and 32/28°C (HT, grey bar) day/night temperature conditions. The reference ratio of curvature angles, $\alpha_1:\alpha_2:\alpha_3$ (Fig. 5-1) was 1:2:2; MC1 = 1:1:1; MC2 = 1:1:2; MC3 = 1:2:3; and MC4 = 2:1:1. Reference area ratio of leaflet 1: leaflet 2: leaflet 3: terminal leaflet was 0.12:0.17:0.13:0.16; ML1 = 0.143:0.143:0.143:0.142; ML2 = 0.2:0.15:0.11:0.08; and ML3 = 0.08:0.15:0.17:0.2. 85
- Fig. 5-8** The simulated influence of the leaf angle (A) and internode length (B) on shoot dry mass at 22/18°C (LT, solid lines) and 32/28°C (HT, dashed lines) day/night temperature conditions. Black and red lines represent that the morphological traits are 70% and 130% of the reference values, respectively. 86
- Fig. 6-1** Effect of salinity on shoot dry mass on day 77 after the first leaf appearance under 22/18°C (LT) and 32/28°C (HT) day/night temperature conditions. 101
- Fig. 6-2** Measured (symbols) and simulated (lines) leaf length (A,B) and internode length (C,D) at 22/18°C (LT, A,C) and 32/28°C (HT, B,D) day/night temperature regimes under 40 (circles), 60 (triangles) and 80 (squares) mM NaCl. 102
- Fig. 6-3** Measured (symbols) and simulated (lines) total plant leaf area (A,B) and shoot dry weight (C,D) at 22/18°C (LT, A,C) and 32/28°C (HT, B,D) day/night temperature regimes under 40 (circles), 60 (triangles) and 80 (squares) mM NaCl. The measured and simulated total leaf area and shoot dry weight of non-stress plants can be found in Chen *et al.* (2014). Measured data were the averages of four replicates (two plants per replicate). The simulated shoot dry weights were the results with light use efficiency equal to ε_0 (Eqn 6-6a). 104
- Fig. 6-4** Measured (A,B) and simulated (C, D) allometric relationships between shoot dry weight and whole plant leaf area ($\text{cm}^2 \text{ plant}^{-1}$) at 22/18°C (LT, closed symbols and solid lines) and 32/28°C (HT, open symbols and dotted lines) day/night temperature regimes under non-stress (A) and under 40, 60 and 80 mM NaCl (B). Black lines represent the regression lines fitted by the data collected in Expt. 5 according to Eqn 6-5a (non-stress) and Eqn 6-5b (salinity stress). The red lines show the allometric relationships before adjusting ε by k_0 in Eqn 6-6a (C) and by k_{80} in Eqn 6-6b (D). The blue lines show the allometric relationships after adjusting ε . 105

Chapter 1

Introduction

Expanding salinization reduces crop yield worldwide (FAO, 2005). Since most crop species are glycophytes (plants which are not adapted to saline conditions; Flower, 2004) and the crop yield has to increase to fulfil the predicted food demands in 2050 (Tester and Langridge, 2010), knowledge for enhancing salt tolerance of crop species are necessary for designing new cultivars or strategies to improve crop performance under saline conditions (Munns and Tester, 2008).

Salinity effects on dry mass production

The presence of Na^+ and Cl^- ions reduce the osmotic potential of soil and nutrient solution. This results in the osmotic effects of salinity, which reduce the expansion of leaves and internodes (Rajendran *et al.*, 2009; Harris *et al.*, 2010) as well as stomatal conductance (James *et al.*, 2008). The consequence of the morphological changes under salinity is alterations in plant architecture, decrease in light interception and the size of photosynthetic apparatus. A lower stomatal conductance due to osmotic stress results in a less efficient use of light for carbon assimilation. Furthermore, the uptake of Na^+ and Cl^- from the roots and then the accumulation of these two ion species in the leaf tissues may further disturb stomatal regulation and reduce photosynthetic capacity (Delfine *et al.*, 1999; James *et al.*, 2002; James *et al.*, 2006; Shapira *et al.*, 2009). This is referred to as ionic effects of salinity which further decrease the light use efficiency for carbon assimilation. Although there are some speculations about the relative impacts of different salinity effects on photosynthesis in the literature (for example, Munns, 1993; Munns & Tester, 2008; Pérez-López *et al.*, 2012), no quantitative assessment of these impacts at the whole plant level exists in the literature, except in Rajendran *et al.* (2009). The latter developed three indices, each one with values between 0 and 1, and combined them in a regression model to predict dry mass production under salinity:

$$W_{d,s}/W_{d,n} = 0.14 X_{oT} + 0.5 X_{Na} + 0.38 X_{TT} + 0.06 \quad (\text{Eqn 1.1})$$

where $W_{d,s}$ and $W_{d,n}$ are shoot dry masses under saline and non-saline conditions, respectively, X_{oT} represents osmotic tolerance, X_{Na} quantifies the ability of Na^+ exclusion, and X_{TT} indicates tissue tolerance. The low coefficient for osmotic tolerance indicates that osmotic tolerance has relatively small influence on improving dry mass production under salinity. However, this conflicts with the view of Munns and Tester (2008) stating that osmotic stress has a greater effect on growth than ionic stress.

Quantitative assessment of limitations to dry mass production under salinity

The major difficulties in assessing the relative impact of an architectural (e.g. leaf size and internode length) or a physiological trait (e.g. stomatal and mesophyll conductance) on crop dry mass production under salinity might be the complex interactions between plant structure, physiological functions and environmental conditions. For example, there are interactions between physiological functions and environmental factors, e.g. severity of salinity (Stępień and Kłobus, 2006) and temperature (Rivero *et al.*, 2014). There are drastic environmental and physiological gradients within a plant (Niinemets *et al.*, 2015) and these gradients result in that the quantitative assessment of salinity effects on photosynthesis obtained from leaf level (e.g., Pérez-López *et al.*, 2012) would not correspond to it at the whole plant level (Cano *et al.*, 2013). Therefore, the salinity effects at the leaf level should be scaled up to the whole plant level. Furthermore, since strong seasonal variations in the components of photosynthetic limitations may occur (under non-stressed and drought stress, Wilson *et al.*, 2000; Grassi and Magnani, 2005; Limousin *et al.*, 2010; Egea *et al.*, 2011), the salinity effects on architectural and photosynthetic properties of a canopy at different developmental stages should be considered. Due to this complexity, it is experimentally almost impossible to quantify the different impacts of salinity stress on whole plant dry mass production. Therefore, Munns and Tester (2008) may only roughly suggest that the relative importance of a physiological mechanism to salinity tolerance may vary with the species, local environmental conditions, severity of salinity and the length exposure to it.

Using functional-structural plant models

It has been proposed that the integration of low-level traits and resource-use efficiency, e.g. light use, is required in predicting salinity effect on crop development (Harris *et al.*, 2010). Functional-structural plant models (FSPM), where the plant architecture, physiological processes and environmental conditions (Vos *et al.*, 2010) are described, is a tool for the simulations of the interactions between environment, plant architecture and architecture-related physiological processes. For example, static FSPMs have been used for the prediction of light distribution in the canopy (Sarlikioti *et al.*, 2011; Wiechers *et al.*, 2011a; Song *et al.*, 2013). Parametric Lindenmayer-Systems (L-systems) are formal grammars which can be used to describe the dynamics of plant growth and canopy architecture (Prusinkiewicz and Lindenmayer 1990). Based on this formalism, dynamic FSPM can be constructed to predict the dynamic growths of plants and the morphological

adaption of canopy elements to light environment (e.g. Kahlen *et al.* 2008, Cieslak *et al.* 2011, Kahlen & Stützel, 2011). Therefore, FSPMs may be a suitable methodology to scale up the salinity effects on whole-plant performance and were chosen for studying the architectural and physiological effects of salinity on dry mass production in this work.

Objectives

Cucumber, a salt sensitive (Stępień and Kłobus, 2006), and tomato, a moderately sensitive species (Maggio *et al.*, 2007), belong to the most important greenhouse vegetable crops (Heuvelink, 2005; Stępień and Kłobus, 2006) and are often cultivated in regions exposed to salinity, or in hydroponic systems, where the presence of salt in the irrigation water may result in salt accumulation (Savvas *et al.*, 2005). Therefore, they are selected as model crops in this work. This thesis aims at quantifying the impacts of plant architecture on light interception and photosynthesis under non-stressed and salinity conditions. Both static and dynamic functional-structural plant models are used to achieve the following objectives:

- 1) developing a novel approach (combining functional-structural plant model, photosynthesis model and quantitative limitation analysis of photosynthesis) to upscale the stomatal, mesophyll, biochemical and light limitations to cucumber photosynthesis from leaf to canopy level under non-stressed conditions (chapter 2);
- 2) construction and parameterization of a model describing salinity effects on cucumber photosynthesis and quantifying different components of photosynthetic limitations at the leaf level (chapter 3);
- 3) combining the modelling approach proposed in chapter 2 and the photosynthesis model proposed in chapter 3 to dissect the contributions of architectural and physiological limitations to cucumber canopy photosynthesis under salinity (chapter 4);
- 4) developing a dynamic functional-structural plant model of tomato under non-stressed condition to quantify the impacts of architectural traits on dry mass production (chapter 5) and
- 5) introducing the salinity effects on plant architecture into the tomato model proposed in chapter 5 for analysing the architectural and non-architectural effects of salinity on dry mass production (chapter 6).

Each chapter focuses on a step towards the quantification of architectural and non-architectural effects of salinity. All of them can be also read individually.

Chapter 2

What is the most prominent factor limiting photosynthesis in different layers of a greenhouse cucumber canopy?

Tsu-Wei Chen¹, Michael Henke², Pieter H.B. de Visser³, Gerhard Buck-Sorlin⁴, Dirk Wiechers⁵, Katrin Kahlen⁶ and Hartmut Stützel¹

¹*Institute of Horticultural Production Systems, Leibniz Universität Hannover, Herrenhäuser Straße 2, 30419 Hannover, Germany,* ²*Department Ecoinformatics, Biometrics and Forest Growth, Georg-August University of Göttingen, Göttingen, Germany,* ³*Greenhouse Horticulture, Wageningen UR, Droevendaalsesteeg 1, 6708 PB Wageningen, the Netherlands,* ⁴*UMR1345 Institut de Recherche en Horticulture et Semences (IRHS), AGROCAMPUS OUEST, Centre d'Angers, 2 rue André le Nôtre 2, 49045 Angers Cedex 01, France,* ⁵*KWS SAAT AG, 373555 Einbeck, Germany and* ⁶*Geisenheim University, Von-Lade-Straße 1, 65366 Geisenheim, Germany*

Published in: *Annals of Botany* **114**: 677-688, 2014

Abstract

Background and Aims Maximizing photosynthesis at the canopy level is important for enhancing crop yield. This requires insights into limiting factors of photosynthesis. Using greenhouse cucumber as an example, we provide a novel approach to quantify different components of photosynthetic limitations at the leaf level and upscale these limitations to different canopy layers and the whole plant.

Methods A static virtual three-dimensional canopy structure was constructed using digitized plant data in *GroIMP*. Light interception of the leaves was simulated by an advanced GPU-based ray-tracer and used to compute leaf photosynthesis. Different components of photosynthetic limitations, i.e. stomatal (S_L), mesophyll (M_L), biochemical (B_L) and light (L_L) limitations, were calculated by a quantitative limitation analysis of photosynthesis under different light regimes.

Key Results In the virtual cucumber canopy, B_L and L_L were the most prominent factors limiting whole-plant photosynthesis. Diffusional limitations ($S_L + M_L$) contributed less than 15% to total limitation. Photosynthesis in the lower canopy was more limited by the biochemical capacity and the upper canopy was more sensitive to light than other canopy parts. Although leaves in the upper canopy received more light, their photosynthesis was more light-restricted than in the leaves of the lower canopy, especially when the light

condition above the canopy was poor. An increase in whole-plant photosynthesis under diffuse light did not result from an improvement of light use efficiency but from an increase in light interception. Diffuse light increased photosynthesis of leaves, which were directly shaded by other leaves in the canopy, by up to 55%.

Conclusions Maintaining biochemical capacity of the middle-lower canopy and increasing the leaf area of the upper canopy would be promising strategies to improve canopy photosynthesis in a high-wire cropping system. Further analyses using our approach are expected to provide insights into the influences of horticultural practices on canopy photosynthesis and the design of optimal crop canopies.

Key words: Canopy photosynthesis, photosynthetic limitations, FvCB model, quantitative limitation analysis, *Cucumis sativus*, diffuse light, functional-structural plant model

Introduction

Improving productivity is a major goal in crop production. This can be achieved by genetic crop improvement or by the optimization of the cropping system. Important tasks to optimize the cropping system are to maximize crop photosynthesis at the canopy level (Murchie *et al.*, 2009; Zhu *et al.*, 2010; Reynolds *et al.*, 2012) and to optimize the photosynthetic resource distribution within the canopy (Buckley *et al.*; 2013). However, since it is difficult to measure canopy photosynthesis, modelling approaches are necessary for its study (Zhu *et al.*, 2012). To date, several approaches for modelling canopy photosynthesis have been proposed: 1) big leaf models, where the whole canopy is assumed to consist of one leaf (Thornley *et al.*, 1992); 2) sunlit-shaded models, where a plant canopy is represented by two leaves and where one of which is shaded by the other (de Pury and Farquhar, 1997; Peltoniemi *et al.*, 2012); 3) multi-layer models, where the plant canopy is divided into leaf clusters exposed to different light environments (Zhu *et al.*, 2012); 4) functional-structural plant models (FSPM), where the plants and the canopy are constructed spatially explicitly at the organ level with geometry and topology and the physiological functions of plants, e.g. photosynthesis, and interactions between canopy structure and environmental factors, such as light, are described (Vos *et al.*, 2010; DeJong *et al.*, 2011). A key feature of FSPMs is that the heterogeneities of microclimate, especially local light conditions, can be simulated and used to compute photosynthesis at the leaf level and upscale it to the canopy level (Buck-Sorlin *et al.*, 2011; Sarlikioti *et al.*, 2011b; Wiechers *et al.*, 2011a; Song *et al.*, 2013).

For decades, plant physiologists have searched for methods to identify and to quantify the factors restricting photosynthesis (Jones, 1985). So far, it is not possible to “measure” the photosynthetic limitation. The relative or quantitative magnitude of photosynthetic limitations can be only quantified by mathematical approaches (see Jones, 1985; Wilson *et al.*, 2000; Grassi and Magnani, 2005; Grassi *et al.*, 2009). By combining the Farquhar-von Caemmerer-Berry model (FvCB model, Farquhar *et al.*, 1980) with the state function method (Jones, 1985), Grassi and Magnani (2005) have dissected and quantified the contribution of different photosynthetic limitations. By their approach (in the following referred to as quantitative limitation analysis) the absolute total limitation of photosynthesis (% of a reference photosynthesis rate at ambient CO₂ concentration and saturating light, A_{\max}^{ref} , $\mu\text{mol CO}_2 \text{ m}^{-2}\text{s}^{-1}$) can be quantitatively partitioned into stomatal, mesophyll and biochemical components. In their study, the reference photosynthesis rate

is $16.8 \mu\text{mol CO}_2 \text{ m}^{-2}\text{s}^{-1}$ and their finding that the stomatal limitation of sun leaves in oak trees in summer is 9-14% indicates that photosynthesis rates can be increased by 1.51-2.35 $\mu\text{mol CO}_2 \text{ m}^{-2}\text{s}^{-1}$ if the stomata would fully open. Quantitative limitation analysis is a helpful methodology to quantify the photosynthetic limitations based on measured data and allows plant physiologist to disentangle the contributions of different physiological and environmental factors to photosynthetic limitations on the leaf level (Flexas *et al.*, 2009; Egea *et al.*, 2011). However, whether the results from the quantitative limitation analysis at leaf level would correspond to the photosynthetic limitations at the canopy level, is questionable for two reasons: Firstly, quantitative limitation analysis has been only applied under light-saturated (Rubisco-limited) conditions but most leaves in the canopy (except for leaves grown in the upper part of the canopy) are normally exposed to non-saturating light conditions (RuBP-limited, Song *et al.*, 2013). Secondly, a recent study has shown that the kind and extent of photosynthetic limitations vary between different tree canopy layers (Cano *et al.*, 2013). Therefore, the compositions of photosynthetic limitations at the canopy or whole plant level may be quite different from those at the leaf level. To date, it is still unknown to which extent the different factors restrict photosynthesis in different canopy layers and at the whole plant level.

Recently, a quantitative limitation analysis for the RuBP-limited phase of photosynthesis was proposed (Chen *et al.*, 2013). In this approach, the influence of light on limiting photosynthesis is taken into account and the total limitation of leaf photosynthesis (A_L , % of $A_{\text{max}}^{\text{ref}}$) is partitioned into four components:

$$A_L = S_L + M_L + B_L + L_L \quad \text{Eqn 2-1}$$

where S_L , M_L , B_L and L_L are stomatal, mesophyll, biochemical and light limitation, respectively. The fact that the contribution of different limitations calculated by this method can be treated additively (Grassi *et al.*, 2009) allows straightforward interpretation and allows the computation of the photosynthetic limitation at canopy levels by summing up the limitations of all leaves of a plant. For example, the stomatal limitation of a plant with n leaves (S_{Lp} , $\mu\text{mol CO}_2 \text{ plant}^{-1}\text{s}^{-1}$) can be calculated by:

$$S_{Lp} = A_{\text{max}}^{\text{ref}} \cdot \sum_{k=1}^n (S_{L,k} \cdot LA_k) \quad \text{Eqn 2-2}$$

where LA_k is the area of leaf k , $S_{L,k}$ is the stomatal limitation of leaf k . This approach allows the calculation of the total limitation of a plant (A_{Lp} , $\mu\text{mol CO}_2 \text{ plant}^{-1}\text{s}^{-1}$):

$$A_{Lp} = A_{\max}^{\text{ref}} \cdot \sum_{k=1}^n (LA_k \cdot (S_{L,k} + M_{L,k} + B_{L,k} + L_{L,k})) \quad \text{Eqn 2-3}$$

where $M_{L,k}$, $B_{L,k}$, $L_{L,k}$, are the mesophyll, biochemical and light limitations of leaf k . This up-scaling approach may provide insights into the sources of photosynthetic limitations in the cropping system. Since it is almost impossible to measure all of the parameters (light interception by the leaves, FvCB model parameters, stomatal and mesophyll conductance) required for the quantitative limitation analysis of all leaves of a plant, a modelling approach would be desirable for investigating the photosynthetic limitation of both different canopy layers and the whole plant. We suggest to combine a structural model and the FvCB model, as has been done in several studies (Wiechers *et al.*, 2011a; Sarlikioti *et al.*, 2011b; Buck-Sorlin *et al.*, 2011; Song *et al.*, 2013), to quantify different components of photosynthetic limitation at the canopy level.

Both experimental and model-based investigations have demonstrated that canopy photosynthesis and light use efficiency may be improved under diffuse light conditions (Alton *et al.*, 2007; Wohlfahrt *et al.*, 2008; Mercado *et al.*, 2009). Greenhouse experiments have shown that transforming direct light entering the greenhouses to diffuse light by a plastic film results in a more even light distribution in the canopy and increases the yield of cucumber by 5% (Hemming *et al.*, 2008). However, the effects of diffuse radiation on canopy photosynthesis change with environmental and biological conditions. For example, they are less significant when the radiation above the canopy is low (Alton *et al.*, 2007), and they depend on plant species and planting season (Jongschaap *et al.*, 2006). Moreover, Wohlfahrt *et al.* (2008) have found that the effect of diffuse radiation on canopy photosynthesis is more significant in a canopy with a higher leaf area index, suggesting that canopy structure might influence the impact of diffuse radiation on canopy photosynthesis, but this has not been examined.

In this work, we used data from plant digitization to construct a static FSPM, a representative cucumber canopy structure, using the interactive modelling platform *GroIMP* (Kniemeyer, 2008) and applied the quantitative limitation of photosynthesis (Chen *et al.*, 2013), to 1) determine the most prominent factor limiting leaf and canopy photosynthesis; 2) quantify the variations in photosynthetic limitations at different canopy layers; 3) investigate the dependence of photosynthesis and light use efficiency on light interception at different canopy layers; and 4) examine the effect of diffuse light on leaf-level light interception and photosynthesis.

Materials and Methods

Constructing the virtual cucumber canopy

The whole plant architecture of cucumber plants (*Cucumis sativus* L. cv. Aramon, Rijk Zwaan, De Lier, Netherlands) with 21 mature leaves grown in a greenhouse experiment (treatment D1R2 in Kahlen and Stützel, 2007) was digitized. The reconstruction of the leaves using digitizing data is described by Wiechers *et al.* (2011b). In short, the coordinates of 13 points per leaf lamina were digitized by a 3D digitizer (Fastrak, Polhemus, USA). Each lamina was represented by a predefined set of triangles and was reconstructed using the commands *FloatList* and *PolygonMesh* in *GroIMP* (Kniemeyer, 2008). For constructing the virtual canopy structure, 18 cucumber plants placed at a density of 1 plant per m² were distributed in 3 rows (Fig. 2-1). Distances between virtual plants in a row and between rows were 0.5 m and 2 m, respectively. Furthermore, the whole canopy was divided into four canopy layers: 1) lower canopy (leaf rank 1-5), 2) middle-lower canopy (leaf rank 6-10), 3) middle-upper canopy (leaf rank 11-15) and 4) upper canopy (leaf rank 16-21). Leaf age (days) and leaf area (m²) are summarized in Table 2-1.

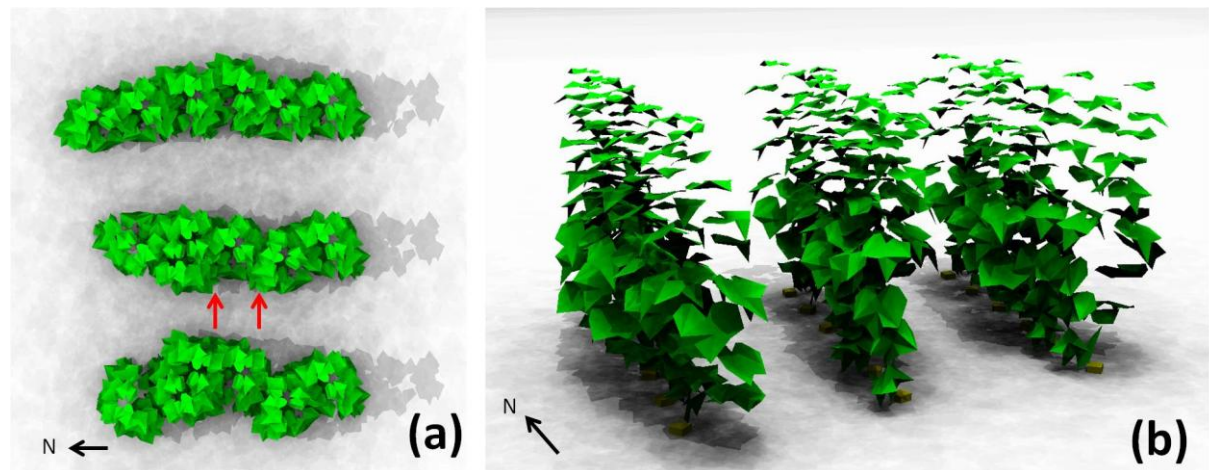


Fig. 2-1. The virtual 2-meter cucumber canopy with 18 plants, constructed using digitized data in *GroIMP*, in top view (a) and side view (b). The black arrows show the north. The simulated results were from the plants indicated by red arrows.

Table 2-1. Characteristics of the leaves at different leaf ranks. Leaf age (day after leaf appearance) is calculated by assuming a constant leaf appearance rate (0.625 day leaf⁻¹). Canopy layer leaf area is the sum of the leaf area in the part of the canopy

Leaf rank (-)	Leaf age (d)	Leaf area (m ²)	Canopy layer (-)	Canopy layer leaf area (m ²)
1	40	0.0462	lower	0.3630
2	38.4	0.0725	lower	
3	36.8	0.0747	lower	
4	35.2	0.0774	lower	
5	33.6	0.0922	lower	
6	32	0.1016	middle-lower	0.4788
7	30.4	0.0953	middle-lower	
8	28.8	0.1063	middle-lower	
9	27.2	0.0900	middle-lower	
10	25.6	0.0855	middle-lower	
11	24	0.0799	middle-upper	0.3349
12	22.4	0.0719	middle-upper	
13	20.8	0.0593	middle-upper	
14	19.2	0.0589	middle-upper	
15	17.6	0.0650	middle-upper	
16	16	0.0550	upper	0.2734
17	14.4	0.0560	upper	
18	12.8	0.0417	upper	
19	11.2	0.0454	upper	
20	9.6	0.0382	upper	
21	8	0.0371	upper	
1-21	-	-	whole plant	1.4501

Simulating local light environment

The light environment was simulated according to Buck-Sorlin *et al.* (2011). In short, the virtual canopy was surrounded by sun and sky providing direct and diffuse light, respectively (Fig. 2-S1). The sun was a single object providing light in the direction of the corresponding location and time (in our simulation: Hannover, Germany, lat. 52°23'N, long. 9°37'E, on 1 Jul. at 1200 h). The sky was approximated by an array of 72 directional light sources arranged in a hemisphere. For computing the light distribution array-tracer, integrated into *GroIMP*, was used with 10 million rays and a recursion depth of 10 reflections (Buck-Sorlin *et al.*, 2011). It was assumed that a leaf absorbs 87%, transmits 7% and reflects 6% of the incident PAR (Kahlen *et al.*, 2008). Since the ground in the greenhouse of the experiment was covered by a white film, the ground in the model

(30m x 30m), above which the virtual canopy was constructed, was assumed to absorb 20% and reflect 80% of the incident PAR.

Modelling leaf photosynthesis

Two assumptions were made for all simulations: 1) leaf temperature = 25°C and 2) constant ambient CO₂ concentration ($C_a = 380 \mu\text{mol mol}^{-1}$). To simulate the stomatal conductance to CO₂ (g_{sc} , $\text{mol m}^{-2} \text{s}^{-1}$), the model proposed by Medlyn *et al.* (2011) was used:

$$g_{sc} = g_0 + (1 + g_1/\sqrt{D}) \cdot (A/C_a) \quad \text{Eqn 2-4}$$

where D is leaf-to-air vapour pressure deficit (0.87 kPa assuming the relative humidity in the greenhouse is around 70%), parameters g_0 and g_1 are $0.009 \text{ mol m}^{-2} \text{s}^{-1}$ and 3.51 (unitless) respectively (Chen *et al.*, Leibniz Universität Hannover, unpubl. res.), and A ($\mu\text{mol CO}_2 \text{ m}^{-2} \text{s}^{-1}$) is the minimum of the Rubisco-limited (A_c , $\mu\text{mol CO}_2 \text{ m}^{-2} \text{s}^{-1}$) and RuBP-regeneration-limited (A_j , $\mu\text{mol CO}_2 \text{ m}^{-2} \text{s}^{-1}$) photosynthesis rate (Farquhar *et al.*, 1980):

$$A_c = V_{cmax} \cdot (C_c - \Gamma^*) / (C_c + K_c(1 + O/K_o)) - R_d \quad \text{Eqn 2-5a}$$

$$A_j = J \cdot (C_c - \Gamma^*) / (4C_c + 8\Gamma^*) - R_d \quad \text{Eqn 2-5b}$$

where V_{cmax} is the maximum rate of Rubisco carboxylation ($\mu\text{mol CO}_2 \text{ m}^{-2} \text{s}^{-1}$), Γ^* is the CO₂ compensation point in the absence of dark respiration (for cucumber: $43.02 \mu\text{mol mol}^{-1}$, Singaas *et al.*, 2003), K_c ($404 \mu\text{mol mol}^{-1}$) and K_o ($278 \text{ mmol mol}^{-1}$) are Michaelis-Menten constants of Rubisco for CO₂ and O₂, O ($210 \text{ mmol mol}^{-1}$) is mol fraction of O₂ at the site of carboxylation, R_d is the respiration rate ($1.08 \mu\text{mol CO}_2 \text{ m}^{-2} \text{s}^{-1}$, Chen *et al.*, Leibniz Universität Hannover, unpubl. res.). C_c (chloroplastic CO₂ concentration, $\mu\text{mol mol}^{-1}$) and J (rate of electron transport, $\mu\text{mol m}^{-2} \text{s}^{-1}$) were calculated by (Archontoulis *et al.*, 2012):

$$C_c = C_a - A(1/g_{sc} + 1/g_m) \quad \text{Eqn 2-6}$$

$$J = (K_{2LL} \cdot I_{int} + J_{max} - \sqrt{((K_{2LL} \cdot I_{int} + J_{max})^2 - 4\theta \cdot J_{max} \cdot K_{2LL} \cdot I_{int})}) / (2\theta) \quad \text{Eqn 2-7}$$

where g_m is mesophyll conductance ($\text{mol m}^{-2} \text{s}^{-1}$), I_{int} is intercepted PAR ($\mu\text{mol photons m}^{-2} \text{s}^{-1}$), J_{max} is the maximum electron transport rate ($\mu\text{mol e}^- \text{ m}^{-2} \text{s}^{-1}$), K_{2LL} is a constant

describing the conversion efficiency of I_{Int} to J ($0.425 \text{ mol e}^- \text{ mol}^{-1}$ photons, Wiechers *et al.*, 2011a) and θ is a constant convexity factor describing the response of J to I_{Int} (0.7, Wiechers *et al.*, 2011a). The dependency of V_{cmax} , J_{max} and g_{m} on leaf age is fitted to a log-normal curve (Irving and Robinson, 2006):

$$X(t) = X_{\text{max}} \cdot \exp(-0.5(\log(t/b)/c)^2) \quad \text{Eqn 2-8}$$

where X_{max} is the maximum of the variables (Table 2-2), t is leaf age (day), b is the time (8.56 day) when the X_{max} occurs, and c is curve standard deviation (0.952). These parameters for cucumber were taken from the work of Wiechers (2011). From our previous study (Chen *et al.*, Leibniz Universität Hannover, unpubl. res., see also Egea *et al.*, 2011 and Buckley *et al.*, 2013), parameters b and c for V_{cmax} , J_{max} and g_{m} were not significantly different and well correlated. Therefore, the same parameter set for these three variables was used. Finally, A_j , A_c , g_{sc} and C_c were obtained by solving Eqns 2-4, 2-5 and 2-6 analytically.

Table 2-2. Reference values of photosynthesis rate (A_j^{ref}), maximum electron transport rate ($J_{\text{max}}^{\text{ref}}$), electron transport rate at PAR = 1300 $\mu\text{mol m}^{-2} \text{ s}^{-1}$ (J_s^{ref}), stomatal ($g_{\text{sc}}^{\text{ref}}$) and mesophyll ($g_{\text{m}}^{\text{ref}}$) conductance for the quantitative limitation analysis at non-saturated light conditions

Reference	A_j^{ref}	$J_{\text{max}}^{\text{ref}}$	J_s^{ref}	$V_{\text{cmax}}^{\text{ref}}$	$g_{\text{sc}}^{\text{ref}}$	$g_{\text{m}}^{\text{ref}}$
	$\mu\text{mol m}^{-2} \text{ s}^{-1}$				$\text{mol m}^{-2} \text{ s}^{-1}$	
Value	26.7 ¹	191.1	168.8	140.7	0.37	1.67

¹ A_j^{ref} is calculated by Eqn 2-13.

Evaluation of the photosynthesis model

To evaluate the photosynthesis model, leaf gas exchange measurements were conducted in a greenhouse experiment in 2013. Cucumber seedlings at the three-leaf stage were transplanted into the greenhouses of the Institute of Horticultural Production Systems, Leibniz Universität Hannover, Germany (lat. 52°23'N, long. 9°37'E) on 20 Mar. 2013. In our model, leaf 21 was 8 days past leaf appearance ($\approx 5\text{cm}$ in leaf length). In the experiment, leaf 21 appeared on 17 Apr., and photosynthesis was measured on 24 Apr. 2013. The experimental setup was similar to the experiment described by Kahlen and Stützel (2007). Root mean squared deviation of photosynthesis rate ($\mu\text{mol m}^{-2} \text{ s}^{-1}$) and accuracy (%) were calculated according to Kahlen and Stützel (2011).

Leaves on ten ranks (1, 3, 5, 7, 9, 11, 14, 17, 19 and 21) were measured using a portable gas exchange system (Li-6400; Licor, Lincoln, NE, USA) at $C_a = 380 \mu\text{mol mol}^{-1}$, leaf temperature = 25°C and 70% relative humidity, corresponding to the model conditions.

Four leaves per rank were measured at the corresponding light conditions simulated in the model. For example, when the PAR above the canopy in the model was 100, 500, 900 and 1300 $\mu\text{mol photons m}^{-2} \text{s}^{-1}$, leaf 5 absorbed on average 27, 133, 247 and 346 $\mu\text{mol photons m}^{-2} \text{s}^{-1}$, respectively. Therefore, leaf 5 in the experiment was measured at 27, 133, 247 and 346 $\mu\text{mol photon m}^{-2} \text{s}^{-1}$ (the input PAR in the Li-6400 chamber was 1.15 times of these values, corresponding to 87% leaf absorbance). All measurements were done between 0900 h and 1400 h.

Quantitative limitation analyses

To test if photosynthesis rate is limited by Rubisco-carboxylation rate or by RuBP-regeneration rate, C_c and the intersection point of the FvCB model (C_{ctr} , Dubois *et al.*, 2007) were compared:

$$C_{\text{ctr}} = (K_c \cdot J \cdot (K_o + O) - 8K_o \cdot \Gamma^* \cdot V_{\text{cmax}}) / (K_o \cdot (4V_{\text{cmax}} - J)) \quad \text{Eqn 2-9}$$

When $C_c < C_{\text{ctr}}$, photosynthesis is Rubisco-limited. In this case, quantitative limitation analysis for saturating light condition, proposed by Grassi and Magnani (2005), was used. When $C_c > C_{\text{ctr}}$, photosynthesis is limited by the RuBP-regeneration rate and the quantitative limitation analysis for non-saturating light condition (Chen *et al.*, 2013, see Supplementary data S1) was used. According to the quantitative limitation analysis for non-saturating light conditions, the relative change of photosynthesis can be described as:

$$dA_j/A_j = S_L + M_L + B_L + L_L = A_L = l_s \cdot dg_{\text{sc}}/g_{\text{sc}} + l_{\text{mc}} \cdot dg_{\text{m}}/g_{\text{m}} + l_j \cdot J_{\text{dB}}/J + l_j \cdot J_{\text{dl}}/J \quad \text{Eqn 2-10}$$

$$l_s = ((g_{\text{tot}}/g_{\text{sc}}) \cdot (\partial A_j / \partial C_c)) / (g_{\text{tot}} + \partial A_j / \partial C_c) \quad \text{Eqn 2-11a}$$

$$l_{\text{mc}} = ((g_{\text{tot}}/g_{\text{m}}) \cdot (\partial A_j / \partial C_c)) / (g_{\text{tot}} + \partial A_j / \partial C_c) \quad \text{Eqn 2-11b}$$

$$l_j = g_{\text{tot}} / (g_{\text{tot}} + \partial A_j / \partial C_c) \quad \text{Eqn 2-11c}$$

$$\partial A_j / \partial C_c = 12J \cdot \Gamma^* / (4C_c + 8\Gamma^*)^2 \quad \text{Eqn 2-11d}$$

where S_L , M_L , B_L and L_L are the contributions of stomatal conductance, mesophyll conductance, biochemical capacity and light to photosynthetic limitation, A_L is the total limitation, l_s , l_{mc} and l_j are the *relative* limitations of stomatal and mesophyll conductance and of electron transport rate, J_{dB} and J_{dl} are the changes of electron transport rate due to

biochemical capacity and irradiance, respectively, and dA_j/A_j , dg_{sc}/g_{sc} , dg_m/g_m , J_{dB}/J and J_{dl}/J are approximated by:

$$dA_j/A_j \approx (A_j^{\text{ref}} - A_j)/A_j^{\text{ref}} \quad \text{Eqn 2-12a}$$

$$dg_{sc}/g_{sc} \approx (g_{sc}^{\text{ref}} - g_{sc})/g_{sc}^{\text{ref}} \quad \text{Eqn 2-12b}$$

$$dg_m/g_m \approx (g_m^{\text{ref}} - g_m)/g_m^{\text{ref}} \quad \text{Eqn 2-12c}$$

$$J_{dB}/J \approx (J_s^{\text{ref}} - J_s)/J_s^{\text{ref}} \quad \text{Eqn 2-12d}$$

$$J_{dl}/J \approx (J_s - J)/J_s^{\text{ref}} \quad \text{Eqn 2-12e}$$

where g_{sc}^{ref} and g_m^{ref} are the reference values of stomatal and mesophyll conductance, J_s is the electron transport rate at saturating light condition (PAR = 1300 $\mu\text{mol m}^{-2}\text{s}^{-1}$, achieve >95% of photosynthesis rate for cucumber), J_s^{ref} is the electron transport rate with maximum J_{max} (with highest biochemical capacity, Eqn 2-7) at saturating light condition and A_j^{ref} is calculated by solving the following function:

$$A_j^{\text{ref}} = J_s^{\text{ref}} \cdot (C_a - A_j^{\text{ref}} \cdot (1/g_{sc}^{\text{ref}} + 1/g_m^{\text{ref}}) - \Gamma^*) / (4(C_a - A_j^{\text{ref}} \cdot (1/g_{sc}^{\text{ref}} + 1/g_m^{\text{ref}})) + 8\Gamma^*) - R_d \quad \text{Eqn 2-13}$$

Reference values are listed in Table 2-2. Furthermore, sensitivity of stomatal limitation to model parameters, g_1 and D (in Eqn 2-4) was tested. These parameters were chosen because their changes have no influence on the reference photosynthesis rate (A_j^{ref} in Eqn 2-13). Simulations for sensitivity analyses were run for leaves intercepting 700 $\mu\text{mol m}^{-2}\text{s}^{-1}$ PAR, on days 15, 25 and 35 after leaf appearance.

Simulation and statistical analysis

To investigate the compositions of photosynthetic limitations at the leaf level, PAR above the virtual canopy was assumed to be 100, 500, 900 and 1300 $\mu\text{mol photon m}^{-2} \text{s}^{-1}$, consisting of 79% direct and 21% diffuse light. These four scenarios were also used to upscale the photosynthetic limitations from leaf to the canopy layers and to the whole plant by using Eqn 2-2 and 2-3. Canopy light interception (I_C , $\mu\text{mol photon canopy layer}^{-1} \text{s}^{-1}$), canopy photosynthesis (A_C , $\mu\text{mol CO}_2 \text{ canopy layer}^{-1} \text{s}^{-1}$) and canopy light use efficiency (LUE_C , $\mu\text{mol CO}_2 \mu\text{mol}^{-1} \text{ photon}$) were calculated by:

$$I_C = \sum_{k=1}^n (I_C \cdot LA_k) \quad \text{Eqn 2-14a}$$

$$A_C = \sum_{k=1}^n (A \cdot LA_k) \quad \text{Eqn 2-14b}$$

$$LUE_C = A_C / I_C \quad \text{Eqn 2-14c}$$

To investigate the relationship between I_C , A_C and LUE_C , a wide range of PAR above the virtual canopy was simulated (between 100 and 1500 $\mu\text{mol photon m}^{-2} \text{s}^{-1}$). For the analysis of the influence of diffuse light on canopy photosynthesis, PAR above the virtual canopy was assumed to be 1000 $\mu\text{mol photons m}^{-2} \text{s}^{-1}$ and the diffuse light consisted of 0 and 100% of the total light.

Only the simulated results from the two plants in the center of the middle row (Fig. 2-1a) were taken for statistical analysis. To avoid model artefacts, simulations for each scenario were repeated 10 times, each run with a slight difference in orientation ($\pm 30^\circ$) of the tested plants in the virtual canopy. Averages, standard errors and regression analyses were calculated in *R* (v.2.12.0; R Foundation for Statistical Computing).

Results

Influence of light regimes on light interception

Simulated PAR interception at the leaf level with different PAR above the canopy is shown in Fig. 2-2a. For the leaves on the top and at the bottom of the canopy, values of PAR interception ($\mu\text{mol m}^{-2} \text{leaf area s}^{-1}$) were about 97% and 21% of the PAR values above the canopy ($\mu\text{mol m}^{-2} \text{ground area s}^{-1}$), respectively.

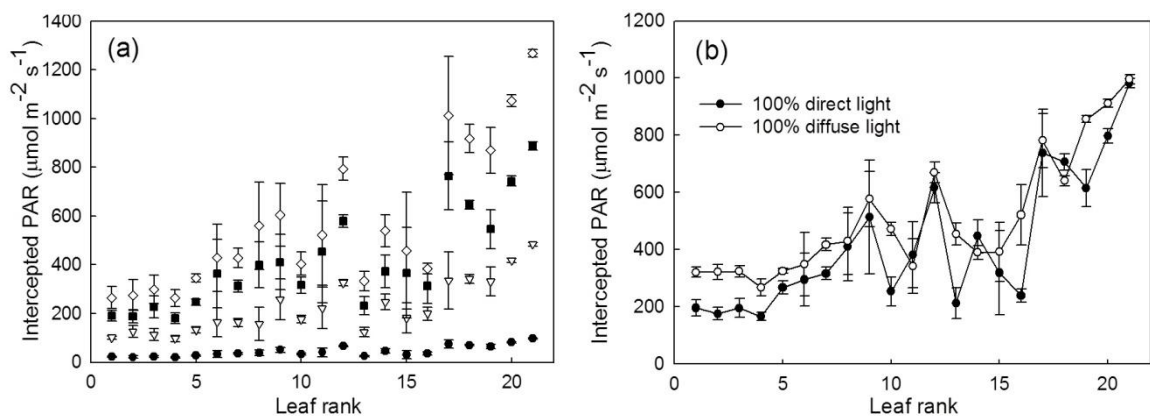


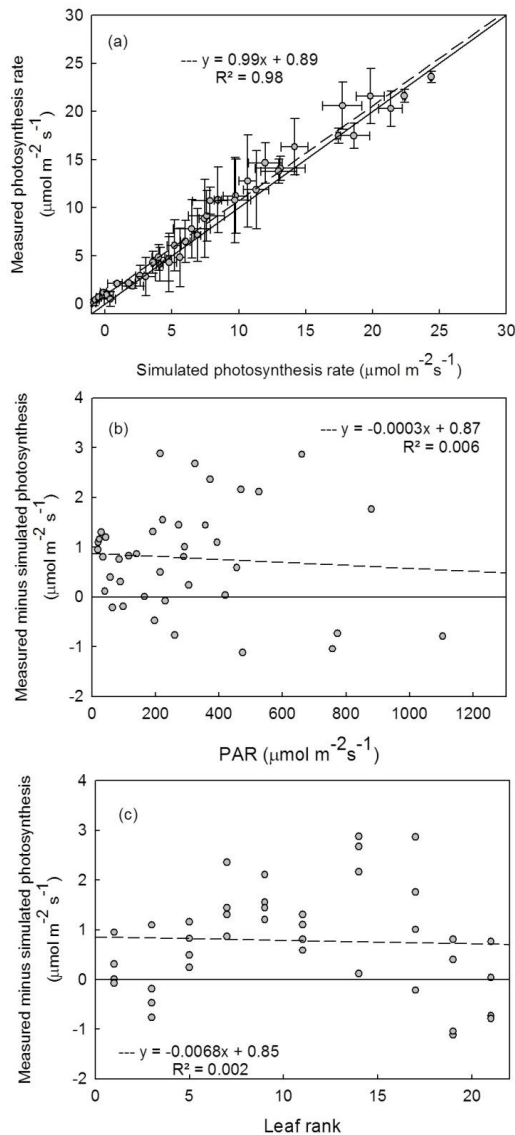
Fig. 2-2. Simulated intercepted PAR of leaves on all ranks with sun position in Hannover, Germany, lat. $52^\circ 23' \text{N}$, long. $9^\circ 37' \text{E}$, on 1 July at 1200h. (a) Light interception of leaves at four light conditions (PAR above the canopy = 100 (closed circle), 500 (open triangle down), 900 (closed square) and 1300 (open diamond) $\mu\text{mol photon m}^{-2} \text{s}^{-1}$, 79% direct light and 21% diffuse light. (b) Light interception of leaves under 100% direct light or 100% diffuse light. PAR above the canopy was assumed to be 1000 $\mu\text{mol photon m}^{-2} \text{s}^{-1}$. Means of 10 simulations with slightly rotated ($\leq \pm 30^\circ$) plants, bars represent standard deviation.

The lower, middle-lower, middle upper and upper canopy received 14, 30, 25 and 31%, respectively, of the light intercepted by the whole canopy.

Under 100% diffuse light, most of the leaves in the canopy intercepted more PAR than under 100% direct light, especially the leaves in the lower canopy (Fig. 2-2b). The increase of light interception was most prominent at leaf ranks 10, 13 and 16 (86, 114 and 118%, respectively).

Evaluation of the photosynthesis model

A clear linear relationship was found between measured and simulated photosynthesis rates (Fig. 2-3a, $R^2 = 0.98$, $p < 0.001$). The 95% confidence intervals of the slope and the intercept were 0.94-1.04 and 0.37-1.42. Root mean squared deviation was $1.30 \mu\text{mol m}^{-2} \text{s}^{-1}$ and accuracy was 86%. The model slightly underestimated the photosynthesis rate. No relationships between model errors and PAR (Fig. 2-3b) or leaf rank (Fig. 2-3c) were found.



s^{-1} and accuracy was 86%. The model slightly underestimated the photosynthesis rate. No relationships between model errors and PAR (Fig. 2-3b) or leaf rank (Fig. 2-3c) were found. Furthermore, in all simulations photosynthesis was limited by RuBP regeneration rate ($C_c > C_{\text{ctr}}$, Fig. 2-S2). Therefore, only the quantitative limitation analysis for non-saturating light conditions was used for calculating the photosynthetic limitations in this study.

Fig. 2-3. Evaluation of the photosynthesis model. (a) Simulated and measured photosynthesis; each point represents mean values of simulated and measured photosynthesis rates (for measurement and simulation, $n = 4$ and 10 , respectively) Bars represent standard deviations. (b) Difference between measured and simulated data at different PAR levels ($R^2 = 0.006$, $p = 0.50$, 95% confidence intervals of the slope and the intercept were -0.002-0.001 and 0.39-1.43). (c) Difference between measured and simulated data at different leaf ranks ($R^2 = 0.002$, $p = 0.79$, 95% confidence intervals of the slope and the intercept were -0.06-0.05 and 0.20-1.50). The solid line is 1:1 line in (a), and $y = 0$ in (b) and (c). The dashed lines are the regression lines.

Photosynthetic limitations at single leaf level

The compositions of photosynthetic limitations changed strongly with the light condition above the canopy and with canopy depth (Fig. 2-4). In general, stomatal limitations (S_L) decreased photosynthesis of the leaves in the upper canopy by 2-4% and this reduction increased with leaf age to 8% (Fig. 2-4a). Furthermore, S_L decreased when light interception increased. The maximal mesophyll limitation (M_L) was about 3% (Fig. 2-4b). In contrast to S_L , M_L increased with the light above the canopy. Diffusional limitations of photosynthesis ($D_L = S_L + M_L$) were stronger in the lower than in the upper canopy (Fig. 2-4c). Biochemical limitations (B_L) increased with canopy depth (Fig. 2-4d) and restricted photosynthesis of the lowest leaves by more than 60%. Interestingly, although the leaves in the lower canopy received less light than those located in the upper canopy (Fig. 2-2a), photosynthesis of lower leaves was less restricted by light (Fig. 2-4e). Reduction of the light above the canopy increased the light limitation (L_L) of all leaves, especially of the upper ones. Total limitation (A_L) reduced with leaf rank and light (Fig. 2-4f). In all cases, B_L and L_L were the most prominent components (80-93%) in A_L .

An increase in water vapour deficit enhanced S_L (Fig. 2-5a), whereas an increase of g_1 reduced S_L (Fig. 2-5b). Changes in water vapour deficit and g_1 influenced S_L by up to 12% and 8% of the reference photosynthesis rate, respectively. S_L in upper leaves was as sensitive as it was in lower leaves to g_1 and to water vapour deficit. Intercepted light had negligible effects on the sensitivity of S_L to water vapour deficit (data not shown). Furthermore, these two parameters had very small effects on M_L , B_L and L_L (less than 1%).

Photosynthetic limitations on different canopy layers and whole plant

Table 2-3 shows photosynthesis and the compositions of photosynthetic limitations on different canopy layers and the whole plant. Stomatal limitation contributed about 10% of the total limitation. This contribution was stronger in young canopies and at high light conditions than in old canopies and at low light conditions. The middle-lower canopy contributed more than one third to the whole plant stomatal limitation. Mesophyll limitations contributed less than 4% of the total limitation on the different canopy layers and the whole plant. Light conditions above the canopy had little effect on biochemical limitations. Both, middle-lower and lower canopy contributed about 40% of the biochemical limitation to the whole plant. Light limitations in all parts of the canopy were decreased when PAR above the canopy increased, especially in the upper canopy. At the

whole plant level, about 30% of the light limitation occurred in the upper and middle-upper part of the canopy (Table 2-3). Independent of the PAR above the canopy, the total limitation in the different parts of the canopy ranged middle-lower > lower > middle-upper > upper. The upper canopy made the highest contribution to the whole plant photosynthesis (over 30% of whole plant photosynthesis), but both, middle-upper and middle-lower canopy also assimilated more than 25% of the whole plant photosynthetic products.

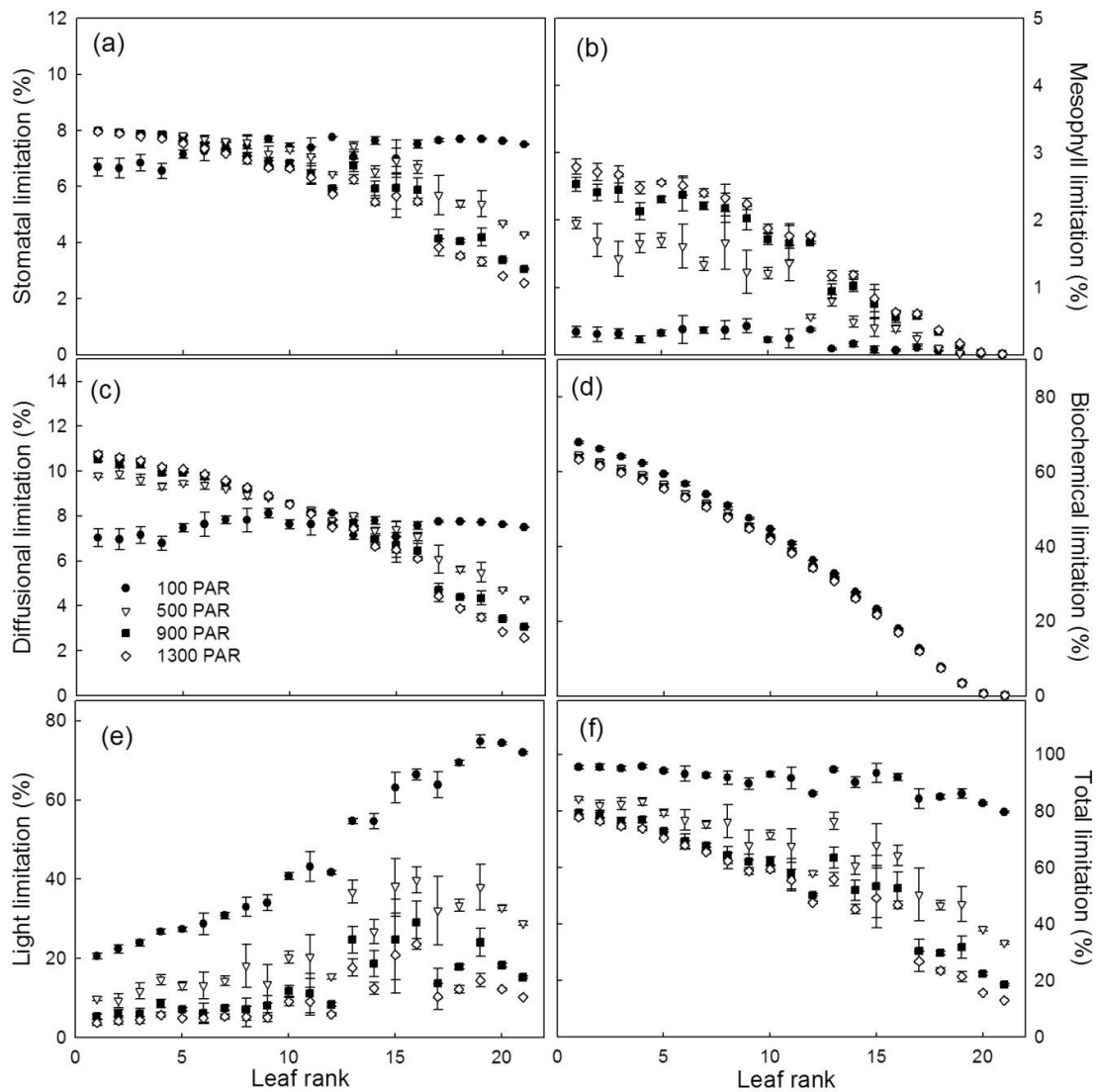


Fig. 2-4. Changes of (a) stomatal, (b) mesophyll, (c) diffusional (stomatal + mesophyll), (d) biochemical, (e) light and (f) total (diffusional + biochemical + light) limitation with leaf rank and light conditions above the canopy (100, 500, 900 and 1300 $\mu\text{mol photon m}^{-2} \text{s}^{-1}$). Symbols are described in Fig. 2-2a ($n = 10$).

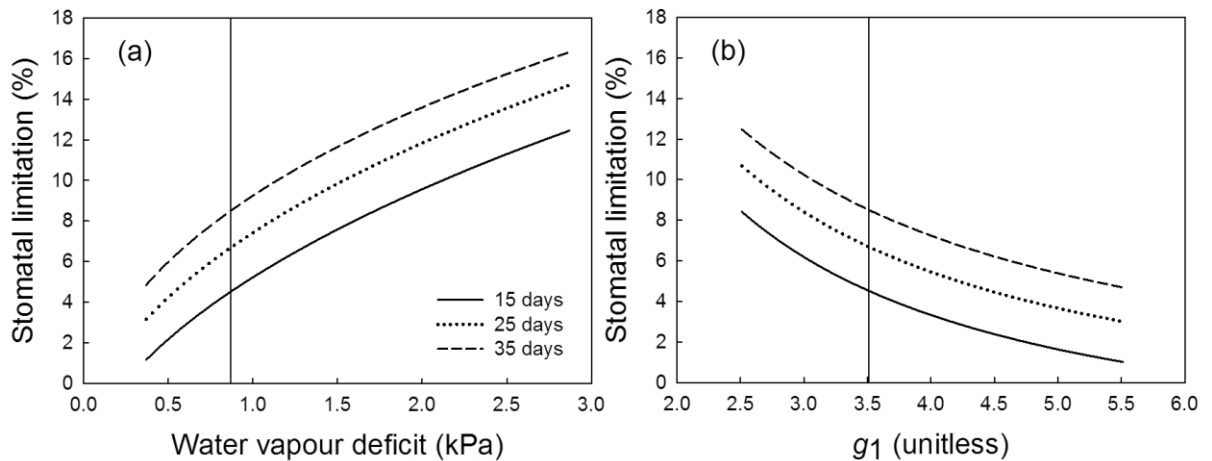


Fig. 2-5. Sensitivity of stomatal limitation to (a) water vapour deficit and (b) parameter g_1 (in Eqn 2-4). Simulations were run for leaves on days 15 (solid line), 25 (dotted line) and 35 (dashed line) after leaf appearance. The vertical solid lines indicate the default parameter values used for analysing the canopy photosynthetic limitation.

Table 2-3. Canopy layers and whole plant photosynthesis and compositions of photosynthetic limitations at four PAR levels above the canopy. S_{Lp} , M_{Lp} , B_{Lp} , and L_{Lp} are stomatal, mesophyll, biochemical, and light limitation, respectively. Leaf area of different canopy layers is shown in Table 2-1.

Canopy part	PAR	Photosynthesis	S_{Lp}	M_{Lp}	B_{Lp}	L_{Lp}
	($\mu\text{mol m}^{-2} \text{s}^{-1}$)	($\mu\text{mol CO}_2 \text{ plant}^{-1} \text{s}^{-1}$)	($\mu\text{mol CO}_2 \text{ plant}^{-1} \text{s}^{-1}$)			
upper	100	0.98	0.56	0.00	0.60	5.08
	500	4.14	0.40	0.01	0.57	2.52
	900	5.48	0.31	0.02	0.57	1.46
	1300	6.01	0.27	0.03	0.56	1.04
middle-upper	100	0.61	0.66	0.02	2.93	4.54
	500	3.21	0.62	0.07	2.81	2.40
	900	4.33	0.56	0.11	2.77	1.51
	1300	4.79	0.53	0.12	2.75	1.15
middle-lower	100	0.72	0.95	0.05	6.53	4.25
	500	3.44	0.96	0.18	6.26	2.03
	900	4.70	0.91	0.27	6.15	1.03
	1300	5.05	0.89	0.29	6.12	0.75
lower	100	0.20	0.66	0.03	6.15	2.39
	500	1.68	0.77	0.16	5.86	1.16
	900	2.31	0.76	0.23	5.77	0.66
	1300	2.57	0.75	0.26	5.73	0.46
whole plant	100	2.51	2.83	0.10	16.21	16.26
	500	12.47	2.75	0.42	15.50	8.11
	900	16.82	2.54	0.63	15.26	4.66
	1300	18.42	2.44	0.70	15.16	3.40

Canopy light interception, photosynthesis rate, and light use efficiency

Responses of canopy photosynthesis (A_C , $\mu\text{mol CO}_2 \text{ plant}^{-1} \text{ s}^{-1}$) and light use efficiency (LUE_C , $\mu\text{mol CO}_2 \mu\text{mol}^{-1} \text{ photon}$) to incident light (I_C , $\mu\text{mol photon plant}^{-1} \text{ s}^{-1}$) on different canopy layers were essentially different from those at the whole plant level (Fig. 2-6). The maximum A_C and LUE_C occurred at the upper canopy and decreased with canopy depth (Table 2-4).

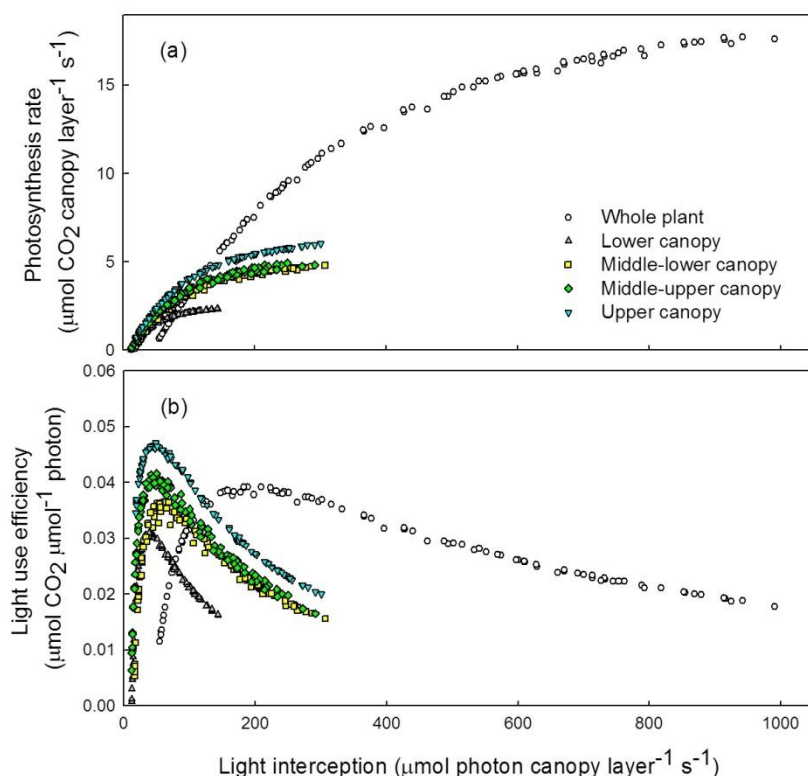


Fig. 2-6. Dependence of (a) canopy photosynthesis rate and (b) light use efficiency on light interception of different canopy layers.

Table 2-4. Values of parameters for the dependence of canopy photosynthesis (A_C , $\mu\text{mol CO}_2 \text{ plant}^{-1} \text{ s}^{-1}$) and light use efficiency (LUE_C , $\mu\text{mol CO}_2 \mu\text{mol}^{-1} \text{ photon}$) on light interception (I_C , $\mu\text{mol photon plant}^{-1} \text{ s}^{-1}$) at different canopy layers and whole plant level

	Canopy part				
	upper	middle-upper	middle-lower	lower	whole plant
Maximum A_C	6.02	4.93	4.78	2.33	17.74
I_C for reaching 95% A_C	235	200	230	113	753
Maximum LUE_C	0.046	0.041	0.035	0.031	0.39
I_C for maximum LUE_C	48.3	55.3	70.2	46.0	224.3

Influence of diffuse light on canopy photosynthesis

Under 100% diffuse light leaves in the lower canopy intercepted more PAR than under 100% direct light. This increase in light interception only resulted in an about 20% increase of leaf photosynthesis (Fig. 2-7). Interestingly, diffuse light had most significant effects on the leaves at the ranks 10, 13 and 16. Under 100% diffuse light these leaves intercepted 86, 113 and 117%, respectively, more light than under 100% direct light (Fig. 2-2b), and their photosynthesis increased 28, 54 and 55%, respectively (Fig. 2-7). These leaves made the biggest contribution to the increase of canopy photosynthesis under 100% diffuse light.

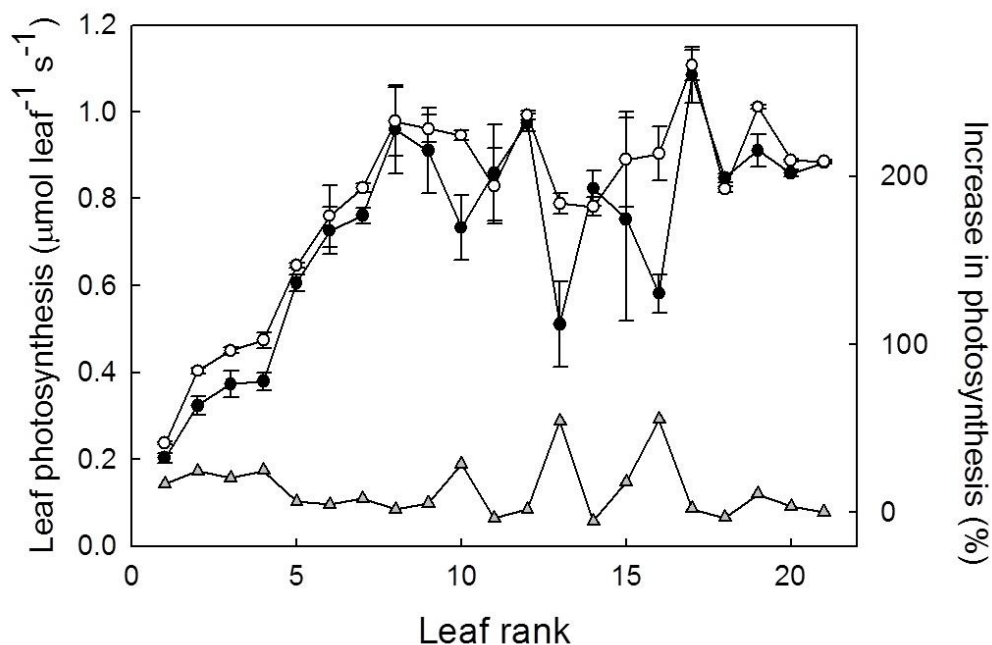


Fig. 2-7. Simulated leaf photosynthesis rate under 100% direct light (closed circle) and 100% diffuse light (open circle, $n = 10$). PAR above the canopy was assumed to be $1000 \mu\text{mol m}^{-2} \text{s}^{-1}$. The grey triangles indicate the increases in photosynthesis under 100% diffuse light condition (% of value at 100% direct light).

Discussion

The quantitative limitation analysis is a useful tool to disentangle the contributions of different physiological and environmental factors to photosynthetic limitations. However, it requires complicated calculations. To aid other researchers in conducting this analysis, we provide a Microsoft Excel file for this calculation online:

<http://aob.oxfordjournals.org/content/114/4/677/suppl/DC1>

This is the first approach to quantify the components of photosynthetic limitations of different canopy layers and the whole plant. Methodological considerations of quantitative limitation analysis have been sufficiently discussed in previous papers (Grassi and Magnani, 2005; Grassi *et al.*, 2009). To our knowledge, it is not possible to experimentally validate our approach because photosynthetic limitations cannot be measured directly. Therefore, we took a step back and evaluated our model for photosynthesis. The slight underestimation of photosynthesis rates in our model (about 0.5-1.0 $\mu\text{mol m}^{-2} \text{s}^{-1}$, i.e. 2-4% of reference photosynthesis rate, Fig. 2-3, Table 2-2) may result in small overestimations of photosynthetic limitations. One reason for this slight inaccuracy could be that R_d in our photosynthetic model was constant. In many modelling works, R_d is scaled with V_{cmax} (e.g. Buckley *et al.* 2013; Cano *et al.* 2013), which is a function of leaf age (Eqn 2-8). Implementing the dependency of R_d on leaf age in the photosynthetic model may reduce the underestimation of the simulated photosynthesis in the middle and lower canopy (Fig. 2-3c). However, quantitative limitation analysis for the RuBP-regeneration-limited phase of photosynthesis may underestimate the total limitation by 0.5-3% (Chen *et al.*, Leibniz Universität Hannover, unpubl. res.). This indicates that the errors from the photosynthesis model could be counterbalanced, but not amplified by the quantitative limitation analysis. Furthermore, fruit and stem structures, which may contribute to the whole plant carbon assimilation (Ashan and Pfanz, 2003), were not included in the architectural model. Due to this simplification, the whole plant photosynthesis might be slightly overestimated because more light may reach the leaves. However, the absence of non-foliar carbon assimilation in the model would counterbalance this effect.

In this work, we combined a light model, a static structural model of a cucumber canopy, a FvCB photosynthesis model and the quantitative limitation analysis of photosynthesis to examine the following questions:

What is the most prominent factor limiting greenhouse cucumber leaf and canopy photosynthesis?

The most prominent factors limiting cucumber photosynthesis were B_L and L_L and they changed strongly with leaf rank. It seems to be contradictive that the leaves in the upper canopy received the highest light intensities (Fig. 2-2a) but their photosynthesis could be more restricted by light (Fig. 2-4e) than those in the lower canopy. This can be explained by the fact that the electron transport rate (J in Eqn 2-7), which is determined by the biochemical capacity (J_{max}) and light interception (I_{Int}), of the older leaves is mainly

reduced by low J_{\max} . Therefore, an increase in I_{int} of the leaves below rank 10 may only increase their photosynthesis rate by up to 20% of the reference.

Here we found that diffusional resistances had less importance in limiting photosynthesis (8-14% of total limitation, Table 2-3) than biochemical capacity and light interception under non-stressed conditions. In the model used here, parameter g_1 was assumed to be constant but in reality it could decrease with the leaf age. According to Eqn 2-4, a reduction in g_1 results in a lower g_{sc} and an increased S_L (Fig. 2-5b). This indicates that S_L could be higher than our estimates in the lower canopy and lower in the upper canopy. In all our simulations, M_L comprised less than 4% of the total limitation. This results conflicts with the recently prevailing opinion that g_m would be the target for increasing photosynthesis and water use efficiency (Flexas *et al.*, 2013). This contradiction may be the consequence of the following reasons: 1) in our study plants were assumed to grow under non-stressed conditions, comparable, e.g., with M_L of 5% estimated in non-stressed grape (Flexas *et al.*, 2009); 2) cucumber has a relatively high g_m in comparison with other plant species (Loreto *et al.*, 1992); and 3) all leaves in our simulations were in RuBP-regeneration-limited phase of photosynthesis (Fig. 2-S2). In this phase, increasing C_c is less effective on enhancing net photosynthesis rate than in Rubisco-carboxylation-limited phase because the slope of A_j - C_c function at $C_c > C_{\text{ctr}}$ is, in general, lower than the slope of A_c - C_c function at $C_c < C_{\text{ctr}}$.

Sensitivity analysis showed that young and old leaves had a similar sensitivity of S_L to water vapour deficit (Fig. 2-5a). This indicates that changes in water vapour deficit may affect whole plant photosynthesis by up to 10%.

Do the compositions of photosynthetic limitations vary between different canopy layers?

Our results showed strong variations in the compositions of photosynthetic limitations between different canopy layers and between different light regimes. The upper canopy, where the young leaves were located (Table 2-1), had the smallest B_L and S_L (Fig. 2-4a and 4d). This is the reason why the upper canopy had the highest maximum LUE_C (Table 2-4). Our simulations, showing that M_L increased with canopy depth, are in accordance with the results of a recent publication by Cano *et al.* (2013), who suggested that in beech and sessile oak M_L in the lower canopy is twice as high as in the upper canopy.

How to improve cucumber canopy photosynthesis?

Based on analyzing the virtual canopy, we suggest three possibilities to improve canopy photosynthesis in a high-wire cucumber cropping system: Firstly, an increase in leaf size of the upper canopy could improve whole plant photosynthesis. The upper canopy had lower B_L and higher LUE_C (Fig. 2-6) than other canopy layers, but a small photosynthetic apparatus (leaf area, Table 2-1). Thus, it would be very interesting to investigate the factors limiting the final leaf size of the upper canopy. Possible causes might be the competition between vegetative and generative growth (Wiechers *et al.*, 2011a). However, an increase in leaf size of the upper canopy could shade the lower canopy layers and increase their light limitation. Thus, it is worth to use dynamic structural models to find out the optimal leaf area profile (see also Kahlen and Stützel, 2011). Using a Y-shape training system, instead of a single-stem system, might be a possibility to increase the leaf area of the upper canopy. Secondly, improving light interception of the middle-lower and middle-upper canopy layers would be also of importance for increasing whole plant photosynthesis, because L_L may contribute up to 55% of the total limitation of these canopy layers (Table 2-3). This could explain why inter-lighting seems to be more efficient than top-lighting in such a production system (Hovi *et al.*, 2004; Hovi-Pekkanen and Tahvonen, 2008; de Visser *et al.*, 2014). Finally, maintaining the biochemical capacity of the middle-lower canopy layer would be of special importance for increasing whole plant photosynthesis. It is often observed that the final size of an individual leaf in the single-stem high-wire cropping system reaches its maximum at rank 6-10 and then decreases with leaf rank (see also Table 2-1). Therefore, the middle-lower canopy in this system has the largest photosynthetic apparatus. Using genotypes with a higher value of parameter c (in Eqn 2-8) may reduce B_L in the middle-lower and lower canopy because this parameter has strong influence on the shape of the B_L -profile (Fig. 2-4d). A recent study has revealed that this parameter varies two fold between different genotypes (Khaembah *et al.*, 2013). Using inter-lighting would be another method to maintain the photosynthetic capacity of the middle canopy as leaves acclimatizing a to better light environment may maintain their photosynthetic capacity (Trouwborst *et al.*, 2011).

Perspectives and limitations of combining FSPM and quantitative limitation analysis

We would like to stress that our results may not be generalized to all plant species, although we suppose that similar results may be obtained by analysing other greenhouse crops (*e.g.* melon, tomato, pepper and aubergine). However, our approach, combining FSPM and quantitative limitation analyses (for both saturating and non-saturating light conditions), can be applied to all plant species and we merely use cucumber as a model plant to demonstrate this approach. It will be fruitful to apply this analysis to investigate other plant species and the influence of horticultural practices on canopy photosynthesis or to search the optimal cropping systems for yield maximization, *e.g.* row distance, plant density and training system. Another question might be the necessity of supplemental lighting and the efficiency of its energy use. Furthermore, implementing the physiological responses to temperature would aid in revealing the importance of temperature to canopy photosynthesis. It is very likely that temperature is the key factor determining whether photosynthesis is at Rubisco-limited or RuBP-limited phase in the FvCB model (von Caemmerer, 2013). Carmo-Silva and Salvucci (2012) also showed that temperature strongly affects the position of the transition point (C_{ctr}) in the FvCB model. However, temperature changes the reference photosynthesis rate and this makes the comparison difficult. It would be interesting to implement stress responses of g_{sc} and g_{m} into the model to investigate the changes in D_{L} on the canopy level under stress. In general, g_{sc} and g_{m} decrease under stress conditions. These decreases may result in 1) increase in D_{L} , 2) decrease in C_{c} and 3) higher leaf temperature due to a lower g_{sc} and transpiration. Since photosynthesis tends to be Rubisco-limited at low C_{c} and high temperature and D_{L} is more prominent at Rubisco-limited phase (see above), D_{L} would be significantly higher under stress conditions.

Moreover, implementing this analysis in a dynamic structural model (Wiechers *et al.*, 2011a; Kahlen and Stützel, 2011) would enable us to explore the effect of developmental stage on photosynthetic limitations at canopy level.

How does diffuse light improve the leaf and canopy photosynthesis?

Our findings suggest that the increase in whole plant photosynthesis under diffuse light is not the result of a higher *LUE* (with respect to leaf area) but a higher light interception per plant or unit ground area. Indeed, leaves use direct light more efficiently than diffuse light (Brodersen *et al.*, 2008; Brodersen and Vogelmann, 2010) and this was not taken into account in our model. Diffuse light might increase canopy photosynthesis by improving

light interception of leaves directly shaded by leaves above them in the canopy. This might explain that the effects of diffuse light were most significant on leaves (Fig. 2-2b, Fig. 2-7), which were directly shaded by the leaves above them in the virtual canopy (Fig. 2-S3). Furthermore, leaves in the lower canopy may acclimatize to the light environment under diffuse light and maintain their photosynthetic capacity (Trouwborst *et al.*, 2011). Therefore, we speculate that the long-term effect of diffuse light could reduce B_L in the lower and middle-lower canopy.

Conclusion

Our novel model approach, combining an FSPM with quantitative limitation analysis of photosynthesis, allows us to quantify the different photosynthetic limitations at the leaf level and to upscale them to the canopy level. Under non-stressed conditions, the biochemical capacity is the most prominent limitation in the lower canopy, whereas light interception is the most important factor limiting photosynthesis in the upper canopy whereas diffusional limitations contribute less to total limitation. Methods for maintaining the biochemical capacity of the middle-lower canopy and optimizing the vertical leaf area profile would be promising strategies to improve canopy photosynthesis. Further analyses using our model approach would provide insights into the influence of horticultural practices on canopy photosynthesis and the design of optimal cropping systems.

Chapter 3

Disentangling the contributions of osmotic and ionic effects of salinity on stomatal, mesophyll, biochemical and light limitations to photosynthesis

Tsu-Wei Chen¹, Katrin Kahlen², Hartmut Stützel¹

¹*Institute of Horticultural Production Systems, Leibniz Universität Hannover, Herrenhäuser Straße 2, 30419 Hannover, Germany* ²*Department of Vegetable Crops, Geisenheim University, Von-Lade-Straße 1, 65366 Geisenheim, Germany*

Published in: *Plant, Cell & Environment* (2015), DOI: 10.1111/pce.12504

Abstract

There are conflicting opinions on the relative importance of photosynthetic limitations under salinity. Quantitative limitation analysis of photosynthesis provides insight into the contributions of different photosynthetic limitations, but it has only been applied under saturating light conditions. Using experimental data and modeling approaches, we examined the influence of light intensity on photosynthetic limitations and quantified the osmotic and ionic effects of salinity on stomatal (L_S), mesophyll (L_M), biochemical (L_B) and light (L_L) limitations in cucumber (*Cucumis sativus* L.) under different light intensities. Non-linear dependencies of L_S , L_M and L_L to light intensity were found. Osmotic effects on L_S and L_M increased with the salt concentration in the nutrient solution (S_s) and the magnitude of L_M depended on light intensity. L_S increased with the Na^+ concentration in the leaf water (S_l) and its magnitude depended on S_s . Biochemical capacity declined linearly with S_l but, surprisingly, the relationship between L_B and S_l was influenced by S_s . Our results suggest that 1) improvement of stomatal regulation under ionic stress would be the most effective way to alleviate salinity stress in cucumber, and 2) osmotic stress may alleviate the ionic effects on L_B but aggravate the ionic effects on L_S .

Key words: *Cucumis sativus*, quantitative limitation analysis, salinity, osmotic stress, ionic stress, FvCB model, light condition

Introduction

Salinity reduces crop production in agriculture worldwide (Munns and Tester 2008). The effects of salinity on plant growth and photosynthesis are often viewed in two time-related phases: osmotic and ionic (Munns, 1993; Munns and Tester 2008; Harris *et al.*, 2010). The first phase is due to the reduction of the osmotic potential of the soil/nutrient solution which reduces leaf expansion and stomatal conductance (g_s) immediately (Maggio *et al.*, 2007; Shapira *et al.*, 2009). These have been referred to as the “osmotic effects” of salinity (Munns and Tester 2008). The second phase is due to the uptake and the accumulation of sodium and chloride in the cells of photosynthetic tissues which cause the “ionic effects” under salinity (Munns and Tester 2008; Harris *et al.*, 2010). These decrease biochemical capacity of leaves and disturb the stomatal regulation (James *et al.*, 2002; James *et al.*, 2006; Tavakkoli *et al.*, 2010; Tavakkoli *et al.*, 2011). Because of the complex responses of plants to salinity, it is still controversial whether the osmotic or the ionic components of salinity should be considered the primary limitation of photosynthesis (Flexas *et al.*, 2004; Chaves *et al.*, 2009).

For decades plant physiologists have made efforts to identify and quantify the limiting factors of photosynthesis (Jones 1985). Several approaches, such as resistance analysis, elimination methods and quantitative limitation analysis (Jones 1985; Wilson *et al.*, 2000; Grassi and Magnani 2005; Grassi *et al.*, 2009), have been proposed to partition and quantify diffusional (stomatal and mesophyll resistance to CO_2) and non-diffusional (biochemical and temperature) limitations to photosynthesis. In resistance analysis, photosynthetic limitations due to stomata and mesophyll are calculated by dividing their resistances to CO_2 by the total resistances to CO_2 . However, resistance analysis is not applicable where the relationship between photosynthesis and CO_2 concentration is non-linear (Jones 1985). In the elimination method, the limitation of a physiological process is the difference between the measured photosynthesis rate and the photosynthesis rate assuming this physiological limitation is eliminated (for example, stomatal conductance is infinite). Therefore, extrapolations to extreme conditions (e.g. intercellular CO_2 concentration is zero or equal to ambient CO_2 concentration) are required. Based on the Farquhar, von Caemmerer and Berry model of C_3 photosynthesis (FvCB model, Farquhar *et al.*, 1980), Grassi and Magnani (2005) used a quantitative limitation analysis to partition the stomatal, mesophyll and biochemical limitations quantitatively (% of a

reference photosynthesis rate, e.g. $35 \mu\text{mol CO}_2 \text{ m}^{-2} \text{ leaf area s}^{-1}$. In this case, a 10% biochemical limitation indicates that the photosynthesis rate would be $3.5 \mu\text{mol m}^{-2} \text{ s}^{-1}$ higher if biochemical capacity would be at its maximum). This approach is considered to be ‘*more realistic*’ than the resistance analysis and the elimination method because the different components of limitations can be summed up, but to be ‘*more complex*’ because it requires elaborative calculations (Grassi *et al.*, 2009).

Quantitative limitation analysis can also be a helpful tool to analyze stress effects on the sources of photosynthetic limitations. It has been applied to investigate the contributions of ontogeny and drought stress to photosynthetic limitations (Wilson *et al.*, 2000; Grassi and Magnani 2005; Egea *et al.*, 2011), the causes of midday depression (Grassi *et al.*, 2009), plant acclimation to and recovery from water stress (Flexas *et al.*, 2009), differences in limiting factors between species (Gago *et al.*, 2013) and the interactions between water potential and the components of limitations (Limosin *et al.*, 2010). To our knowledge, only one study has quantified different components of photosynthetic limitations under salinity (Pérez-López *et al.*, 2012). However, Pérez-López *et al.*, (2012) focused on analyzing the limitations in plants subjected to different stress levels on day 28 after exposure to salinity. Since the ion concentrations in leaves may change daily after the start of salinity, their findings may not be interpreted in the context of osmotic and ionic stress. Indeed, salinity affects all components of photosynthetic limitations. Stomatal closure and disturbance of stomatal regulation, due to osmotic stress (Maggio *et al.*, 2007; Shapira *et al.*, 2009) and ion accumulation in the guard cells (James *et al.*, 2006), respectively, increase stomatal limitations (L_S). Recent studies have reported that mesophyll conductance (g_m) is reduced by drought and salinity stress (Delfine *et al.*, 1999; Flexas *et al.*, 2009; Flexas *et al.*, 2012). There is no clear evidence of ionic stress causing mesophyll limitations. However, salinity stress may induce chloroplast destruction (Shu *et al.*, 2012) which reduces the chloroplast surface area and thereby mesophyll conductance (Tosens *et al.*, 2012). There are no data showing whether the biochemical capacity is influenced by osmotic stress. Although one study suggests that biochemical capacity is not reduced by salinity (Centritto, Loreto & Chartzoulakis 2003), most studies report that toxic effects of Na^+ or Cl^- in the cytosol (James *et al.*, 2002; James *et al.*, 2006; Tavakkoli *et al.*, 2010) increase biochemical limitations.

The quantitative limitation analysis used in the paper of Grassi and Magnani (2005) and the following works has two drawbacks: firstly, it can only be applied at light-saturating (Rubisco-limited) conditions, but except for the leaves grown in the upper part of canopy, large parts of the canopy are exposed to non-saturating (RuBP-limited, Song *et al.*, 2013; Chen *et al.*, 2014) light conditions. Therefore, it would not be justified to scale up the results of the limitation analysis to the whole plant or canopy level (Chen *et al.*, 2014). This has been recently resolved by extending the quantitative limitation analysis to RuBP-limited conditions (Chen *et al.*, 2014). Secondly, stomatal conductance increases with light intensity and this indicates that stomatal limitation might be affected by light conditions. Furthermore, above the light saturation point the stomata may open more with increasing light (e.g. in cucumber, Hogewoning *et al.*, 2010). Therefore, the stomatal limitation calculated by this approach of Grassi and Magnani (2005) may be influenced by the interval between the light saturation point and the light intensity used in the gas-exchange measurement. This could underestimate stomatal limitations, especially when comparing control and stressed plants, since the light saturation point of stressed plants may be considerably lower than that of control plants. This drawback has not been clearly addressed so far and requires further examination.

Using gas-exchange measurements on cucumber (*Cucumis sativus* L., a salt sensitive species), this work aims at answering the following questions: 1) what is the influence of light conditions on the compositions of photosynthetic limitations; 2) to which extent do the osmotic and ionic effects of salinity influence the components of photosynthetic limitations under saturating and non-saturating light conditions. Furthermore, we propose and parameterize a model for disentangling the different osmotic and ionic effects on photosynthesis.

Materials and methods

Plant materials and salt stress treatments

Cucumber seeds (*Cucumis sativus*, 'Aramon' Rijk Zwaan, De Lier, the Netherlands) were sown in rock-wool cubes (36 mm x 36 mm x 40 mm) in the greenhouse of the Institute of Horticultural Production Systems, Leibniz Universität Hannover, Germany (52.5°N, 9.7°E) on 30 July 2012. Seven days after sowing, seedlings were transplanted into larger rock-wool cubes (10 cm x 10 cm x 6.5 cm) for another seven days. After that, each seedling was transplanted upon Styrofoam floating in a container with 25 liters nutrient solution. Each liter of the nutrient solution contained 0.53 g Ca(NO₃)₂ and 0.65 g Fertyl

Basisdünger 1 (Planta GmbH, Regenstauf, Germany, 14% P₂O₅, 38% K₂O, 5% MgO; the solution contained 5.3 mM K⁺, 1.5 mM Na⁺, 3.0 mM Ca²⁺, 0.8 mM Mg²⁺, 1.3 mM H₂PO₄ 5.9 mM NO₃⁻, 1.5 mM Cl⁻ as well as adequate amounts of the micronutrients). The pH value was adjusted to 6.0-6.2 by 1% sulfuric acid. The nutrient solution was changed once a week. The greenhouse was heated to maintain 24/20°C day-night temperature, and roof ventilation was opened when the inside temperature was higher than 26°C. The temperature and light intensity in the greenhouse during the experiment is shown in Fig. 3-S1.

Salt was applied on 26 August, 10 days after the third leaves had appeared and were fully expanded (leaf age = 10 days). Table salt (NaCl) was added to the solution to obtain four salinity levels, 0, 20, 40 and 60 mM. There were 12 plants in each treatment. During the experiment, the third and the fourth leaves were positioned southwards (southwest to southeast). All side shoots and fruits up to the sixth rank were removed.

Gas exchange measurements

All gas exchange measurements were conducted using a Li-6400-40 portable photosynthesis system equipped with a fluorescence chamber head and a Li-6400-20B (LI-COR Inc., Lincoln, NE, USA) between 8:30-13:30. To prevent the possible errors introduced by using different chamber types, possible CO₂ leakage was corrected for each chamber (Flexas *et al.*, 2007a). All measurement types (light response curves, CO₂ response curves and point measurements) were conducted on four leaves from four different plants per treatment.

Light response curves and respiration rate

Light response curves were measured on the fourth leaves on days 2, 7 and 11 after exposure to salinity at 1300, 1000, 800, 600, 400, 200, 100, 80, 65, and 50 $\mu\text{mol m}^{-2} \text{s}^{-1}$ PPFD, $C_a = 380 \mu\text{mol mol}^{-1}$, leaf temperature = 25°C, flow rate = 300 $\mu\text{mol s}^{-1}$ and relative humidity = 70 (± 2.5)%. Data measured at 1000, 800, 600, 400 and 200 $\mu\text{mol m}^{-2} \text{s}^{-1}$ PPFD were used for the limitation analysis at non-saturated light conditions (see below), and leaves were adapted for 5-20 minutes per step to ensure that the stomatal conductance was stable (CV < 0.1 % for 2 minutes). Points measured at and below 200 $\mu\text{mol m}^{-2} \text{s}^{-1}$ PPFD were used to estimate the day respiration rate (R_d , $\mu\text{mol CO}_2 \text{ m}^{-2} \text{ s}^{-1}$) by the Yin method ($R_{d,\text{yin}}$) and the Kok method ($R_{d,\text{kok}}$) Yin *et al.*, 2011).

Photosynthesis CO₂ response curves

Photosynthesis CO₂ response curves (AC_i curves) were conducted on the third leaf on 23 and 26 August, i.e. 3 and 0 days before exposure to salinity, and on the days 3, 6 and 10 after exposure to salinity. Leaves were first adapted for 10-20 minutes at saturated (> 95% of full photosynthesis) photosynthetic photon flux density (PPFD = 1300 $\mu\text{mol m}^{-2} \text{s}^{-1}$) with 10% blue light, 380 $\mu\text{mol mol}^{-1}$ ambient CO₂ concentration (C_a), 25° C leaf temperature, 300 $\mu\text{mol s}^{-1}$ flow rate and 70 (± 2.5)% relative humidity until photosynthesis rate and stomatal conductance were stable. Data were recorded and the AC_i curves were established by an adapted auto-program of the *Open 6.2* software (LI-COR Inc., Lincoln, NE, USA). In short, C_a was changed in 10 steps: 300, 200, 100, 50, 400, 400, 600, 900, 1200 and 1500 $\mu\text{mol mol}^{-1}$. Measured data were not used for further calculations if patchy stomatal behavior was detected, i.e. if there were transient variations of the AC_i relationship at steady-state photosynthesis or oscillation of stomatal conductance (Mott and Buckley 1998). This only occurred in some plants grown at 60 mM NaCl after 8 days.

To estimate the maximum rate of Rubisco carboxylation (V_{cmax} , $\mu\text{mol CO}_2 \text{ m}^{-2} \text{s}^{-1}$) and electron transport rate at saturating light conditions (J , $\mu\text{mol m}^{-2} \text{s}^{-1}$), AC_i curves were analyzed by the non-linear curve fitting method in Microsoft Excel (Sharkey *et al.*, 2007) with slight modifications: 1) leaf temperature was 25°C; 2) CO₂ compensation point in the absence of mitochondrial respiration (Γ^* , $\mu\text{mol mol}^{-1}$) was assumed to be 43.02 $\mu\text{mol mol}^{-1}$ for cucumber (Singsaas *et al.*, 2003); and 3) day respiration rate (R_d , $\mu\text{mol CO}_2 \text{ m}^{-2} \text{s}^{-1}$) and mesophyll conductance to CO₂ (g_m , $\text{mol m}^{-2} \text{s}^{-1}$) were considered as input parameters with the values estimated in this experiment. To estimate g_m , the curve-fitting method (Sharkey *et al.*, 2007), variable J method and constant J method (Harley *et al.*, 1992) were used. Over 90% of the g_m values estimated by the curve-fitting method were larger than 3 $\text{mol m}^{-2} \text{s}^{-1}$ and far from the values reported in the literature (Loreto *et al.*, 1992; Singsaas *et al.*, 2003). As the results of the variable and constant J methods were not different, the values from the variable J method were used throughout. For g_m estimation, Γ^* and R_d are required. The value of Γ^* was taken from the literature (43.02 $\mu\text{mol mol}^{-1}$ for cucumber, Singsaas *et al.*, 2003). Since no difference in R_d was found between treatments in this experiment (data not shown), the average value of R_d estimated by the Yin method ($R_{d,\text{yin}}$, $1.08 \pm 0.43 \mu\text{mol CO}_2 \text{ m}^{-2} \text{s}^{-1}$) were used. Furthermore, the respiration rate estimated by the Kok method ($R_{d,\text{kok}}$) was lower than the rate estimated by the Yin method ($R_{d,\text{yin}}$), but they were well correlated ($R_{d,\text{yin}} = 1.03 R_{d,\text{kok}} + 0.37$; $R^2 = 0.91$). The electron transport rate, J ($\mu\text{mol m}^{-2} \text{s}^{-1}$) is the product of incident PPFD, leaf

absorptance (α , 87% for cucumber, Kahlen *et al.*, 2008), the partitioning factor of light between the two photosystems (β , 0.5 for cucumber, Juszczuk *et al.*, 2007), and photochemical efficiency of photosystem II (Φ_{PSII}), calculated by steady-state fluorescence (F_s) and maximum fluorescence (F_m') following a saturating light pulse ($> 7000 \mu\text{mol m}^{-2} \text{s}^{-1}$ for 0.8 s; $\Phi_{\text{PSII}} = (F_m' - F_s)/F_m'$). From our previous experience in cucumber, salinity has no influence on the relationship between Φ_{PSII} and Φ_{CO_2} ($\Phi_{\text{CO}_2} = 4 \cdot (A + R_d)/\text{PPFD}$, Hassiotou *et al.*, 2009) under non-photorespiratory conditions (2% O_2) and the slope (0.40 ± 0.02) between Φ_{PSII} and Φ_{CO_2} was not different from 0.435 ($\alpha \cdot \beta$ using in this study). Fluorescence data were also used to assure that our measured data points were assigned correctly to the Rubisco-limited or RuBP-limited phase of photosynthesis for the quantitative limitation analysis (see below).

Furthermore, on days 4 and 8 after treatment started, photosynthesis at saturating ($1300 \mu\text{mol m}^{-2} \text{s}^{-1}$ PPFD) and non-saturating light conditions ($600 \mu\text{mol m}^{-2} \text{s}^{-1}$ PPFD) was measured on the third and fourth leaves. V_{cmax} and J_{max} were estimated by the one point method (Wilson *et al.*, 2000; Grassi & Magnani, 2005; Flexas *et al.*, 2009; Egea *et al.*, 2011).

Quantitative limitation analysis

Photosynthesis under saturating light conditions can be expressed as (Farquhar *et al.*, 1980):

$$A_c = \frac{V_{\text{cmax}} \cdot (C_c - \Gamma^*)}{C_c + K_c(1 + O/K_o)} - R_d \quad (\text{Eqn 3-1})$$

where A_c is the photosynthesis rate in the Rubisco carboxylation-limited stage ($\mu\text{mol CO}_2 \text{m}^{-2} \text{s}^{-1}$), V_{cmax} is the maximum rate of Rubisco carboxylation ($\mu\text{mol CO}_2 \text{m}^{-2} \text{s}^{-1}$), C_c ($\mu\text{mol mol}^{-1}$) and O ($210 \text{ mmol mol}^{-1}$) are mol fractions of CO_2 and O_2 at the site of carboxylation, and K_c ($405 \mu\text{mol mol}^{-1}$) and K_o ($278 \text{ mmol mol}^{-1}$) are Michaelis-Menten constants of Rubisco for CO_2 and O_2 , respectively (Dubois *et al.*, 2007), and R_d is respiration rate ($\mu\text{mol CO}_2 \text{m}^{-2} \text{s}^{-1}$). According to Grassi & Magnani (2005), the relative changes in photosynthesis rate under saturated light conditions, dA_c/A_c , can be expressed by:

$$\frac{dA_c}{A_c} = l_{\text{sc}} \cdot \frac{dg_{\text{sc}}}{g_{\text{sc}}} + l_{\text{mc}} \cdot \frac{dg_{\text{m}}}{g_{\text{m}}} + l_{\text{bc}} \cdot \frac{dV_{\text{cmax}}}{V_{\text{cmax}}} = L_{\text{Sc}} + L_{\text{Mc}} + L_{\text{Bc}} \quad (\text{Eqn 3-2})$$

$$l_{\text{sc}} = \frac{g_{\text{tot}}/g_{\text{sc}} \cdot \partial A_c / \partial C_c}{g_{\text{tot}} + \partial A_c / \partial C_c} \quad (\text{Eqn 3-3a})$$

$$l_{\text{mc}} = \frac{g_{\text{tot}}/g_{\text{m}} \cdot \partial A_c / \partial C_c}{g_{\text{tot}} + \partial A_c / \partial C_c} \quad (\text{Eqn 3-3b})$$

$$l_{bc} = \frac{g_{tot}}{g_{tot} + \partial A_c / \partial C_c} \quad (\text{Eqn 3-3c})$$

$$\frac{\partial A_c}{\partial C_c} = \frac{V_{cmax} \cdot (\Gamma_* + K_c(1+O/K_o))}{(C_c + K_c(1+O/K_o))^2} \quad (\text{Eqn 3-4})$$

where l_{sc} , l_{mc} and l_{bc} are the *relative* limitations of stomatal conductance to CO₂ (g_{sc} , mol m⁻²s⁻¹), mesophyll conductance (g_m) and biochemical capacity (V_{cmax}), respectively, summing up to a value of one. Total resistance to CO₂ ($1/g_{tot}$) is the sum of stomatal and mesophyll resistances ($1/g_{sc} + 1/g_m$). L_{Sc} , L_{Mc} and L_{Bc} are the contribution of g_{sc} , g_m and V_{cmax} to dA_c/A_c respectively. Then the relative change of A_c , g_{sc} , g_m and V_{cmax} in Eqn 3-2 can be approximated by (Chen *et al.*, 2014):

$$\frac{dA_c}{A_c} \approx \frac{A_c^{ref} - A_c}{A_c^{ref}} \quad (\text{Eqn 3-5a})$$

$$\frac{dg_{sc}}{g_{sc}} \approx \frac{g_{sc}^{ref} - g_{sc}}{g_{sc}^{ref}} \quad (\text{Eqn 3-5b})$$

$$\frac{dg_m}{g_m} \approx \frac{g_m^{ref} - g_m}{g_m^{ref}} \quad (\text{Eqn 3-5c})$$

$$\frac{dV_{cmax}}{V_{cmax}} \approx \frac{V_{cmax}^{ref} - V_{cmax}}{V_{cmax}^{ref}} \quad (\text{Eqn 3-5d})$$

where g_{sc}^{ref} , g_m^{ref} , and V_{cmax}^{ref} are the reference values of stomatal and mesophyll conductances and of maximum carboxylation rate, defined as the maximum values measured in an experiment (Grassi and Magnani 2005, see below). A_c^{ref} is the photosynthesis rate assuming g_{sc} , g_m and V_{cmax} reach their maxima concomitantly (Grassi *et al.*, 2009):

$$A_c^{ref} = \frac{V_{cmax}^{ref} \cdot (C_a - A_{cmax}^{ref} (1/g_{sc}^{ref} + 1/g_m^{ref}) - \Gamma_*)}{C_a - A_{cmax}^{ref} (1/g_{sc}^{ref} + 1/g_m^{ref}) + K_c(1+O/K_o)} - R_d \quad (\text{Eqn 3-6})$$

where C_a is the ambient CO₂ concentration (380 μmol mol⁻¹).

Under non-saturating light conditions, photosynthesis is limited by RuBP regeneration rate (or electron transport rate, J , μmol m⁻²s⁻¹) and photosynthesis rate (A_j) can be expressed as (Farquhar *et al.*, 1980):

$$A_j = \frac{J(C_c - \Gamma_*)}{4C_c + 8\Gamma_*} - R_d \quad (\text{Eqn 3-7})$$

where J is the rate of electron transport (μmol m⁻²s⁻¹), which is related to absorbed photosynthetically active irradiance (I_{ab} , μmol photons m⁻²s⁻¹) and maximum electron transport rate (J_{max} , μmol m⁻²s⁻¹):

$$J = \frac{(\mathcal{K}_{2LL} \cdot I_{ab} + J_{max} - \sqrt{(\mathcal{K}_{2LL} \cdot I_{ab} + J_{max})^2 - 4\theta \cdot J_{max} \cdot \mathcal{K}_{2LL} \cdot I_{ab}})}{2\theta} \quad (\text{Eqn 3-8})$$

where K_{2LL} denotes the conversion efficiency of I_{ab} to J ($\text{mol e}^- \text{mol}^{-1}$ photons) and θ is the convexity factor for the response of J to I_{ab} . According to Chen *et al.*, (2014), the relative change of photosynthesis can be described as:

$$\frac{dA_j}{A_j} = l_{sj} \cdot \frac{dg_{sc}}{g_{sc}} + l_{mj} \cdot \frac{dg_m}{g_m} + l_j \cdot \frac{dJ_B}{J} + l_j \cdot \frac{dJ_I}{J} = L_{Sj} + L_{Mj} + L_{Bj} + L_{Lj} \quad (\text{Eqn 3-9})$$

with

$$l_{sj} = \frac{g_{\text{tot}} / g_{sc} \cdot \partial A_j / \partial C_c}{g_{\text{tot}} + \partial A_j / \partial C_c} \quad (\text{Eqn 3-10a})$$

$$l_{mj} = \frac{g_{\text{tot}} / g_m \cdot \partial A_j / \partial C_c}{g_{\text{tot}} + \partial A_j / \partial C_c} \quad (\text{Eqn 3-10b})$$

$$l_j = \frac{g_{\text{tot}}}{g_{\text{tot}} + \partial A_j / \partial C_c} \quad (\text{Eqn 3-10c})$$

$$\frac{\partial A_j}{\partial C_c} = \frac{12J \cdot \Gamma_*}{(4C_c + 8\Gamma_*)^2} \quad (\text{Eqn 3-11})$$

where L_{Sj} , L_{Mj} , L_{Bj} and L_{Lj} are the contributions of stomatal conductance, mesophyll conductance, biochemical capacity and light to photosynthetic limitation under non-saturating light conditions, respectively; l_{sj} , l_{mj} and l_j are the *relative* limitations of stomatal and mesophyll conductance and of electron transport rate, respectively; dA_j/A_j , dg_{sc}/g_{sc} and dg_m/g_m were obtained in a way similar to Eqns 3-5a-c; dJ_B and dJ_I represent the change of electron transport rate due to biochemical capacity and due to irradiance, respectively. Furthermore, it was assumed that g_m is not dependent on the light conditions (Yamori *et al.*, 2010b). Finally, dJ_B and dJ_I are approximated by (Chen *et al.*, 2014):

$$\frac{dJ_B}{J} \approx \frac{J_s^{\text{ref}} - J_s}{J_s^{\text{ref}}} \quad (\text{Eqn 3-12a})$$

$$\frac{dJ_I}{J} \approx \frac{J_s - J}{J_s^{\text{ref}}} \quad (\text{Eqn 3-12b})$$

where J_s^{ref} is the J with maximum J_{max} (with highest biochemical capacity) at light saturation (PPFD = 1300 $\mu\text{mol m}^{-2}\text{s}^{-1}$ in the experiment), J_s and J are the electron transport rates of the sample plants at the saturating and the measured light conditions, respectively. Furthermore, A_j^{ref} is calculated by solving the following equation at $C_a = 380 \mu\text{mol mol}^{-1}$:

$$A_j^{\text{ref}} = \frac{J_{\text{max}}^{\text{ref}} (C_a - A_{j\text{max}}^{\text{ref}} (1/g_{sc}^{\text{ref}} + 1/g_m^{\text{ref}}) - \Gamma_*)}{4(C_a - A_{j\text{max}}^{\text{ref}} (1/g_{sc}^{\text{ref}} + 1/g_m^{\text{ref}})) + 8\Gamma_*} - R_d \quad (\text{Eqn 3-13})$$

Chemical analysis

After each photosynthesis measurement, the measured part of the leaf was harvested and the fresh weight was recorded. Leaf samples were weighed after drying at 70°C for 72

hours for recording dry weight, then ground into fine powder. For sodium analysis, 50-100 mg of the powder was dry ashed at 500°C for removing the organic components. After ashing, the samples were dissolved in nitric acid before being measured by an atom absorption spectrometer (Perkin Elmer, 1100B, USA). Soluble chloride was extracted from 100 mg of the powder by distilled water and the extract was titrated with AgNO₃ by TitroLine®6000 (SI Analytics GmbH, Mainz, Germany) to determine the Cl⁻ concentrations.

*Disentangling the osmotic and ionic effects on photosynthetic parameters –
model approach*

Assuming that the effects of osmotic and ionic stresses on photosynthetic parameters X are additive and can be described by:

$$X_{\text{stress}} = (1 + m_x S_s + n_x S_l) X_n \quad (\text{Eqn 3-14})$$

where X_{stress} and X_n are the photosynthetic parameters X (stomatal conductance, g_{sc} , mesophyll conductance, g_m , maximum rate of Rubisco carboxylation rate, V_{cmax} , and maximum electron transport rate, J_{max}) under stressed and non-stressed conditions, respectively; S_s and S_l are the sodium concentrations in the nutrient solution and in the leaf water (mM), respectively; and m_x and n_x are empirical parameters for osmotic and ionic effects of salt, respectively. Using these empirical parameters, the dependencies of stomatal, mesophyll and biochemical limitations to S_l were simulated for saturating and non-saturating light conditions.

Data analysis and model fitting

The averages of g_{sc} , g_m , V_{cmax} , J_{max} and J were used ($n = 4$) for quantitative limitation analyses. Therefore, no standard errors are shown in the results of the quantitative limitation analyses (see also Wilson *et al.*, 2000; Grassi and Magnani 2005; Flexas *et al.*, 2009; Grassi *et al.*, 2009; Limosin *et al.*, 2010; Egea *et al.*, 2011; Pérez-López *et al.*, 2012). Stomatal, mesophyll biochemical and light limitations were calculated by the EXCEL file provided in Chen *et al.*, (2014) using the measured gas-exchange data. Linear regressions were conducted to (i) estimate the day respiration rate, R_d , and (ii) parameterize Eqn 3-14. These analyses were conducted in R v.2.12.0 (R Foundation for Statistical Computing).

Results

Dependency of photosynthetic limitations on light conditions

Light intensity had strong influences on stomatal (L_{Sj} , Fig. 3-1a), mesophyll (L_{Mj} , Fig. 3-1c), and light (L_{Lj} , Fig. 3-1e) limitations and their relationships were non-linear (Fig. 3-1a, 1c, 1e). Light intensity had negligible effects on biochemical limitations (L_{Bj} , data not shown). The relative stomatal and mesophyll limitations (l_{sj} and l_{mj} in Eqn 3-10a and 3-10b, respectively, Fig. 3-1b, 1d) increased with the light intensity, whereas the relative limitation of electron transport rate (l_j in Eqn 3-10c, Fig. 3-1f) decreased.

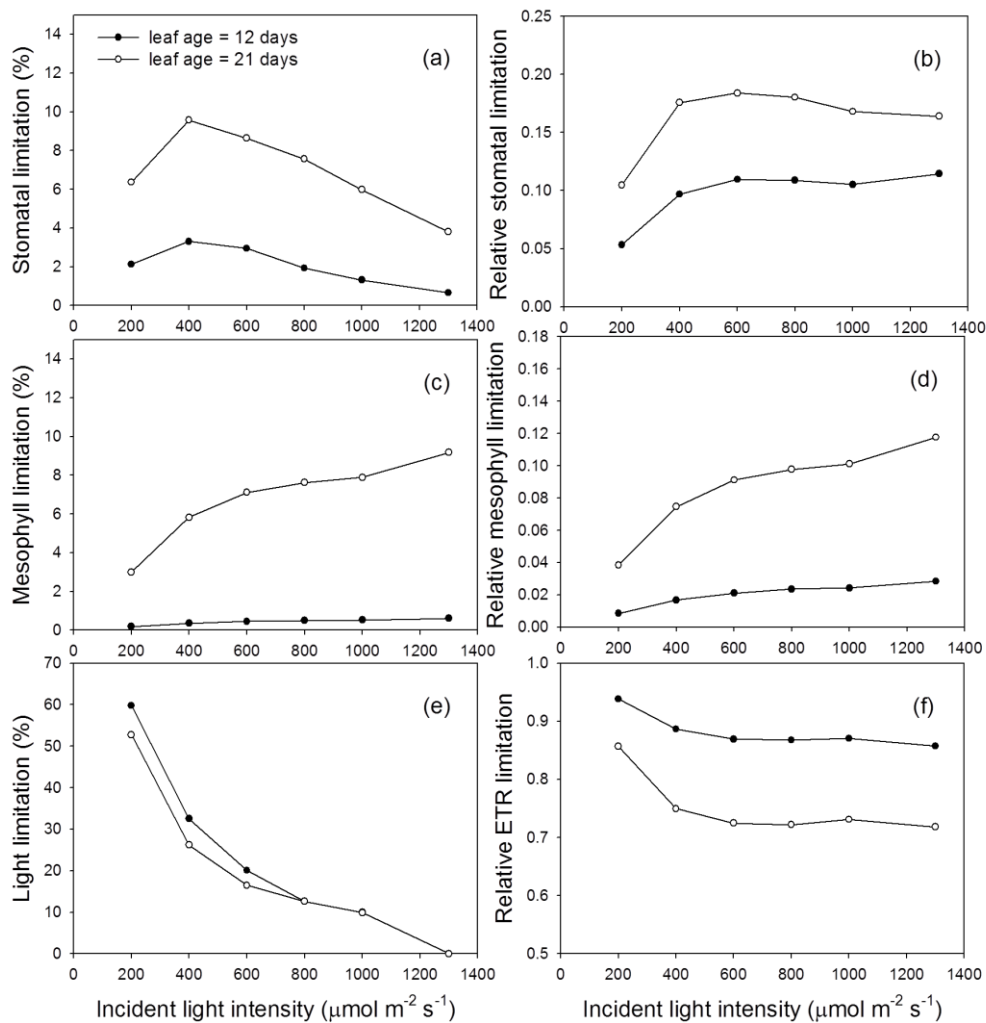


Fig. 3-1. Influence of incident light intensity on (a) absolute stomatal limitation, L_{Sj} in Eqn 3-9; (b) relative stomatal limitation, l_{sj} in Eqn 3-10a; (c) absolute mesophyll limitation, L_{Mj} in Eqn 3-9; (d) relative mesophyll limitation, l_{mj} in Eqn 3-10b; (e) absolute light limitation, L_{Lj} in Eqn 3-9; and (f) relative limitation of electron transport rate (ETR), l_j in Eqn 3-10c. Data were obtained from cucumber leaves on days 12 (closed circles) and 21 (open circles) after leaf appearance. Each point was calculated from the averages of four measurements on a given date, on the fourth leaves under non-stress conditions.

Under non-stress and salinity stress conditions, L_{Sj} was lower at 200 than at 400 $\mu\text{mol m}^{-2}\text{s}^{-1}$ PPFD (Fig. 3-S2). L_{Sj} reached its maximum between 400 – 600 $\mu\text{mol m}^{-2}\text{s}^{-1}$ and decreased at 800 and 1000 $\mu\text{mol m}^{-2}\text{s}^{-1}$. L_{Mj} increased with light intensity, and was about 3-fold higher at 1000 than at 200 $\mu\text{mol m}^{-2}\text{s}^{-1}$ PPFD. However, the restriction of photosynthesis due to L_{Mj} was less than 9% in all cases. L_{Bj} remained fairly constant between 400 – 1000 $\mu\text{mol m}^{-2}\text{s}^{-1}$ PPFD and slightly increased at 200 $\mu\text{mol m}^{-2}\text{s}^{-1}$ PPFD. L_{Lj} decreased significantly with increasing light, and approached zero at light saturation conditions (Fig. 3-1e, Fig. 3-S2).

Effects of salinity on photosynthetic parameters and photosynthetic limitations

The reference values of g_{sc} , g_m , V_{cmax} and J are shown in Table 3-1 (averages from four measurements). The reference photosynthesis rates under saturating and non-saturating light conditions, A_c^{ref} and A_j^{ref} , were calculated using Eqn 3-6 and Eqn 3-13, respectively. The results of the quantitative limitation analysis are expressed as percentages of these reference values. Furthermore, Na^+ and Cl^- concentrations in leaves under salinity stress were well correlated (Fig. 3-S3, $R^2 = 0.84$, $p < 0.001$). Therefore, we only focused on the relationships between Na^+ concentration (in the tissue water) and photosynthetic parameters.

Table 3-1. Photosynthetic parameters for the quantitative limitation analysis at saturated and non-saturated light conditions and parameters of osmotic and ionic effects.

Parameter	Unit	Equation	Value	p value	R^2
A_c^{ref}	$\mu\text{mol CO}_2 \text{ m}^{-2}\text{s}^{-1}$	Eqn 3-6	30.24*	-	-
A_j^{ref}	$\mu\text{mol CO}_2 \text{ m}^{-2}\text{s}^{-1}$	Eqn 3-13	26.71*	-	-
V_{cmax}^{ref}	$\mu\text{mol CO}_2 \text{ m}^{-2}\text{s}^{-1}$	Eqn 3-6	130.84*	-	-
J_{max}^{ref}	$\mu\text{mol CO}_2 \text{ m}^{-2}\text{s}^{-1}$	Eqn 3-13	168.80*	-	-
g_{sc}^{ref}	$\text{mol m}^{-2}\text{s}^{-1}$	Eqn 3-6 & 3-13	0.37*	-	-
g_m^{ref}	$\text{mol m}^{-2}\text{s}^{-1}$	Eqn 3-6 & 3-13	1.68*	-	-
m_{gsc}	mM^{-1}	Eqn 3-14	$-6.15 \pm 1.40 \cdot 10^{-3}$	$p < 0.001$	0.75
n_{gsc}	mM^{-1}	Eqn 3-14	$-2.69 \pm 0.83 \cdot 10^{-3}$	$p < 0.01$	0.75
m_{gm}	mM^{-1}	Eqn 3-14 ^A	$-9.34 \pm 1.25 \cdot 10^{-3}$	$p < 0.001$	0.70
n_{gm}	mM^{-1}	Eqn 3-14	n.s.	0.88	-
m_{vcmax}	mM^{-1}	Eqn 3-14	n.s.	0.13	-
n_{vcmax}	mM^{-1}	Eqn 3-14 ^B	$-2.84 \pm 0.20 \cdot 10^{-3}$	$p < 0.001$	0.61
m_{jmax}	mM^{-1}	Eqn 3-14	n.s.	0.98	-
n_{jmax}	mM^{-1}	Eqn 3-14 ^B	$-2.06 \pm 0.13 \cdot 10^{-3}$	$p < 0.001$	0.59

* Reference values are the maximum values of control plants measured or estimated in the experiment; ^A Since n_{gm} was not significant, Eqn 3-14 was simplified as $g_{m,s} = (1 + m_{gm}S_s) g_{m,n}$; ^B Since parameters for osmotic effect were not significant, Eqn 3-14 was simplified as $X_{stress} = (1 + n_x S_i) X_n$.

Photosynthetic limitations under saturating light conditions

Stomatal limitation, L_{Sc} , of plants in control and 20 mM NaCl during the experiment was less than 7% (Fig. 3-2a, 2b). After three days of exposure to 40 and 60 mM NaCl, L_{Sc}

increased from 5% to 11% and 16%, respectively (Fig. 3-2c, 2d). In both treatments, L_{Sc} increased with time and reached 22% and 28% after 10 days. After full expansion of leaves (day 0), L_{Mc} increased from 0% to 14% in control plants. The rapid reduction of g_m after 3 days in the 60 mM NaCl (from 1.68 ± 0.39 to 0.53 ± 0.28) resulted in an 8% reduction of photosynthesis. L_{Bc} of control plants was within 10% at treatment start and reached about 20% after 10 days of exposure to 60 mM NaCl.

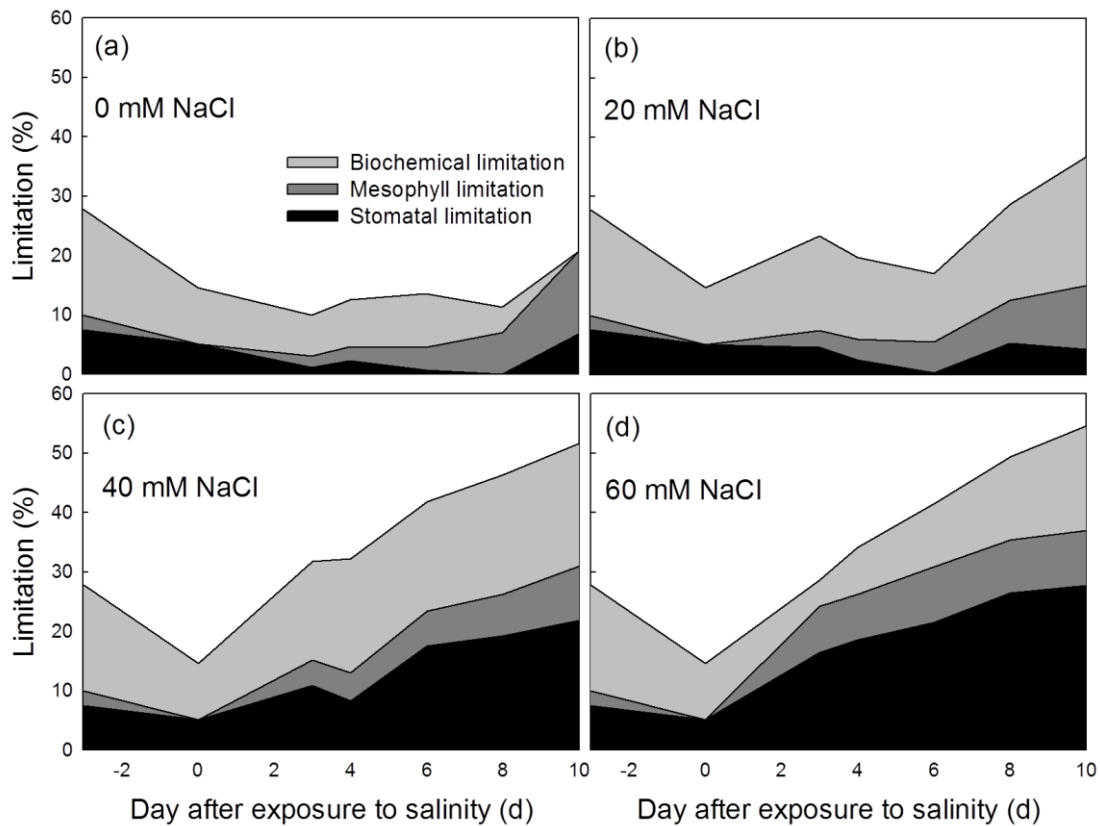


Fig. 3-2. Stacked graphs describing the effects of ontogeny and salinity levels on the components of photosynthetic limitation at saturated light conditions (PPFD = $1300 \mu\text{mol m}^{-2}\text{s}^{-1}$ and $C_a = 380 \mu\text{mol mol}^{-1}$). (a) - (d) represent 0, 20, 40 and 60 mM NaCl in the solution, respectively. The black, dark grey and grey areas represent the stomatal, mesophyll and biochemical limitations, respectively. Limitations are expressed as percentages of the reference values at saturated light conditions given in Table 3-1. Each value was calculated from four measurements on the given dates and salt treatments.

Photosynthetic limitations at non-saturating light conditions

The total photosynthetic limitations of control plants at PPFD = $600 \mu\text{mol photons m}^{-2}\text{s}^{-1}$ increased between day 2 and day 11 after exposure to salinity from 24% to 32% (Fig. 3-3a). The major component of the limitations on day 11 was due to light (L_{Lj} , 17-20%). Stomatal limitation (L_{Sj}) and mesophyll limitation (L_{Mj}) were 9% and 7%, respectively.

L_{Sj} increased with salinity level and time of exposure to salinity. The changes of L_{Sj} between day 2 and 11 were 4-10% in 20 mM NaCl, 7-15% in 40 mM NaCl and 15-27% in 60 mM NaCl (Fig. 3-3b-3d). In all treatments, L_{Mj} increased with time and remained below 7%. The biochemical limitation (L_{Bj}) also increased with salinity level and time of exposure to salinity (between day 2 and 11, 7-31% in 20 mM NaCl, 4-37% in 40 mM NaCl and 7-23% in 60 mM NaCl, respectively). Interestingly, L_{Lj} decreased with time under salinity. After 11 days in 40 and 60 mM NaCl, L_{Lj} at PPFD = 600 $\mu\text{mol m}^{-2}\text{s}^{-1}$ approached zero.

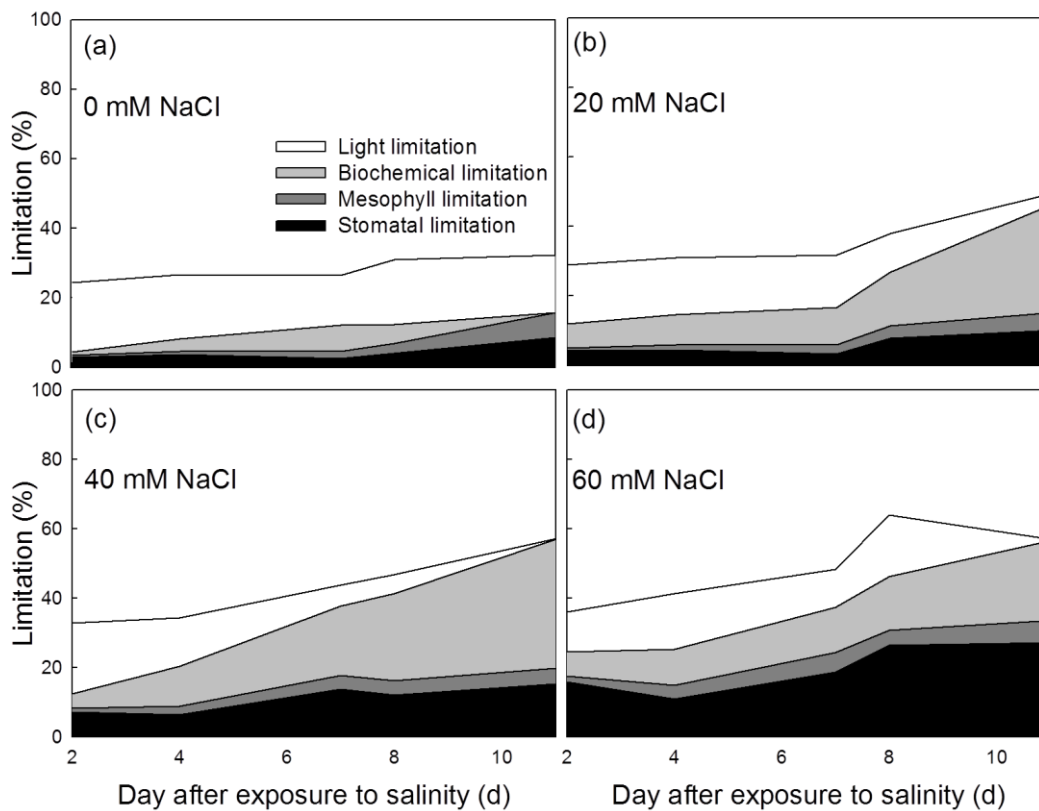


Fig. 3-3. Stacked graphs describing the effects of ontogeny and salinity levels on the components of photosynthetic limitation at non-saturated light conditions (PPFD = 600 $\mu\text{mol m}^{-2}\text{s}^{-1}$ and $C_{as} = 380 \mu\text{mol mol}^{-1}$). (a) - (d) represent 0, 20, 40 and 60 mM NaCl in the solution, respectively. The black, dark grey, grey and white areas represent the stomatal, mesophyll, biochemical and light limitations, respectively. Limitations are expressed as percentages of the reference values at non-saturated light conditions given in Table 3-1. Each value was calculated from four measurements on the given dates and salt treatments.

Effects of osmotic and ionic stress on photosynthetic parameters

The significances of the regression coefficients, m_x and n_x in Eqn 3-14 were used as criteria to determine whether photosynthetic parameters, g_{sc} , g_m , V_{cmax} and J_{max} , were influenced by osmotic and ionic stress. Our results showed that osmotic stress strongly

affected g_{sc} and g_m , but had no influence on V_{cmax} and J_{max} (Table 3-1). In contrast, ionic stress had influenced g_{sc} , V_{cmax} and J_{max} , but not g_m . Since n_{gm} was not significant, Eqn 3-14 was simplified as $g_{m, stress} = (1 + m_{gm}S_s)g_{m,n}$. Parameters describing osmotic effects on biochemical capacity (m_{vcmax} and m_{jmax}) were not significant, therefore, Eqn 3-14 was simplified as $X_{stress} = (1 + n_x S_l)X_n$. Furthermore, n_{vcmax} and n_{jmax} were also analyzed separately for different salinity levels in the nutrient solution. At 20, 40 and 60 mM NaCl, n_{vcmax} was $-3.81 \pm 0.81 \cdot 10^{-3}$, $-2.24 \pm 0.44 \cdot 10^{-3}$ and $-2.98 \pm 0.29 \cdot 10^{-3}$, respectively. At 20, 40 and 60 mM NaCl, n_{jmax} , were $-3.48 \pm 0.71 \cdot 10^{-3}$, $-2.94 \pm 0.30 \cdot 10^{-3}$ and $-1.83 \pm 0.17 \cdot 10^{-3}$, respectively. Both n_{vcmax} and n_{jmax} were not different between salinity levels in the nutrient solution. Therefore, data collected from all salinity levels were pooled for regression analysis (Fig. 3-S4). Between salinity levels and stomatal limitations, after 2-3 days of exposure to salinity, linear relationships were found (Fig. 3-4a, intercepts and slopes were not different between saturating and non-saturating light conditions and the data were pooled). Mesophyll limitation also increased with salinity (Fig. 3-4b) and was more prominent under saturating than under non-saturating light.

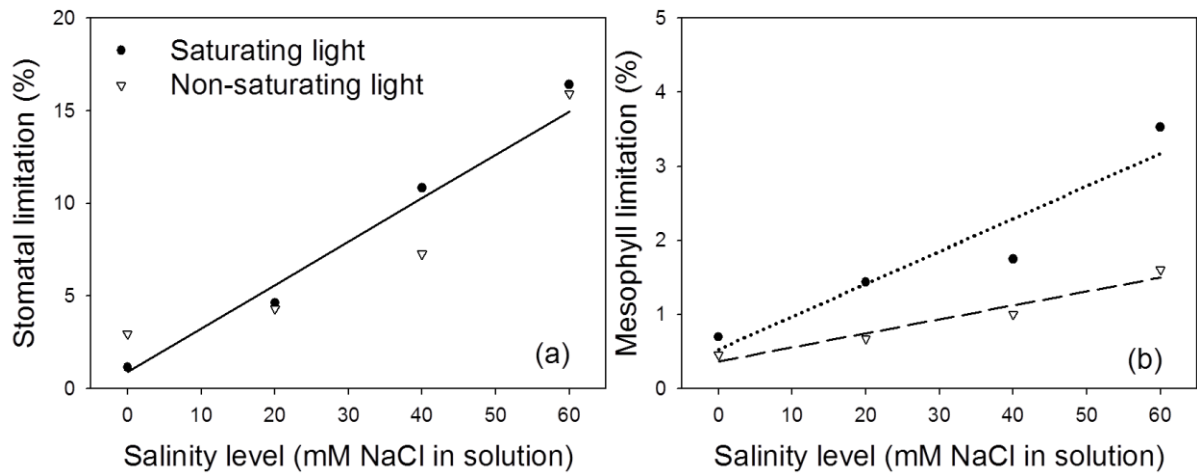


Fig. 3-4. Effects of osmotic stress on photosynthetic limitations at saturating (PPFD = $1300 \mu\text{mol m}^{-2}\text{s}^{-1}$, close circle) and non-saturating ($600 \mu\text{mol m}^{-2}\text{s}^{-1}$, reversed triangle) light conditions. (a) The stomatal limitation increased linearly with the salinity level in the nutrient solution. The solid line represents the regression line of the pooled data because the slopes between saturating and non-saturating light conditions were not different; $y = 0.24x + 0.89$, $R^2 = 0.92$, $p < 0.001$; standard errors of intercept and slope were 1.39 and 0.02 \%mM^{-1} , respectively. (b) The mesophyll limitation increased linearly with the salinity level. Dotted and dashed lines are regression lines under saturating ($y = 0.044x + 0.531$, $R^2 = 0.90$, $p = 0.054$; standard errors of intercept and slope were 0.399 and 0.011, respectively) and non-saturating ($y = 0.019x + 0.368$, $R^2 = 0.95$, $p = 0.025$; standard errors of intercept and slope were 0.114 and 0.003, respectively) light conditions, respectively. Each value was calculated from four measurements under the given light conditions and salt treatments. Measurements were taken on day 2 (non-saturating light) and day 3 (saturating light) after start of salinity treatment.

Stomatal and biochemical limitations increased linearly with Na^+ concentration in leaf water (S_l) but the slopes tended to decrease with increasing salinity levels in the nutrient solution (S_s , Fig. 3-5). Under both light conditions, the relationships between stomatal limitation and S_l were non-linear and the increase in stomatal limitation due to S_l depended on S_s (Fig. 3-6a, 6b). The slopes between biochemical limitation and S_l were influenced by the salinity levels in the nutrient solution (Fig. 3-6c, 6d). The effect of S_l on mesophyll limitation was less than 4% (data not shown).

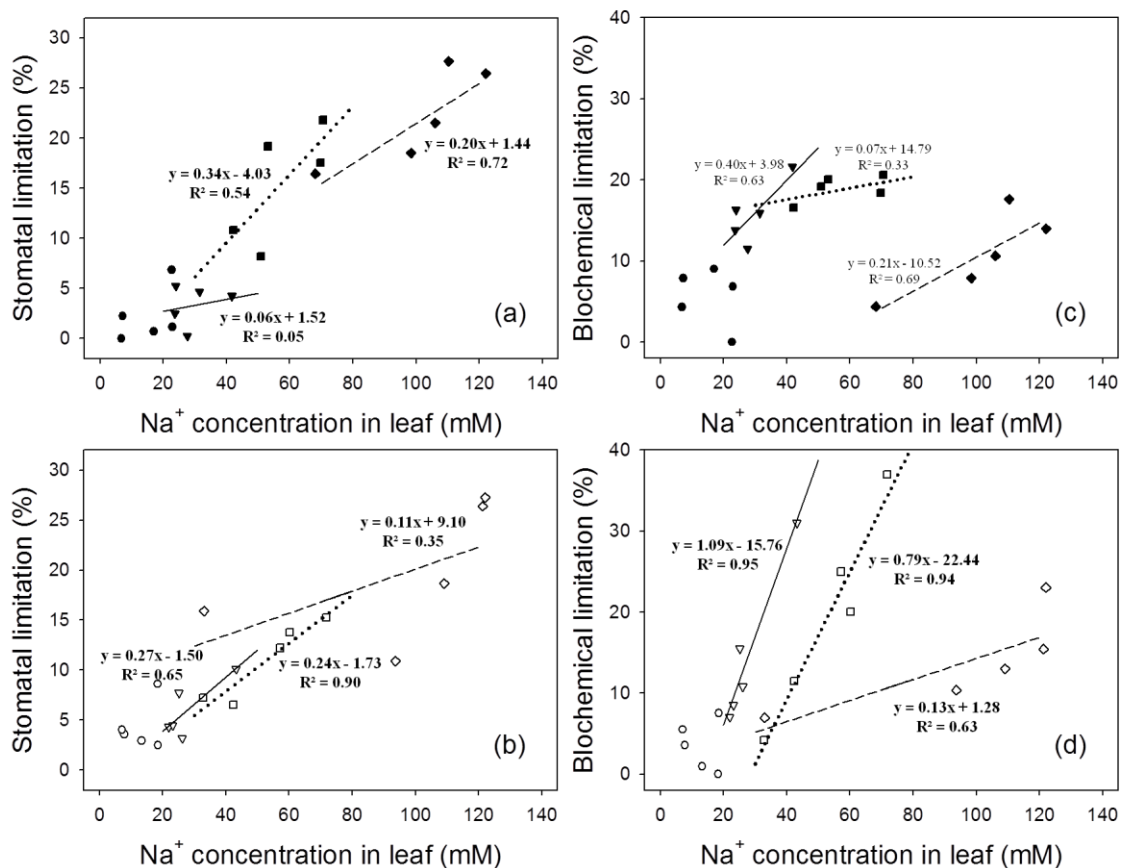


Fig. 3-5. Effects of ionic stress on stomatal (a, b) and biochemical limitation (c, d) at saturated (PPFD = $1300 \mu\text{mol m}^{-2}\text{s}^{-1}$, a, c) and non-saturated ($600 \mu\text{mol m}^{-2}\text{s}^{-1}$, b, d) light conditions. Circles, reverse triangles, squares and rhombi represent data collected from plants subjected to 0, 20, 40 and 60 mM NaCl in the nutrient solution, respectively. The solid, dotted and dashed lines represent the regression lines of the data collected from plants subjected to 20, 40 and 60 mM NaCl in the nutrient solution, respectively. Each point was calculated from four measurements under the given light conditions and salt treatments. Measurements were taken between day 2-11 after start of salinity treatment.

Salinity effects on water use efficiency

Under saturated light conditions, the photosynthetic rate (A_c) decreased linearly with stomatal limitation (Fig. 3-7a, $y = -0.46x + 25.44$, $R^2 = 0.77$, $p < 0.001$). However, this

relationship was less close under non-saturating light conditions (Fig. 3-7b, $y = -0.37x + 19.57$, $R^2 = 0.27$, $p < 0.001$). Clear relationships were found between stomatal conductance to water vapor (g_{sw} , $\text{mol H}_2\text{O m}^{-2}\text{s}^{-1}$) and stomatal limitation (S_c in Fig. 3-7c and L_{sj} in Fig. 3-7d), and these relationships seemed to be independent of salinity levels. The intrinsic water use efficiency ($iWUE$, A/g_{sw} $\mu\text{mol CO}_2 \text{ mol}^{-1} \text{ H}_2\text{O}$) increased linearly with stomatal limitation in all treatments and the slopes and intercepts of this relationship were not different between treatments ($p < 0.05$). Therefore, linear regression was conducted by pooling the data of all treatments (Fig. 3-7e, $y = 1.23x + 45.11$, $R^2 = 0.79$, $p < 0.001$; Fig. 7f, $y = 2.21x + 39.32$, $R^2 = 0.87$, $p < 0.001$).

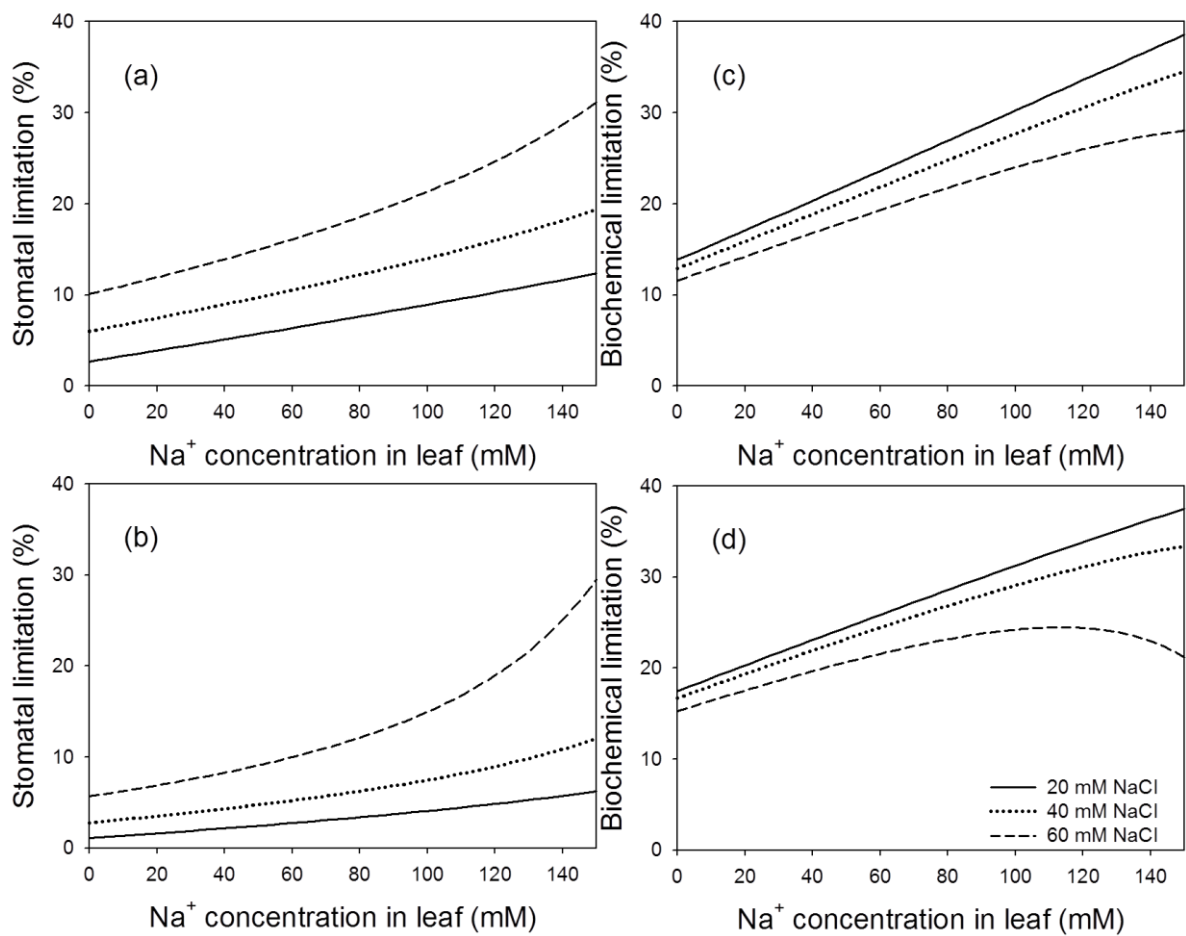


Fig. 3-6. Simulated relationships between Na^+ concentrations in leaves and stomatal (a, b) and biochemical limitations (c, d) under saturating ($1300 \mu\text{mol m}^{-2}\text{s}^{-1}$; a, c) and non-saturation ($600 \mu\text{mol m}^{-2}\text{s}^{-1}$; b, d) light conditions under 20, 40 and 60 mM NaCl in the solution. Parameters listed in Table 3-1 were used for simulations; stomatal conductance, mesophyll conductance, maximum Rubisco-carboxylation rate and maximum electron transport rate at Na^+ concentration in leaves with 0 mM Na^+ were assumed to be $0.3 \text{ mol m}^{-2}\text{s}^{-1}$, $0.8 \text{ mol m}^{-2}\text{s}^{-1}$, $104 \mu\text{mol CO}_2 \text{ m}^{-2}\text{s}^{-1}$ and $135 \mu\text{mol e}^- \text{ m}^{-2}\text{s}^{-1}$, respectively, which were similar to the values measured in the middle of the experiment.

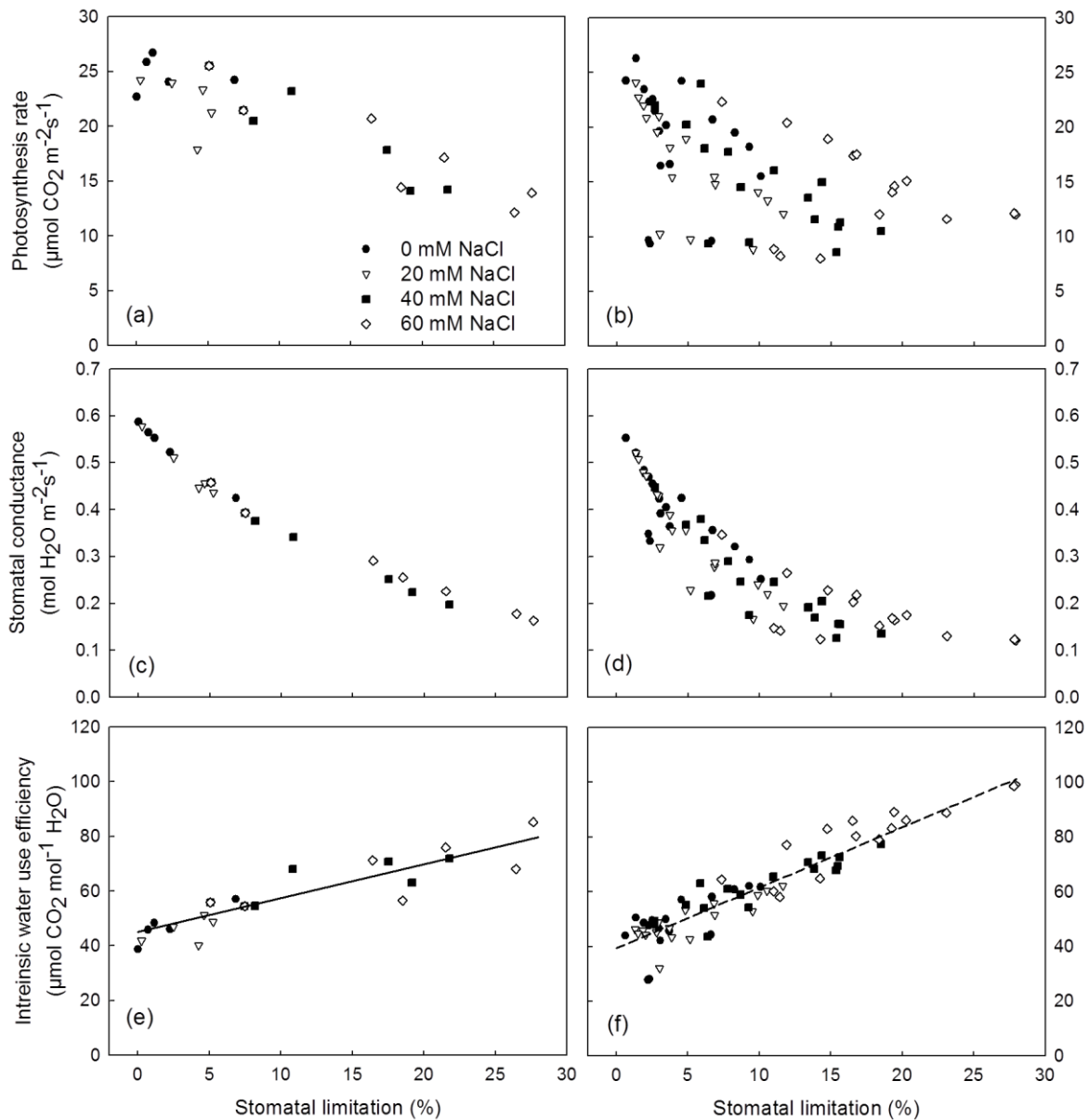


Fig. 3-7 Relationships between stomatal limitation and photosynthesis rate (a, b), stomatal conductance to water vapor (c, d) and intrinsic water use efficiency (e, f) at saturating (a, c and e) and non-saturating (b, d and f) light conditions. Each point represents the mean values of 4 measurements. Linear regression was used to describe the relationships between stomatal limitation and intrinsic water use efficiency.

Discussion

Importance of quantitative limitation analysis under non-saturating light condition

Quantitative limitation analysis is a helpful tool in analyzing stress and acclimation effects on the sources of photosynthetic limitations. However, except in a model study (Chen *et al.*, 2014), it has only been applied for saturating light condition (see Wilson *et al.*, 2000; Grassi and Magnani 2005; Flexas *et al.*, 2009; Grassi *et al.*, 2009; Limosin *et*

al., 2010; Egea *et al.*, 2011; Pérez-López *et al.*, 2012). Very recently, Buckley & Diaz-Espejo (2015) also proposed a new approach to partition changes in photosynthetic rate by using numerical integration of Eqn 3-2. They demonstrated that their new approach is more accurate (error was less than 0.07% with step for numerical integration = 1000) than the quantitative limitation analysis proposed by Grassi and Magnani (2005). Our previous results show that the potential errors of the quantitative limitation analyses proposed by Grassi and Magnani (2005) and Chen *et al.* (2014) are less than 3% of the reference photosynthetic rate (Chen *et al.*, unpublished results), sufficient accuracy for a sound limitation analysis. Nevertheless, it would be interesting to analyze published datasets with the new method and compare the results from different approaches.

Except for the leaves grown in the upper part of canopy, large parts of the canopy, especially under greenhouse conditions, are usually exposed to non-saturating light conditions (RuBP-limited, Song *et al.*, 2013; Chen *et al.*, 2014). Therefore, the results and conclusions in the past studies would not be representative at the canopy level. Our results show non-linear relationships between L_{Sj} , L_{Mj} and measuring light intensity (Fig. 3-1a, 1c). In the quantitative limitation analysis, each limitation is the product of two components: relative limitation and relative change (Eqns 2 and 9). For example, the light limitation (% of reference) in Fig. 3-1c is the product of relative limitation of electron transport rate, l_j (Eqn 3-10c), and the relative change in electron transport rate due to light intensity, dJ_l/J in Eqn 3-12b. According to Eqns 4 and 11, a decrease in C_c increases $\partial A_c/\partial C_c$ and $\partial A_j/\partial C_c$, which are important components for calculating relative limitations (Eqns 3 and 10). Higher $\partial A_c/\partial C_c$ and $\partial A_j/\partial C_c$ values decrease the proportions of non-diffusional limitations (l_{bc} and l_j in Eqns 3c and 10c, respectively). Therefore, the relative importance of diffusional limitations increases with decreasing C_c . It is often observed that C_c is close to ambient CO_2 concentration at low light conditions ($< 50 \mu\text{mol m}^{-2}\text{s}^{-1}$), decreases with light intensity up to 400-500 $\mu\text{mol m}^{-2}\text{s}^{-1}$ and stays relatively constant (up to saturating light, data not shown, see also Hogewoning *et al.*, 2010). This explains the dependencies of relative limitations to light as shown in Fig. 3-1b, 1d and 1f which result in the non-linear dependencies of L_{Sj} , L_{Mj} and L_{Lj} to light (Fig. 3-1a, 1c, 1e). An increase in L_{Sj} from PPF = 200 $\mu\text{mol m}^{-2}\text{s}^{-1}$ to PPF = 400 $\mu\text{mol m}^{-2}\text{s}^{-1}$ was due to the increase in l_{sj} (Fig. 3-1a). The decrease in L_{Sj} from PPF = 400 $\mu\text{mol m}^{-2}\text{s}^{-1}$ to PPF = 1300 $\mu\text{mol m}^{-2}\text{s}^{-1}$ was due to the increase in g_{sc} and the resulting decrease in relative change of g_{sc} (dg_{sc}/g_{sc} in Eqn 3-10a). In our analyses, g_m was assumed to be constant in the range of the

measuring light conditions (Yamori *et al.*, 2010b). Therefore, the dependency of L_{Mj} (Fig. 3-1c) was similar to the dependency of I_{mj} (Fig. 3-1d).

Quantitative limitation analysis for non-saturating light conditions may facilitate further studies on partitioning and quantifying the components of limitation to photosynthesis at canopy level (Chen *et al.*, 2014). This may be achieved with the help of a functional-structural plant model (FSPM), in which the plant structure, physiological functions and the interactions of both with environmental factors are described (Vos *et al.*, 2010). Combining quantitative limitation analysis and FSPM should give insights into the sources of photosynthetic limitations in the canopy (Chen *et al.*, 2014).

Salinity effects on photosynthesis

Conflicting opinions about the relative importance of the tolerance mechanisms to salinity can be found in the literature. Munns and Tester (2008) suggested that ‘*osmotic stress has a greater effect on growth rates than ionic stress.*’ However, several studies concluded that mechanisms related to ionic tolerance (e.g. Na^+ exclusion, tissue tolerance or K^+ homeostasis) have stronger influences on total plant tolerance (Shabala and Cuin 2008; Rajendran *et al.*, 2009). Here we quantified the effects of the osmotic and ionic components of salinity on cucumber photosynthesis by 1) comparing the regression coefficients of photosynthetic parameters of the multiple linear regression analyses (Eqn 3-14); and by 2) using quantitative limitation analyses. The quantities of photosynthetic limitations are shown as percentages of the reference values in Table 3-1.

Effects of osmotic stress

The decreases in photosynthesis in the osmotic phase are ascribed to the reductions of the CO_2 diffusion conductivities (g_{sc} and g_m) due to osmotic stress. Regression analyses show that osmotic stress has strong influence on g_{sc} and g_m and has no influence on biochemical capacity (V_{cmax} and J_{max} , Table 3-1), which is in accordance with the results in the literature (Drew *et al.*, 1990; Delfine *et al.*, 1999; James *et al.*, 2008; Flexas *et al.*, 2009; Rajendran *et al.*, 2009). To quantify the osmotic effects on g_{sc} , measurements should be taken before reaching toxic salt concentrations (James *et al.*, 2008). According to our results the stomatal limitation after 2 and 3 days of exposure to salinity increases by about 2.4% per 10 mM NaCl in the nutrient solution (Fig. 3-4a), similar to the modeling results

(Fig. 3-6a). Therefore, the reduction of cucumber photosynthesis due to the osmotic effects on g_{sc} would be about 9.6% under 40 mM NaCl.

Osmotic stress also increases the mesophyll limitation (L_{Mc}). An explanation would be that g_m responds quickly to the changed hydraulic conditions of the leaves (Chaves *et al.*, 2009; Flexas *et al.*, 2009; Flexas *et al.*, 2012). The rapid increase of L_{Mc} after exposure to salinity seems to be the effect of osmotic stress (Fig. 3-2 and Fig. 3-3). However, our results suggest that long-term impact of mesophyll limitation due to osmotic stress may be considerably less than other limiting factors. We propose three reasons for this. Firstly, the increase of mesophyll limitation due to osmotic stress was relatively small (6% of reference photosynthesis), which is in accordance with previous observations (in almond under drought, Egea *et al.*, 2011 and in barley under salinity, Pérez-López *et al.*, 2012). In contrast, stomatal and biochemical limitations may reach 30% (Fig. 3-5 and Fig. 3-6). Secondly, L_{Mc} in control plants on day 10 was higher than in 60 mM NaCl (Fig. 3-2a, 2d). This can be explained by the diffusional limitations being more prominent when the biochemical capacity is high (Chen *et al.*, 2014). Finally, mesophyll limitation is in general more prominent under saturating than non-saturating light (Fig. 3-1c, Fig. 3-2, Fig. 3-3). Since most of the leaves in the canopy operate under non-saturating light conditions, the contribution of mesophyll limitation to whole plant photosynthesis should be relatively small. One consideration would be that our measurements were conducted on the leaves developed and expanded before the commencement of salinity treatments. As salinity would change the anatomical structures of leaves developing under salinity (Hu *et al.*, 2005) and the leaf structure affects g_m (Tosens *et al.*, 2012), further studies providing insights into the impacts of salinity on mesophyll conductance are required.

Effects of ionic stress

At the end of the experiment, slight chlorosis, a symptom of ionic stress, was observed on the measured leaves in the 40 and 60 mM NaCl treatments. James *et al.* (2006) showed good linear relationships between S_1 and Na^+ concentrations in vacuole and in cytoplasm in barley and durum wheat. We assumed that this is also the case in cucumber. Their results suggest that the slopes and intercepts of these linear relationships could be different between genotypes due to their capacity in compartmentalizing sodium in different cells or organelles. Therefore, it is possible that a genotype which can compartmentalize more sodium in vacuole may have less negative values of n_x . Ion

accumulation in the leaves disturbs stomatal function (Tavakkoli *et al.*, 2011) and g_{sc} decreases with the salt concentrations in leaves (Gibberd *et al.*, 2002; James *et al.*, 2002). Therefore, it is not surprising that a significant decrease of g_{sc} with the Na^+ concentration in leaves, S_1 , was found ($n_{g_{sc}}$ in Table 3-1). So far, no study has shown that mesophyll limitation may be influenced by ionic stress, and our present results also suggest that there may be no ionic effects on mesophyll limitation (Table 3-1). Surprisingly, while regression analyses show that V_{cmax} and J_{max} decreased linearly with S_1 (Fig. 3-S4, parameter n_{vcmax} and n_{jmax} in Table 3-1), which is in accordance with the results in the literature (Drew *et al.*, 1990; Delfine *et al.*, 1999; James *et al.*, 2006), the increases in biochemical limitations with S_1 depended on the salinity level in the nutrient solution (S_s , Fig. 3-5c, 5d, 6c, 6d). These surprising relationships may be due the fact that osmotic stress induces stomata closure, which lowers C_c and reduces the relative importance of biochemical capacity and electron transport rate in limiting photosynthesis (see the section “Importance of quantitative limitation analysis under non-saturating light condition”). It indicates that 1) osmotic stress reduces biochemical limitations and 2) the ionic effect on g_{sc} reduces the importance of biochemical limitation (especially at 60 mM NaCl in the nutrient solution, Fig. 3-6c, 6d). Therefore, photosynthesis of a leaf with high S_s and high S_1 will be predominantly limited by g_{sc} (Fig. 3-6a, 6b). This explains the prevailing opinions that the photosynthesis under salinity is mostly restricted by diffusional limitations (James *et al.*, 2002; Loreto *et al.*, 2003; Flexas *et al.*, 2004; Chaves *et al.*, 2009; Pérez-López *et al.*, 2012). Moreover, our results suggest that improvement of stomatal regulation under ionic stress would be the most important mechanism to alleviate salinity stress in cucumber.

Salinity effects on water use efficiency

High WUE can be achieved by several physiological mechanisms: 1) increase of mesophyll conductance (Flexas *et al.*, 2012), 2) decrease of stomatal conductance and 3) increase in biochemical capacity. In this study, the relatively small reduction of photosynthesis due to g_m indicates that the first mechanism would not have a great effect on WUE improvement for cucumber, a species with relatively high mesophyll conductance in comparison with other species (Loreto *et al.*, 1992). The clear linear relationships between intrinsic WUE (iWUE, $\mu\text{mol CO}_2 \text{ mol}^{-1} \text{ H}_2\text{O}$) and stomatal limitation (Fig. 3-7c, 7f) also strongly suggest that increasing WUE by reducing g_{sc} would always be associated with a loss of assimilation. These results provide an explanation of

the inverse relationship between WUE and yield, which has often been observed (Condon *et al.*, 2004), and suggest that WUE could be improved by improvements in maintenance of biochemical capacity. Therefore, mechanisms reducing the ionic effects on biochemical capacity may be of primary importance in maintaining high WUE under salinity.

Conclusion

Using experimental data and a modeling approach, we disentangled the contribution of osmotic and ionic stress on different components of photosynthetic limitations. Our data suggest that the improvement of stomatal regulation under ionic stress would be the most effective way to alleviate salinity stress in cucumber, a salt-sensitive species. Non-linear dependencies of stomatal, mesophyll and light limitations on light intensity, and the intriguing interactions between osmotic and ionic effects on photosynthetic limitations suggest that quantitative limitation analysis for saturating light conditions do not represent the photosynthetic limitation at canopy level. We suggest future research on combining functional-structural plant modelling and quantitative limitation analysis to quantify the effects of salinity on photosynthetic limitations on the canopy level.

Chapter 4

Architectural and functional limitations of whole-plant cucumber photosynthesis under salinity

Tsu-Wei Chen¹, Katrin Kahlen², Hartmut Stützel¹

¹*Institute of Horticultural Production Systems, Leibniz Universität Hannover, Herrenhäuser Straße 2, 30419 Hannover, Germany* ²*Department of Vegetable Crops, Geisenheim University, Von-Lade-Straße 1, 65366 Geisenheim, Germany*

Abstract

Most of the crop species are glycophytes and salinity stress is one of the most severe abiotic stress reducing crop yields worldwide. Salinity affects plant architecture and physiological functions but there is no quantitative assessment of the relative impacts of these effects on whole plant photosynthetic limitations. Using cucumber (*Cucumis sativus*, a salt sensitive species) grown at three salinity levels in the nutrient solution as an example, this work aimed to systematically and quantitatively assess the impacts of architectural and functional limitations to whole plant photosynthesis due to salinity during different developmental stages and at different light environments. Combining functional-structural plant model (FSPM) and quantitative limitation analysis, functional limitations were further dissected into stomatal (L_s), mesophyll (L_m) and biochemical (L_b) limitations. Architectural limitations had greater impact on photosynthesis than functional limitations, especially under high salinity. Relative importance of diffusional limitations ($L_s + L_m$) increased with salinity level and light intensity above the canopy. Our results suggest that architectural limitations are related to the hydraulic processes of the plant, and functional limitations were mainly due to toxic effects of Na^+ accumulation in leaves affecting stomatal regulation. Based on these results, possibilities to improve whole plant photosynthesis under salinity are proposed.

Key words: Plant architectural, photosynthetic limitation, canopy level, salinity, osmotic stress, ionic stress, light environment, functional-structural plant model

Introduction

Salinity stress is one of the most severe abiotic stresses reducing crop yields worldwide (Munns & Tester, 2008). It affects both plant architecture and physiological functions. Typical salinity effects on whole plant architecture are the reduction in organ size, e.g. leaf area (Rajendran *et al.*, 2009; Harris *et al.*, 2010), which affect canopy light interception, light distribution within the canopy and the size of photosynthetic apparatus (referred to as architectural effects). Salt in the soil and salt accumulation in the leaves (mainly Na⁺, James *et al.*, 2002; Stępień & Kłobus, 2006; Shapira *et al.*, 2009) disturb stomatal regulation, increase diffusional resistance to CO₂ transport to the chloroplast, and reduce biochemical capacity and light use efficiency (referred to as functional effects, Delfine *et al.*, 1999; James *et al.*, 2006). Both architectural and functional effects of salinity limit whole plant photosynthesis and consequently yields (for this reason, they are also referred to as architectural or functional limitations in this article).

Although there are some speculations in the literature about the relative impact of different components of salinity effects on photosynthesis (for example, Munns, 1993; Munns & Tester, 2008; Rajendran *et al.*, 2009; Pérez-López *et al.*, 2012), no quantitative assessment of these impacts at the whole plant level exists in the literature. The major difficulty of this assessment might its multi-dimensionality. One dimension is the up-scaling from leaf to whole plant level. Within a plant, there are drastic gradients and heterogeneity, particularly the light gradients and the variations in leaf functional traits (Niinemets *et al.*, 2015). From the within-canopy heterogeneities results that the quantitative assessment of salinity effects on photosynthesis obtained from leaf level (e.g., Pérez-López *et al.*, 2012) and the whole plant level would not necessarily correspond. This argument is supported by both theoretical and experimental results showing that the compositions of photosynthetic limitations vary between different canopy layers (see Chen *et al.*, 2014b and Cano *et al.*, 2013, respectively). Furthermore, Chen *et al.* (2015) have also shown the complex interactions between light interception, Na⁺ concentration in the leaves and the compositions of photosynthetic limitations under different salinity levels in the nutrient solution. Their results imply that 1) the compositions of photosynthetic limitations depend on the light interception of a leaf, and 2) within-canopy variations in leaf age, which is usually associated with the Na⁺ concentration in the leaf under salinity, (Munns, 1993; Munns & Tester, 2008), should be considered in the quantitative assessment of photosynthetic limitations under salinity. The second dimension is time: the architectural and functional properties of a canopy change with its

developmental stages. Recently, it has been demonstrated that the dynamic development of canopy architecture has to be taken into account when quantifying the impact of a plant trait, such as internode length and leaf angle, on canopy photosynthesis (Chen *et al.*, 2014a). Furthermore, the environmental effects on physiological functions generate other dimensions, e.g. severity of salinity, light condition and temperature. This multi-dimensionality makes it experimentally almost impossible to quantify the different components of salinity stress on whole plant photosynthesis.

Because of these difficulties in assessing photosynthetic limitations at the whole plant level, several different speculations about the relative importance of these limitations can be found in the literature. For example, it has been proposed that the reduction in leaf area and stomatal closure due to the osmotic components of salinity have greater impact on growth than physiological disturbances due to ion accumulation in the plant (Munns & Tester, 2008). In contrast, it has also been proposed that ion exclusion and tolerance to toxic ions in leaves are the main mechanisms to maintain plant growth under salinity (Rajendran *et al.*, 2009). There are prevailing opinions considering stomatal conductance the primary photosynthetic limitation under salinity (Centritto *et al.*, 2003; Flexas *et al.*, 2004; Pérez-López *et al.*, 2012), while there are data showing that biochemical limitation is equally or even more prominent than stomatal limitation (Drew *et al.*, 1990; Chen *et al.*, 2015). According to the quantitative limitation analysis of photosynthesis proposed by Grassi and Magnani (2005), the functional limitations to leaf photosynthesis can be quantitatively dissected into stomatal, mesophyll and biochemical limitations (Grassi & Magnani, 2005; Pérez-López *et al.*, 2012; Chen *et al.*, 2015). This approach has been demonstrated to be a useful tool for dissecting the contributions of physiological parameters to photosynthetic limitations under saturating light conditions (Grassi & Magnani, 2005; Flexas *et al.*, 2009; Egea *et al.*, 2011; Cano *et al.*, 2013). Recently, quantitative limitation analysis has been extended to non-saturating light conditions (Chen *et al.*, 2014b). More recently, an alternative approach of quantitative limitation analysis has been proposed to partition photosynthetic limitations into more variables (Buckley & Diaz-Espejo, 2015). These new approaches allow studying the effects of diurnal and seasonal climatic variations on photosynthetic rate (Chen *et al.*, 2014b; Chen *et al.*, 2015). Combining the quantitative limitation analysis and functional-structural plant model (FSPM), Chen *et al.* (2014b) have shown the possibility to scale up the contributions of different physiological traits to photosynthetic limitations from leaf to whole plant level. The main advance of FSPM is that the interactions between plant architecture, physiological functions and microclimate (mainly light environment of

individual leaves within the canopy) can be simulated (Vos *et al.*, 2010). This advance may overcome the difficulty in assessing the impacts of various components of salinity on plant growth. However, in the work of Chen *et al.* (2014b), the magnitude of stomatal limitations depends on the total leaf area of the plant. Therefore, whole plant photosynthetic limitations for different plants (e.g. stressed and non-stressed plant, or the same plant at different developmental stages), differing in leaf area, are not comparable based on their approach.

Cucumber is a salt sensitive crop (Stępień & Kłobus, 2006) and often subjected to saline conditions in the greenhouse production systems (Savvas *et al.*, 2005). Using cucumber plants grown in a single-stem training system as a model system, this work aims to systematically dissect the impacts of architectural and functional responses of plants to salinity on whole plant photosynthesis. This was achieved in three steps: 1) to analyze the salinity effects on canopy light interception efficiency and light use efficiency at different developmental stages; 2) to propose a revised approach of Chen *et al.* (Chen *et al.*, 2014b), which is able to dissect the contributions of different physiological processes to whole plant photosynthetic limitations; 3) to quantify the architectural and functional (i.e. stomatal, mesophyll and biochemical) limitations of salinity at different developmental stages, light environments and severity of salinity by using an FSPM.

Materials and Methods

Plant materials

Cucumber seeds (*Cucumis sativus* 'Aramon' Rijk Zwaan, De Lier, the Netherlands) were sown in rock-wool cubes (36 mm x 36 mm x 40 mm) on 12 June 2013. Seven days after sowing, seedlings were transplanted into larger rock-wool cubes (10 cm x 10 cm x 6.5 cm). On 25 June, plants were transplanted on rock-wool slabs (Grodan, Grodania A/S, Hedehusene, Denmark) in two greenhouses (two replications) of the Institute of Horticultural Production Systems, Leibniz Universität Hannover, Germany (lat. 52°23'N, long. 9°37'E). The greenhouses were heated to maintain 22/20°C day/night temperature and roof ventilation was opened when the inside temperature was higher than 24°C during the whole experiments. Each litre of the standard nutrient solution contained 0.5 g Ferty Basisdünger 2 (Planta GmbH, Regenstauf, Germany, 0.9 mM NO₃⁻, 1.5 mM NH₄⁻, 2.8 mM K⁺, 3.0 mM Ca²⁺, 0.4 mM Mg²⁺, 0.4 mM H₂PO₄, as well as adequate amounts of the micronutrients) and extra 0.9 g Ca(NO₃)₂ was added in the solution (5.5 mM Ca²⁺ and 11 mM NO₃⁻) after the first fruit set. In each greenhouse, 50 cucumber plants were grown

in five rows (north-south oriented). Plant and row distances were 60 and 120 cm, respectively. The plants in the left and right border rows were not used for measurements and irrigated with the standard nutrient solution. Three different salinity levels, obtained by adding 0, 25 and 50 mM NaCl to the standard nutrient solution, were randomly applied to the three rows in the middle on 08 July 2013. The northernmost and southernmost plants in the three middle rows were also border plants, which were not used for measurements. All side shoots were removed to maintain monopodial growth and plants were decapitated at the 25th leaf to maintain a canopy height of two metres. Whole plants were harvested on day 35 after exposure to salinity (DAS). Leaf area (measured by LI-COR 3100 area meter, LI-COR, Lincoln, USA), fresh weight of leaf, fruit, internode and petiole were measured. Dry weights were measured after drying at 70°C for at least 72 hours. Weather data during the experiment was recorded by the sensors above and inside the greenhouse (see Fig. 4-S1).

Plant digitizing

The whole plant architectures of cucumber plants were digitized weekly by a 3D digitizer (Fastrak, Polhemus, USA). For internodes, petioles and fruits, the 3D coordinates of the beginning and end points were recorded and their lengths were calculated by these coordinates. For leaves, 13 points per leaf lamina were digitized. Using these points, a leaf lamina was reconstructed with 10 predefined triangles. Details are described in Chen *et al.* (2014b). Three plants per salinity level were digitized on 0, 7, 14, 21, 28 and 35 DAS. In the end of the experiment, the leaf area measured with a leaf area meter and the area estimated by plant digitization were compared to ensure the accuracy of plant digitization.

Simulating the virtual canopies and light interceptions of the leaves

Using the digitized data, cucumber plants were reconstructed in *GroIMP* (Kniemeyer, 2008) according to Chen *et al.* (2014b). For constructing the virtual canopy structure, 50 cucumber plants were distributed in 5 rows and distances between virtual plants in a row and between rows were 60 cm and 120 cm, respectively, as in the experiment (1.39 plants per m²). Two reconstructed one-row canopies are shown in Fig. 4-1. To simulate the light environment, the virtual canopy was surrounded by sun and sky providing direct and diffuse light, respectively (79% direct light and 21% diffuse light). The sun was a single object providing light in the direction of the corresponding location (Hannover, Germany, lat. 52°23'N, long. 9°37'E) and time (at 1200 h on the dates of digitizing).

Photosynthetically active radiation (PAR) above the canopy was assumed to be $600 \mu\text{mol m}^{-2}\text{s}^{-1}$, similar to the daily average during the experiment (Fig. 4-S1). The sky was approximated by an array of 72 directional light sources arranged in a hemisphere. For computing the light distribution a ray-tracer, integrated into *GroIMP*, was used with 10 million rays and a recursion depth of 10 reflections (Buck-Sorlin *et al.*, 2011). Leaf absorption, transmission and reflection of PAR were 87%, 7% and 6%, respectively (Kahlen *et al.*, 2008). The ground in the model (30m x 30m), above which the virtual canopy was constructed, was assumed to absorb 80% and reflect 20% of the incident PAR.

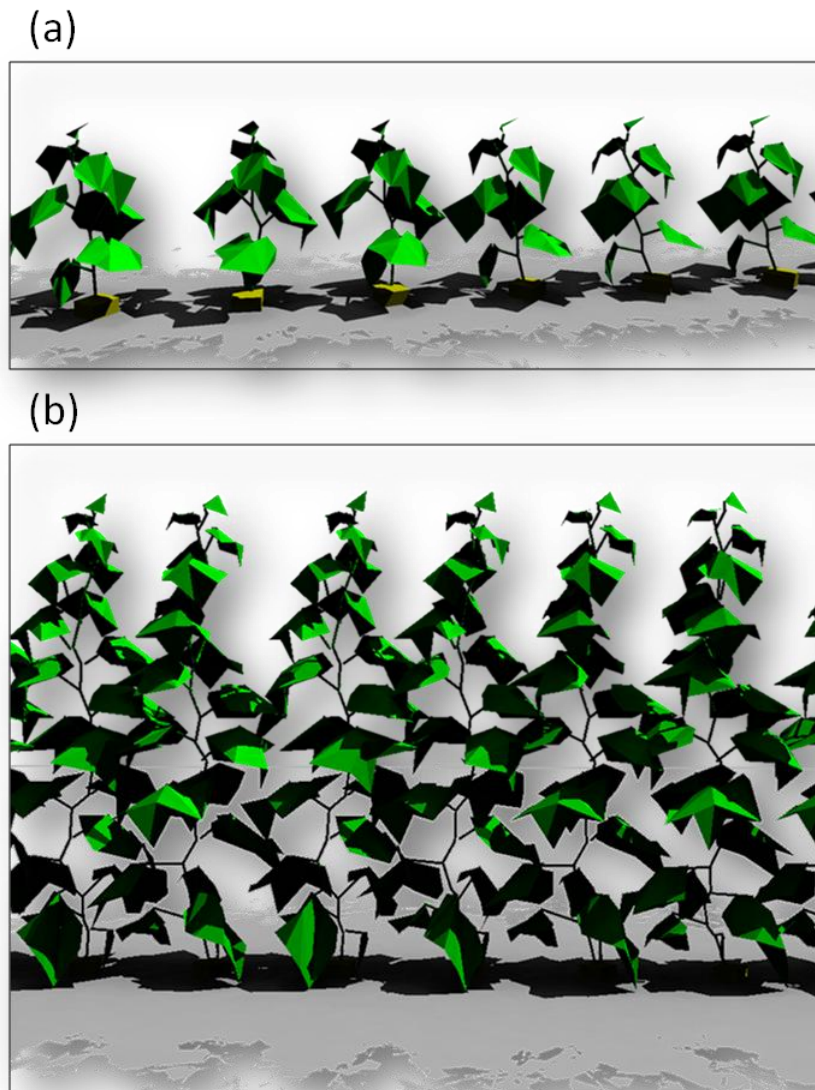


Figure 4-1. Side view of the 3D virtual cucumber canopies on day 0 (a) and day 14 (b) after exposure to 50 mM NaCl salinity. For a clear visual representation, only six plants in one row are shown, instead of 50 plants in five rows used for the simulations. Plants are reconstructed in *GroIMP* by digitized data.

Modelling leaf photosynthesis

For all simulations leaf temperature was assumed to be 25°C and ambient CO₂ concentration (C_a) was 380 $\mu\text{mol mol}^{-1}$. Leaf photosynthesis under non-stressed condition was simulated based on Chen *et al.* (2014b). In short, stomatal conductance was simulated based on the model proposed by Medlyn *et al.* (Medlyn *et al.*, 2011):

$$g_{sc} = g_0 + \left(1 + \frac{g_1}{\sqrt{D}}\right) \frac{A}{C_a} \quad (\text{Eqn 4-1})$$

where D is leaf-to-air vapour pressure deficit (1.2 kPa assuming a relative humidity in the greenhouse of around 60%), parameters g_0 and g_1 are the minimum stomatal conductance and an empirical parameter respectively, and A ($\mu\text{mol CO}_2 \text{ m}^{-2} \text{ s}^{-1}$) is the minimum of the RuBP-regeneration-limited and Rubisco-carboxylation-limited photosynthesis rate (A_j and A_c , respectively, $\mu\text{mol CO}_2 \text{ m}^{-2} \text{ s}^{-1}$, Farquhar *et al.*, 1980):

$$A_c = \frac{V_{cmax} (C_c - \Gamma_*)}{C_c + K_c (1 + O/K_o)} - R_d \quad (\text{Eqn 4-2})$$

$$A_j = \frac{J(C_c - \Gamma_*)}{4C_c + 8\Gamma_*} - R_d \quad (\text{Eqn 4-3})$$

where V_{cmax} is the maximum rate of Rubisco carboxylation ($\mu\text{mol CO}_2 \text{ m}^{-2} \text{ s}^{-1}$), Γ_* is the CO₂ compensation point in the absence of dark respiration (for cucumber: 43.02 $\mu\text{mol mol}^{-1}$, Grassi & Magnani, 2005), K_c (404 $\mu\text{mol mol}^{-1}$) and K_o (278 mmol mol^{-1}) are Michaelis-Menten constants of Rubisco for CO₂ and O₂, O (210 mmol mol^{-1}) is mol fraction of O₂ at the site of carboxylation, R_d is the respiration rate. C_c (chloroplastic CO₂ concentration, $\mu\text{mol mol}^{-1}$) and J (rate of electron transport, $\mu\text{mol m}^{-2} \text{ s}^{-1}$) were calculated by (Chen *et al.*, 2014b):

$$C_c = C_a - A \left(\frac{1}{g_{sc}} + \frac{1}{g_m} \right) \quad (\text{Eqn 4-4})$$

$$J = \frac{(\kappa_{2LL} \cdot I_{ab} + J_{max} - \sqrt{(\kappa_{2LL} \cdot I_{ab} + J_{max})^2 - 4\theta \cdot J_{max} \cdot \kappa_{2LL} \cdot I_{ab}})}{2\theta} \quad (\text{Eqn 4-5})$$

where g_m is mesophyll conductance ($\text{mol m}^{-2} \text{ s}^{-1}$), I_{ab} is intercepted PAR ($\mu\text{mol photons m}^{-2} \text{ s}^{-1}$), J_{max} is the maximum electron transport rate ($\mu\text{mol e}^- \text{ m}^{-2} \text{ s}^{-1}$), κ_{2LL} is a constant describing the conversion efficiency of I_{ab} to J (0.425 $\text{mol e}^- \text{ mol}^{-1} \text{ photons}$) and θ is a constant convexity factor describing the response of J to I_{ab} (0.7). The dependency of V_{cmax} , J_{max} , g_m and R_d on leaf age is fitted to a log-normal curve (Irving & Robinson, 2006):

$$X_n(t) = X^{\text{ref}} e^{(-0.5(\log(t/t_{max})/c_{sd})^2)} \quad (\text{Eqn 4-6})$$

where $X_n(t)$ is the photosynthetic variable on day t under non-stressed conditions, X^{ref} is the maximum of the variables, t_{max} is the time (day) when the X_{max} occurs, and c_{sd} is curve standard deviation. Because of the good coordination between V_{cmax} , J_{max} , g_m and R_d (Egea *et al.*, 2011; Buckley *et al.*, 2013; Chen *et al.*, 2014b), parameters t_{max} and c_{sd} for them are the same. Finally, A_j , A_c , g_{sc} and C_c were obtained by solving Eqns 4-1, 4-2, 4-3 and 4-4 analytically. To avoid the discontinuity at the transition point between A_j and A_c functions, if the difference between A_j and A_c was smaller than 5% of their average, photosynthesis was considered to be co-limited by both Rubisco-carboxylation and RuBP-regeneration rate (Yamori *et al.*, 2010; Yamori *et al.*, 2011). In this case, A is the interpolation between A_j and A_c . A similar approach can be found in other modelling studies (Peltoniemi *et al.*, 2012; Buckley *et al.*, 2013).

The effects of osmotic and ionic stresses on photosynthetic variables X are assumed to be additive and can be described by (Chen *et al.*, 2015):

$$X_{\text{stress}}(t, S_s, S_l) = (1 + m_x S_s + n_x S_l) \cdot X_n(t) \quad (\text{Eqn 4-7})$$

where $X_{\text{stress}}(t)$ and $X_n(t)$ are the photosynthetic variables X (g_{sc} , g_m , V_{cmax} , and J_{max}) under stressed and non-stressed conditions, respectively; S_s and S_l are the sodium concentrations in the nutrient solution and in the leaf water (mM), respectively; and m_x and n_x are empirical parameters for osmotic and ionic effects of salt, respectively. The parameter values were taken from Chen *et al.* (2015). All parameters and their values are listed in Table 4-1.

Evaluation of the photosynthesis model

The 3rd and 8th leaves of the plants were measured using a portable gas exchange system (Li-6400; Licor, Lincoln, NE, USA) at $C_a = 380 \mu\text{mol mol}^{-1}$, leaf temperature = 25°C, incoming light = 600 and 1300 $\mu\text{mol m}^{-2}\text{s}^{-1}$ (average daily light intensity and saturating light intensity, respectively) and relative humidity $\approx 65\text{-}70\%$, corresponding to the model conditions. Eight leaves per treatment were measured 3, 6, 9, 12, 15, 19 and 23 DAS. All measurements were conducted between 0900 h and 1400 h.

Chemicals analyses

After gas exchange measurements, the measured part of the leaf was cut (circa 300 cm²) and the fresh weight and cut area were recorded. Leaf samples were weighed after drying at 70°C for 72 hours for recording dry weight, then ground into fine powder. For sodium

analysis, 50-100 mg of the powder was dry ashed at 500°C and subsequently dissolved in nitric acid before being measured by an atom absorption spectrometer (Perkin Elmer, 1100B, USA). Na⁺ concentration in the leaf water (mM) was used as input for the photosynthesis model. Furthermore, Na⁺ concentrations in leaves 3, 6, 8, 10, 13, 15, 18, 20, 23 and 25 were also measured on day 35 after the whole-plant harvest. The measured relationships between the time of a leaf grown under salinity (d) and Na⁺ concentrations in that leaf were used to estimate the Na⁺ concentrations in leaves of the simulated canopies.

Table 4-1. Parameter list of the photosynthesis model.

Parameters (Eqn)	Description	Value and unit
<i>Environmental parameters</i>		
D (4-1)	Leaf-to-air vapour pressure deficit	1.2 kPa
C_a (4-1, 4)	Ambient CO ₂ concentration	380 $\mu\text{mol mol}^{-1}$
O (4-2)	mol fraction of O ₂ at the site of carboxylation	210 mmol mol^{-1}
<i>Physiological parameters</i>		
g_0 (4-1)	Minimum stomatal conductance	0.09 $\text{mol m}^{-2}\text{s}^{-1}$
g_1 (4-1)		3.51
Γ^* (4-2, 3)	CO ₂ compensation point in the absence of dark respiration	43.02 $\mu\text{mol mol}^{-1}$
K_c (4-2)	Michaelis-Menten constants of Rubisco for CO ₂	404 $\mu\text{mol mol}^{-1}$
K_o (4-2)	Michaelis-Menten constants of Rubisco for O ₂	278 mmol mol^{-1}
K_{2LL} (4-5)	conversion efficiency of I_{ab} to J	0.425 $\text{mol e}^- \text{mol}^{-1} \text{photons}$
θ (4-5)	constant convexity factor	0.7
g_{sc}^{ref} (4-8,9)	Maximum value of g_{sc}	0.55 $\text{mol m}^{-2}\text{s}^{-1}$
g_m^{ref} (4-6,8,9)	Maximum value of g_m	0.8 $\text{mol m}^{-2}\text{s}^{-1}$
V_{cmax}^{ref} (4-6,8)	Maximum value of V_{cmax}	140.7 $\mu\text{mol m}^{-2}\text{s}^{-1}$
J_{max}^{ref} (4-6,9)	Maximum value of J_{max}	191.1 $\mu\text{mol m}^{-2}\text{s}^{-1}$
R_d^{ref} (4-6,8)	Maximum value of R_d	1.08 $\mu\text{mol m}^{-2}\text{s}^{-1}$
b (4-6)	Leaf age when the X_{max} occurs	8.56 day
c (4-6)	Curve standard deviation	0.662
m_{gsc} (4-7)	Osmotic effect on g_{sc}	$-6.15 \cdot 10^{-3}$
m_{gm} (4-7)	Osmotic effect on g_m	$-9.34 \cdot 10^{-3}$
m_{vcmax} (4-7)	Osmotic effect on V_{cmax}	0
m_{jmax} (4-7)	Osmotic effect on J_{max}	0
m_{rd} (4-7)	Osmotic effect on R_d	0
n_{gsc} (4-7)	Ionic effect on g_{sc}	$-2.69 \cdot 10^{-3}$
n_{gm} (4-7)	Ionic effect on g_m	0
n_{vcmax} (4-7)	Ionic effect on V_{cmax}	$-2.84 \cdot 10^{-3}$
n_{jmax} (4-7)	Ionic effect on J_{max}	$-2.06 \cdot 10^{-3}$
n_{rd} (4-7)	Ionic effect on R_d	0

Quantitative limitation analyses at leaf level

The relative change of photosynthesis under RuBP-regeneration-limited (dA_j/A_j) and Rubisco-carboxylation-limited conditions (dA_c/A_c) can be described as (Chen *et al.*, 2014b):

$$\frac{dA_j}{A_j} = l_{sj} \cdot \frac{dg_{sc}}{g_{sc}} + l_{mj} \cdot \frac{dg_m}{g_m} + l_{ej} \cdot \frac{dJ_B}{J} + l_{ej} \cdot \frac{dJ_I}{J} = L_{sj} + L_{mj} + L_{bj} + L_{lj} \quad (\text{Eqn 4-8})$$

$$\frac{dA_c}{A_c} = l_{sc} \cdot \frac{dg_{sc}}{g_{sc}} + l_{mc} \cdot \frac{dg_m}{g_m} + l_{bc} \cdot \frac{dV_{cmax}}{V_{cmax}} = L_{sc} + L_{mc} + L_{bc} \quad (\text{Eqn 4-9})$$

where the subscripts j and c denote the RuBP-regeneration-limited and Rubisco-carboxylation-limited conditions, respectively; the subscripts s , m , b and l indicate the contributions of stomatal conductance, mesophyll conductance, biochemical capacity and light to photosynthetic limitation; l_s , l_{mc} , l_e and l_b are the *relative* limitations of stomatal and mesophyll conductance, electron transport rate and biochemical capacity, respectively; J_{dB} and J_{dI} are the changes of electron transport rate due to biochemical capacity and irradiance, respectively. A complete description of Eqns 4-8 and 4-9 can be found in Chen *et al.* (2015). Furthermore, if photosynthesis is co-limited by both Rubisco-carboxylation and RuBP-regeneration rate, photosynthetic limitation, for example, stomatal limitation, is the linear interpolation between L_{sj} and L_{sc} .

Revised approach of quantitative limitation analyses at whole plant level

The photosynthetic limitations at whole plant levels were computed by summing up the limitations of all leaves of a plant (Chen *et al.*, 2014b). For example, the stomatal limitation of a plant with n leaves (L_{sW} , $\mu\text{mol CO}_2 \text{ plant}^{-1} \text{ s}^{-1}$) can be calculated by:

$$L_{sW} = A_{\max}^{\text{ref}} \cdot \sum_{k=1}^n L_{s,k} \cdot LA_k \quad (\text{Eqn 4-10})$$

where A_{\max}^{ref} ($\mu\text{mol CO}_2 \text{ m}^{-2} \text{ s}^{-1}$) is the reference photosynthesis rate, calculated by assuming that all photosynthetic parameters reach their maximums simultaneously, LA_k is the area of leaf k (m^2), $L_{s,k}$ is the stomatal limitation of leaf k (% of A_{\max}^{ref}). L_{sW} represents the whole plant stomatal limitation. Since the magnitude of L_{sW} depends on the total leaf area of a plant, which differs between developmental stages and between salinity levels, L_{sW} between salt treatments and developmental stages is not comparable. Therefore, the whole plant stomatal limitation was normalized by the whole plant leaf area:

$$L_{sP} = \frac{A_{\max}^{\text{ref}} \cdot \sum_{k=1}^n L_{s,k} \cdot LA_k}{A_{\max}^{\text{ref}} \cdot \sum_{k=1}^n LA_k} = \frac{\sum_{k=1}^n L_{s,k} \cdot LA_k}{\sum_{k=1}^n LA_k} \quad (\text{Eqn 4-11})$$

L_{sP} represents the average of the whole plant stomatal limitation (%). Whole plant mesophyll (L_{mP}), biochemical (L_{bP}) and light (L_{lP}) limitations were calculated by the same way. The compositions of whole plant limitations were quantified for different salinity level (0, 25 and 50 mM NaCl in the nutrient solution), developmental stages (0, 7, 14, 21, 28 and 35 DAS) and light intensities above the canopy (150, 300, 600, 900 and 1200 $\mu\text{mol m}^{-2}\text{s}^{-1}$).

Disentangling the architectural and functional effects of salinity on whole plant photosynthesis

The architectural effects ($E_{a,x}$, %) and functional effects ($E_{f,x}$, %) of salinity on cucumber canopy photosynthesis under x mM NaCl were quantified by:

$$E_{a,x} = \frac{(P_{W,0} - P_{W,ax})}{P_{W,0}} \quad (\text{Eqn 4-12a})$$

$$E_{f,x} = \frac{(P_{W,ax} - P_{W,x})}{P_{W,0}} \quad (\text{Eqn 4-12b})$$

where $P_{W,0}$, $P_{W,ax}$, and $P_{W,x}$ are the simulated whole plant photosynthesis rate ($\mu\text{mol plant}^{-1}\text{s}^{-1}$) of plants under non-stressed condition, plants with x mM NaCl architecture but non-stressed photosynthetic capacity, and plants under x mM NaCl, respectively. The term $P_{W,0} - P_{W,ax}$ in Eqn 4-12a represents the difference in simulated whole plant photosynthesis between non-stressed and stressed canopies having the same photosynthetic capacity (but differing in size of photosynthetic apparatus). Therefore, this difference should be a result of reduced leaf area and changed plant architecture under salinity (the architectural effects). Since $P_{W,x}$ represents the photosynthesis of plants under x mM NaCl, the term $P_{W,ax} - P_{W,x}$ in Eqn 4-12b is the reduction of photosynthesis due to the salinity effects on photosynthetic function (the functional effect). Furthermore, canopy light use efficiency (ϵ_i , $\mu\text{mol CO}_2 \text{ mmol}^{-1} \text{ photon}$) was obtained from dividing whole plant photosynthesis rate ($\mu\text{mol CO}_2 \text{ plant}^{-1}\text{s}^{-1}$) by whole plant light interception ($\text{mmol photon plant}^{-1}\text{s}^{-1}$).

Statistical analysis

Only the simulated results from the two plants in the middle of the middle row were taken for the statistical analysis. To avoid model artefacts, simulations for each digitized plant were repeated 10 times, each run with a slight difference in the plant orientation ($\pm 30^\circ$) in the virtual canopy. Average values of the 10 replications were used for data analyses. The whole plant light interception efficiency (ϵ_i , unitless) and light use efficiency (ϵ_u) were:

$$\varepsilon_i = I_p \cdot D_p / I_{inc} \quad (\text{Eqn 4-13a})$$

$$\varepsilon_u = P_W / I_p \quad (\text{Eqn 4-13b})$$

where I_p is the light absorption per plant ($\mu\text{mol photon plant}^{-1} \text{s}^{-1}$), D_p is the plant density (plant m^{-2} ground area), I_{inc} is the total income radiation ($\mu\text{mol photon m}^{-2}$ ground area s^{-1}) and P_W is the whole plant photosynthesis rate ($\mu\text{mol plant}^{-1}\text{s}^{-1}$). All statistical analyses were conducted in *R* (v.2.12.0; R Foundation for Statistical Computing). The root mean square deviation (RMSD) and bias of photosynthesis model were evaluated based on Kobayashi and Salam (Kobayashi K & Salam MS., 2000).

Results

The digitized leaf area was in good agreement with leaf area measured by leaf area meter (Table 4-2). Plant digitizing detected the salinity effects on leaf area (Table 4-2), petiole length and internode length (data not shown). On day 35 after exposure to salinity (DAS), total shoot dry weights between treatments were different (291 ± 9 , 223 ± 5 and 140 ± 5 g for plant grown under 0, 25 and 50 mM NaCl, respectively). Strong relationships between the time of a leaf grown under salinity and Na^+ concentrations in that leaf were found (Fig. 4-2).

Table 4-2. Measured whole plant leaf area (LA, m^2) and simulated light interception efficiency (ε_i , unit-less).

Day after salinity start	LA			ε_i		
	0 mM	25 mM	50 mM	0 mM	25 mM	50 mM
0 ^A	0.22±0.02 ^a	0.21±0.05 ^a	0.21±0.01 ^a	0.24±0.06 ^a	0.25±0.05 ^a	0.25±0.06 ^a
7 ^A	0.77±0.01 ^a	0.69±0.05 ^a	0.59±0.11 ^a	0.48±0.07 ^a	0.52±0.06 ^b	0.46±0.06 ^a
14 ^A	1.61±0.13 ^a	1.39±0.15 ^{ab}	1.11±0.08 ^b	0.75±0.07 ^a	0.66±0.07 ^b	0.63±0.12 ^b
21 ^A	2.02±0.13 ^a	1.69±0.12 ^b	1.15±0.07 ^c	0.80±0.11 ^a	0.70±0.06 ^b	0.68±0.04 ^b
28 ^A	2.05±0.11 ^a	1.81±0.09 ^a	1.07±0.12 ^b	0.77±0.10 ^a	0.79±0.10 ^a	0.68±0.06 ^b
35 ^A	2.18±0.15 ^a	1.74±0.03 ^b	1.07±0.14 ^c	0.78±0.08 ^a	0.72±0.08 ^b	0.72±0.10 ^b
35 ^B	2.16±0.10 ^a	1.77±0.06 ^b	0.94±0.02 ^c			

^A measured by plant digitizing; ^B measured by leaf area meter.

Evaluation of photosynthetic model of salinity stress

The model slightly underestimated photosynthetic rate (A_{net} , $\mu\text{mol m}^{-2} \text{s}^{-1}$, Fig. 4-3a and Table 4-3). The intercept and the slope of the regression line were 1.81 ± 0.79 and 0.96 ± 0.06 , respectively (95% confidence interval (CI) of the intercept was 0.23-3.39; 95% CI of the slope was 0.85-1.08). Stomatal conductance to CO_2 (g_{sc} , $\text{mol m}^{-2} \text{s}^{-1}$) was

slightly overestimated by the model (Fig. 4-3b). The intercept and the slope of the regression line were 0.01 ± 0.01 and 0.79 ± 0.07 , respectively (95% CI of the intercept was -0.02 - 0.03 ; 95% CI of the slope was 0.64 - 0.94). No dependencies of the bias of A_{net} and g_{sc} to leaf age, A_{net} and Na^+ concentrations in leaf were found (Fig. 4-S2).

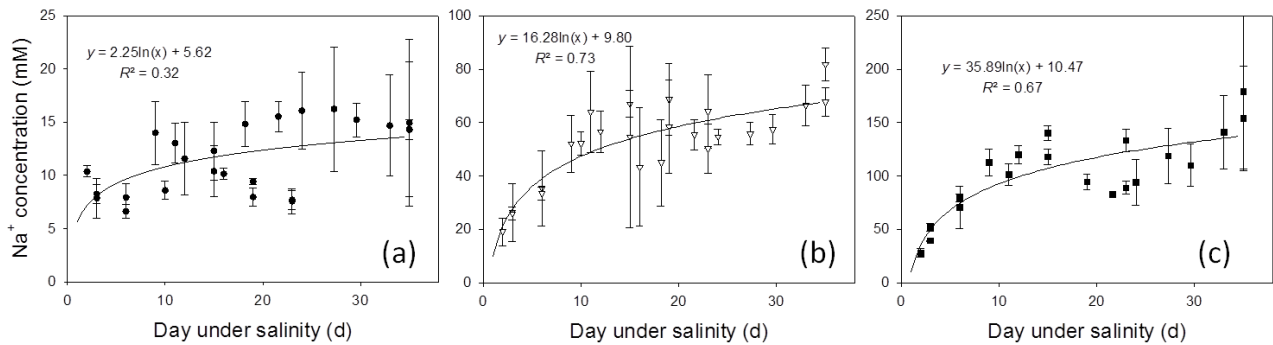


Figure 4-2. Relationships between day under salinity and Na^+ concentrations in leaf water under 0 mM (a), 25 mM (b) and 50 mM (c) NaCl. These relationships were used to estimate the Na^+ concentrations in leaves for simulating canopy photosynthesis. Each point and bar represents the average and standard deviation of four leaves.

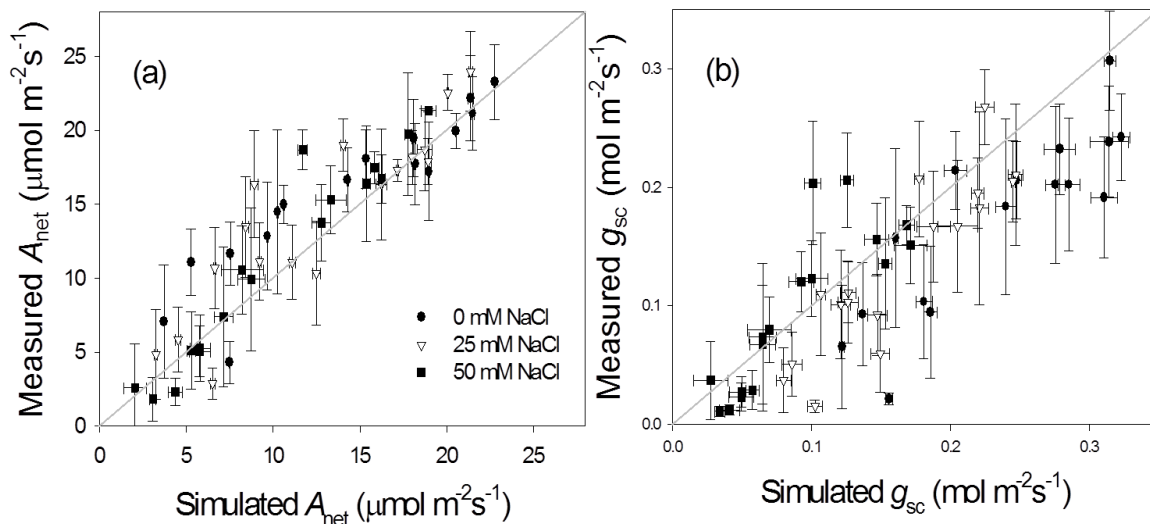


Figure 4-3. Measured and simulated simulated photosynthesis rate (A_{net} , a) and stomatal conductance to CO_2 (g_{sc} , b). Each point and bar represents the average and standard deviation of eight point measurements and simulations. The grey lines are 1:1 lines.

Table 4-3. Statistical analyses for the comparison between simulated and measured data for photosynthesis rate (A_{net} , $\mu\text{mol m}^{-2} \text{s}^{-1}$) and stomatal conductance to CO_2 (g_{sc} , $\text{mol m}^{-2} \text{s}^{-1}$). RMSD, root mean square deviation.

Parameter	Salinity level	RMSD	Bias
A_{net}	0 mM	2.85	1.58
	25 mM	2.92	1.31
	50 mM	2.43	1.23
g_{sc}	0 mM	0.07	-0.06
	25 mM	0.04	-0.03
	50 mM	0.04	0.01

Salinity effects on photosynthetic limitations – leaf level

Salinity enhanced the stomatal limitation (L_s , Fig. 4-4a), mesophyll limitation (L_m , Fig. 4-4b) and biochemical limitation (L_b , Fig. 4-4c) of all leaves in a plant (except L_b in the older leaves), but decreased the light limitation (L_l , Fig. 4-4d). While the rise in salinity level from 0 to 25 mM only increased L_s and L_m of the leaves by 2-4% and 1-2%, respectively, the rise in salinity level from 25 to 50 mM strongly increased L_s and L_m at all leaves (8-15% and 2-6%, respectively, Fig. 4-4a,b). The increase of L_b in the middle-upper canopy (leaf rank = 15-20) due to salinity stress was stronger than in the lower canopy (leaf rank = 1-10, Fig. 4-4c). The salinity effect on decreasing L_l was the strongest in the middle canopy (leaf rank = 10-20, Fig. 4-4d).

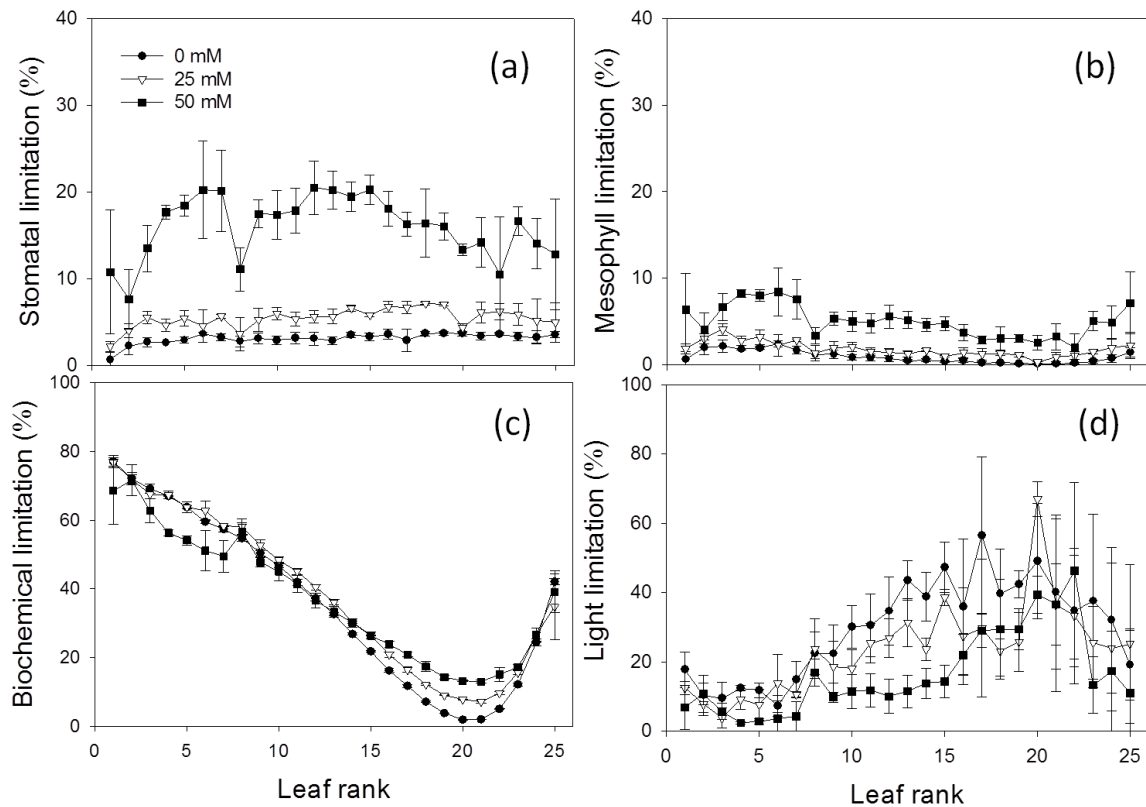


Figure 4-4. Changes of (a) stomatal, (b) mesophyll, (c) biochemical and (d) light limitation with leaf rank and salinity level in the nutrient solution (closed circle, open reverse triangle and closed square represent additional 0, 25 and 50 mM NaCl in the nutrient solution) on day 21 after exposure to salinity. Photosynthetically active radiation above the canopy was assumed to be $600 \mu\text{mol photons m}^{-2} \text{s}^{-1}$. The leaves with higher leaf rank were the younger leaves in the canopy

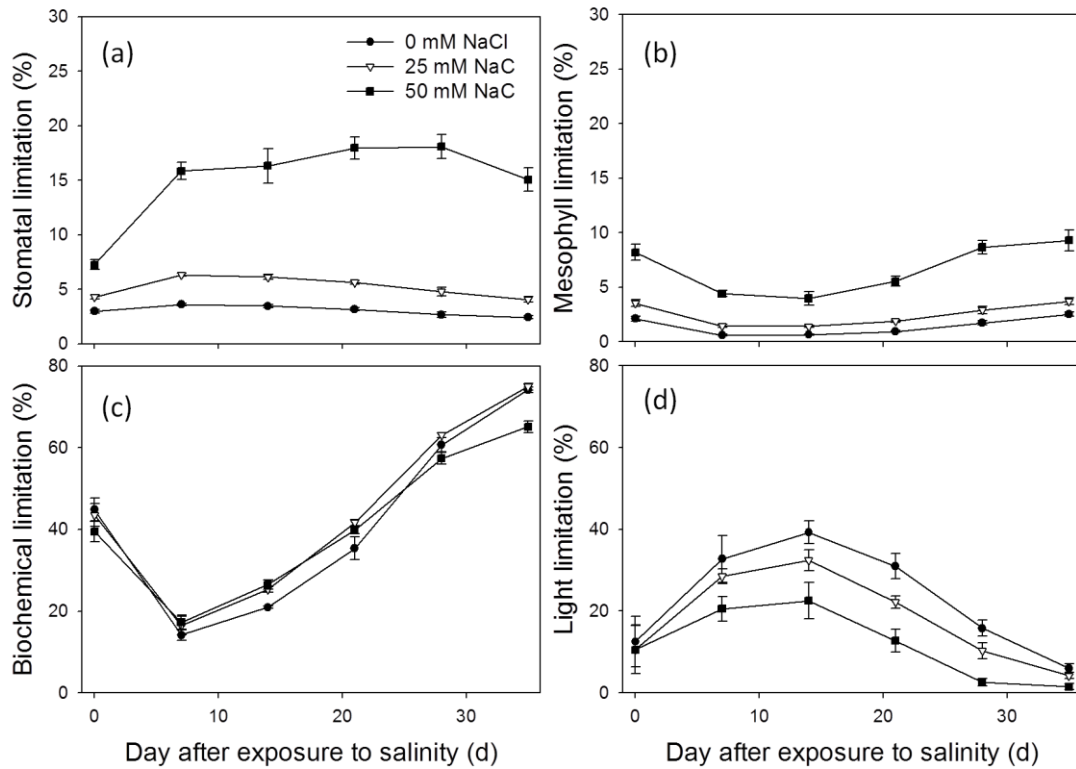


Figure 4-5. Simulated whole plant stomatal (a), mesophyll (b), biochemical (c) and light (d) limitations between days 0-35 after exposure to salinity ($n = 3$, each replication represents the average value of 10 simulations). Photosynthetically active radiation above the canopy was assumed to be $600 \mu\text{mol photons m}^{-2} \text{s}^{-1}$.

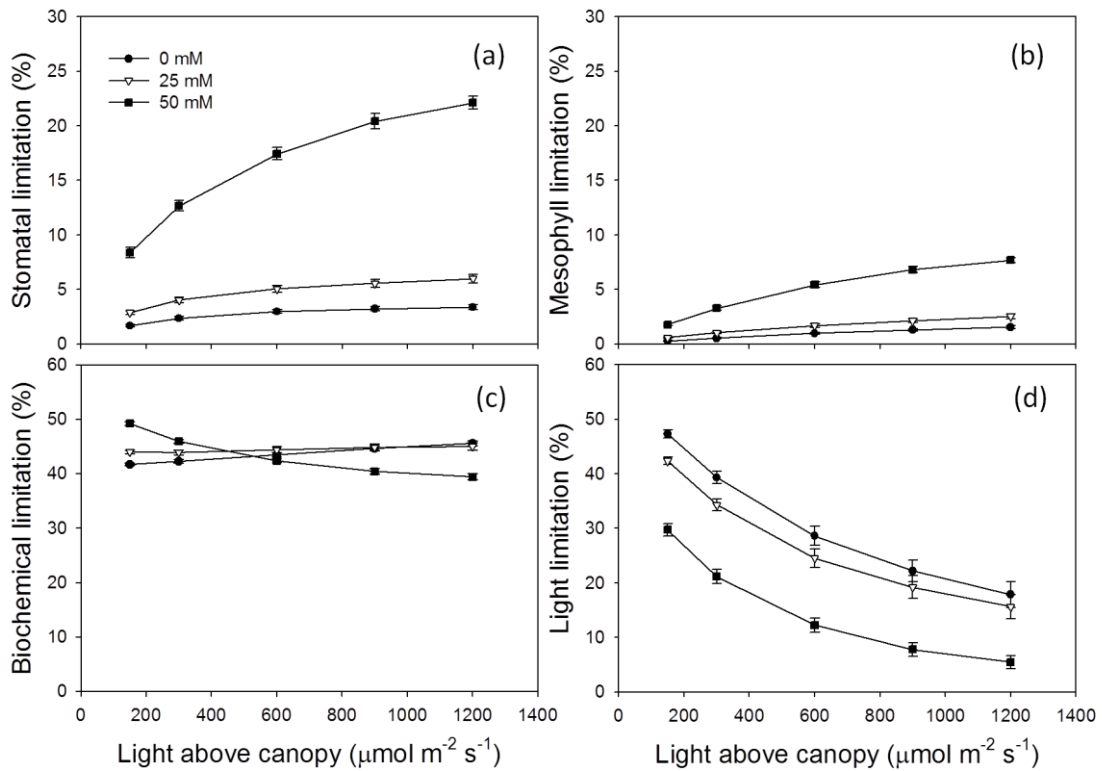


Figure 4-6. Changes of whole plant stomatal (a), mesophyll (b), biochemical (c) and light (d) limitations with light (photosynthetically active radiation) above the canopy and salinity level in the nutrient solution (closed circle, open reverse triangle and closed square represent additional 0, 25 and 50 mM NaCl in the nutrient solution) on day 21 after exposure to salinity.

Salinity effects on photosynthetic limitations – whole plant level

At whole plant level, the compositions of photosynthetic limitation changed with developmental stages and salinity levels (PAR above the canopy = $600 \mu\text{mol m}^{-2}\text{s}^{-1}$). Under non-stressed conditions, whole plant stomatal (L_{sP} , Fig.4-5a) and mesophyll limitation (L_{mP} , Fig.4-5b) were constantly lower than 4% and 3%, respectively. In contrast to the small increases in L_{sP} and L_{mP} under 25 mM NaCl (3% and 1%, respectively), L_{sP} and L_{mP} under 50 mM NaCl were about 15% and 6% higher than non-stressed condition, respectively. In comparison with L_{sP} and L_{mP} , salinity had relative small effects on whole plant biochemical limitation (L_{bP} , Fig. 4-5c). The strongest increase in L_{bP} (~7%) occurred on 14 and 21 DAS. Salinity stress reduced the whole plant light limitation (L_{lP}), especially on 14 and 21 DAS (up to 18%). Similar responses were obtained by changing the light conditions above the canopy (data not shown, but see also Fig. 4-6).

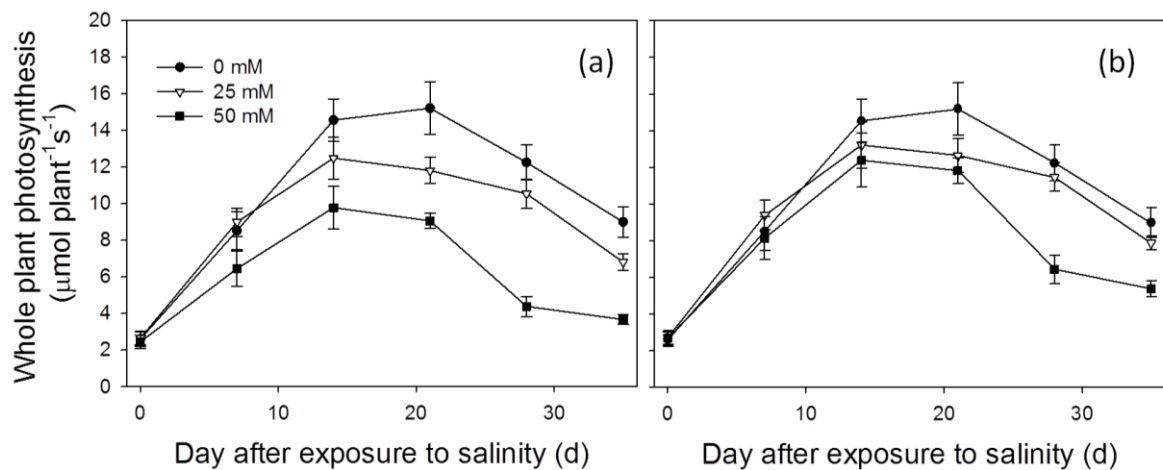


Figure 4-7. (a) Simulated whole plant photosynthesis rate ($P_{w,x}$, $\mu\text{mol plant}^{-1}\text{s}^{-1}$, Eqn 4-12) under different salinity levels. (b) Simulated whole plant photosynthesis rate ($P_{w,ax}$, $\mu\text{mol plant}^{-1}\text{s}^{-1}$, Eqn 4-12) of plants plants with x mM NaCl architecture but non-stressed photosynthetic capacity.

On 21 DAS, increasing light conditions above the canopy slightly enhanced L_{sP} , L_{mP} and L_{bP} (<3%) of plants grown under 0 and 25 mM NaCl (Fig. 4-6a, b, c). Under 50 mM NaCl, a rise of light intensity from 150 to $1200 \mu\text{mol m}^{-2}\text{s}^{-1}$ increased L_{sP} and L_{mP} by 14 and 6%, respectively (Fig. 4-6a, b). In all treatments, L_{lP} decreased with light intensity above the canopy (Fig. 4-6d).

Architectural and functional effects of salinity

Decreases in whole plant photosynthetic rates increased with salinity level and DAS (Fig. 4-7a). If the photosynthetic capacity of the plants grown under 25 and 50 mM NaCl was

not influenced by salinity stress, whole plant photosynthesis would be increased by 5-12% and 17-20%, respectively (Fig. 4-7b, the photosynthetic effects, Table 4-4). Under 25 mM NaCl, both structural and functional effects contributed to the increase in salinity effects with DAS. Under 50 mM, photosynthetic effects was relative constant during the whole growing period (17-20%), while architectural effect increased from 4.4-47.5% between 7-28 DAS (Table 4-4).

Table 4-4. Whole plant light use efficiency ($\epsilon_{u,x}$, $\mu\text{mol CO}_2 \text{ mmol}^{-1} \text{ photon}$), architectural effect ($E_{a,x}$, %, Eqn. 4-12a) and functional effects ($E_{f,x}$, %, Eqn. 4-12b) of salinity on reducing whole plant photosynthesis under x mM NaCl. Data represented simulations under $600 \mu\text{mol m}^{-2}\text{s}^{-1}$ PAR above the canopy.

Day	$\epsilon_{u,0}$	$\epsilon_{u,25}$	$\epsilon_{u,50}$	$E_{a,25}$	$E_{a,50}$	$E_{f,25}$	$E_{f,50}$
0*	24.8	24.1	22.5	-	-	2.4	9.0
7**	40.8	39.6	32.5	-	4.4	4.9	19.9
14	44.7	43.7	35.9	9.2	14.8	5.1	18.0
21	43.8	39.0	30.7	16.8	22.2	5.5	18.2
28	36.8	30.9	17.4	6.3	47.5	7.7	16.7
35	26.8	21.8	11.8	12.4	40.2	11.9	19.1

* The salinity effects were not significant. ** The effects of 25 mM NaCl were not significant.

Discussion

Although the salinity effects on photosynthesis at the leaf level have been studied for a long time in many different species (Drew *et al.*, 1990; Delfine *et al.*, 1999; Centritto *et al.*, 2003; James *et al.*, 2006; Tavakkoli *et al.*, 2010), there are very few data reporting salinity effects on whole plant photosynthesis or light use efficiency (but see Wang *et al.*, 2001 and Qian & Fu, 2005). Using greenhouse cucumber as a model crop, the present modeling study demonstrates a framework to assess the architectural and physiological limitations of whole plant photosynthesis under salinity. This framework allows the dissection of the physiological limitations into stomatal, mesophyll, biochemical and light limitations quantitatively. This advance may be used to identify the traits to be improved for salinity tolerance in cucumber and any other crop species.

Plant architecture is the main limitation on whole plant photosynthesis under salinity

The architectural effects of salinity are mainly resulted from the decrease in whole plant leaf area (LA). Based on the equation of Monteith (Monteith, 1977), architectural traits may influence dry mass production by light interception efficiency (ϵ_i , Eqn 4-13a) and light use efficiency (ϵ_u , Eqn 4-13b). Smaller LA indicates not only less ϵ_i but also less photosynthetic apparatus (Table 4-2), which may lead to decrease in ϵ_u . According to Eqn

4-13b, a decrease in ε_u may be resulted from an increase of whole plant light absorption (I_p) or a decrease in whole plant photosynthesis rate (P_w), the sum of photosynthesis of all leaves in a plant. Since ε_i under salinity was slightly lower than under control condition (Table 4-2), the decrease in ε_u under salinity was resulted from the salinity effects on P_w . P_w can be considered the product of LA and average leaf photosynthesis rate of a plant. Therefore, smaller LA under salinity (architectural effects) may strongly reduce ε_u , especially under high salinity (50 mM NaCl in the nutrient solution). This explains that architectural effects are more prominent than functional effects (Table 4-4). Since the strongest reduction in leaf area occurred at the upper canopy (leaf rank from 15-25, data not shown), maintaining the build up of young leaves, a trait related to osmotic tolerance (Rawson & Munns, 1984), is crucial for reducing architectural effects. Unfortunately, the exact mechanisms and signal pathways controlling leaf growth under osmotic stress is still unclear (Munns & Tester, 2008; Roy *et al.*, 2014). Except the osmotic effects on LA, leaf burn at the shoot tip in some plants under high salinity level after a sunny day (in the greenhouse, PAR above the canopy could reach $1500 \mu\text{mol m}^{-2}\text{s}^{-1}$ at the midday) further reduced LA. The high light conditions at the midday increase the transpirational demand of the upper canopy for leaf cooling and once the transpirational demand of a leaf is larger than the amount of water which can be transported into it, the leaf can be overheated and then injured. Since leaf burn was not observed in the plants under non-stress and low salinity level, it might be resulted from this salt-induced hydraulic failure in water transport. Under high salinity, the size and number of leaf veins decrease (Hu *et al.*, 2005). These changes in vein anatomy may reduce the hydraulic supply capacity (Brodribb *et al.*, 2007), increase the vulnerability to cavitation (Comstock & Sperry, 2000) and then result in hydraulic failure. Both osmotic effects and leaf burn indicate that the negative architectural effects could be reduced by improving the hydraulic processes of plant. Furthermore, it has been reported that canopy structure has strong influence on the canopy photosynthesis in plants growing in a salt marsh (Turitzin & Drake, 1981). This indicates that architectural effects could be reduced by using different training systems. However, these possibilities to reduce architectural effects of salinity are hypothetical. Further studies are required for testing these hypotheses.

Methodological considerations on partitioning contributions to photosynthetic limitations

Recently, it has been proposed that using numerical integration instead of using partial differentiation of Eqn 4-8 and 4-9 provides more accurate results of dissecting photosynthetic limitation (Buckley & Diaz-Espejo, 2015). Therefore, we compared the potential differences between two approaches systematically (see Supplementary Note 4-S1) and found that errors of the partial differentiation approach were less than 4%, while the potential errors of numerical integration approach could be up to 9%. Both approaches are with sufficient accuracy for a sound limitation analysis but they mainly differ in partitioning the contributions of photosynthetic limitations into diffusional processes (CO₂ diffusion through stomata and mesophyll) or biochemical processes (Rubisco carboxylation or electron transport rate). Furthermore, for partitioning the contribution of biochemical capacity (J_{\max}) and light absorption (I_{ab}) to the limitation of electron transport rate, the approach proposed by Chen *et al.* (2014b) may mathematically (according to Eqn 4-5) overestimate biochemical limitation (L_b) and underestimate, light limitation (L_l) especially when J_{\max} and I_{ab} of a leaf are far from their references (for detail, see Supplementary Note S1). This indicates that L_l at the lower canopy, where J_{\max} and I_{ab} are low, may be more dominant than suggested in Chen *et al.* (2014b), an encouraging news for greenhouse farmer using inter-lighting system. For instance, based on the numerical integration approach, the light limitations at the lower canopy (rank 1-10) under non-stressed condition (Fig. 4-4, results of non-stressed plants in Fig. 4-4 are similar to those in Chen *et al.* 2014b) was 13% (of reference) higher than those calculated by the approach proposed by Chen *et al.* (2014b).

Functional limitations on whole plant photosynthesis under salinity

Even if there are potential discrepancies between partial differentiation and numerical integration approaches, consensus on the functional limitations exist at the whole plant level. Firstly, processes related to electron transport contribute to the most part of limitation in a canopy under stress and non-stress conditions, similar to the analyses conducted at leaf (Chen *et al.*, 2015) and canopy (Chen *et al.*, 2014b) level in the non-stressed plants.

Secondly, although salinity increased L_b , it reduced the absolute contributions of biochemical processes (Rubisco carboxylation or electron transport rate) electron transport to photosynthetic limitation (Fig. 4-5c, 4-6c) by the decrease in L_l (Fig. 4-5d, 4-

6d). This effect is due to the fact that a lower C_c under salinity (Delfine *et al.*, 1999; Loreto *et al.*, 2003; Pérez-López *et al.*, 2012) reduces the relative biochemical limitation (Chen *et al.*, 2015). Therefore, the diffusional limitations (L_d , the sum of stomatal, L_s , and mesophyll, L_m , limitations) made the main contribution to photosynthetic limitation under salinity. Furthermore, it also indicates that the relative importance of L_d increased with the level of salinity in the nutrient solution due to its effect on reducing C_c . This is in accordance with our results showing that salt-induced L_d was only slightly higher than L_b under low salinity but much stronger under high salinity. Finally, the changes in photosynthetic limitation on 0 DAS is purely due to osmotic effect (Fig. 4-5) and the increases in photosynthetic limitations on the other days can be considered to be resulted from the ionic effects. Therefore, our results suggest that L_d was mainly contributed by the osmotic effects on both L_s and L_m under low salinity (75% of total L_d) but, in contrast, mainly contributed by the ionic effects on L_s under high salinity (55% of total L_d , Fig. 4-5a, 4-5b). Furthermore, the contributions of ionic effects on L_s to the total limitation increase with light intensity above the canopy (Fig.4-6a, 4-6b). For these reasons, ionic effects on stomatal regulation make the major contribution to the functional effects.

In summary, the present study, using salt-sensitive cucumber as a model crop, provides a novel modelling approach to quantify different components of the whole plant photosynthetic limitations under salinity. The analyses of this model indicated that plant architecture and stomatal regulation are the main factors limiting cucumber canopy photosynthesis under salinity. Further studies using this approach in other species would provide insights into physiological limits due to salinity and improve our understanding of salinity tolerance. For example, it may help in defining target traits of a crop species to be improved by breeder or in designing cropping systems (e.g. training system, intercropping or orchard) more suitable to saline conditions.

Chapter 5

Quantification of the effects of architectural traits on dry mass production and light interception of tomato canopy under different temperature regimes using a dynamic functional-structural plant model

Tsu-Wei Chen¹, Thi My Nguyet Nguyen¹, Katrin Kahlen², Hartmut Stützel¹

¹*Institute of Horticultural Production Systems, Leibniz Universität Hannover, Herrenhäuser Straße 2, 30419 Hannover, Germany;* ²*Department of Vegetable Crops, Geisenheim University, Von-Lade-Straße 1, 65366 Geisenheim, Germany*

Published in: *Journal of Experimental Botany* **65**: 6399-6410, 2014

Abstract

There is increasing interest in evaluating the environmental effects on crop architectural traits and yield improvement. However, crop models describing the dynamic changes in canopy structure with environmental conditions and the complex interactions between canopy structure, light interception and dry mass production are only gradually emerging. Using tomato (*Solanum lycopersicum L.*) as a model crop, a dynamic functional-structural plant model (FSPM) was constructed, parameterized and evaluated to analyze the effects of temperature on architectural traits, which strongly influence canopy light interception and shoot dry mass. The FSPM predicted the organ growth, organ size and shoot dry mass over time with high accuracy (> 85%). Analyses of this FSPM showed that, in comparison with the reference canopy, shoot dry mass may be affected by leaf angle by as much as 20%, leaf curvature by up to 7%, leaf length:width ratio by up to 5%, internode length by up to 9%, curvature ratios and leaf arrangement by up to 6%. Tomato canopies at low temperature had higher canopy density and were more clumped due to higher leaf area and shorter internodes. Interestingly, dry mass production and light interception of the clumped canopy was more sensitive to changes in architectural traits. The complex interactions between architectural traits, canopy light interception, dry mass production and environmental conditions can be studied by the dynamic FSPM, which may serve as a tool for designing a canopy structure which is “ideal” in a given environment.

Key Words: Functional-structural plant model, canopy photosynthesis, light interception, dynamic model, tomato, temperature, plant architecture

Introduction

Increasing crop productivity is an important objective of current plant science. Many approaches, such as improving photosynthesis (Zhu *et al.*, 2010; Zhu *et al.*, 2012; Evans, 2013), nutrient use efficiency (Xu *et al.*, 2012), tolerance to biotic and abiotic stress (Munns and Tester, 2008; Roy *et al.*, 2011), have been proposed in the past decades. An interesting and important question is to which extent alterations in single processes and traits may improve yield on the canopy level (Zhu *et al.*, 2012; Evans, 2013). Without credible assessment of these impacts '*prioritizing the choice of target is a gamble* (Evans, 2013). To assess the impact of a single trait on improving yield, plant scientists and statisticians have started to develop tools and methods to evaluate the relative importance of these targets in the recent years.

Although there are urgent needs and increasing interest on using crop models to quantify the relative importance of plant traits on improving yields, reliable crop models are not available (Evans, 2013). A big challenge is the prediction of canopy photosynthesis in fluctuating environments. Most of the existing models predicting canopy photosynthesis consist of three main components: whole plant leaf area (or leaf area index, LAI), light interception by leaves and photosynthetic rates of leaves. Accurate prediction of leaf area under a certain range of environmental conditions remains a challenge. One reason is that leaf area is strongly affected by many factors such as temperature, vapor pressure deficit and environmental stress (Tardieu *et al.*, 2000; Heuvelink, 2005; Najla *et al.*, 2009). Furthermore, changes of environmental conditions at the leaf level may not necessarily influence final plant leaf area (Granier and Tardieu, 2009), since the latter is not only a function of individual leaf area but also of the number of leaves and leaf senescence (Yin *et al.*, 2000).

Significant temperature effects have been shown to occur on the rates of tissue initiation and expansion and the duration of tissue expansion (Tardieu *et al.*, 2000; van der Ploeg and Heuvelink, 2005; Granier and Tardieu, 2009; Parent and Tardieu, 2012). This indicates that temperature has strong influences on architectural traits such as the leaf number, leaf area and internode length. These modifications of leaf and stem properties by temperature alter canopy structure such as crown density and leaf dispersion, consequently affecting light interception and dry mass production. However, there is only a very limited number of studies on quantifying the influence of temperature regime on plant architecture and light regime at the canopy level.

The amount of light intercepted by individual leaves or layers in the canopy is required to calculate photosynthesis rate. One classical approach is using the Beer-Lambert's law, according to which light passing through the canopy is reduced exponentially with LAI and a light extinction coefficient, k , (Monsi and Saeki, 1953; Hirose, 2005). However, k is not a constant in a growing canopy as it varies with developmental stage, plant structure, canopy configurations (Evers *et al.*, 2009) and architectural traits, such as leaf shape, leaf angle, and internode length (Hirose, 2005; Kahlen *et al.*, 2008). The importance of architectural traits on light interception has been widely reported (Takenaka, 1994; Zhu *et al.*, 2010; Sarlikioti *et al.*, 2011b; Zhu *et al.*, 2012; Song *et al.*, 2013). For example, plants with longer internodes increase light harvest (Weijschede *et al.*, 2008). Leaf curvature (curvature of midrib) has received some attention mostly in maize (e.g., Espana *et al.*, 1999; Ford *et al.*, 2008). Leaf angle has been considered as an important architectural trait for a very long time (Evers *et al.*, 2009; Sarlikioti *et al.*, 2011b; Song *et al.*, 2013). Furthermore, canopy structure and these architectural traits change dynamically with the growth of plants. The complexity of architectural influence on light interception raises the necessity to combine all architectural information in a functional-structural model (FSPM) to describe canopy architecture more accurately which in turn determines light interception and canopy photosynthesis (Vos *et al.*, 2010; Buck-Sorlin *et al.*, 2011; Song *et al.*, 2013). The influences of architectural traits on canopy photosynthesis have been evaluated by static FSPMs in tomato (Sarlikioti *et al.*, 2011b) and in rice (Song *et al.*, 2013). However, these influences were analyzed based on static canopy architecture at a specific developmental stage of plant. The long-term impacts of architectural changes on canopy photosynthesis in a dynamic environment remain unknown.

Lindenmayer systems (L-systems) are a widely used approach to construct dynamic plant architectural models using empirically derived functions. L-systems were first used to describe the development of multi-cellular organisms (Lindenmayer, 1968). They have been extended to plant growth modeling for many crops such as rose (Buck-Sorlin *et al.*, 2011), kiwi (Cieslak *et al.*, 2011), wheat (Evers *et al.*, 2009), cucumber (Kahlen *et al.*, 2008; Wiechers *et al.*, 2011; Kahlen and Stützel, 2011) and tomato (Najla *et al.*, 2009). L-systems have been widely used because they are an elegant formalism for generating branching structures and describing complicated structural dynamics (Prusinkiewicz and Lindenmayer, 1990). Virtual plants expressed by L-systems interfacing with a light environmental model allow estimating the distribution of irradiance from direct and indirect light sources at leaf level (e.g., Cieslak *et al.*, 2008).

The objective of this study was to assess the potential impacts of architectural traits on canopy light interception and canopy photosynthesis at different temperature regimes. Using tomato (*Solanum lycopersicum* L.) as a model crop, this objective was achieved in four steps: 1) Experiments were conducted for parameterizing models for single organ expansion and shape alteration; 2) Combining these models at organ level with L-system and light model, a dynamic FSPM for tomato canopies was constructed; 3) The model was evaluated at both single organ and plant levels using an independent data set; and 4) the FSPM was used to quantify the effects of architectural traits on canopy dry mass production.

Materials and methods

Plant cultivation and data collection

Tomato (*Solanum lycopersicum* L. 'Pannovy,' Syngenta) was used in all experiments. Five experiments were conducted in the growth chambers and greenhouses of Leibniz Universität Hannover, Germany. Experiments 1, 2 and 3 were carried out in growth chambers with a variation of air temperatures, vapor pressure deficits and light intensities (Table 5-S1) to obtain data for parameterization of the leaf model. Experiments 4 and 5 were performed in greenhouses in 2009 and 2010, respectively, for parameterization (Expt. 4) and evaluation (Expt. 5) of the canopy model. The plants in all experiments were raised in the same way throughout, starting with sowing into small rock wool cubes of 2.5 cm x 2.5 cm x 2.5 cm in growth chambers with a light intensity of 300 $\mu\text{mol m}^{-2} \text{s}^{-1}$ photosynthetically active radiation (PAR), VPD of 0.8 kPa, and day/night temperatures of 22/18°C. The seedlings in the cotyledon stage were transplanted to larger rock wool cubes with 10 cm x 10 cm x 10 cm. When the first true leaves appeared, seedlings were transplanted into the hydroponic system with the desired treatments for growth chamber experiments. For the greenhouse experiments, the plants were maintained in the growth chambers until they had five true leaves before transplanting to the greenhouses (for detail, see Table 5-S2). In all experiments, side shoots were removed daily to maintain one stem per plant which was trained upright. Plant protection was conducted as necessary to keep plants free from damage.

In the growth chamber experiments, each treatment consisted of six plants grown in three 50L hydroponic containers. The nutrient solution had an electrical conductivity (EC) of 2 dS m^{-1} with concentrations of 175 mg L^{-1} N, 40 mg L^{-1} P, 300 mg L^{-1} K, 40 mg L^{-1} Mg, 175 mg L^{-1} Ca, 120 mg L^{-1} S and 0.8 mg L^{-1} Fe. Styrofoam covered the surface of the

nutrient solution to prevent the growth of algae and to maintain the plants floating on the nutrient solution. Holes in the Styrofoam with the size of the rock wool cubes fixed the plants inside these holes. The nutrient solution was renewed weekly. Air stones supplied air to the nutrient solution.

In experiment 4, greenhouse ventilation opened when day temperature reached 24°C. The nutrient solution was the same as in the growth chamber experiments except that a drip irrigation system was used. The tomatoes were planted on rock wool slabs (Grodan B.V, Roermond, The Netherlands) with 1 m spacing between rows and within each row. There were four replications each consisting of four plants. Experiment 5 was established in two greenhouses with 22/18°C (low) and 32/28°C (high) day/night temperature. Ventilation opened when day temperature reached 24°C and 34°C in the low and high temperature regimes, respectively. The drip irrigation system was similar to experiment 4. There were two replications, each consisting of eight plants.

In experiment 1 and 2, the length of the leaves at rank 8, i.e. the leaves below the first trusses (Fig. 5-1A), were measured daily, and the lengths of the other leaves were measured weekly. All the lengths were measured manually using a ruler. Leaf length was defined as the distance from the tip of the terminal leaflet to the insertion of the rachis on the stem.

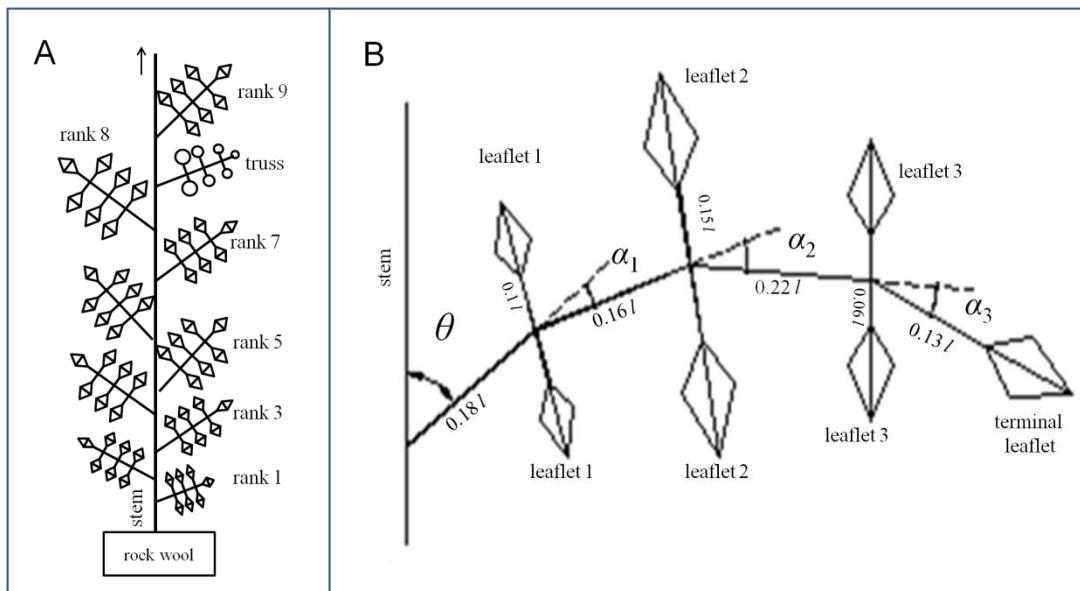


Fig. 5-1. Representation of a tomato plant architecture (A) and a tomato leaf architecture with leaf length = l (B). Leaf angle (θ) is the angle between stem and petiole. Leaf curvature is defined as the sum of α_1 , α_2 and α_3 . Reference ratio of $\alpha_1 : \alpha_2 : \alpha_3 = 1:2:2$. Reference area of leaflet 1 : leaflet 2 : leaflet 3 : terminal leaflet = 0.12 : 0.17 : 0.13 : 0.16. Reference ratio of the length and width of all leaflets is 1.33. Reference values were derived from leaves grown in expt. 1.

By the end of these experiments, the area of each leaf was measured using a LI-COR 3100 area meter (LI-COR, Lincoln, USA) to establish the relationship between leaf length and area. In addition, a leaf was counted when its length was ≥ 1 cm and the number of leaves was counted daily. Internode lengths at rank 8 were measured daily in experiments 1, 2 and 3.

In experiment 4, leaf angle, leaf curvature and leaf senescence were recorded. Leaf angle is the angle between the stem and the line between leaf insertion and the point where the first leaflet appeared, while leaf curvature is sum of the angles describing curvature of the midrib (Fig. 5-1B). The points to calculate these angles were obtained from digitizing using a Fastrak 3D digitizer (Polhemus Inc, Colchester, VT, USA). A leaf was defined senescent when more than 30% of its lamina area (by visual assessment) had turned yellow. In addition, leaf optical properties (reflectance and transmittance) of the full spectrum of the upper and the lower sides of leaves were also measured for different leaf ages: young, mature and old leaves of three plants per treatment using a LI-1800 spectrometer (Li-Cor, Lincoln, NE, USA).

In experiment 5, lengths of leaves and internodes at ranks 8 and 13, the number of leaves and plant height were recorded twice a week. The first truss appeared after the leaf at rank 8 and truss clusters alternated with every three leaves throughout. Therefore, leaf appearance rates of leaves above rank 8 was three times the truss appearance rates on average. Leaf appearance rate was calculated as the slope of the relationship between time and leaf number. Shoot dry weight and plant leaf area were sampled once a week starting 28 days after the first true leaf appeared (DAFLA). Air temperature, VPD and PAR in the greenhouse experiments were recorded hourly. At the end of all experiments, all plant organs were dried at 70°C for at least 96 hours and weighted to determine dry mass.

Additionally, to enhance the data set for deriving base temperature, data for maximum leaf elongation rate of the leaves at rank 5 from Fanwoua (2007) were used. In this work (referred to as Expt. 6), tomato cv. Pannovy was grown in growth chambers under different temperature regimes: 8/12, 14/18, 20/24, 26/30 and 32/36°C for day/night temperature.

Canopy composition and light model

An L-system was used to construct the model for plant architecture. The model was established using *lpg* where L-system specific constructs were added to the C++ programming language (Karwowski and Lane, 2008). A Quasi-Monte Carlo algorithm

based light model was utilized for estimating light absorption of the canopy (for details, see Kahlen and Stützel, 2011).

The virtual canopy comprised 16 plants (4x4), in which four plants in the center of the canopy were analyzed using mean values. The virtual ground was covered by a white rectangle, reflecting 80% of incident light without transmittance, which is in agreement with the setup of the greenhouse experiments.

Geometrical properties of leaf

The arrangement of leaves at the main stem was defined by a phyllotaxis angle of 144° (Najla *et al.*, 2009). Each leaf consisted of seven leaflets, one terminal leaflet and three pairs of lateral leaflets arranged opposite to each other (Fig. 5-1B). In the L-systems, each leaflet was represented by a rhombus. Based on data from experiment 1, geometrical relationships between leaflet length, leaflet width, petiole length of leaflets, and leaf length were derived. Petioles and internodes were interpreted by cylinders.

Architecture model of leaf and internode

The elongation rate $E_l(t, TS, r)$ (cm d⁻¹) of a leaf at time t (d), with a given temperature sum, TS (°Cd, calculated by accumulating the difference between the average air temperature and the base temperature each day from the date of leaf appearance) and at rank r was calculated as the product of the maximum leaf elongation rate of the leaf at rank 8, $E_{l,max}(t)$ (cm d⁻¹), normalized effect of temperature sum, $E_{l,norm}(TS)$, and normalized rank effect, $R_{l,norm}(r)$:

$$E_l(t, TS, r) = E_{l,max}(t) \cdot E_{l,norm}(TS) \cdot R_{l,norm}(r) \quad (\text{Eqn 5-1})$$

$E_{l,max}(t)$ was computed based on the approach proposed by Tardieu *et al.* (2000), but only depending on daily temperature and VPD. Additionally, the model assumed that when temperature is above an optimal temperature, T_{opt} (°C), then $E_{l,max}(t)$ would decrease at the same rate as it increases in the range of temperatures below the T_{opt} :

$$E_{l,max}(t) = (T(t) - T_b)(a_{El,max} + b_{El,max} \cdot VPD(t)) \quad \text{for } T_b \leq T(t) \leq T_{opt} \quad (\text{Eqn 5-2a})$$

$$E_{l,max}(t) = (2T_{opt} - T(t) - T_b)(a_{El,max} + b_{El,max} \cdot VPD(t)) \quad \text{for } T(t) > T_{opt} \quad (\text{Eqn 5-2b})$$

where $T(t)$ and T_b are air temperature at time t and base temperature (°C), respectively. $VPD(t)$ is vapor pressure deficit (kPa) at time t . The base temperature of 6.8 °C was obtained by extrapolation of a linear relationship between normalized maximum leaf

elongation rates and air temperature. The normalized effect of temperature sum, $E_{l,norm}(TS)$, was considered as a bell shaped function depending on leaf temperature sum:

$$E_{l,norm}(TS) = \exp(-0.5((TS-TS_{l,max})/h_l)^2) \quad (\text{Eqn 5-3})$$

where $TS_{l,max}$ ($^{\circ}\text{Cd}$) is the temperature sum required by a leaf to reach its maximum elongation rate. Normalized rank effects, $R_{r,norm}(r)$, on leaf elongation were assumed to follow a bell shaped function for ranks below 14:

$$R_{r,norm}(r) = \exp(-0.5((r-R_{max})/h_r)^2) \quad (\text{Eqn 5-4})$$

where R_{max} is the rank where a leaf has the maximum leaf length. Due to the short duration of the growth chamber experiments the measurement of rank effects could be done only for leaves on ranks 1 to 13. The maximum elongation rate $E_{l,max}$ of leaves above rank 13 was assumed to be the same as of the leaves at rank 13.

Leaf length L_l (cm) was calculated as the cumulative E_l and the area of a leaf, A_l (cm^2), was computed based on the relationship between leaf length and area for this specific cultivar:

$$A_l = a_{Al} \cdot L_l^g \quad (\text{Eqn 5-5})$$

where a_{Al} and g are empirical coefficients. Leaf appearance rate at time t , $R_l(t)$ (leaf d^{-1}) was:

$$R_l(t) = a_r \cdot \ln(T(t)) - b_r \quad \text{for } T(t) \leq 30^{\circ}\text{C} \quad (\text{Eqn 5-6a})$$

$$R_l(t) = R_{l,max} \quad \text{for } T(t) > 30^{\circ}\text{C} \quad (\text{Eqn 5-6b})$$

where a_{rl} and b_{rl} are empirical parameters and if $R_l(t)$ reached its maximum value, $R_{l,max}$, at 30°C , a further increase in temperature did not increase $R_l(t)$. The number of leaves was calculated as the integral of R_l over time. Total plant leaf area, A_p ($\text{cm}^2 \text{ plant}^{-1}$), was the accumulated leaf area of all leaves on the main stem.

Leaf angle, θ ($^{\circ}$), and leaf curvature, C_l ($^{\circ}$) were assumed to be leaf length dependent and followed logistic and linear functions for leaf angle and curvature, respectively.

$$\theta = a_{\theta} \cdot (1 - \exp(-(b_{\theta} \cdot L_l))) \quad (\text{Eqn 5-7})$$

$$C_l = a_{Cl} - b_{Cl} \cdot L_l \quad \text{for } L_l \leq 50 \text{ cm} \quad (\text{Eqn 5-8b})$$

$$C_l = a_{1Cl} + b_{1Cl} \cdot L_l \quad \text{for } L_l > 50 \text{ cm} \quad (\text{Eqn 5-8b})$$

where a_θ , b_θ , a_{Cl} and b_{Cl} , are empirical coefficients.

Internode elongation rate, E_i (cm d⁻¹), was modeled as the product of maximum internode elongation rate, $E_{i,max}(t)$ (cm d⁻¹) and normalized internode elongation rate, $E_{i,norm}$. $E_{i,max}$ was computed similarly to $E_{l,max}$ but was considered to be dependent on temperature and photosynthetically active radiation (PAR):

$$E_{i,max}(t) = (T(t)-T_{bi})(a_{Ei,max}-b_{Ei,max} \cdot PAR(t)) \quad (\text{Eqn 5-9})$$

$$E_{i,norm}(TS) = \exp(-0.5((TS-TS_{i,max,})/h_i)^2) \quad (\text{Eqn 5-10})$$

where T_{bi} is the base temperature for internode growth. It was derived using the same procedure as base temperature for leaf growth. TS is temperature sum (°Cd) and $TS_{i,max}$ is the temperature sum when the internode reaches its maximum elongation rate (°Cd). $PAR(t)$ is photosynthetically active radiation of day t (μmol m⁻² s⁻¹). The parameters h_i , $a_{Ei,max}$ and $b_{Ei,max}$ are shape coefficient. Internode length, L_i (cm), is the accumulation of E_i . Internode diameter, D_i (cm), increases linearly with the age of internode in terms of TS :

$$D_i = a_{Di} + b_{Di} \cdot TS \quad (\text{Eqn 5-11})$$

where a_{Di} and b_{Di} are empirical parameters.

Dry matter production

Dry matter production of a leaf, W_l (g d⁻¹), was the product of leaf area (A_l , m²), light absorption (I_{abs} , J m⁻²d⁻¹) and light use efficiency, ε (g CO₂ J⁻¹):

$$W_l = I_{abs} \cdot \varepsilon(I_{abs}) \cdot (1-\kappa(T(t)-T^*)^2) \cdot A_l \quad (\text{Eqn 5-12})$$

where $\varepsilon(I_{abs})$ is an empirical light-dependent function for tomato derived from the literature (Warren-Wilson *et al.*, 1992), and the term $(1-\kappa(T(t)-T^*)^2)$, a concave parabola reaching its maximum at T^* , describes the temperature response of light use efficiency. Parameter κ (0.0013°C⁻²) and T^* (25°C) for tomato were taken from Gent and Seginer (2012). To simulate leaf senescence when the temperature sum of a leaf is larger than a threshold value, $TS_{l,sen}$ (°Cd), representing that 30% visible yellow symptoms can be observed on leaf lamina, this leaf does not produce dry mass any longer.

Plant dry weight, W_p (g), is then the accumulation of dry weight produced by all leaves. Thus, shoot dry weight, W_s (g), is a proportion of plant dry weight:

$$W_s = \mu \cdot W_p \quad (\text{Eqn 5-13})$$

where μ is a partitioning factor of dry weight to above-ground organs.

Simulation procedures and model evaluation

Simulations were run for two different temperature regimes with the measured climate data in the Expt. 5 (set point temperatures 22/18°C, referred to as “LT”, and 32/28°C, referred to as “HT”). Simulations were run five times with randomized changes of phyllotaxis angle ($144 \pm 10^\circ$). At the organ level, measured and simulated leaf and internode lengths over time were compared for rank 8 and 13. At the canopy level, measured and simulated leaf number, plant height (sum of all internode lengths of a plant), leaf area and shoot dry weight were evaluated. Measured total leaf area and shoot dry weight were compared with the simulated data, which are the average values of the four plants in the middle of the virtual canopy. Statistics of comparison were root mean square deviation (RMSD), bias and accuracy (%):

$$\text{RMSD} = \sqrt{\frac{1}{n} \sum_{i=1}^n (x_i - y_i)^2} \quad (\text{Eqn 5-14a})$$

$$\text{Bias} = \frac{1}{n} \sum_{i=1}^n (x_i - y_i) \quad (\text{Eqn 5-14b})$$

$$\text{Accuracy} = 1 - \frac{\text{RMSD}}{\frac{1}{n} \sum_{i=1}^n (x_i)} \quad (\text{Eqn 5-14c})$$

where x_i and y_i are measured and simulated data, respectively (Kobyashi and Salam, 2000; Kahlen and Stützel, 2011).

Analyses of morphological traits

To quantify the effect of the changes in morphological traits on light interception and dry mass production, analyses were conducted, separately for both temperature regimes. Leaf angles (θ), leaf curvature angles ($\alpha_1 + \alpha_2 + \alpha_3$) and internode lengths were simulated with 70-130% of the reference values (100%). Furthermore, the ratio of curvature angles, $\alpha_1:\alpha_2:\alpha_3$, was modified (reference = 1:2:2; MC1 scenario = 1:1:1; MC2 scenario = 1:1:2; MC3 scenario = 1:2:3; MC4 scenario = 2:1:1). Leaflet length/width ratio was changed between 0.5 and 1.5 (reference = 1.33). Different arrangements of the leaflets, which was represented by the variation in area ratio between leaflets, were simulated (reference area ratio of leaflet 1: leaflet 2: leaflet 3: terminal leaflet = 0.12:0.17:0.13:0.16; ML1 = 0.143:0.143:0.143:0.142; ML2 = 0.2:0.15:0.11:0.08; ML3 = 0.08:0.15:0.17:0.2). When one morphological trait was changed all the other traits were kept identically to those of the reference plants.

Canopy light interception

Four virtual sensors of one square meter were added to the ground in the middle of the center plants to estimate light transmittance through the canopy (Q_t , $\mu\text{mol m}^{-2}\text{s}^{-1}$). The sensors had no reflectance and no transmittance. The estimated absorption therefore corresponded to the transmittance of light through the canopy. To avoid effects of the virtual sensors on light distribution, they were only available on 28, 44, 56 and 64 DAFLA. Light extinction coefficient (k) was calculated by Beer-Lambert's law (Monsi and Saeki, 1953)

$$Q_t/Q_0 = e^{-k \cdot \text{LAI}} \quad (\text{Eqn 5-15})$$

where LAI is the leaf area index (m^2 leaf area per m^2 ground area) and Q_0 ($\mu\text{mol m}^{-2}\text{s}^{-1}$) is the total incoming irradiance.

Results

The climate data in the Expt. 5 are shown in Fig. 5-S1. The values of model parameters are summarized in Table 5-S3. Details for parameterization can be found in the supplementary information (Fig. 5-S2-S6). The adaxial and abaxial sides of tomato leaves reflect 7.3% and 12.7% of incident light and transmit 2.4% and 2.5% of incident light, respectively.

Model evaluation at organ level

The simulation showed that maximum leaf elongation rates, $E_{l,\text{max}}$ (cm d^{-1}), of the leaves at rank 8 and 13 were lower in the 22/18 °C day/night temperature treatment (LT) than in the 32/28 °C day/night temperature treatment (HT, Fig. 5-2) and the time (days) taken to complete leaf growth was longer in the LT than in the HT treatment (Fig. 5-3A,B).

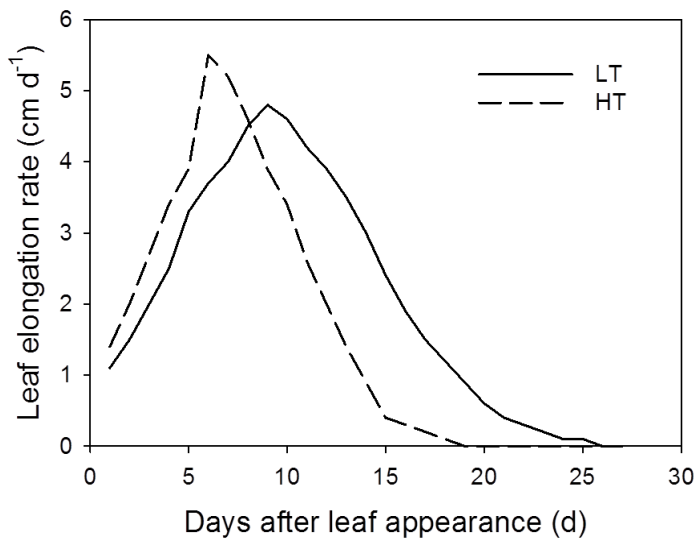


Fig. 5-2. Time course of simulated leaf elongation rates of the leaves at rank 8. Solid and dashed lines represent the simulated leaf elongation rates at 22/18°C (LT) and 32/28°C (HT) day/night temperature conditions.

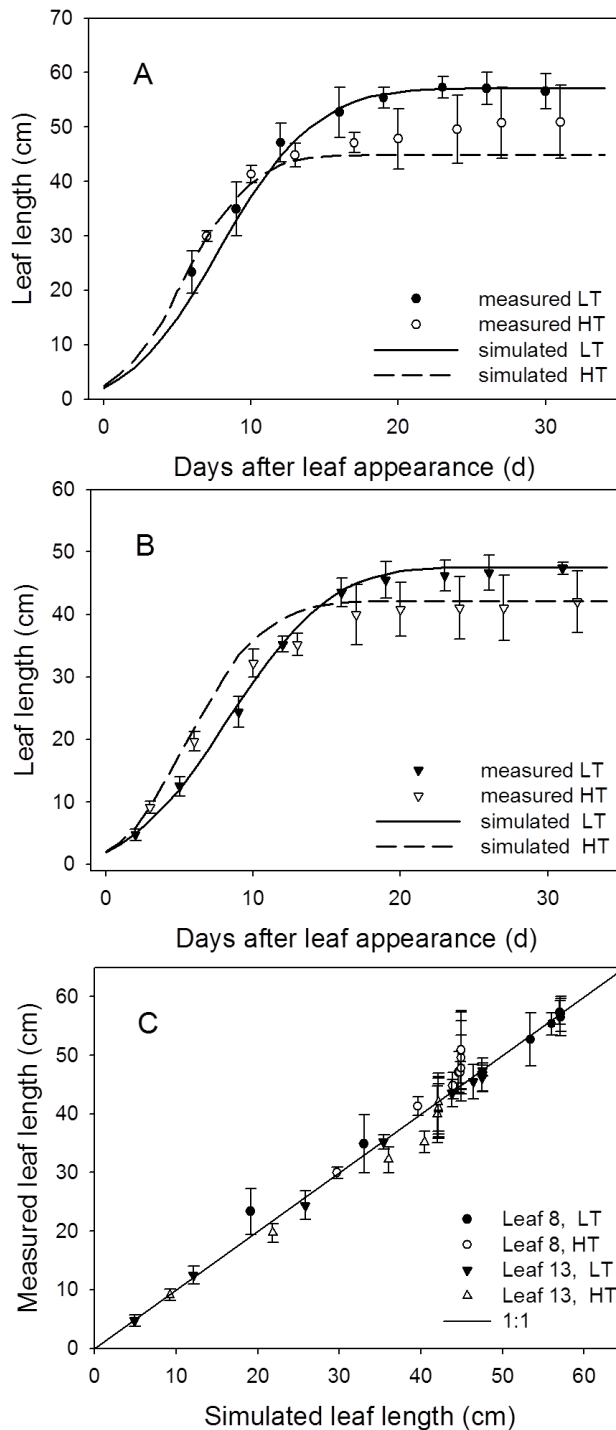


Fig. 5-3. Measured (symbols) and simulated (lines) leaf lengths at rank 8 (A) and rank 13 (B) under 22/18°C (LT, closed symbols) and 32/28°C (HT, open symbols) day/night temperature conditions (Expt. 5, $n = 4$). Bars indicate standard errors. The solid line in (C) is the 1:1 line between simulated and measured data. By plotting all data, $y = 1.00x + 0.04$, $R^2 = 0.97$, $p < 0.001$, intercept was not different from zero and slope was not different from one.

Leaves of plants grown under LT were larger than of those grown under HT conditions, for both rank 8 and 13. Furthermore, the random factor in the model only resulted in a very slight difference (< 0.1 cm) between simulations. Therefore, in Fig. 5-3A and 3B the results of a single simulation are presented which are in good correspondence with measured leaf lengths (Fig. 5-3C). The accuracies for both ranks and temperature conditions were higher than 90%, but the model predicted leaf growth under LT better

than under HT for both ranks (8 and 13) as indicated by the RMSDs and bias (Table 5-1). Simulated internode growth was faster under high than low temperatures in the early phase (Fig. 5-S7). However, final internode length differed only slightly between these two conditions. Simulated leaf angles under LT and HT were well in accordance with measurements (Fig. 5-4) with 76% and 80% accuracies, respectively (Table 5-1).

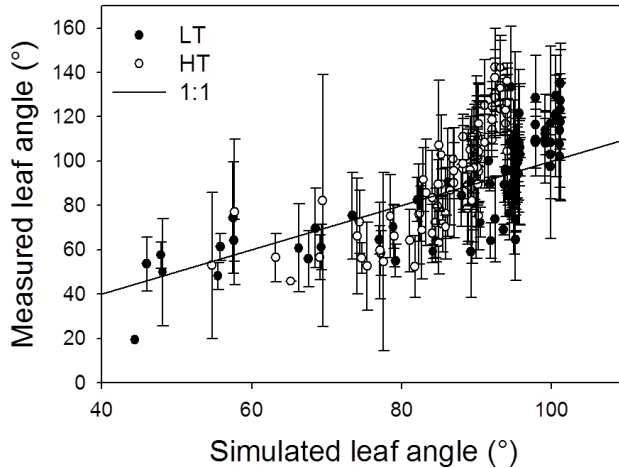


Fig. 5-4. Measured and simulated leaf angles at 22/18°C (LT, closed circle) and 32/28°C (HT, open circle) day/night temperature conditions (Expt. 5, $n = 4$). Data were taken from the plants on 50, 56, 63 and 64 DAFLA. Bars are standard errors. The solid line is the 1:1 line between simulations and measurements.

Model evaluation at canopy level

Plants exposed to HT produced more leaves than those grown under LT, but the differences between temperature regimes were less than three leaves (Fig. 5-5A). For both conditions, the model predicted leaf number with accuracies higher than 95% (Table 5-1). Plant height at LT was 74% - 80% of that at HT (Fig. 5-5B). The simulated plant heights were in good agreement with the measured data, with differences not exceeding 10%. Both measured and simulated results showed that plants under LT had larger total leaf area than those under HT throughout. At the last measurement (77 DAFLA), HT plants had total leaf areas amounting to only 65% and 66% of the leaf area of the plants at LT for simulation and measurement, respectively (Fig. 5-5C). The accuracies of our model at both temperatures were 95%. Total shoot dry mass, W_s , at LT was 15-20% higher than at HT from day 50 on (Fig. 5-5D). Our model predicted W_s at HT with a 93% accuracy but less exactly at LT (Fig. 5-5D). After 77 DAFLA, our model overestimated W_s at HT by 2% and underestimated it at LT by 8%. The standard errors of the simulated total leaf area and W_s between simulations were a very small ($< 1\%$). Therefore, only average values are shown in Fig. 5-5C and 5D.

Table 5-1. Statistical analysis for the comparison between simulated and measured data for organ and canopy levels over the whole duration of leaf and plant growth at 22/18°C (LT) and 32/28°C (HT) day/night temperatures (L_1 , leaf length; L_i , internode length; RMSD: root mean square deviation in Eqn 5-14a).

Traits	Figure	LT			HT		
		RMSD	Bias	Accuracy (%)	RMSD	Bias	Accuracy (%)
L_1 at rank 8	Fig. 5-3A	2.04	0.98	96	3.25	2.66	93
L_1 at rank 13	Fig. 5-3B	0.82	-0.59	97	2.51	-2.03	92
L_i at rank 8	Fig. 5-S7	0.38	-0.07	89	0.35	-0.08	91
Leaf angle	Fig. 5-4	21.35	16.46	76	17.05	7.54	80
Leaf number	Fig. 5-5A	0.96	0.89	96	0.86	-0.26	97
Plant height	Fig. 5-5B	5.36	-0.18	95	3.39	-2.65	97
Total leaf area	Fig. 5-5C	1038	649	95	765	-133	95
Shoot dry mass	Fig. 5-5D	44.94	37.84	85	17.39	-1.55	93

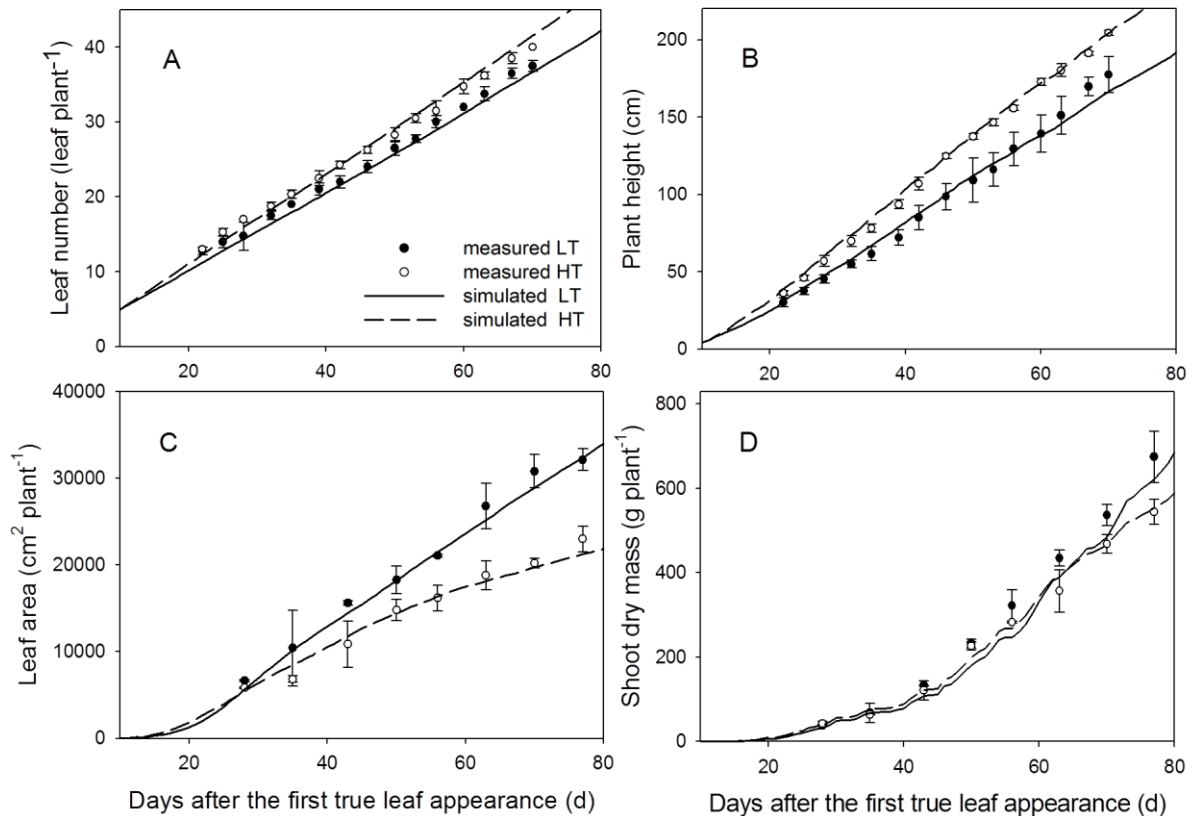


Fig. 5-5. Comparison between simulated and measured leaf number (A), plant height (B), total leaf area (C) and shoot dry mass (D) at 22/18°C (LT, closed circle) and 32/28°C (HT, open circle) day/night temperature conditions (Expt. 5, $n = 4$). Bars are standard errors. Lines represent the averages of simulated data under LT (solid line) and HT conditions.

Interestingly, simulations of shoot dry mass with (Fig. 5-5D) and without (Fig. 5-S8) the temperature effect on light use efficiency (the term $(1-\kappa(T(t)-T^*)^2)$ in Eqn 5-12) were not strongly different. Therefore, temperature effect on light use efficiency was excluded for the analyses of morphological traits.

Analyses of morphological traits

At LT, decreasing leaf angles by 30% resulted in a 17% increase in W_s (Fig. 5-6A) on 77 DAFLA. Interestingly, the corresponding increase at HT was only 2.2%. In contrast, increases in leaf angle reduced dry mass production: A 30% increase in leaf angle resulted in 19.8% and 14.1% reduction of W_s at LT and HT, respectively.

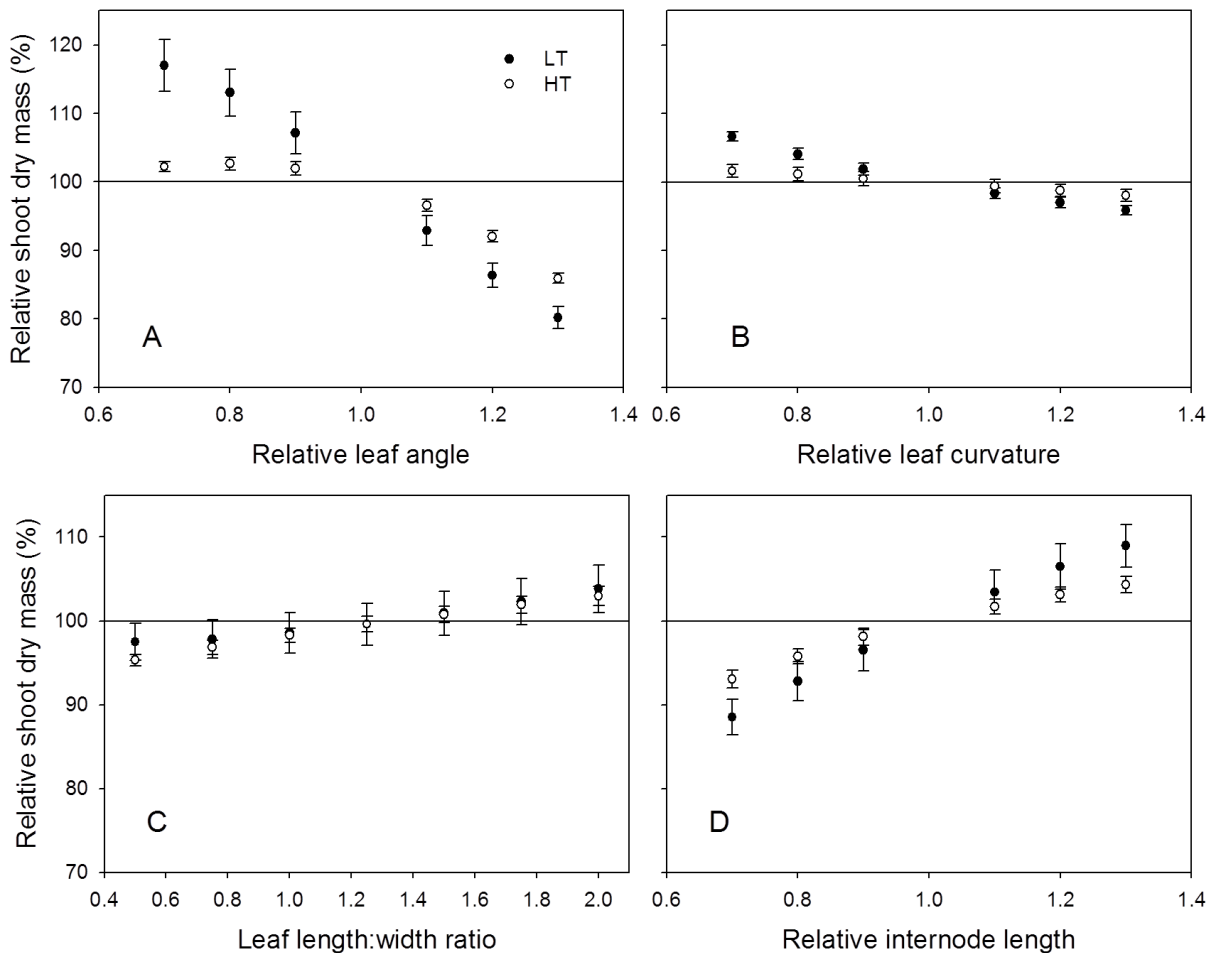


Fig. 5-6. The predicted influence of the leaf angle (A), leaf curvature (B), leaf length and width ratio (C) and internode length (D) on shoot dry mass on 77 DAFLA at 22/18°C (LT, closed circle) and 32/28°C (HT, open circle) day/night temperature conditions. The reference values for relative leaf angle, leaf curvature and internode length were 1. The reference value for leaf length and width ratio was 1.33. Simulated shoot dry mass on 77 DAFLA with the reference values was set to 100%.

In comparison with the leaf angle, leaf curvature and leaf length: leaf width ratio had less effect on W_s . For example, a decrease in leaf curvature by 30% increased shoot dry mass by 6.6% and 1.5% at LT and HT, respectively (Fig. 5-6B); and plants with narrow leaves (e.g. leaf length: width ratio = 2) had an up to 3.8% higher W_s (Fig. 5-6C). Shorter internodes had negative effects on W_s . So was W_s of the plants with 30% shorter internodes reduced by 11.5% and 6.9% at LT and HT, respectively (Fig. 5-6D).

Changes in ratios of the leaf curvature angles affected W_s to a lesser extent, both at LT and HT (Fig. 5-7A). The strongest reduction of 6%, occurred in plants with leaves more curved at the leaf base (MC4, $\alpha_1:\alpha_2:\alpha_3 = 2:1:1$). For leaflet arrangement, the ML1 scenario, where all leaflets were equal in size, had nearly the same shoot dry mass as the reference leaflet arrangement (Fig. 5-7B). In the ML2 scenario, where the leaflet 1 was larger and the terminal leaf was smaller, W_s was reduced by 2.2 and 6.4% at LT and HT conditions, respectively. In the ML3 scenario, where the leaflet 1 was smaller and the terminal leaf was larger, W_s at HT increased slightly by 3.4%.

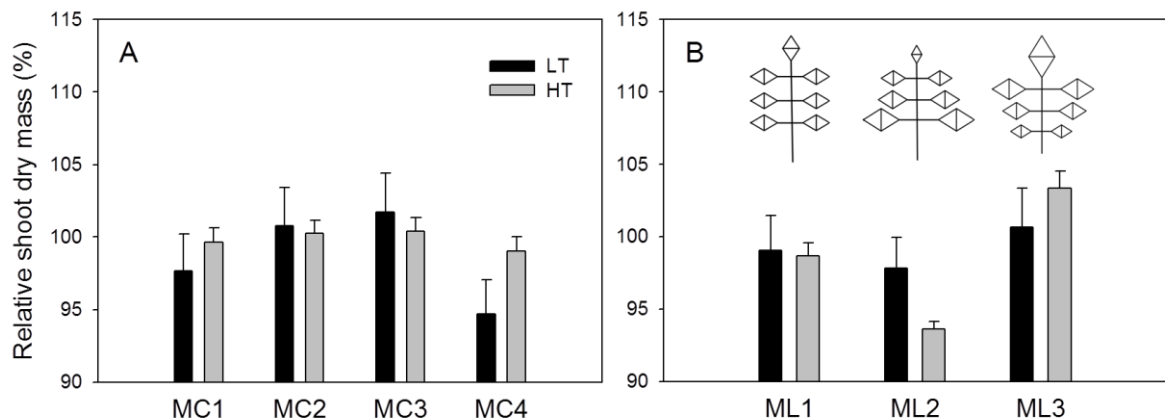


Fig. 5-7. The predicted influence of the leaf curvature angle ratio (A) and leaflet arrangement (B) on total shoot dry mass on 77 DAFLA at 22/18°C (LT, black bar) and 32/28°C (HT, grey bar) day/night temperature conditions. The reference ratio of curvature angles, $\alpha_1:\alpha_2:\alpha_3$ (Fig. 5-1) was 1:2:2; MC1 = 1:1:1; MC2 = 1:1:2; MC3 = 1:2:3; and MC4 = 2:1:1. Reference area ratio of leaflet 1: leaflet 2: leaflet 3: terminal leaflet was 0.12:0.17:0.13:0.16; ML1 = 0.143:0.143:0.143:0.142; ML2 = 0.2:0.15:0.11:0.08; and ML3 = 0.08:0.15:0.17:0.2.

Among the all morphological traits tested by the analyses in this study, leaf angle and internode length were the traits having the strongest effects on W_s (Fig. 5-8A, 8B). These effects were most prominent between 25-40 DAFLA when the LAI was between 0.4 and 1 (Fig. 5-5C). All the results from the analyses suggested that, in general, changes in morphological traits at HT had less influence on W_s than at LT.

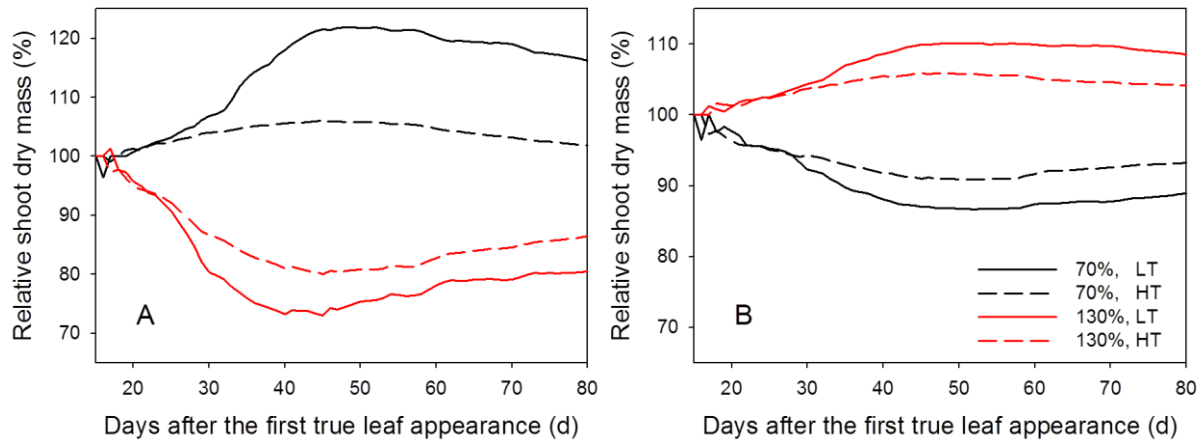


Fig. 5-8. The simulated influence of the leaf angle (A) and internode length (B) on shoot dry mass at 22/18°C (LT, solid lines) and 32/28°C (HT, dashed lines) day/night temperature conditions. Black and red lines represent that the morphological traits are 70% and 130% of the reference values, respectively.

Canopy light interception

Simulated light transmission (Q_t/Q_0) through the canopy decreased with time regardless of temperature conditions. HT allowed more light to be transmitted through the canopy than LT (Table 5-2). Except on 28 DAFLA, a 30% decrease in leaf angle, θ , reduced Q_t/Q_0 by about 10% at LT but had no effect at HT (Table 5-2). Conversely, an increase in leaf angle by 30% increased the Q_t/Q_0 by 15-20% at both LT and HT. The light extinction coefficient, k , decreased over time and was higher at LT than at HT. At LT, a decrease in leaf angle increased k and an increase of θ reduced k . At HT, a decrease of θ had no effect on k and an increase of θ reduced k . Interestingly, changes in internode length had no effects on Q_t/Q_0 and k . Further data about the effects of changing architectural traits on canopy light interceptions and k can be found in the supplementary data (Table 5-S4).

Table. 5-2 Influence of leaf angle and internode length on light transmission through the simulated tomato canopy (Q_t/Q_0), light extinction coefficient (k), and on different days expressed in days after appearance of the first true leaf (DAFLA) at 22/18°C (LT, black bar) and 32/28°C (HT, grey bar) day/night temperature conditions. Numbers are means with standard error in parentheses.

Scenario	DAFLA	LT		HT	
		Q_t/Q_0	k	Q_t/Q_0	k
Reference					
	28	0.67 (0.01)	0.71 (0.03)	0.71 (0.02)	0.63 (0.05)
	43	0.44 (0.02)	0.58 (0.04)	0.50 (0.02)	0.59 (0.04)
	56	0.35 (0.02)	0.49 (0.02)	0.41 (0.02)	0.54 (0.03)
	63	0.32 (0.02)	0.45 (0.02)	0.39 (0.02)	0.52 (0.02)
70% leaf angle					
	28	0.70 (0.01)	0.62 (0.01)	0.75 (0.01)	0.52 (0.03)
	43	0.35 (0.02)	0.73 (0.04)	0.51 (0.42)	0.56 (0.03)
	56	0.25 (0.02)	0.64 (0.03)	0.42 (0.01)	0.53 (0.02)
	63	0.22 (0.01)	0.60 (0.02)	0.40 (0.01)	0.50 (0.02)
130% leaf angle					
	28	0.83 (0.01)	0.33 (0.02)	0.81 (0.01)	0.39 (0.01)
	43	0.62 (0.01)	0.33 (0.01)	0.66 (0.01)	0.35 (0.01)
	56	0.53 (0.02)	0.29 (0.01)	0.58 (0.01)	0.33 (0.01)
	63	0.51 (0.01)	0.27 (0.01)	0.55 (0.01)	0.33 (0.01)
70% internode					
	28	0.68 (0.01)	0.68 (0.04)	0.68 (0.02)	0.70 (0.06)
	43	0.43 (0.03)	0.59 (0.05)	0.48 (0.02)	0.63 (0.04)
	56	0.35 (0.02)	0.49 (0.03)	0.40 (0.02)	0.56 (0.03)
	63	0.33 (0.02)	0.45 (0.03)	0.38 (0.02)	0.53 (0.03)
130% internode					
	28	0.68 (0.02)	0.68 (0.04)	0.73 (0.02)	0.58 (0.05)
	43	0.44 (0.02)	0.57 (0.03)	0.51 (0.02)	0.56 (0.03)
	56	0.35 (0.02)	0.49 (0.03)	0.42 (0.02)	0.53 (0.03)
	63	0.32 (0.01)	0.45 (0.02)	0.41 (0.02)	0.50 (0.03)

Discussion

Functional-structural plant models (FSPM) are particularly suitable for studying structure-related research questions (Vos *et al.*, 2010; DeJong *et al.*, 2011; Poorter *et al.*, 2013). In comparison with traditional crop models, it requires more parameters to construct a dynamic FSPM (Evers *et al.*, 2010), but a precise and detailed description of canopy structure is a condition for the accurate evaluation of the sensitivity of canopy light interception and dry mass production to architectural traits (Song *et al.*, 2013). To assure that the results from the analyses are plausible the careful evaluation of the model is a prerequisite (Evers *et al.*, 2010; Evans, 2013).

Evaluation of model performance

The simulated results, both at organ and canopy levels, were well in accordance with the measurements in the experiment for model evaluation (Figs. 5-2, 3, 4). The accuracies of our model in predicting architectural traits were higher than 90% (Table 5-1), except for the internode length at LT conditions (89%). The number of leaves at HT was slightly overestimated after 60 DAFLA (Fig. 5-5A). This may have resulted from day temperatures above 30°C (Fig. 5-S1). Probably, above 30°C, leaf appearance rate (R_l) slightly decreases instead of maintaining R_{lmax} as it was assumed (Eqn 5-6). Nevertheless, simulation and measurement were still in good agreement (Fig. 5-5A). The less accurate prediction of internode length was due to an overestimation of internode elongation rate (Fig. 5-3), which was dependent on temperature and light quantity (Eqn 5-9). However, it has been shown that both light quantity and light quality (e. g. red:far red ratio) may affect internode growth (Ballaré, 2009). By using a dynamic FSPM, Kahlen and Stützel (2011) have demonstrated that introducing the effect of light quality on internode length may improve its prediction in cucumber. It will be interesting to study whether their approach can be used for predicting tomato internode length more accurately. The predicted shoot dry mass over time was similar to the measurements, but less satisfactory (86% and 90% accuracies for LT and HT conditions, respectively, Table 5-1). Nevertheless, we may conclude that our model has already good performance in predicting dynamic plant architecture and dry mass production at LT and HT conditions.

Temperature effects on canopy structure and light interception

Temperature increased leaf elongation rate, E_l , between base temperature and optimum temperature. Above optimum temperature, further increasing temperatures would decrease leaf elongation rate. This response of E_l to temperature in our study followed a similar pattern as found in other plant species (Parent and Tardieu, 2012). Although the leaf elongation rates at HT were higher than those at LT (Fig. 5-2), final leaf lengths at HT were 87% and 86% of those at LT for the leaves at ranks 8 and 13, respectively (Fig. 5-3). This is due to ca. five days shorter duration of leaf growth at HT (Fig. 5-2). Whole plant leaf area consists of two components: leaf number and leaf area. Although tomato plants produce more leaves at HT than at LT, this was not sufficient to compensate for the smaller single leaf area. Consequently, plants at LT had more leaf area. Furthermore, plants at HT had longer internodes than at LT (Fig. 5-S7, Fig. 5-5B). The differences in leaf area and internode length between LT and HT resulted in the change in canopy structure. Smaller leaves and longer internodes at HT constructed a canopy with lower crown density (canopy surface area: canopy leaf area) and probably higher leaf dispersion (less clumped leaves, Duursma *et al.*, 2012). This resulted in a higher transmittance of light through the canopy but a larger light extinction coefficient, k , (Table 5-2). A larger k value indicates that more light is intercepted per unit leaf area (Duursma *et al.*, 2012). This might explain that plants at HT produced more dry matter per unit leaf area than those at LT (Fig. 5-5C, 5D). Therefore, the higher shoot dry mass in LT was not in proportion to the larger plant leaf area.

There are two possible reasons for the differences of k between canopies at low and high temperature regimes. The first could be a different leaf angle distribution in the middle layer of the canopy. In the top of the canopy, leaf angle distribution between the two canopies was similar. However, the leaf angle in the middle of the canopy at HT was more horizontal (85° - 90°) than at LT (around 100° , Fig. 5-S9A). From our model analyses, smaller leaf angle increases the light absorption from the canopy, increase k (Table 5-2) and shoot dry mass (Fig. 5-6A). The second reason might be leaf curvature. Similarly, the curvatures of leaves in the upper layer between the two temperature conditions were not different. Again, the leaves in the middle section of the plants in the LT treatment were about 20° more curved than those in the HT treatment (Fig. 5-S9B). More curvature would increase mutual leaf shading due to overlapping; this leads to a reduction in area available for light interception in the canopy at LT. Therefore, a

decrease in leaf curvature would be associated with an increase in shoot dry mass (Fig. 5-6B).

Potential impacts of architectural traits on dry mass production

Our results strongly suggest that 1) there are substantial impacts of plant architectural traits on dry mass production and canopy light interception and leaf angle and internode length have the strongest impacts; 2) there are interactions between these effects and temperature; 3) for dry mass production, canopies with more clumped structure are more sensitive to changes in architectural traits.

Clearly, all architectural traits, leaf angle (Fig. 5-6A), leaf curvature (Fig. 5-6B), leaf length:width ratio (Fig. 5-6C), internode length (Fig. 5-6D), curvature ratio (Fig. 5-7A) and leaflet arrangement (Fig. 5-7B) affect light interception and dry mass production of tomato. According to our results, leaf angle and internode length would affect plant productivity more than other morphological changes, which is in accordance with the results of Sarlikioti *et al.* (2011a) and Song *et al.* (2013). For leaf angle, it has been suggested that an ideal plant for light interception has small and vertical leaves in the upper part, which allow more light to penetrate to the lower part where leaves are large and horizontal (Zhu *et al.*, 2010). This could explain the increase in shoot dry mass as leaf angle decreased (Fig. 5-6A). However, the magnitudes of our results were quite discrepant from the values reported in the literature. Sarlikioti *et al.* (2011a) and Song *et al.* (2013) reported that changes in leaf angle and internode length could increase or decrease canopy photosynthesis by 3-7%, but our results suggested that these changes could influence the shoot dry mass by up to 20% (Fig. 5-6A). An easy explanation is that the canopy models used in these two papers were static models and the simulations were only run for one day and for several specific environmental conditions. In reality, the increase of canopy photosynthesis due to changes in architectural traits on one day affects canopy growth and therefore light interception of the next day, so that this self-enforcing effects has to be taken into account, which can be done only in dynamic models as the one presented here. This effect could be observed between 20-40 DAFLA (Fig. 5-8). Moreover, in reality plants grow in a fluctuating environment and canopy structure changes daily. Since there are strong interactions between canopy structure and light interception and the relationship, both at leaf and organ levels, between light interception and photosynthesis rate is not linear (Warren-Wilson *et al.*, 1992; Sarlikioti *et al.*, 2011a;

Zhu *et al.*, 2012; Song *et al.*, 2013; von Caemmerer, 2013), running simulation for one specific condition may not be valid to generalize the architectural effects on canopy photosynthesis.

Longer internodes could increase dry mass production (Fig. 5-6D, Fig. 5-8B) because increased internode length would increase the distance between leaves and hence reduce canopy density and self-shading which improves light interception (Takenaka, 1994; Sarlikioti *et al.*, 2011a). However, no difference in light transmittance and light extinction coefficient was found between reference and $\pm 30\%$ internode length (Table 5-2). This suggests that a canopy with plants having longer internodes does not intercept more light, but the light might be better distributed in the canopy.

Analyses of architectural traits showed that dry mass production at HT, in most cases, was less influenced by changes in architectural traits than at LT (Fig. 5-6, Fig. 5-7 and Fig. 5-8). Dry mass production at LT and HT was modeled by the same parameter set and light intensity above the canopy. As discussed above, canopy structure at HT was less clumped, had lower crown density, and the leaves in the canopy were less self-shaded. Therefore, the degree of improving light distribution within the canopy structure at HT through a better leaf distribution would be less than in a more closed canopy structure. This idea can be supported by the finding that light interception is more sensitive to canopy structure when the crown density is high and the leaves in the canopy are more clumped (Duursma *et al.*, 2012). These results imply that there are interactions between temperature regime and the impacts of architectural traits on dry mass production. Another interesting question is, if the high temperature always results in a more open canopy structure for different species but answering this question is beyond the scope of this study.

We want to emphasize that not only the precise description of the canopy structure, but also the dynamic changes in canopy architecture and environment over time must be taken into account when quantifying the potential impacts of the architectural traits on light interception and consequently on plant productivity. We conclude that dynamic functional-structural plant models may serve as a suitable tool to achieve this objective. Further studies using dynamic FSPM may help in designing the ‘ideotype’ and ideal canopy structure for different environmental conditions.

Chapter 6

High temperatures aggravate architectural effects but ameliorate non-architectural effects of salinity on dry mass production of tomato

Tsu-Wei Chen¹, Thi My Nguyet Nguyen¹, Katrin Kahlen², Hartmut Stützel¹

¹*Institute of Horticultural Production Systems, Leibniz Universität Hannover, Herrenhäuser Straße 2, 30419 Hannover, Germany;* ²*Department of Vegetable Crops, Geisenheim University, Von-Lade-Straße 1, 65366 Geisenheim, Germany*

Abstract

Tomato (*Solanum lycopersicum L.*) is an important vegetable crop and often cultivated in regions exposed to salinity (S) and high temperatures (HT) which change plant morphology, decrease light interception of the canopy and disturb physiological functions. However, our knowledge about the effects of high temperature on plant responses to salinity (S+HT) is restricted. The objective of this study was to investigate the long-term responses (77 days) of tomato plants to S+HT and quantify the contribution of morphological changes (architectural effects) and physiological disturbances (non-architectural effects) on dry mass production under S+HT. To dissect architectural from non-architectural effects of salinity, which is impossible to be done experimentally, a dynamic functional-structural plant model (FSPM) of tomato was constructed, parameterized and evaluated using data from five experiments. The model accuracies in predicting dynamic plant architecture were high (> 85%). Furthermore, a novel approach is proposed to estimate relative canopy light use efficiency by analyzing the dynamic FSPM. HT enhanced architectural effects but reduced non-architectural effects of salinity on dry mass production. The stronger negative architectural effects of salinity on productivity under HT could not be counterbalanced by the smaller (positive) non-architectural effects. Therefore, long-term influences of HT on shoot dry mass under salinity were negative at the whole plant level. Our results highlight the importance of plant architecture at canopy level in studying the plant responses to the environment and show the merits of dynamic FSPM as a heuristic tool.

Key Words: dynamic functional-structural plant model, canopy architecture, canopy photosynthesis, allometric relationship, tomato, high temperature, salinity, stress combination

Introduction

Salinity is a severe problem for agricultural production in many parts of the world (Munns and Tester, 2008). Salinity stress has negative effects on plant morphology (referred to as architectural effects) which may reduce light interception of the canopy, and physiology (referred to as non-architectural effects), and is a combination of osmotic stress and ionic stress (Munns and Tester, 2008; Rajendran et al., 2009; Harris et al., 2010). Osmotic stress affects plant growth and development due to low water potential in the root zone (Munns, 1993; Hasegawa and Bressan, 2000; Munns, 2002). The primary architectural effects of osmotic stress are the decrease in leaf size and leaf number which reduces light interception (Al-Karaki, 2000; Rajendran et al., 2009; Najla et al., 2009). The non-architectural effects of osmotic stress are the reduction of stomatal and mesophyll conductance that restrict CO₂ diffusion into the chloroplast and reduce photosynthesis rate per unit leaf area (James et al., 2002; Maggio et al., 2007; Pérez-López et al., 2012). Therefore, whole plant photosynthesis and dry mass production may be restricted by architectural and non-architectural effects of osmotic stress, at the canopy and leaf levels. Ionic stress results from the accumulation of ions in leaf cells above certain concentrations. High ion concentrations in the leaf cells are toxic, disturb stomatal regulation and reduce photosynthetic capacity (James et al., 2002; Munns, 2002; Munns and Tester, 2008; Rajendran et al., 2009). Therefore, ionic stress enhances the non-architectural effect of salinity.

Tomato is one of the most widely produced and consumed vegetable crops (Heuvelink, 2005) and is often cultivated in regions exposed to salinity (Maggio et al., 2007). Tomato can tolerate an electrical conductivity (EC) of up to 2.5 dS m⁻¹ without any yield loss and is classified as moderately sensitive to salinity (Cuartero and Fernández-Muñoz, 1998). In tomato, the most obvious and visible symptoms of salinity are the changes in plant architectural traits, e.g., leaf length, leaf number, leaf area (Li and Stanghellini, 2001; Maggio et al., 2004; Maggio et al., 2007; Najla et al., 2009), internode and stem length (Romero-Aranda et al., 2001; Shibli et al., 2007; Zribi et al., 2009; Najla et al., 2009) and leaf angle (Jones and El-Beltagy, 1989; Shibli et al., 2007). By using a dynamic functional-structural plant model (FSPM, Vos et al., 2010), where the detailed 3D architecture of plant and physiological functions were combined, Chen *et al.* (2014) have demonstrated that changes in individual architectural traits may affect dry mass production by up to 20% and that the sensitivity of dry mass production to architectural modifications is not only trait but also temperature dependent. This study using dynamic

FSPM highlights that the architectural effects on dry mass production are stronger than suggested in the literature (e.g. 8% in Sarlikioti et al., 2011a and 5% in Song et al., 2013), where static FSPMs were used for studying architectural effects. Their results raise the question to which extend the reductions of dry mass production under salinity result from architectural effects and light interception? However, it is experimentally impossible to assess the pure architectural effects of salinity on dry mass production because in reality they occur together with non-architectural effects such as the reduction of stomatal and mesophyll conductance.

The degree to which architectural traits are influenced by salinity is genotype-dependent. For example, in comparison with non-stressed plants, reductions of leaf number and leaf area have been shown to range between 0-9% and 7.4-17.1%, per 10 mM NaCl in the solution (Table 6-S1). Jones and El-Beltagy (1989) reported a three-fold difference in the change of leaf angle due to salinity between tomato genotypes. These experimental results suggest that there should be a wide spectrum of salt-induced morphological changes in the tomato genome. Although these changes have received some attentions, no study, to our knowledge, has quantified the effects of these alterations on light interception and, as a result, on dry mass production.

Salinity is often associated with high temperatures (Rivero et al., 2014; Suzuki et al., 2014). It is surprising that the combined effects of salinity and high temperature are rarely studied (Colmenero-Flores and Rosales, 2014; Rivero et al., 2014; Suzuki et al., 2014). Keleş and Öncel (2002) showed that high temperatures aggravate the salinity effects on leaf and root length of wheat seedlings (architectural effects). However, their results contradict with a recent study in tomato (Rivero et al., 2014) addressing the short-term responses of tomato to the combined effects of salinity and high temperature (first 72 hours after exposing to 120mM NaCl in nutrient solution of a hydroponic system). The findings of this study suggest that heat stress ameliorates the negative non-architectural effects of salinity and highlight the fact that the combined impact of two stresses must not be the sum of their individual effects. This may be explained by the complex interactions between salinity and temperature. For example, stomatal and mesophyll conductance increase with leaf temperature (Carmo-Silva and Salvucci, 2012; Evans and von Caemmerer, 2013) but salinity reduces them (Delfine et al., 1999; Pérez-López et al., 2012). Furthermore, salinity increases the Na^+/K^+ ratio in the leaves which results in physiological disturbances (Munns and Tester, 2008), whereas high temperature reduces Na^+ uptake by the roots and lowers the Na^+/K^+ ratio in the leaves (Rivero et al., 2014).

It seems as if the results of Rivero et al. (2014) are not consistent with the previous findings of Keleş and Öncel (2002). However, this can be explained by the different target traits in their studies: Keleş and Öncel (2002) investigated the combined effects on architectural traits (leaf and root length) and Rivero et al. (2014) focused on non-architectural traits (stomatal conductance, photosynthesis and Na⁺ uptake). Combining the knowledge from these studies, it seems that high temperature aggravates the architectural effects of salinity but ameliorates the non-architectural effects. However, the magnitudes of these aggravation and amelioration and the long-term effects (more than weeks) of them on dry mass production at the whole plant level are still unknown.

In this paper, we implemented the salinity effects on plant architecture in a dynamic functional-structural plant model of tomato (Chen *et al.* 2014), where the detailed 3D architecture of tomato canopy and physiological functions were combined, and evaluate the new model. Furthermore, we proposed a new method to estimate the relative canopy light use efficiency by using experimental data and this model. We test the hypothesis that high temperature increases architectural effects of salinity but reduces non-architectural effects of salinity. Furthermore, we analyze the architectural parameters in the new model to quantify the reductions of dry mass production under salinity due to the reduction in light interception as a result of architectural effects.

Materials and Methods

Plant materials

Tomato (*Solanum lycopersicum* L. ‘Pannovy,’ Syngenta) was used in five experiments conducted in the growth chambers (Expt. 1, 2 and 3) and greenhouses (Expt. 4 and 5) of Leibniz Universität Hannover, Germany. The growth chamber experiments were set up with four levels of salinity (0, 20, 40 and 60 mM NaCl in nutrient solution for expt. 1 and 0, 40, 60 and 80 mM NaCl in nutrient solution for expts 2 and 3) in combination with a variation of temperature, air vapour pressure deficit (VPD) and photosynthetically active radiation (PAR). Salinity treatments in experiments 4 and 5 were identical with those in experiments 2 and 3 (for details, see Table 6-S2). Air temperature, VPD and PAR in the greenhouses were recorded hourly. In the growth chambers, the experiments were arranged in split plot designs with environmental conditions as main plot factors and salt stress as the sub plot factor. There were seven plants for each stress level. The greenhouse experiment was set up as a randomized complete block design with four replications and four plants per plot. Furthermore, experiment 5 was established in two greenhouses with

22/18°C and 32/28°C day/night temperature, representing low temperature (LT) and high temperature (HT) conditions, respectively. Details of the experimental set-ups, cultivation schedule and weather data of the greenhouse experiments can be found in Table 6-S2 and in Chen et al. (2014). Plant protection was applied when necessary.

Measurements of architectural traits

The growth chamber experiments were designed to investigate the environmental effects (temperature, VPD and light intensity) on leaf and internode responses to salinity, while Expt. 4 was used to examine the effects of salinity on leaf shape and curvature. Expt. 5 was used for model evaluation. In the growth chamber experiments, leaf length (cm) and internode length (cm) at rank 8 were measured by a ruler daily. In the greenhouse experiments, leaf and internode length, leaf number and plant height were also recorded twice a week. Leaf angle and leaf curvature were derived from plant digitizing using a Fastrak 3D digitizer (Polhemus Inc, Colchester, VT, USA). At the end of each experiment, all plant organs were dried at 70°C for at least 96 hours and weighted to determine dry mass.

Model structure

Details of the dynamic functional-structural plant model describing the growth of a tomato crop under non-stress conditions can be found in Chen et al. (2014). In short, the whole plant architecture was reconstructed by an L-System using *lpg* where L-system specific constructs were added to the C++ code. Each leaf consisted of seven leaflets with a phyllotaxis angle of 144°. Each leaflet was represented by a rhombus. The adaxial and abaxial sides of tomato leaves reflect 7.3% and 12.7% of incident light and transmit 2.4% and 2.5% of incident light, respectively. A Quasi-Monte Carlo algorithm-based light model was utilized for estimating light absorption of each leaflet in the canopies (Cieslak et al., 2008), which comprised 16 plants (4x4) with row and plant distances equal to one meter. The virtual ground was a rectangle, reflecting 80% of incident light without transmittance. The canopy and ground setups were in agreement with the setups of the Expt. 5.

Influence of salinity stress on architectural traits

Leaf elongation rate $E_l(t, TS, r)$ (cm d⁻¹) at leaf rank r , at a given leaf temperature sum, TS (°Cd, calculated by accumulating the difference between the average air temperature and the base temperature each day from the date of leaf appearance), and at time t was

calculated as the product of the maximum leaf elongation rate of the leaf at rank 8, $E_{l,\max}(t)$ (cm d^{-1}), the normalized effect of temperature sum, $E_{l,\text{norm}}(TS)$, and a normalized rank effect, $R_{l,\text{norm}}(r)$ (Chen et al. 2014):

$$E_l(t, TS, r) = E_{l,\max}(t) \cdot E_{l,\text{norm}}(TS) \cdot R_{l,\text{norm}}(r) \quad (\text{Eqn 6-1})$$

$E_{l,\max}(t)$ was a function of temperature ($T(t)$, °C), vapor pressure deficit ($\text{VPD}(t)$, kPa) and the salt concentration S_S (mM NaCl) in the solution (Reymond et al., 2003):

$$E_{l,\max}(t) = (T(t) - T_b)(a_{\text{El,max}} + b_{\text{El,max}} \cdot \text{VPD}(t) + c_{\text{El,max}} \cdot S_S) \quad \text{for } T_b \leq T(t) \leq T_{\text{opt}} \quad (\text{Eqn 6-2a})$$

$$E_{l,\max}(t) = (2T_{\text{opt}} - T(t) - T_b)(a_{\text{El,max}} + b_{\text{El,max}} \cdot \text{VPD}(t) + c_{\text{El,max}} \cdot S_S) \quad \text{for } T(t) > T_{\text{opt}} \quad (\text{Eqn 6-2b})$$

where T_b and T_{opt} are base and optimal temperatures, respectively. When $T(t)$ is above T_{opt} , $E_{l,\max}(t)$ decreases at the same rate as it increases in the range of temperatures below the T_{opt} . Normalized temperature effect, $E_{l,\text{norm}}(TS)$, normalized rank effects, $R_{r,\text{norm}}(r)$, and parameters T_b (6.8°C), T_{opt} (28 °C), $a_{\text{El,max}}$ (0.318) and $b_{\text{El,max}}$ (-0.029) were as described in Chen *et al.* (2014). The parameter $c_{\text{El,max}}$ was estimated from the data of Expt. 3, where the light intensity in the growth chamber was similar to typical greenhouse production conditions in the spring in Germany. The effects of salinity on other architectural parameters, X , including leaf appearance rate, maximum internode elongation rate, leaf angle and leaf curvature, were quantified by:

$$X = (1 + \alpha_x S_S) \cdot X_0 \quad (\text{Eqn 6-3})$$

where S_S is the salinity level in the root zone (mM NaCl), α_x is an experimentally derived parameter describing the change of X due to salinity and X_0 is the value of each architectural parameter at non-stress conditions.

Simulations and model evaluation

Simulations were run for two different temperature regimes with the measured climate data from Expt. 5 (set point temperatures 22/18°C, referred to as “LT”, and 32/28°C, referred to as “HT”) and for four salinity levels (0, 40, 60 and 80 mM NaCl in the nutrient solution). Simulations were run five times with a randomized variation in phyllotaxis angle ($144 \pm 10^\circ$). At the organ level, measured and simulated leaf and internode growth over time was compared for rank 8. At the canopy level, measured and simulated leaf number, plant height (sum of all internode lengths of a plant), leaf area and shoot dry weight were compared. Simulated and measured data were compared using root mean

square deviation (RMSD), bias and accuracy (Kobayashi and Salam, 2000; Kahlen and Stützel, 2011).

Estimating relative canopy light use efficiency under salinity stress

Daily dry mass production by a leaf, ΔW_1 (g d⁻¹), was the product of leaf area (A_1 , m²), light absorption of the leaf (I_{abs} , J m⁻²d⁻¹, see above section “*Model structure*”) and light use efficiency, ε (g CO₂ J⁻¹):

$$\Delta W_1 = I_{\text{abs}} \cdot \varepsilon(I_{\text{abs}}) \cdot k_{T,x} \cdot A_1 \quad (\text{Eqn 6-4})$$

where $\varepsilon(I_{\text{abs}})$ is an empirical light-dependent function for tomato derived from Warren-Wilson et al. (1992) and is defined as the reference canopy light use efficiency, $k_{T,x}$ is the effect of temperature and salinity on light use efficiency (the subscripts T and x indicate the temperature and salinity effects, respectively). Total plant dry weight (W_p , g) is then the integration of ΔW_1 produced by all leaves. The shoot weight W_{sh} (g) and is considered a constant proportion of W_p ($W_{\text{sh}} = \mu \cdot W_p$, where μ is a partitioning factor of dry weight to above-ground organs). To predict canopy dry mass production under various environmental conditions, using canopy light use efficiency has been demonstrated to be a robust approach (Kahlen & Stützel, 2011; Chen et al., 2014). Furthermore, it has been experimentally shown that estimated canopy light use efficiency reflects the environmental effects on it (Warren-Wilson et al., 1992; Hui et al., 2001; Benincasa et al., 2006). In Eqn 6-4, $k_{T,x}$ represents the relative canopy light use efficiency, the integrated effects of the complicated interactions between temperature, osmotic and ionic effects on photosynthetic parameters (which are also related to ion transport to and ion accumulation in leaf). Here we present a new method to estimate the changes in $k_{T,x}$ during the growing period using the dynamic FSPM and measured allometric relationships between shoot dry mass and total leaf area.

Allometric relationships between plant traits have been shown from cell to population levels (Enquist et al., 1998; Harmens et al., 2000; Kahlen and Stützel, 2007; Niklas et al., 2009; John et al., 2013). For example, strong relationships between total leaf area and shoot dry mass have been widely reported (Bartelink, 1997; Gunn et al., 1999; Harmens et al., 2000; Niklas et al., 2009). Allometric relationships between measured total leaf area (A_n) and shoot dry mass under non-stress conditions, $W_{\text{sh},n}$, were described by Bartelink (1997), Gunn et al. (1999), Harmens et al. (2000) and Niklas et al. (2009):

$$\ln(A_n) = p_n \cdot \ln(W_{\text{sh},n}) + q_n \quad (\text{Eqn 6-5a})$$

where p_n and q_n are empirical coefficients for non-stress conditions. Since salinity slightly changes the allometric relationship between total leaf area and shoot dry mass (Poorter et al., 2012), coefficients p_s and q_s are estimated from leaf area and shoot dry weight under salinity (A_s and $W_{sh,s}$, respectively):

$$\ln(A_s) = p_s \cdot \ln(W_{sh,s}) + q_s \quad (\text{Eqn 6-5b})$$

Data from LT and HT conditions were analyzed separately, because leaf and stem mass fractions of the whole plant mass, which have a strong influence on the slope (p) and intercept (q) parameters, are influenced by temperature (Poorter et al., 2012). Data collected from different salt levels were pooled because salinity is the environmental factor which has least effect on this allometry (Poorter et al. 2012), but analyzed separately for LT and HT.

A crop model where W_{sh} and total leaf area are accurately simulated should reflect the measured allometric relationships. Achieving accurate predictions of allometric relationships requires accurate predictions of 1) leaf growth dynamics, 2) leaf distribution in the space and 3) canopy light use efficiency. Our model predicts leaf growth dynamics and leaf distribution with high accuracies (see *Model evaluation* in the Results section and Chen et al., 2014) but uses a very simple function as the reference canopy light use efficiency ($\varepsilon(I_{abs})$ in Eqn 6-4), which can be influenced by leaf age, temperature (Gent and Seginer, 2012) and both, osmotic and ionic stress of salinity (James et al., 2002; James et al., 2008). Therefore, the ratio between measured dry mass production and simulated dry mass production using reference canopy light use efficiency represents the relative canopy light use efficiency, $k_{T,x}$ (the subscript T and x denote temperature or salinity conditions, respectively) :

$$k_{T,x}(t) = (W_{sh,m}(t+1) - W_{sh,m}(t)) / (W_{sh,r}(t+1) - W_{sh,r}(t)) \quad (\text{Eqn 6-6a})$$

where $W_{sh,m}$ and $W_{sh,r}$ are the shoot dry mass at time t based on the measured allometric relationships (Eqn 6-5a and 5b) and simulations with reference canopy light use efficiency, respectively. The steps for time t were 28, 35, 43, 50, 56, 63, 70 and 77 days after the appearance of the first leaf. By running the model for unstressed conditions with $k_{T,0} \cdot \varepsilon(I_{abs})$ instead of $\varepsilon(I_{abs})$, the simulated allometric relationships between total leaf area and shoot dry mass should fit the measured relationships (Eqn 6-5a). The same, by running the model for stress conditions with $k_{T,x} \cdot \varepsilon(I_{abs})$, the simulated allometric relationships should match Eqn 6-5b. Here we want to emphasize that the biological

meaning of $k_{T,x}$ is the relative photosynthetic capacity of a whole plant, an outcome of combined effects of temperature, salinity, leaf and canopy age. For this reason, temperature and salinity effects on relative canopy light use efficiency were further dissected:

$$k_{T,x} = k_{LT,0} \cdot k_{HT} \cdot k_x \quad (\text{Eqn 6-6b})$$

where $k_{LT,0}$ is the relative canopy light use efficiency under LT and non-salinity condition, k_{HT} is the effects of high temperature (set to 1 for LT conditions) and k_x is the effects of x mM NaCl in the nutrient solution (set to 1 for 0 mM NaCl).

Dissecting the architectural and non-architectural effects of salinity

The architectural and non-architectural effects of salinity on dry mass production ($R_{a,x}$ and $R_{n,x}$, respectively, %) at x mM NaCl was calculated by:

$$R_{a,x} = (W_{sh,0} - W_{sh,a}) / W_{sh,0} \quad (\text{Eqn 6-7a})$$

$$R_{n,x} = (W_{sh,a} - W_{sh,x}) / W_{sh,0} \quad (\text{Eqn 6-7b})$$

where $W_{sh,0}$, $W_{sh,a}$ and $W_{sh,x}$ are the simulated shoot dry mass under non-stress condition with light use efficiency equal to $k_{T,0} \cdot \varepsilon(I_{abs})$, under x mM NaCl with light use efficiency equal to $k_{T,0} \cdot \varepsilon(I_{abs})$ and under x mM NaCl with light use efficiency equal to $k_{T,x} \cdot \varepsilon(I_{abs})$, respectively. The term $W_{sh,0} - W_{sh,a}$ in Eqn 6-7a represents the difference in simulated shoot dry mass between non-stressed and stressed plants both with light use efficiency equal to $k_{T,0} \cdot \varepsilon(I_{abs})$, i.e. the light use efficiency estimated under non-stress conditions (Eqn 6-6). Therefore, this difference should be a result of decreases in total leaf area, changes in leaf angle and canopy light interception under salinity, in other words, the architectural effects. The term $W_{sh,a}$ and $W_{sh,x}$ in Eqn 6-7b are the simulated shoot dry mass of stressed plants with light use efficiency equal to $k_{T,0} \cdot \varepsilon(I_{abs})$ and $k_{T,x} \cdot \varepsilon(I_{abs})$, respectively. Therefore, the term $W_{sh,a} - W_{sh,x}$ in Eqn 6-7b is the reduction of shoot dry mass due to the salinity effects on light use efficiency (non-architectural effect).

Analyses of architectural traits

The model with light use efficiency equal to ε_x was used for quantifying the effects of architectural traits on light interception and dry mass production under 40 and 80 mM NaCl, separately for both temperature regimes. Leaf number (leaf initiation rate), leaf area, internode length and leaf angle were chosen for the analyses because they are most

frequently reported to be influenced by salinity. The testing range for each trait was determined according to the values reported in the literature (Table 6-S1): The reduction of leaf number was by 3, 6 and 9% per 10 mM NaCl in the solution. Reduction of internode length was by 2, 4 and 6% per 10 mM NaCl in the solution. The reduction of leaf area under salinity in the model was due to the parameter $c_{El,max}$ in the Eqn 6-2a and 2b. To evaluate this effect of salinity, $c_{El,max}$ was simulated with 50-150% of the reference value. Leaf angle was simulated with 70-130% of the reference values (100%). Only one morphological trait was changed for each analysis.

Results

High temperatures aggravate salinity effects on shoot dry mass

On day 77 after the first leaf appearance, reduction in shoot dry mass due to salinity stress under HT was stronger than under LT. In comparison with the tomato plants grown under control conditions, measured shoot dry mass of plants grown under 40, 60 and 80 mM NaCl was reduced by 6.1%, 22.5% and 28.6%, respectively, under LT, and 11.6%, 30.3% and 39.4%, under HT conditions (Fig. 6-1).

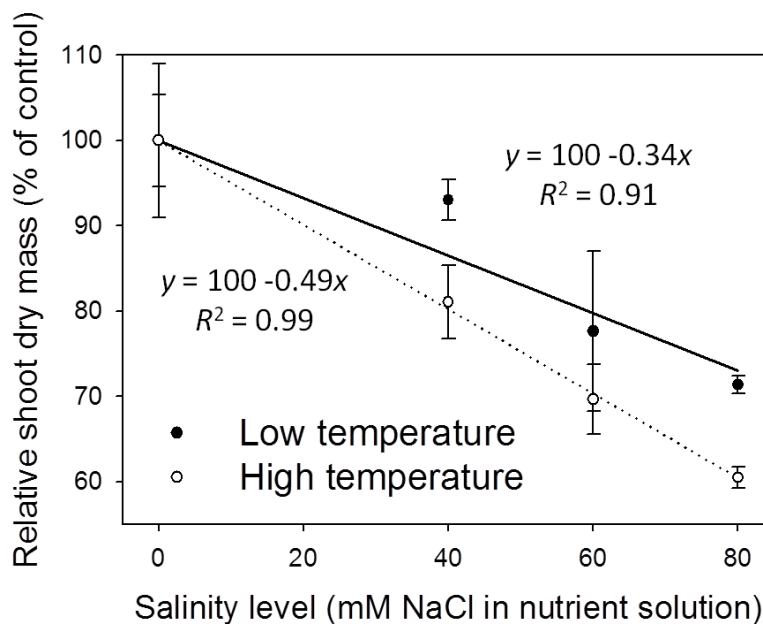


Fig. 6-1. Effect of salinity on shoot dry mass on day 77 after the first leaf appearance under 22/18°C (LT) and 32/28°C (HT) day/night temperature conditions.

Influence of salinity stress on architectural traits

To account for salinity effects on leaf elongation rate, $c_{El,max} = -0.0006 (\pm 0.00003)$ (Eqn 6-2) was estimated. All results from Expts. 1-3 showed that salinity stress had no

influence on leaf appearance rate, maximum internode elongation rate and leaf curvature of tomato cultivar Pannovy and there was no interaction between environmental factors (temperature, light, and VPD) and salinity (Table 6-S2, 6-S3 and 6-S4). Therefore, parameters α_x in Eqn 6-3 were zero for these traits. Leaf angles of salt-treated plants were on average 15.3% higher than in the control, with no significant difference between salinity levels. Therefore, the term $(1 + \alpha_x S_S)$ in Eqn 6-3 for leaf angle was replaced by 1.153 for simulations under all salt stress conditions.

Model evaluation

The model described the reduction of leaf length due to salinity under LT very well (Fig. 6-2A). At HT, final leaf length was underestimated by 2.7-4.8 cm (Fig. 6-2B). Predicted leaf lengths had accuracies higher than 85% (Table 6-1). Salinity had no effect on internode length for both LT and HT (Fig. 6-2C, Fig. 6-2D) and the model overestimated the internode growth in the early phase. This resulted in lower accuracies in predicting internode length (Table 6-1). However, standard deviations of the measured final internode lengths were high and the difference between measured and simulated final internode lengths were less than 1 cm (Fig. 6-2C, Fig. 6-2D).

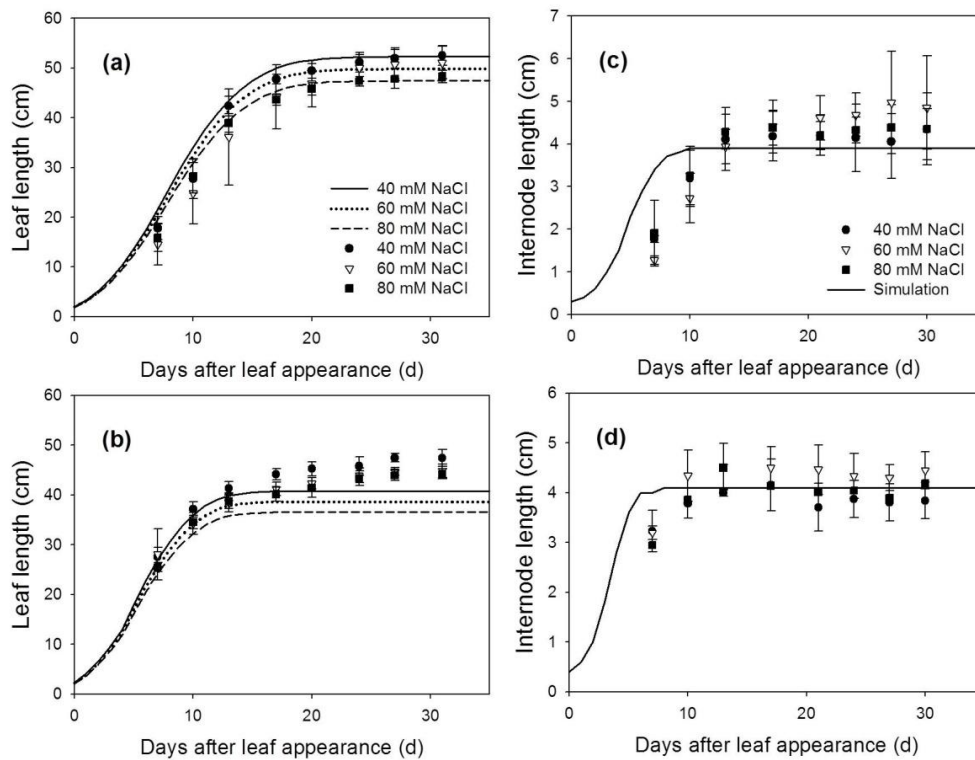


Fig. 6-2. Measured (symbols) and simulated (lines) leaf length (A,B) and internode length (C,D) at 22/18°C (LT, A,C) and 32/28°C (HT, B,D) day/night temperature regimes under 40 (circles), 60 (triangles) and 80 (squares) mM NaCl.

Table 6-1. Statistical analysis for the comparison between simulated and measured data for organ level and canopy level for the whole duration of leaf and plant growth at 22/18°C (LT) and 32/28°C (HT) day/night temperature conditions (L_l , leaf length of rank 8; L_i , internode length of rank 8; A_s and $W_{sh,a}$ are, respectively, total leaf area and shoot dry weight(Eqn 6-6a); RMSD: root mean square deviation)

Salinity level	Traits	LT			HT		
		RMSD	Bias	Accuracy (%)	RMSD	Bias	Accuracy (%)
40 mM NaCl	L_l	2.87	-2.08	93.3	4.19	2.69	89.6
	L_i	0.68	-0.09	81.9	0.44	-0.35	88.2
	A_s	2124	1570	87.8	1048	932	91.3
	$W_{sh,a}$	38.4	30.7	86.3	16.0	5.6	92.5
60 mM NaCl	L_l	4.23	-2.83	89.4	4.14	3.42	89.6
	L_i	1.08	0.10	72.6	0.42	0.02	90.2
	A_s	1865	1488	88.1	455	-222	95.7
	$W_{sh,a}$	23.1	2.5	90.8	29.8	-20.5	84.2
80 mM NaCl	L_l	1.79	-0.98	95.5	5.31	4.75	86.5
	L_i	0.68	-0.04	82.4	0.42	-0.13	89.4
	A_s	1547	1391	89.0	684	343	93.1
	$W_{sh,a}$	37.6	-20.8	83.0	36.5	-29.3	78.0

Both measured and simulated results show that salinity reduced total leaf area and plants produced more leaves under LT (Fig. 6-3A) than under HT (Fig. 6-3B). For all salinity levels and both temperature conditions, the simulated total leaf area was well in accordance with the measurements (accuracies > 87%, Table 6-1). The measured shoot dry mass under 80 mM NaCl was 23% less than under 40 mM NaCl at LT but, interestingly, the simulated 16% reduction of total leaf area under LT (Fig. 6-3A) reduced the simulated dry mass production by only 1.1% (Fig. 6-3C). In contrast, the simulated shoot dry mass under 80 mM NaCl was 13% less than under 40 mM NaCl at HT (Fig. 6-3D). The accuracies of the simulated shoot dry mass with reference canopy light use efficiency (Eqn 6-4) decreased with the salinity level for both LT and HT conditions (Table 6-1). The random factor in the model only resulted in a very slight difference (< 1%) between simulations. Therefore, the simulated data shown in Fig. 6-2 and Fig. 6-3 were the results of one simulation.

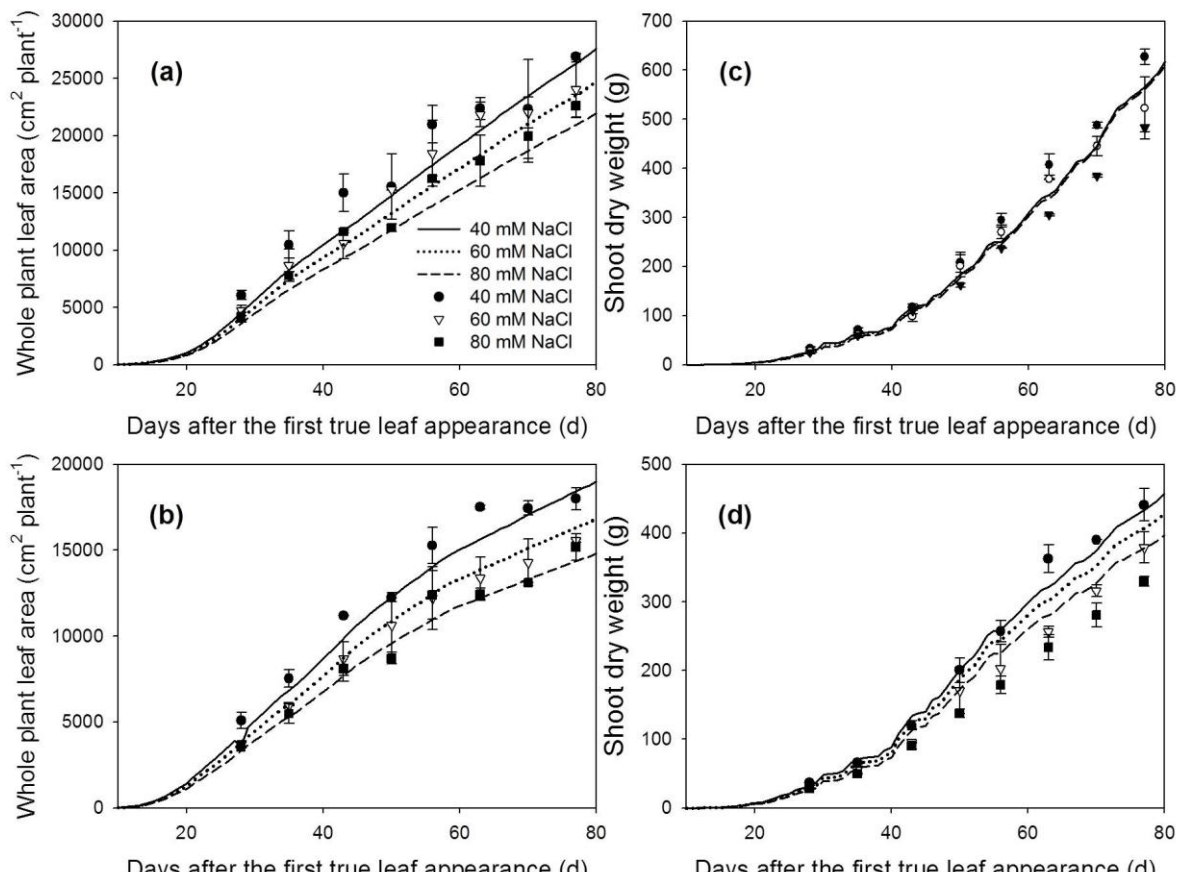


Fig. 6-3. Measured (symbols) and simulated (lines) total plant leaf area (A,B) and shoot dry weight (C,D) at 22/18°C (LT, A,C) and 32/28°C (HT, B,D) day/night temperature regimes under 40 (circles), 60 (triangles) and 80 (squares) mM NaCl. The measured and simulated total leaf area and shoot dry weight of non-stress plants can be found in Chen *et al.* (2014). Measured data were the averages of four replicates (two plants per replicate). The simulated shoot dry weights were the results with light use efficiency equal to ϵ_0 (Eqn 6-6a).

Allometric relationships between shoot dry mass and total leaf area

Significant allometric relationships between total shoot dry mass and total leaf area were found (Fig. 6-4A, Fig. 6-4B, in all cases, $R^2 > 0.95$, $p < 0.0001$). Running the model with canopy light use efficiency equal to $k_{T,x} \cdot \epsilon(I_{\text{abs}})$ instead of the reference light use efficiency, the simulated allometric relationships matched the measured relationships (Fig. 6-4C, Fig. 6-4D).

Temperature and salinity effects on the relative canopy light use efficiency

Under LT conditions, the relative canopy light use efficiency ($k_{T,x}$ in Eqn 6-6a) was higher than 1 for days 29-56 and decreased with time (Table 6-2). Furthermore, high temperature reduced canopy light use efficiency, k_{HT} . Light use efficiency decreased with

the increasing salinity level under both LT and HT condition ($k_{40} < k_{60} < k_{80}$) and with time after exposure to salinity (Table 6-3). The degree of this decrease with time under 60 and 80 mM was stronger than under 40 mM NaCl.

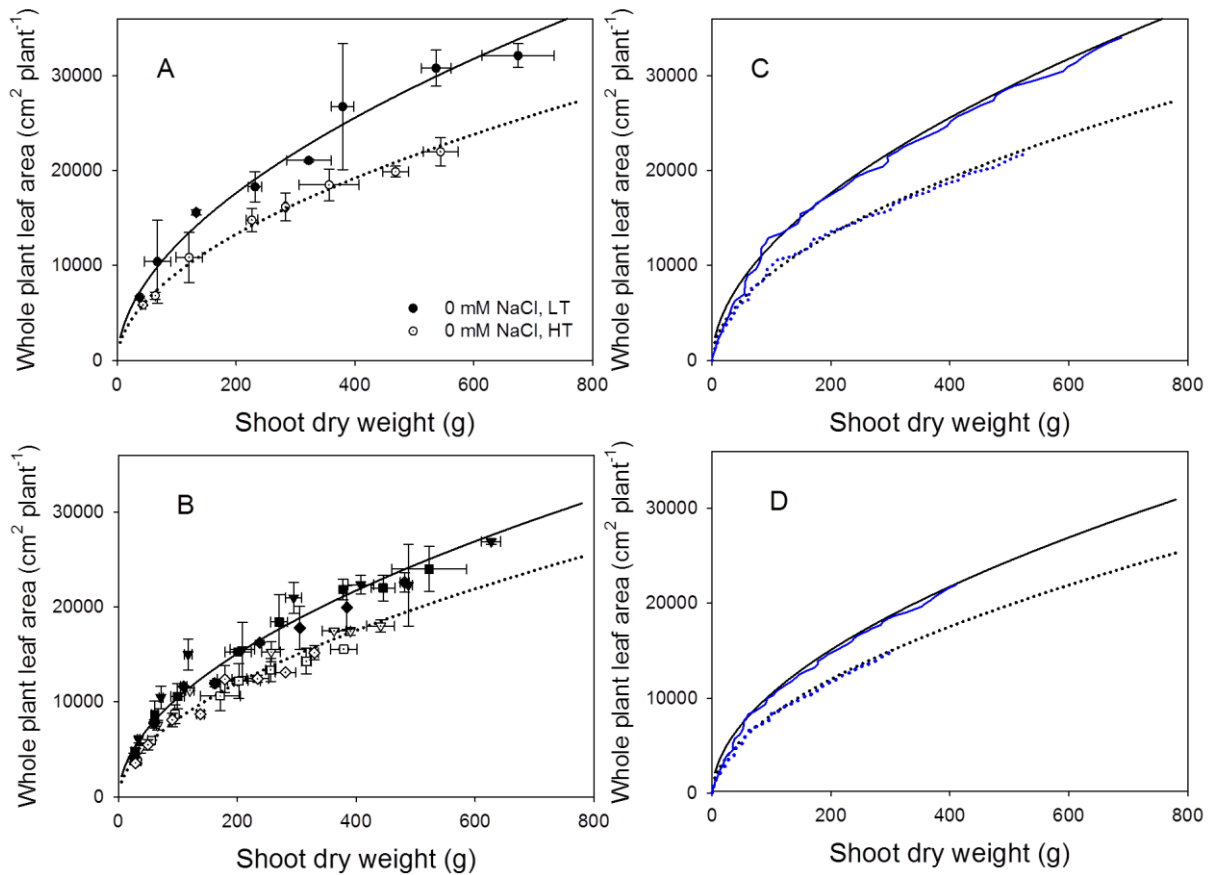


Fig. 6-4. Measured (A,B) and simulated (C, D) allometric relationships between shoot dry weight and whole plant leaf area ($\text{cm}^2 \text{plant}^{-1}$) at 22/18°C (LT, closed symbols and solid lines) and 32/28°C (HT, open symbols and dotted lines) day/night temperature regimes under non-stress (A) and under 40, 60 and 80 mM NaCl (B). Black lines represent the regression lines fitted by the data collected in Expt. 5 according to Eqn 6-5a (non-stress) and Eqn 6-5b (salinity stress). The red lines show the allometric relationships before adjusting ϵ by k_0 in Eqn 6-6a (C) and by k_{80} in Eqn 6-6b (D). The blue lines show the allometric relationships after adjusting ϵ .

Architectural effects of salinity

The reduction in total leaf area under salinity was similar between LT and HT conditions (data not shown). Both under LT and HT conditions, the architectural effects on reducing dry mass production ($R_{a,x}$ in Eqn 6-7a) decreased with time after exposure to salinity (Table 6-3). Architectural effects depended on temperature regimes and increased with salinity level. In general, they were stronger at HT than at LT. For example, architectural effects at 80 mM NaCl over the whole growing period reduced dry mass production by

9.7% and 21.9% under LT and HT, respectively. Furthermore, architectural effects did not change strongly with salinity level under LT conditions while under HT they were twice as high as at 80 than at 40 mM NaCl (Table 6-3).

Table 6-2. Relative canopy light use efficiency, $k_{T,x}$ (Eqn 6-6a) and effects of high temperature (k_{HT} , Eqn 6-6b) and x mM NaCl salinity (k_x , Eqn 6-6b) on canopy light use efficiency under 22/18°C (LT) and 32/28°C (HT) day/night temperature conditions

Day	0 mM		40 mM		60 mM		80 mM	
	LT	HT	LT	HT	LT	HT	LT	HT
	$k_{LT,0}$	$k_{HT,0}$	$k_{LT,40}$	$k_{HT,40}$	$k_{LT,60}$	$k_{HT,60}$	$k_{LT,80}$	$k_{HT,80}$
29-35	1.38	1.33	1.61	1.42	1.32	1.24	1.10	1.08
36-43	1.60	1.59	1.76	1.69	1.41	1.45	1.10	1.24
44-50	1.02	0.91	1.07	0.93	0.87	0.78	0.69	0.66
51-56	1.16	0.88	1.24	0.90	1.00	0.75	0.77	0.63
57-63	0.70	0.49	0.68	0.46	0.55	0.39	0.45	0.33
64-70	1.18	0.76	1.24	0.80	0.86	0.68	0.78	0.57
71-77	0.86	0.71	0.80	0.68	0.65	0.59	0.52	0.50
		k_{HT}	k_{40}	k_{40}	k_{60}	k_{60}	k_{80}	k_{80}
29-35		0.96	1.17	1.07	0.96	0.93	0.80	0.81
36-43		0.99	1.10	1.06	0.88	0.91	0.69	0.78
44-50		0.89	1.05	1.02	0.85	0.86	0.68	0.73
51-56		0.76	1.07	1.02	0.86	0.85	0.66	0.72
57-63		0.70	0.97	0.94	0.79	0.80	0.64	0.67
64-70		0.64	1.05	1.05	0.73	0.89	0.66	0.75
71-77		0.83	0.93	0.96	0.76	0.83	0.60	0.70

Table 6-3 Architectural ($R_{a,x}$, Eqn 6-7a) and non-architectural effects ($R_{n,x}$, Eqn 6-7b) on reducing dry mass production under x mM NaCl at 22/18°C (LT) and 32/28°C (HT) day/night temperature conditions

Day	$R_{a,40}$ (%)		$R_{a,60}$ (%)		$R_{a,80}$ (%)		$R_{n,40}$ (%)		$R_{n,60}$ (%)		$R_{n,80}$ (%)	
	LT	HT	LT	HT	LT	HT	LT	HT	LT	HT	LT	HT
	29-35	23.2	21.2	24.9	27.8	27.5	34.4	-11.1	-4.9	2.6	4.4	12.8
36-43	11.7	13.7	16.4	18.3	15.6	24.0	-8.5	-5.2	9.8	7.3	25.7	16.6
44-50	12.1	8.9	12.5	13.3	12.7	18.7	-4.6	-2.0	13.0	11.8	27.9	21.7
51-56	13.2	9.0	12.3	12.7	12.4	17.8	-5.9	-1.7	12.4	12.9	29.5	22.8
57-63	4.3	1.1	4.2	6.5	5.5	12.8	1.5	5.3	19.9	18.7	33.8	28.0
64-70	11.3	13.0	9.4	17.4	8.4	22.8	-3.7	-3.1	24.0	10.1	31.3	20.0
71-77	0.9	5.7	0.4	13.2	0.8	20.3	4.2	-2.1	25.6	13.7	37.6	22.5
29-77	8.8	10.4	8.9	15.8	9.7	21.9	-2.7	1.2	16.8	10.5	29.0	19.0

Table 6-4. Relative shoot dry mass ($W_{sh,x}$) and total leaf area (A_s , % of the reference canopy architecture), and light transmittance through the canopy (Q_t/Q_0). Values are simulated data on day 77 after the appearance of the first leaf to different architectural traits under 22/18°C (LT) and 32/28°C (HT) day/night temperature. In all cases, standard errors were smaller than 3%. The magnitudes of change in architectural traits are similar to the reported magnitude reported in the literature (Table 6-S1).

Traits	Salinity (mM NaCl)	Magnitude of change of trait	LT			HT		
			$W_{sh,x}$ (%)	A_s (%)	Q_t/Q_0 (%)	$W_{sh,x}$ (%)	A_s (%)	Q_t/Q_0 (%)
LN	40	88%	93.1	87.7	47.8	91.1	87.5	53.1
		76%	84.5	76.3	51.4	80.7	75.8	56.8
		64%	75.2	64.3	55.2	69.6	63.4	62.0
	80	76%	82.3	76.3	55.0	79.1	75.9	67.4
		52%	61.4	53.1	64.2	73.1	50.1	73.1
		28%	27.1	25.2	84.6	12.3	18.1	99.5
$c_{El,max}$	40	-0.0003	99.6	111.2	43.6	104.7	112.2	46.4
		-0.00045	99.8	105.5	44.3	102.6	106.0	47.5
		-0.00075	100.0	94.6	46.3	97.1	94.2	51.6
		-0.0009	99.9	89.5	47.0	93.9	88.6	54.2
	80	-0.0003	101.5	125.7	45.0	115.2	128.3	50.0
		-0.00045	101.1	112.4	47.0	107.9	113.6	54.2
		-0.00075	97.1	88.4	50.0	90.8	87.4	64.6
		-0.0009	92.1	77.7	54.3	80.9	75.7	71.1
IL	40	92%	96.6	100	45.6	98.3	100	49.4
		84%	93.0	100	45.7	96.0	100	49.3
		76%	89.1	100	46.1	93.7	100	49.1
	80	84%	93.8	100	48.8	96.4	100	58.5
		68%	85.7	100	49.1	91.8	100	58.0
		52%	76.2	100	50.5	85.6	100	57.6
θ	40	70%	123.7	100	29.7	106.0	100	46.6
		85%	114.3	100	33.7	104.0	100	45.9
		115%	86.4	100	56.7	91.3	100	58.1
		130%	76.8	100	66.4	79.3	100	70.4
	80	70%	114.4	100	39.2	102.4	100	58.7
		85%	109.7	100	40.1	102.4	100	57.2
		115%	86.9	100	60.8	94.6	100	64.4
		130%	75.8	100	70.7	86.1	100	72.8

LN, leaf number as percentage of leaf number at 0 mM NaCl; $c_{El,max}$, parameter for salinity effect on leaf area in Eqn 6-2 (reference value = -0.0006); IL, internode length as percentage of internode length at 0 mM NaCl; θ , leaf angle in percentage of the leaf angle under stress conditions; $W_{sh,x}$, shoot dry weight, as percentage of the $W_{sh,x}$ under the correspondent stress conditions; A_s , total leaf area, as percentage of the A_s correspondent under stress conditions; Q_t/Q_0 , light transmittance through the canopy as percentage of the light intensity above the canopy.

Non-architectural effects of salinity

Non-architectural effects increased with salinity level. In contrast to architectural effects,

non-architectural effects ($R_{n,x}$ in Eqn 6-7b) increased with time and were higher at LT than at HT for the whole growing period. Both architectural and non-architectural effects increased with salinity level. They were close to zero under 40 mM NaCl and increased to 29% and 19% under 80 mM NaCl at LT and HT, respectively. Furthermore, the sum of architectural and non-architectural effects was similar to the measured reduction of shoot dry mass under salinity (see above “*High temperatures aggravate salinity effects on shoot dry mass*” in the results).

Analyses of architectural traits

Shoot dry mass was most sensitive to leaf number and the reduction of leaf number decreased total leaf area almost linearly (Table 6-4). The sensitivity of dry mass production to architectural traits was temperature dependent. For example, while the change in parameter $c_{El,max}$ (Eqn 6-2), which determined the leaf expansion rate, influenced the total leaf area in the same magnitude at both LT and HT conditions, $c_{El,max}$ had no effect on shoot dry mass at LT but affected shoot dry mass by up to 20% at HT (Table 6-4). Shoot dry mass was less sensitive to internode length and leaf angle at HT than at LT. Changes in leaf angle had less influence on dry mass production under 80 mM NaCl than under 40 mM NaCl. The reduction of dry mass production was linearly related to the light interception by the canopy (Fig. 6-S1). The change in light interception explained 85% and 76% of the reduction in dry mass production at LT and HT, respectively. Furthermore, both at LT and HT conditions, the sensitivity of shoot dry mass to internode length was similar at 0, 40 and 80 mM NaCl (Table 6-S6).

Discussion

There is increasing interest to better understand the plant responses to stress combinations because plants grown in the field are often exposed to more than one stress type (Suzuki et al., 2014) and the effects of stress combinations on plant growth are not equal to the sum of the stresses applied individually (Colmenero-Flores and Rosales, 2014; Rivero et al., 2014). This might be due to the facts that (1) there are complex interactions between stress types, plant structures (e.g. leaf morphology and canopy architecture) and plant functions (e.g. photosynthesis and transpiration) and (2) stress combinations have opposite effects on different traits. For example, Keleş and Öncel (2002) reported that high temperature aggravates the salinity effects on leaf length (structural trait) but Rivero et al. (2014) found that high temperature ameliorates the salinity effects on leaf

photosynthesis (functional trait). Because of the feedbacks between function and structure it is impossible to separate environmental effects on plant structure from those on plant function experimentally. Therefore, we use here a dynamic functional-structural plant model to dissect the architectural effects (effects on plant structure) from non-architectural effects (effects on plant function) of salinity.

High temperature aggravates the architectural effects of salinity on dry mass production

Our model analyses showed that architectural effects of salinity are more prominent under HT than under LT, especially under high salinity (Table 6-3). The measured shoot dry mass of tomato plants grown under 40 mM NaCl was reduced by 6.1% and 11.6% for LT and HT conditions, in comparison with the plants grown under control. This reduction may be mostly explained by the architectural effects (8.8% and 10.4% for LT and HT conditions, respectively). It is interesting to note that the architectural effects decreased with time, both under LT and HT (Table 6-3). This indicates that architectural effects of salinity are stronger in a younger open canopy and decrease with canopy closure. Similar to the canopy age, the fact that canopies under LT had higher leaf areas (Fig. 6-3A, Fig. 6-3B) and were more closed also explains why architectural effects of salinity are smaller under LT than under HT.

In our model, only leaf expansion rates and leaf angles were changed by salinity. Interestingly, under LT condition, the increase of salinity level from 40 mM NaCl to 80 mM NaCl reduced the total leaf area by additional 20% (Fig. 6-3A, Fig. 6-4A) but this reduction in leaf area only resulted in an extra 0.9% of architectural effects on dry mass production (Table 6-3). This could be explained by the fact that light interception of the canopies under 40 and 80 mM NaCl were about equal (55% and 52%, respectively, Table 6-4), indicating that the architectural effects of salinity at LT were mainly an effect of leaf angle, but not of leaf area. This is also the reason why shoot dry weight was less sensitive to the leaf expansion parameter, $c_{El,max}$, at LT (Table 6-4).

High temperature ameliorates the non-architectural effects of salinity on dry mass production

The results from our model analyses support the hypothesis that non-architectural effects are more prominent under LT than under HT (Table 6-3). The primary non-architectural effects of salinity are the reduction of stomatal conductance, mesophyll conductance and

photosynthetic capacity due to ion toxicity (Delfine et al., 1999; Munns and Tester, 2008; Pérez-López et al., 2012). These non-architectural effects of salinity can be ameliorated by increasing temperature. For example, stomatal and mesophyll conductance increase with leaf temperature (Carmo-Silva and Salvucci, 2012; Evans and von Caemmerer, 2013) and Na^+ uptake rate of tomato plant is reduced under high temperature (Rivero et al., 2014). Therefore, our results are in accordance with recent findings of Rivero et al. (2014). Several studies found negative effects of high temperature ($> 35^\circ\text{C}$) on mesophyll conductance and biochemical capacity that reduce leaf photosynthesis (Yamori et al., 2010a; Egea et al., 2011). However, day temperature higher than 35°C only rarely occurred during our experiment. Our results suggest that positive effects of high temperature on plant responses to salinity (lower sodium accumulation and higher photosynthesis) could not counterbalance the negative effects of high temperature on canopy architecture and light interception under salinity. Therefore, high temperatures, in total, aggravate the salinity effects on dry mass production. Here we want to stress that our results are not contradictory to the findings of Keleş and Öncel (2002) and Rivero et al. (2014). They highlight 1) differences in temperature effects on plant responses to salinity between the leaf and the canopy level, 2) that the results based on studying at the leaf level (in this case, the non-architectural effects) must not be the same as the results at canopy level (architectural effects) and 3) the importance of plant architecture at canopy level in studying the plant responses to the environments.

Methodological considerations for dissecting the architectural and non-architectural effects

The measured data showed strong allometric relationships between shoot dry weight and total leaf area (Fig. 6-4A, Fig. 6-4B). The simulated results from a model, where the leaf growth dynamics, distribution of leaves in the space, light interception and photosynthesis are described precisely, should also be able to describe these allometric relationships. Since we have carefully evaluated our architectural model and shown that both at organ and canopy levels, our architectural model may predict the dynamic changes of plant architecture with very high accuracies (Fig. 6-2, Table 6-1 and Chen *et al.* 2014), we may estimate the relative canopy light use efficiency ($k_{T,x}$ in Eqn 6-6a) based on the measured allometric relationships between shoot dry mass and total leaf area. To assure that these

estimations are plausible, we carefully examined the prerequisites and the results of this new method.

Very importantly, we want to emphasize the prerequisite of this method. Model analyses have shown that dry mass production can be strongly influenced by architectural traits while the simulated leaf area maintains the same (Chen *et al.* 2014). This indicates that the three-dimensional distribution of the leaves in the space may influence the allometric relationship between shoot dry mass and total leaf area. Therefore, not only the accurate predictions for total leaf area, but also the accurate distributions of the leaves in the space are crucial for the simulated results reflecting the measured allometry. Hence, the mismatch between simulated and measured allometric relationships between shoot dry mass and total leaf area may be the results of both an inaccurate distribution of leaves and an inaccurate model for photosynthesis. Therefore, the method proposed in this paper may only be applicable for the dynamic functional-structural plant models (dynamic FSPM), where the details in three-dimensional distribution of leaves can be simulated precisely (Evers *et al.*, 2010; Kahlen and Stützel, 2011; Cieslak *et al.*, 2011). This is also the reason why architectural traits in our model should be evaluated by the measured data before estimating $k_{T,x}$. Therefore, this method may not be applied to traditional crop models, where the architectural information of the plant is missing.

The relative canopy light use efficiency, $k_{T,x}$, and effects of high temperature and salinity on it, k_{HT} and k_x , respectively, (Eqn 6-6a, 6b, Table 6-2) showed several trends: (1) k_{HT} was smaller than one; (2) $k_{LT,0}$ and $k_{HT,0}$ decreased with time; (3) k_x decreased with increasing salinity level; (4) k_x decreased with time after exposure to salinity; (5) the magnitude of the decrease in k_x with time under 60 and 80 mM NaCl was stronger than it under 40 mM NaCl ; and (6) k_x under LT, especially under 80 mM NaCl, was smaller than it under HT. Because that all this trends can be well explained by the findings reported in the literature, we consider that our estimations of the relative canopy light use efficiency and the following quantification of architectural and non-architectural effects were plausible. First, under control conditions, tomato has its best photosynthetic performance at around 25°C (Gent and Seginer, 2012; Qian et al., 2012). The average day temperatures in the greenhouses were 23°C and 29°C for LT and HT conditions, respectively. The fact that the average day temperature in LT was closer to the optimal temperature than it was in HT may explain that k_{HT} was smaller than one throughout the

whole growing period. Secondly, the function for canopy light use efficiency ($\epsilon(I_{\text{abs}})$ in Eqn 6-4) was parameterized from a mature tomato canopy (Warren-Wilson et al., 1992). Before day 43, tomato plants were in the young developmental stage with less than 23 leaves and with plant height shorter than 120 cm. This explains that $k_{T,0}$ was larger than one before day 43 because young canopy, which has a higher photosynthesis capacity (Qian et al., 2012). This also explains the trend of $k_{T,0}$ with time. Both osmotic and ionic components of salinity reduce the photosynthesis capacity of the plants and the magnitude of this reductions increase with the salinity level in the nutrient solution (James et al., 2002; Maggio et al., 2007; Munns and Tester, 2008; Rajendran et al., 2009; Pérez-López et al., 2012). This explains the reduction of k_x with increasing salinity level and with time after exposure to salinity (Table 6-2). Furthermore, the magnitude of the decrease in k_x with time under 80 mM NaCl was stronger than it under 40 mM NaCl. This indicates that the ionic effect appeared faster and was more prominent under higher salinity. Finally, that k_x under LT was smaller than it under HT can be explained by the recent finding that tomato grown under LT accumulates more Na^+ in leaves than grown under HT (Rivero et al., 2014). This indicates that leaves grown under HT may maintain low Na^+ concentrations and, therefore, maintain their light use efficiency.

Contributions of architectural traits on yield reduction

The decrease in leaf appearance rate and leaf number under salinity had the strongest effects on reducing total leaf area and dry mass production (Table 6-4). This indicates that maintaining young leaf production under salinity stress is a key architectural trait for salinity tolerance. Furthermore, maintaining young leaf production may also counterbalance the leaf senescence due to the ionic effect (Munns and Tester, 2008). The changes in leaf angle and internode length may also result in up to 25% differences in dry mass production (Table 6-4). This would partly explain the negative relationship between salt tolerance and salt-induced increases in leaf angle (Jones and El-Beltagy, 1989). Changes in leaf angle affected the light interception by the canopy by up to 35% while changes in internode length, in contrast, affected the light interception by the canopy by only 8% (Table 6-4). The light interception by the canopy may explain 85% of the effects of leaf angle on shoot dry mass while no relationship was found between the effects of internode on light interception and on shoot dry weight (Fig. 6-S2). Reduction in internode length decreases the distance between leaves and enhances the self-shading

(Takenaka, 1994; Sarlikioti et al., 2011a), which resulted in a less efficient light use in the canopy (Chen *et al.* 2014).

Conclusion

High temperatures aggravate the negative effects of salinity on dry mass production via plant architecture and light interception but ameliorate the reduction of canopy light use efficiency. These results highlight the different temperature effects on physiological and morphological responses to salinity and the importance of plant architecture in studying plant responses to environmental changes at canopy level. Our analyses suggest that leaf angles influence light interception more than light distribution, and that changes in internode length have stronger effects on light distribution than on light interception. Furthermore, our model analyses enable us to dissect the architectural effect from non-architectural effect of salinity, which is impossible to be done experimentally because in reality both effects occur together under osmotic stress.

Chapter 7

Discussion

Architectural traits strongly influence light interception and, therefore, dry mass production. In the last two decades, there are increasing interests in quantifying the impacts of architectural traits on canopy light interception and canopy photosynthesis. At the canopy level, it has been suggested that three-dimensional details in plant architecture are of specific importance for assessing the potential impacts of light-driven physiological processes on photosynthesis because any change in plant architecture alters the light distribution in the canopy (Bond *et al.*, 1999; Buckley *et al.*, 2013). Therefore, static or dynamic functional-structural plant models (FSPM), where the 3D architecture of plants is explicitly described, are becoming a standard tool for assessing the influence of morphological traits on canopy light interception and dry mass production (e.g. in tomato, Sarlikioti *et al.*, 2011a; Sarlikioti *et al.*, 2011b; in rice, Song *et al.*, 2013; in apple, Da Silva *et al.*, 2014; in wheat-pea mixture, Barillot *et al.*, 2014; and in wheat-maize mixture, Zhu *et al.*, 2015).

The previous chapters present two FSPM-frameworks for quantitative assessments of the architectural and physiological impacts on dry mass production under various environmental conditions. The first framework (chapter 2, 3 and 4) focuses on the influences of salinity, instantaneous light condition and their interactions on the physiological limitations in cucumber. This framework combines a static FSPM of digitized cucumber plants, a biochemical model of photosynthesis and quantitative limitation analysis of photosynthesis to upscale the impacts of physiological processes on limiting photosynthesis from leaf to the whole plant level. The second framework (chapter 5 and 6), a dynamic FSPM of tomato growth, focuses on the impacts of architectural parameters on whole plant dry mass production and their interactions with temperature and salinity.

It is important to emphasize two important assumptions in these frameworks: 1) Plant growth is source-limited, so an increase in photosynthesis improves the dry mass production; 2) The processes of plant growth and the processes of photosynthesis can be decoupled, and no feedbacks and interactions between growth and photosynthesis are considered. Assumptions are inevitable in any modelling work since models are always

simplifications (which mean under a series of assumptions) of the real world. The questions now is, are the above-mentioned assumptions valid for the model analyses?

The first assumption should be valid for the greenhouse cropping systems, although it has been demonstrated that vegetative growth of tomato plants could be sink-limited under cool conditions (air temperature lower than 18°C and the transition temperature between source- and sink-limitation increases with light intensity, Gent and Seginer, 2012). In contrast, in the greenhouse experiments, the temperature was constantly maintained above 20°C and the greenhouse construction reduced the average light intercepted by the plants. Furthermore, carbon-demand for the generative growth is, in general, higher than for vegetative growth. Therefore, it can be assumed that fruit vegetables tend to be source-limited.

The second assumption is that processes of plant growth and the processes of photosynthesis are to some extent independent, similar to many crop model frameworks (e.g. CERES, Lizaso *et al.*; APSIM, Hammer *et al.*, 2010; and CSM-IXIM, Lizaso *et al.*, 2011, for review, see Parent and Tardieu, 2014). This assumption strongly reduces the complexity of model structures and interdependence between the build-up of leaves and the photosynthesis. The benefit of this assumption is to avoid the long-standing debate about if plant growth is controlled by photosynthesis or vice versa (Wardlaw, 1990; Körner, 2003; Kirschbaum, 2011). This debate could be a reason why many FSPMs are only used for evaluating the light interception of canopy, but not for dry mass production. It has been proposed that structure and algorithm of a crop model determine the sensitivity of the model output (in this study, the dry mass production or canopy photosynthesis) to a specific trait (Parent and Tardieu, 2014). This might be due to the fact that, in a model, complex interactions between physiological processes and environments are often simplified in a way of fitting the model structure/algorithm with the model concept. Important is that a model addresses the biological processes accurately (Parent and Tardieu, 2014). In this study, the most important biological processes are the environmental effects on plant architectures (the results of plant growth) and on photosynthesis, which were constructed as independent sub-models. Since the model analyses were all based on the evaluated sub-models (for example, in the cucumber works, plant architectures were constructed by digitized real plants and, in the tomato works, environmental effects on plant architectures were evaluated), the possible issue raised from the second assumption could be minimized.

Many other empirical relationships in the models of this research work (e.g. Eqn 2-7, 2-8, 3-14, 5-4, 5-7, 6-3 *etc.*) mean more assumptions, except the two discussed above, were made for simplifying the modelling work. Due to these simplifications having to be made, George E. P. Box cruelly points out the fact that “*all models are wrong.*” Nevertheless, and fortunately, he also notices that “*but some (models) are useful.*” The models in this work are useful because they all address hypotheses or research questions, which cannot be answered by experimental works. For example, it is not possible to “measure” the photosynthetic limitations experimentally. Therefore, mathematical models, the quantitative limitation analyses, are called for this use (chapter 2 and 3). At the canopy level, it is experimentally almost impossible to estimate all parameters (light interception, biochemical capacity, stomatal and mesophyll conductance) required for the quantitative limitation analyses of all leaves of a plant. Therefore, quantification of the photosynthetic limitations at the whole plant level (chapter 2 and 4) also relies on modelling approaches. It is well known that plant architecture determines canopy light interception and architectural traits are under genetic and environmental control. However, there are still experimental difficulties in disentangling the genetic and environmental effects on architecture and light interception. In terms of dry mass production, architectural effects of an environmental factor mostly occur together with physiological effects. Therefore, it is also experimentally impossible to quantify them separately. For example, changes in temperature and light conditions affect leaf photosynthetic parameters (Yamori *et al.*, 2009; Yamori *et al.*, 2010a), organ morphology and elongation (Kahlen and Stützel, 2011; Caldeira *et al.*, 2014) at the same time, and under salinity, reduction in leaf area occurs together with the reduction of stomatal and mesophyll conductance (Munns and Tester, 2008). In chapter 5, the model analyses were useful because they decouple the temperature effects on architecture and physiological property. The models presented in chapter 4 and chapter 6 were also useful in assessing the pure architectural effects of salinity, which is also experimentally impossible. It can be therefore concluded that these frameworks are useful and provide very valuable theoretical assessments about the impacts of environmental conditions, architectural traits, physiological functions and their interactions on dry mass production.

Future research needs

It is important to stress that the results obtained from this study may not be generalized to all plant species and all cropping system. For example, even in the greenhouse high-wired

cropping system, different architectural effects of salinity were estimated between cucumber and tomato plant grown under similar salinity condition (50 mM NaCl in cucumber, chapter 4 and 40 and 60 mM NaCl in tomato, chapter 6). However, these results highlight the differences in mechanisms of salinity tolerance between species. It also indicates that more insights to salinity tolerance could be obtained by applying these frameworks to other plant species, such as the influences of canopy structure (e.g. cereal crops versus greenhouse crops) or phenology (e.g. fruit tree versus annual crops) on physiological and architectural limitations of plant growth under various environments or stress types. It can also be used for studying the influence of plant morphology on stress tolerance, horticultural practices on canopy photosynthesis and the optimal cropping systems for reducing photosynthetic limitations. Furthermore, functional ecologist would say that having a certain limitation in plant growth, instead of reaching the physiological maximum of growth, may be beneficial for plant development, e.g. to produce mechanically more robust stem or to be less sensible to pathogen (Körner, 2015). It would be also interesting to test, e.g., perhaps through a series of meta-analyses, if this concept should be valid in cropping system.

The quantification of photosynthetic limitations at the canopy level is based on a model for steady-state photosynthesis (von Caemmerer, 2013). For the current simulations, daily average values of photosynthetically active radiation were used to calculate the steady-state photosynthetic limitations. However, plants are constantly subjected to fluctuations in environmental conditions and a steady-state condition is “*an exception rather than a rule*” (Caldeira *et al.*, 2014). Therefore, diurnal variations in photosynthetic limitations have been, but unfortunately rarely, reported in the literature (Grassi *et al.*, 2009; Buckley and Diaz-Espejo, 2015). Recent studies provide more details about the influences of the environmental fluctuations on the dynamics of photosynthetic parameters, e.g. the dynamic behaviour of stomata (Violet-Chabrand *et al.*, 2013; Merilo *et al.*, 2014); rapid change in mesophyll conductance to light interception (Flexas *et al.*, 2007b), CO₂ concentration (Flexas *et al.*, 2007b) or leaf temperature (Evans and von Caemmerer, 2013; von Caemmerer and Evans, 2015), temperature effects on biochemical parameters (Yamori *et al.*, 2009; von Caemmerer, 2013); and light effects on the Rubisco activity (Yamori *et al.*, 2012; Qian *et al.*, 2012). These works provide a solid basis for extending the current static models in order to build a dynamic model. Except the dynamics of photosynthetic parameters, several issues linked to light, temperature and salinity could

be also taken into account when extending the current static model to a dynamic model, e.g. hydraulic processes in the regulation of stomatal conductance and leaf expansion (Caldeira *et al.*, 2014), leaf acclimation to local light (Yamori *et al.*, 2010a) and temperature (Kattge and Knorr, 2007), salt accumulation in leaf (Wolf *et al.*, 1990; Wolf *et al.*, 1991), salt recirculation in plant (Berthomieu *et al.*, 2003; Davenport *et al.*, 2005) and resource allocation within the plant (Buckley *et al.*, 2013; Hirotsuka, 2014). Furthermore, the current models were parameterized for a single cultivar (“Aramon” in cucumber and “Pannovy” in tomato). Using different cultivars in the future research may explore genotypic differences in mechanisms of stress tolerance.

In conclusion, the current study, using cucumber and tomato plants as model crops, demonstrates that FSPM is a valuable tool to disentangle the architectural and non-architectural effects of salinity under different temperature regimes and light conditions, a task which cannot be done experimentally. The two FSPM-frameworks provided in this work may provide insights into inter- and intra-specific differences in the contributions of morphological and physiological mechanisms to stress tolerance.

Supplementary Materials

Text 2-S1: A full mathematical derivation of the limitation analysis under saturating and non-saturating light conditions.

Quantitative limitation analysis at saturating light conditions

Photosynthesis under saturating light conditions can be expressed as (Farquhar *et al.* 1980):

$$A_c = V_{\text{cmax}} \cdot (C_c - \Gamma^*) / (C_c + K_c \cdot (1 + O/K_o)) - R_d \quad (\text{Eqn 2-S1})$$

where A_c is the photosynthesis rate in the Rubisco carboxylation-limited stage ($\mu\text{mol CO}_2 \text{ m}^{-2} \text{ s}^{-1}$), V_{cmax} is the maximum rate of Rubisco carboxylation ($\mu\text{mol CO}_2 \text{ m}^{-2} \text{ s}^{-1}$), C_c ($\mu\text{mol mol}^{-1}$) and O (mmol mol^{-1}) are mol fraction of CO_2 and O_2 at the site of carboxylation, and K_c ($\mu\text{mol mol}^{-1}$) and K_o (mmol mol^{-1}) are Michaelis-Menten constants of Rubisco for CO_2 and O_2 . According to Grassi and Magnani (2005), the relative changes in photosynthesis rate under saturating light conditions, dA_c/A_c , can be expressed by:

$$dA_c/A_c = l_{\text{sc}} \cdot dg_{\text{sc}}/g_{\text{sc}} + l_{\text{mc}} \cdot dg_{\text{m}}/g_{\text{m}} + l_{\text{bc}} \cdot dV_{\text{cmax}}/V_{\text{cmax}} = S_{\text{Lc}} + M_{\text{Lc}} + B_{\text{Lc}} \quad (\text{Eqn 2-S2})$$

$$l_{\text{sc}} = ((g_{\text{tot}}/g_{\text{sc}}) \cdot (\partial A_c / \partial C_c)) / (g_{\text{tot}} + \partial A_c / \partial C_c) \quad (\text{Eqn 2-S3a})$$

$$l_{\text{mc}} = ((g_{\text{tot}}/g_{\text{m}}) \cdot (\partial A_c / \partial C_c)) / (g_{\text{tot}} + \partial A_c / \partial C_c) \quad (\text{Eqn 2-S3b})$$

$$l_{\text{bc}} = g_{\text{tot}} / (g_{\text{tot}} + \partial A_c / \partial C_c) \quad (\text{Eqn 2-S3c})$$

$$\partial A_c / \partial C_c = V_{\text{cmax}} \cdot (\Gamma^* + K_c \cdot (1 + O/K_o)) / (C_c + K_c \cdot (1 + O/K_o))^2 \quad (\text{Eqn 2-S4})$$

where l_{sc} , l_{mc} and l_{bc} are the *relative* limitations of stomatal conductance to CO_2 (g_{sc} , $\text{mol m}^{-2} \text{ s}^{-1}$), mesophyll conductance (g_{m}) and biochemical capacity (V_{cmax}), respectively, summing up to a value of one. Total resistance to CO_2 ($1/g_{\text{tot}}$) is the sum of stomatal and mesophyll resistances ($1/g_{\text{sc}} + 1/g_{\text{m}}$). S_{Lc} , M_{Lc} and B_{Lc} are the contribution of g_{sc} , g_{m} and V_{cmax} to dA_c/A_c respectively. Then the relative change of A_c , g_{sc} , g_{m} and V_{cmax} in Eqn 2-S2 can be approximated by (Grassi and Magnani 2005):

$$dA_c/A_c \approx (A_c^{\text{ref}} - A_c) / A_c^{\text{ref}} \quad (\text{Eqn 2-S5a})$$

$$dg_{\text{sc}}/g_{\text{sc}} \approx (g_{\text{sc}}^{\text{ref}} - g_{\text{sc}}) / g_{\text{sc}}^{\text{ref}} \quad (\text{Eqn 2-S5b})$$

$$dg_{\text{m}}/g_{\text{m}} \approx (g_{\text{m}}^{\text{ref}} - g_{\text{m}}) / g_{\text{m}}^{\text{ref}} \quad (\text{Eqn 2-S5c})$$

$$dV_{\text{cmax}}/V_{\text{cmax}} \approx (V_{\text{cmax}}^{\text{ref}} - V_{\text{cmax}}) / V_{\text{cmax}}^{\text{ref}} \quad (\text{Eqn 2-S5d})$$

where $g_{\text{sc}}^{\text{ref}}$, $g_{\text{m}}^{\text{ref}}$, and $V_{\text{cmax}}^{\text{ref}}$ are the reference values of stomatal and mesophyll conductances and of maximum carboxylation rate, defined as the maximum measured values (Grassi and Magnani 2005). A_c^{ref} is the reference photosynthesis rate assuming g_{sc} , g_{m} and V_{cmax} reach their maxima concomitantly. A_c^{ref} can be calculated by solving the following equation at $C_a = 380 \mu\text{mol mol}^{-1}$ (Grassi *et al.* 2009):

$$A_c^{\text{ref}} = V_{\text{cmax}}^{\text{ref}} \cdot (C_a - A_{\text{cmax}}^{\text{ref}} \cdot (1/g_{\text{sc}}^{\text{ref}} + 1/g_{\text{m}}^{\text{ref}}) - \Gamma^*) / (C_a - A_{\text{cmax}}^{\text{ref}} \cdot (1/g_{\text{sc}}^{\text{ref}} + 1/g_{\text{m}}^{\text{ref}}) + K_c \cdot (1 + O/K_o)) - R_d \quad (\text{Eqn 2-S6})$$

Quantitative limitation analysis at non-saturating light conditions

Here we propose that the quantitative limitation analysis described above can also be applied to non-saturating light conditions. Under non-saturating light conditions, photosynthesis is limited by RuBP regeneration rate (or electron transport rate, J , $\mu\text{mol m}^{-2}\text{s}^{-1}$) and photosynthesis rate (A_j) can be expressed as (Farquhar *et al.* 1980):

$$A_j = J \cdot (C_c - \Gamma^*) / (4C_c + 8\Gamma^*) - R_d \quad (\text{Eqn 2-S7})$$

where J is the rate of electron transport ($\mu\text{mol m}^{-2}\text{s}^{-1}$), which is related to the photosynthetically active irradiance (I_{Int} , $\mu\text{mol photons m}^{-2}\text{s}^{-1}$) and maximum electron transport rate (J_{max} , $\mu\text{mol m}^{-2}\text{s}^{-1}$):

$$J = (K_{2LL} \cdot I_{\text{Int}} + J_{\text{max}} - \sqrt{((K_{2LL} \cdot I_{\text{Int}} + J_{\text{max}})^2 - 4\theta \cdot J_{\text{max}} \cdot K_{2LL} \cdot I_{\text{Int}})}) / (2\theta) \quad (\text{Eqn 2-S8})$$

where K_{2LL} and θ are constants for conversion efficiency of I_{Int} to J ($\text{mol e}^- \text{mol}^{-1}$ photons) and convexity factor for the response of J to I_{Int} , respectively. Applying the method described by Grassi and Magnani (2005) to Eqn 2-S7 and assuming the leaf temperature and respiration rate (R_d) are constants, a small change in photosynthesis (A_j) under non-saturated light condition is the total derivative of Eqn 2-S7:

$$dA_j = (\partial A_j / \partial C_c) \cdot dC_c + (\partial A_j / \partial J) \cdot dJ \quad (\text{Eqn 2-S9})$$

By ignoring the boundary layer conductance, the CO_2 concentration at the site of carboxylation (C_c) is:

$$C_c = C_a - (A_j / g_{sc}) - (A_j / g_m) \quad (\text{Eqn 2-S10})$$

where C_c is the ambient CO_2 concentration (constant). Therefore, the change in C_c is the total derivation of Eqn 2-S10:

$$dC_c = (A_j / g_{sc}) \cdot (dg_{sc} / g_{sc}) + (A_j / g_m) \cdot (dg_m / g_m) - (1 / g_{sc} + 1 / g_m) \cdot dA_j \quad (\text{Eqn 2-S11})$$

The sensitivity of net photosynthesis to electron transport rate can be approximated by:

$$\partial A_j / \partial J \approx A_j / J \quad (\text{Eqn 2-S12})$$

Replacing the dC_c and $\partial A_j / \partial J$ in Eqn 2-S9 by Eqn 2-S11 and Eqn 2-S12, respectively, the following equation can be obtained:

$$dA_j / A_j = l_{sj} \cdot dg_{sc} / g_{sc} + l_{mj} \cdot dg_m / g_m + l_j \cdot dJ / J = S_{Lj} + M_{Lj} + J_L \quad (\text{Eqn 2-S13})$$

$$l_{sj} = ((g_{\text{tot}} / g_{sc}) \cdot (\partial A_j / \partial C_c)) / (g_{\text{tot}} + \partial A_j / \partial C_c) \quad (\text{Eqn 2-S14a})$$

$$l_{mj} = ((g_{\text{tot}} / g_m) \cdot (\partial A_j / \partial C_c)) / (g_{\text{tot}} + \partial A_j / \partial C_c) \quad (\text{Eqn 2-S14b})$$

$$l_j = g_{\text{tot}} / (g_{\text{tot}} + \partial A_j / \partial C_c) \quad (\text{Eqn 2-S14c})$$

$$\partial A_j / \partial C_c = 12J \cdot \Gamma^* / (4C_c + 8\Gamma^*)^2 \quad (\text{Eqn 2-S15})$$

where S_{Lj} , M_{Lj} and J_L are the contributions of stomata and mesophyll conductance and of RuBP regeneration capacity to photosynthetic limitation, l_{sj} , l_{mj} and l_j are the *relative* limitations of stomatal and mesophyll conductance and of electron transport rate, and dA_j / A_j , dg_{sc} / g_{sc} and dg_m / g_m

were obtained in a similar way to Eqn 2-S5a, S5b and 2-S5c, respectively. According to Eqn 2-S8, dJ is:

$$dJ = (\partial J/\partial J_{\max}) \cdot dJ_{\max} + (\partial J/\partial I_{\text{Int}}) \cdot dI_{\text{Int}} \quad (\text{Eqn 2-S16})$$

The first term in Eqn 2-S16 is the change of electron transport rate due to biochemical capacity (J_{dB}) and the second is the change due to irradiance (J_{dI}). Therefore, Eqn 2-S13 can be rewritten by replacing dJ with Eqn 2-S16:

$$dA_j/A_j = l_{\text{sj}} \cdot dg_{\text{sc}}/g_{\text{sc}} + l_{\text{mcj}} \cdot dg_{\text{m}}/g_{\text{m}} + l_j \cdot J_{\text{dB}}/J + l_j \cdot J_{\text{dI}}/J = S_{Lj} + M_{Lj} + B_{Lj} + L_{Lj} \quad (\text{Eqn 2-S17})$$

where B_{Lj} and L_{Lj} are biochemical and light limitation. J_{dB} and J_{dI} represent $\partial J/\partial J_{\max} \cdot dJ_{\max}$ and $\partial J/\partial I_{\text{Int}} \cdot dI_{\text{Int}}$ in Eqn 2-S16, respectively. J_{dB}/J and J_{dI}/J are approximated by:

$$J_{\text{dB}}/J \approx (J_s^{\text{ref}} - J_s)/J_s^{\text{ref}} \quad (\text{Eqn 2-S18a})$$

$$J_{\text{dI}}/J \approx (J_s - J)/J_s^{\text{ref}} \quad (\text{Eqn 2-S18b})$$

where J_s^{ref} is the J with maximum J_{\max} (with highest biochemical capacity) at light saturation, J_s and J are the electron transport rates of the leaves at their the saturating and the intercepted light conditions respectively.

However, Eqn 2-S12 is only satisfied if the respiration rate, R_d , only reduces a small amount of the gross photosynthesis:

$$\partial A_j/\partial J = (C_c - \Gamma^*)/(4C_c + 8\Gamma^*) \quad (\text{Eqn 2-S19a})$$

$$A_j/J = (C_c - \Gamma^*)/(4C_c + 8\Gamma^*) - R_d/J \quad (\text{Eqn S19b})$$

Comparing Eqn 2-S19a and S19b, the approximation in Eqn 2-S12 may introduce small errors in the limitation analysis, especially when the electron transport rate is low.

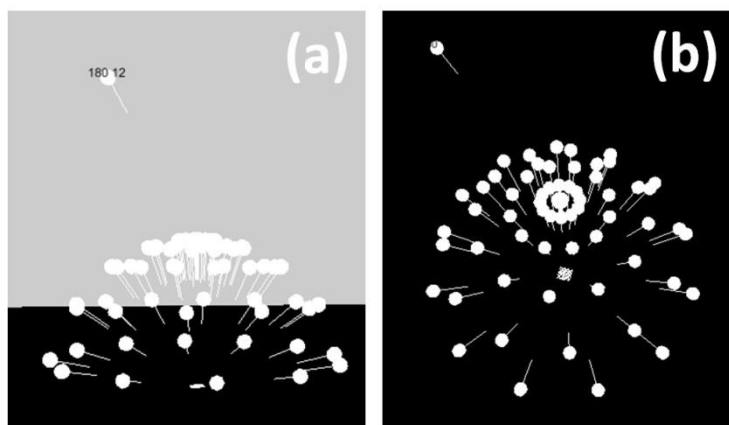


Figure 2-S1: Graphical description of the light model from the side view (a) and the bird view (b).

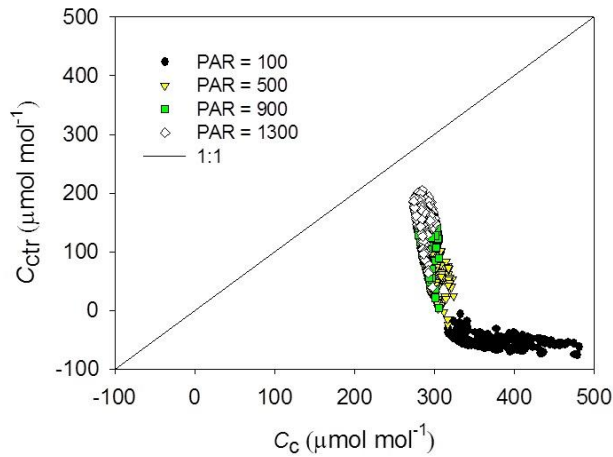


Figure 2-S2: Relationship between C_c and C_{ctr} in all simulations.

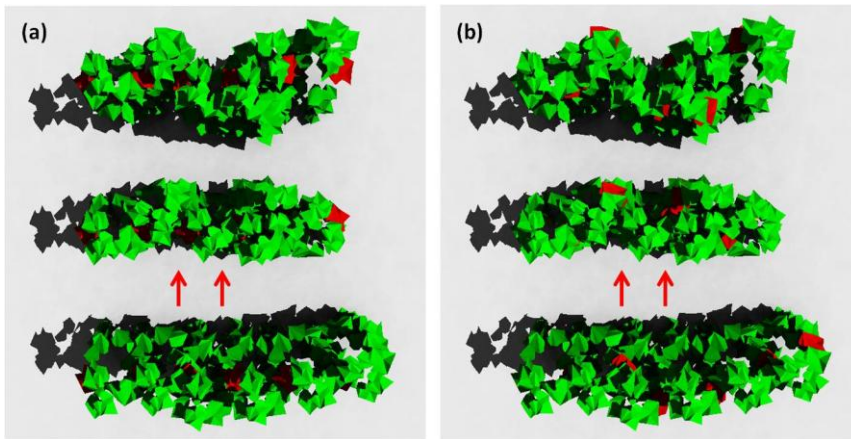


Figure 2-S3: Top view of the virtual canopy. The leaves 10, 13 and 16 of the plants are marked in red colour.

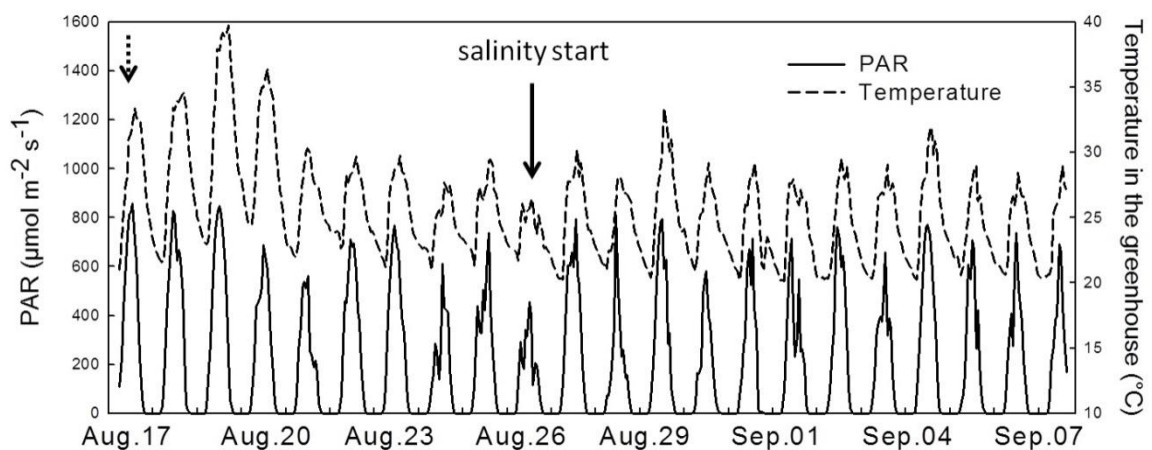


Fig. 3-S1 Variations in daily temperature and photosynthetic active radiation (PAR) in the greenhouse during the experiment. The dotted arrow indicates the day on which the 3rd leaves appeared. The PAR values in the greenhouse represent 60% of the PAR values collected by the PAR sensor (RAM 267.045, Hertsching, Germany) above the greenhouse. The temperature sensor was located 2 meter above ground in the middle of the greenhouse

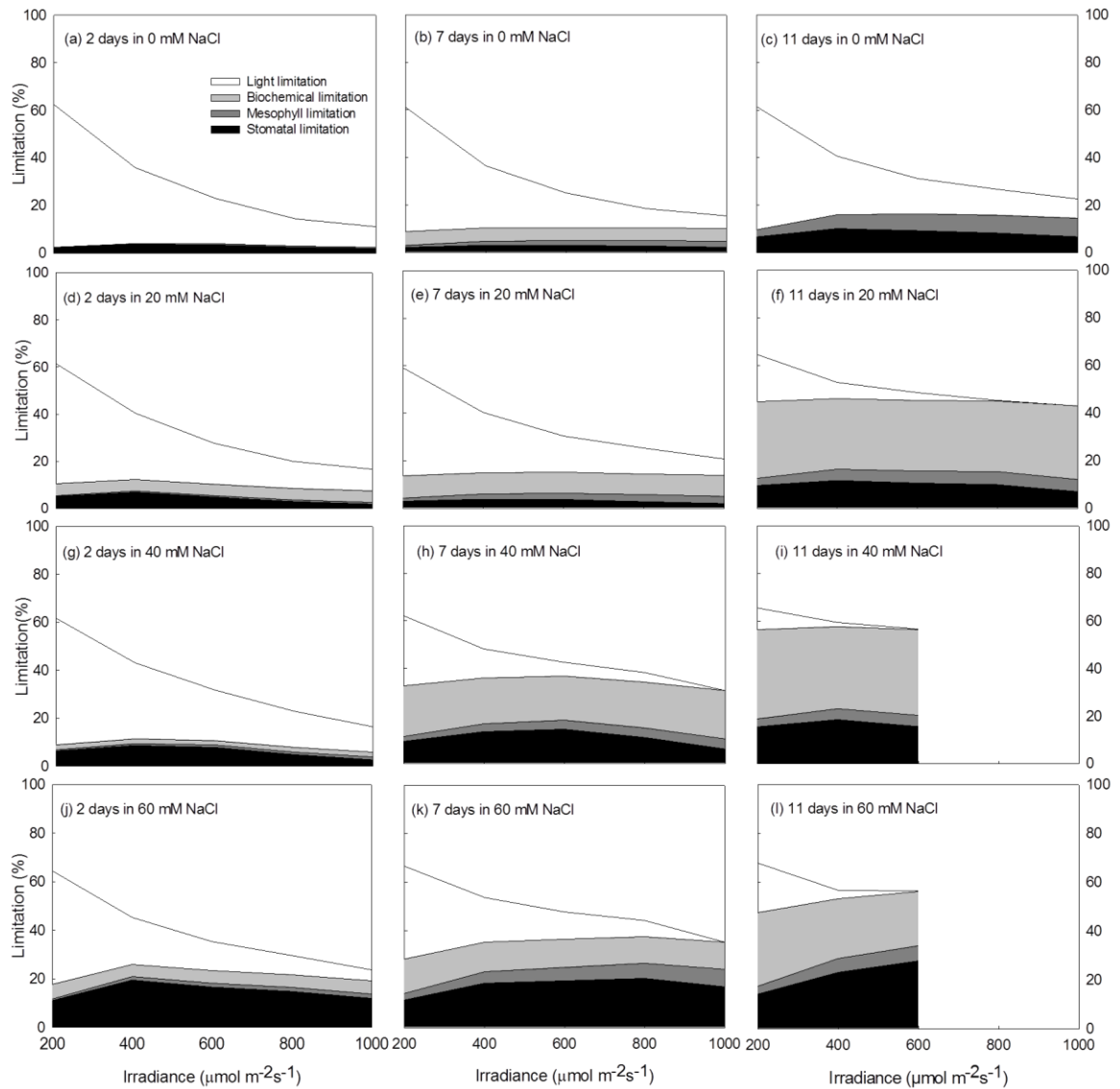


Fig. 3-S2 The results of quantitative limitation analysis at non-saturated light conditions ($C_a = 380 \mu\text{mol mol}^{-1}$) show the photosynthetic limitations of cucumber leaves grown in 0 (a-c), 20 (d-f), 40 (g-i) and 60 (j-l) mM NaCl solution after 2 days (a, d, g and j), 7 days (b, e, j and k) and 11 days (c, f, I and l);. The black, dark grey, grey and white areas represent the stomatal, mesophyll, biochemical and light limitation respectively. On the day 11, limitation analysis was not conducted at PPFD = 800 and 1000 $\mu\text{mol m}^{-2}\text{s}^{-1}$ for the leaves grown in 40 and 60 mM NaCl because these were already the saturated light conditions for the leaves

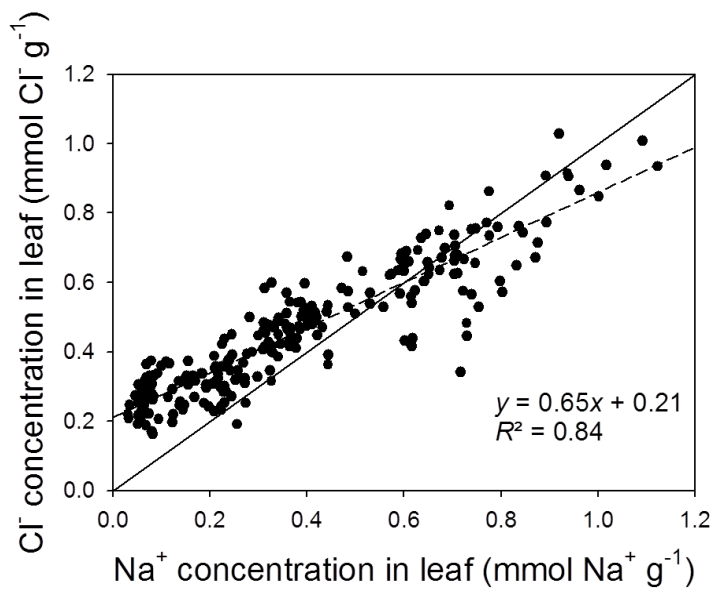


Fig. 3-S3 Relationship between Na^+ and Cl^- concentration in cucumber leaves in the experiments. The solid line represents the 1:1 line and the dashed line is the regression line ($p < 0.001$). 95% Confidence intervals of intercept and slope are 0.19-0.22 and 0.61-0.68, respectively.

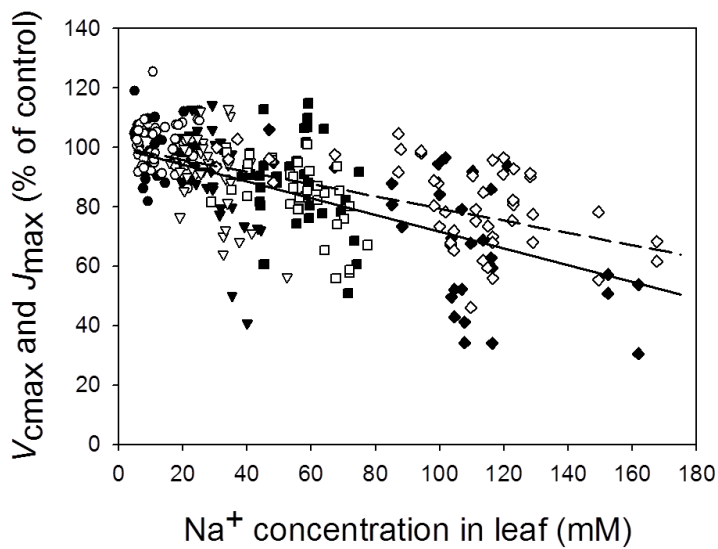


Fig. 3-S4 Relationships between V_{cmax} (closed symbols), J_{max} (open symbols) and Na^+ concentration in leaf. Circle, reverse triangle, square and rhombus represent data collected from plants subjected to 0, 20, 40 and 60 mM NaCl in the nutrient solution, respectively.

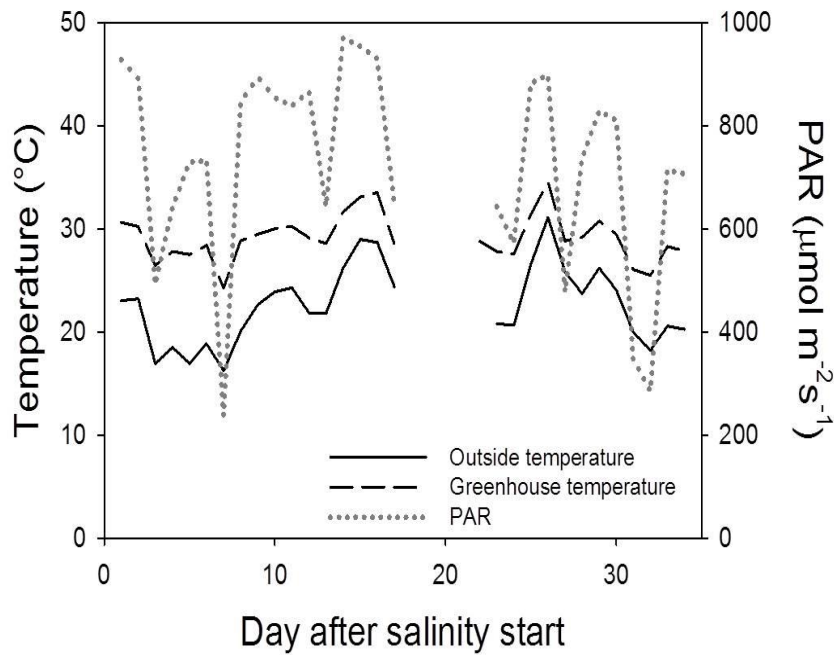
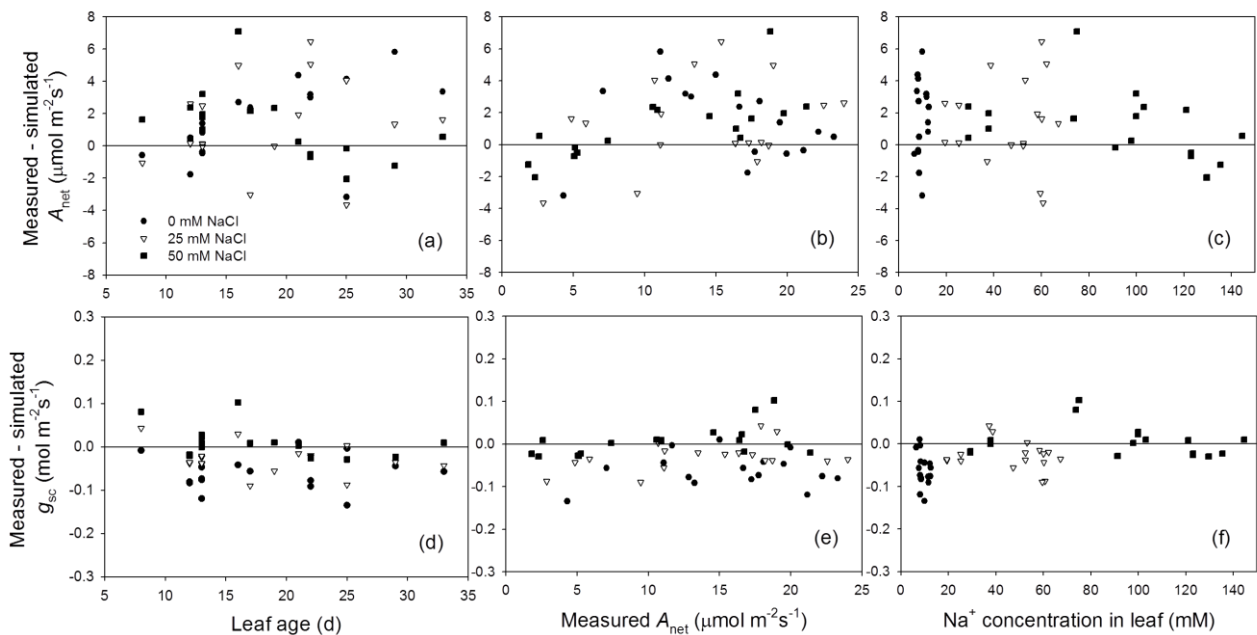


Figure 4-S1. Variations in daily average temperatures and photosynthetic active radiation (PAR) during the experiment (0600-2000 h). Solid and dashed lines represent average temperature out- and inside the greenhouse, respectively. The temperature sensor was located 2 meter above ground in the

middle of the greenhouses and the PAR sensor (RAM 267.045, Herrsching, Germany) was located above the greenhouse. Climate data on days 18-22 after salinity start were not recorded due to technical disturbance. The average differences in air temperature between two greenhouses



were 0.45°C.

Figure 4-S2. Dependencies of the differences between measured and simulated photosynthesis rate (A_{net} , a, b, c) and stomatal conductance to CO_2 (g_{sc} , d, e, f) to leaf age (a,d), measured A_{net} (b, e) and Na^+ concentration in leaf (c, f). Each point represents the average of eight point measurements and simulations.

4-Note S1: Evaluation of the quantitative limitation analysis using numerical integration and using partial differentiation

Buckley and Diaz-Espejo (2015) proposed that using numerical integration method (referred to as BDE approach) instead of using partial differentiation method (proposed by Grassi and Magnani, 2005; referred to as GM approach) provides more accurate results of dissecting photosynthetic limitation. Here we evaluated the GM approach by simulations similar to those used in Buckley and Diaz-Espejo (2015) and compared the outcomes of both approaches. All abbreviations used in this supplementary note are in accordance with those in Chen *et al.* (2015).

Evaluation of the partial differentiation method

To evaluate the partial differentiation method, total limitations calculated by Eqn 4-8 and 4-9 were compared with the theoretical limitations. The total limitations represent the sum of all limitation ($L_{Sj} + L_{Mj} + L_{Bj} + L_{Lj}$ and $L_{Sc} + L_{Mc} + L_{Bc}$ in Eqn 4-8 and 4-9, respectively), and the theoretical limitations are defined as $(A_j^{\text{ref}} - A_j)/A_j^{\text{ref}}$ and $(A_c^{\text{ref}} - A_c)/A_c^{\text{ref}}$, for non-saturating and saturating light conditions, respectively. Errors were defined by the difference between total limitation and theoretical limitation. For the simulations under saturating light conditions, A_c^{ref} was assumed to be the photosynthesis rate at $g_{\text{tot}} = 0.4 \text{ mol m}^{-2}\text{s}^{-1}$ and $V_{\text{cmax}} = 150 \text{ } \mu\text{mol CO}_2 \text{ m}^{-2}\text{s}^{-1}$ ($O = 210 \text{ mmol mol}^{-1}$; $K_c = 405 \text{ } \mu\text{mol mol}^{-1}$; $K_o = 278 \text{ mmol mol}^{-1}$; Γ^* , $43.02 \text{ } \mu\text{mol mol}^{-1}$; $R_d = 1.08 \text{ } \mu\text{mol CO}_2 \text{ m}^{-2} \text{ s}^{-1}$); A_c was simulated with four representative values of g_{tot} (0.05, 0.1, 0.2 and $0.4 \text{ mol m}^{-2}\text{s}^{-1}$, assuming $g_{\text{sc}} = g_m$) and V_{cmax} ranging between 0 and $150 \text{ } \mu\text{mol CO}_2 \text{ m}^{-2}\text{s}^{-1}$. Using the same parameters, the total limitation of photosynthesis was calculated by summing L_{Sc} , L_{Mc} and L_{Bc} in Eqn 9 (assuming $V_{\text{cmax}}^{\text{ref}} = 150 \text{ } \mu\text{mol CO}_2 \text{ m}^{-2}\text{s}^{-1}$, $g_{\text{sc}}^{\text{ref}} = 0.8 \text{ mol m}^{-2}\text{s}^{-1}$ and $g_m^{\text{ref}} = 0.8 \text{ mol m}^{-2}\text{s}^{-1}$, resulting in a $g_{\text{tot}}^{\text{ref}} = 0.4 \text{ mol m}^{-2}\text{s}^{-1}$). To evaluate the GM approach at non-saturating light conditions, A_j^{ref} was assumed to be the photosynthesis rate at $J_{\text{max}} = 200 \text{ } \mu\text{mol m}^{-2}\text{s}^{-1}$, $I_{\text{ab}} = 1500 \text{ } \mu\text{mol m}^{-2}\text{s}^{-1}$, $g_{\text{sc}} = 0.8 \text{ mol m}^{-2}\text{s}^{-1}$, $g_m = 0.8 \text{ mol m}^{-2}\text{s}^{-1}$, $K_{2\text{LL}} = 0.425$ and $\theta = 0.7$. A_j was simulated with $J_{\text{max}} = 150$ or $50 \text{ } \mu\text{mol m}^{-2}\text{s}^{-1}$, $g_m = 0.6$ or $0.4 \text{ mol m}^{-2}\text{s}^{-1}$, and I_{ab} ranging from 50 to $1500 \text{ } \mu\text{mol m}^{-2}\text{s}^{-1}$. For simplification, a linear relationship between g_{sc} and I_{ab} was assumed ($g_{\text{sc}} = 0.16 + 0.00015I_{\text{ab}}$) and the possible dependency of g_m to I_{ab} was assumed to be negligible. The same parameters were used to calculate L_{Sj} , L_{Mj} , L_{Bj} and L_{Lj} in Eqn 4-9.

The results showed that the errors resulted from GM approach were less than 3% of the reference photosynthesis rate, both under saturating (Fig. 4-Note-1) and non-saturating (Fig. 4-Note-2) light conditions.

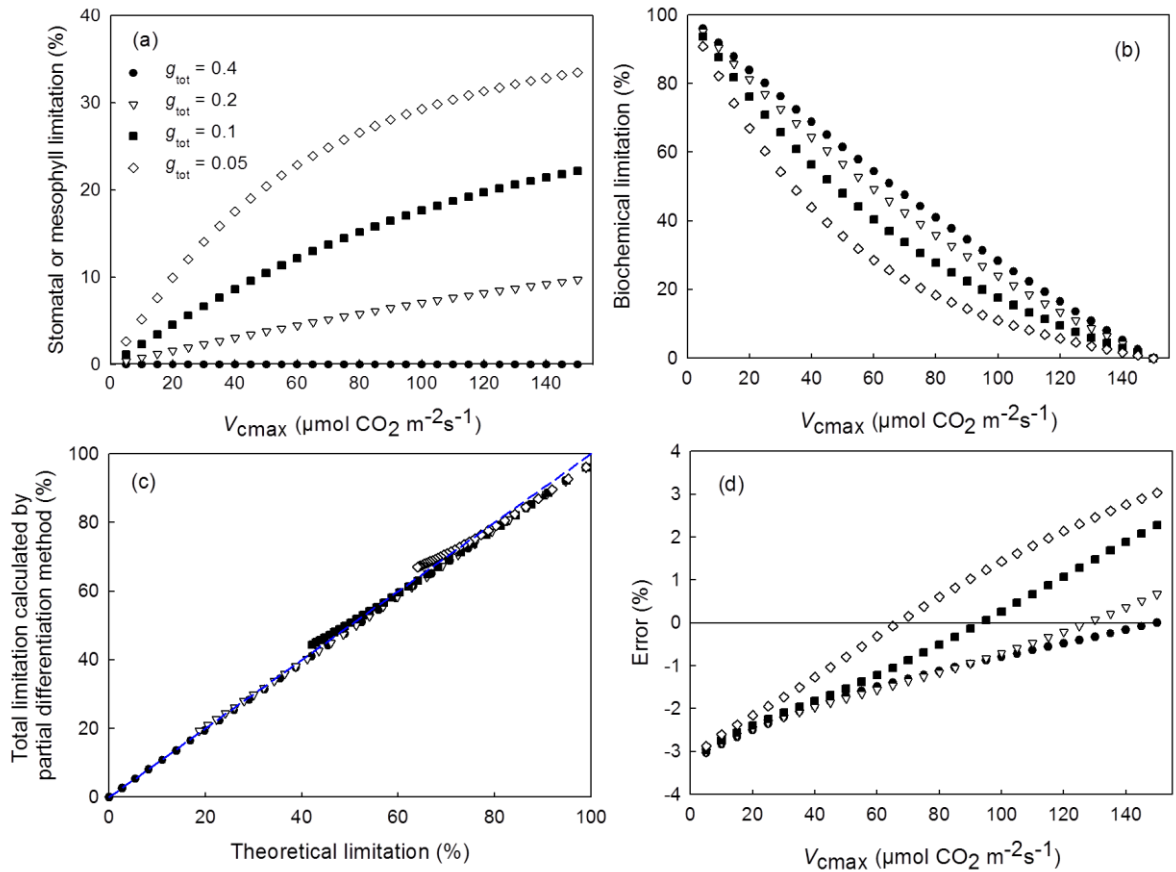


Figure 4-Note-1 Influence of V_{cmax} on diffusional (stomatal or mesophyll) limitations (a) and biochemical limitation (b) at different values of g_{tot} ($\text{mol m}^{-2} \text{ s}^{-1}$). (c) Comparison of the theoretical limitation with the limitation calculated by the quantitative limitation analysis ($L_{Sc} + L_{Mc} + L_{Bc}$ in Eqn 4-9). The dotted line represents the 1:1 relationship. (d) Error of the GM approach at saturating light conditions (% of A_c^{ref}).

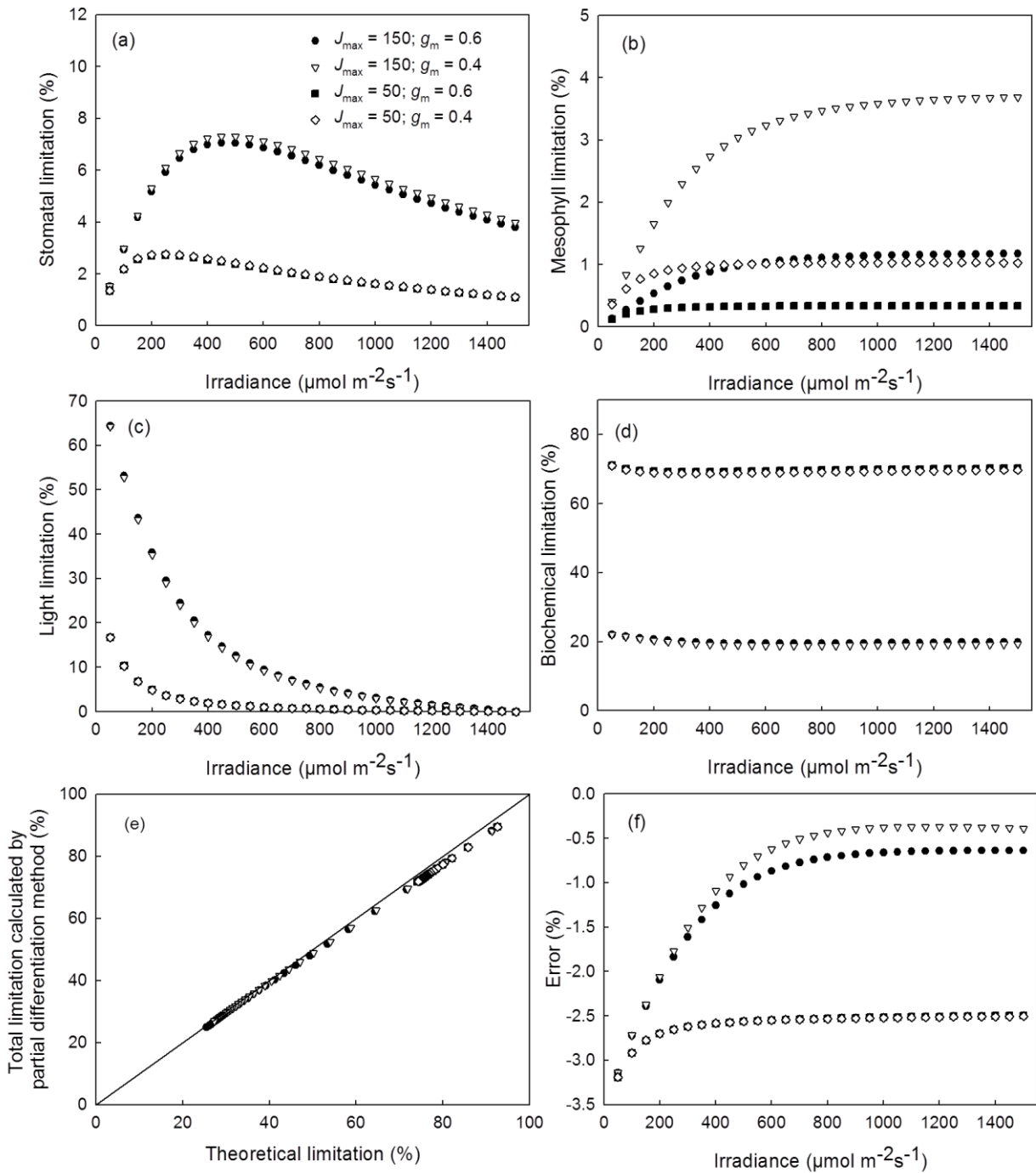


Figure 4-Note-2. Influence of irradiance on the (a) stomatal (L_{Sj}), (b) mesophyll (L_{Mj}), (c) light (L_{Lj}) and (d) biochemical (L_{Bj}) limitation to photosynthesis at four different combinations of electron transport capacity, J_{max} ($\mu\text{mol m}^{-2}\text{s}^{-1}$), and mesophyll conductance, g_m ($\text{mol m}^{-2}\text{s}^{-1}$). (e) Comparing the theoretical limitation with the limitation calculated by the quantitative limitation analysis ($L_{Sj} + L_{Mj} + L_{Bj} + L_{Lj}$ in Eqn 4-8). The solid line represents the 1:1 line. (f) The errors under non-saturating light conditions (% of A_j^{ref}).

Comparisons between GM approach and BDE approach

Using the dataset shown in Fig.4-4, the results from GM approach were compared with those from BDE approach. This dataset contained more than 1000 simulated points including g_{sc} ranging from 0.02 – 0.37 mol m⁻²s⁻¹, g_m ranging from 0.05 – 0.7 mol m⁻²s⁻¹, V_{cmax} ranging from 20 – 140 μmol m⁻²s⁻¹, J_{max} ranging from 30 – 170 μmol m⁻²s⁻¹, R_d ranging from 0.20 – 1.08 μmol m⁻²s⁻¹ and I_{ab} ranging from 10-1000 μmol m⁻²s⁻¹, representing a wide spectrum of variations in photosynthetic parameters. All results and differences between two approaches are described in percentage of the reference photosynthesis rate. Temperature for all simulations was assumed to be 25°C. Total limitations calculated by BDE approach were well in accordance with the total limitation calculated by GM approach (Fig. 4-Note-3a). In general, BDE approached estimated a higher (1.1±1.8%) total limitation than GM approach, especially when the theoretical limitation was low. The errors from GM approach were from -4% to 1% while the errors from BDE approach were from -9% to 7% (Fig. 4-Note 1-3b). BDE approach tended to overestimate total limitation when the photosynthesis rate was high (low theoretical limitation) and the average errors of GM and BDE approaches were -0.8±0.9% and 0.3±1.8%, respectively. The reason that GM approach underestimates the total limitation could be that day respiration rate, R_d , is assumed to be ignorable in the GM approach. However, R_d may contribute up to 4% to photosynthetic limitation.

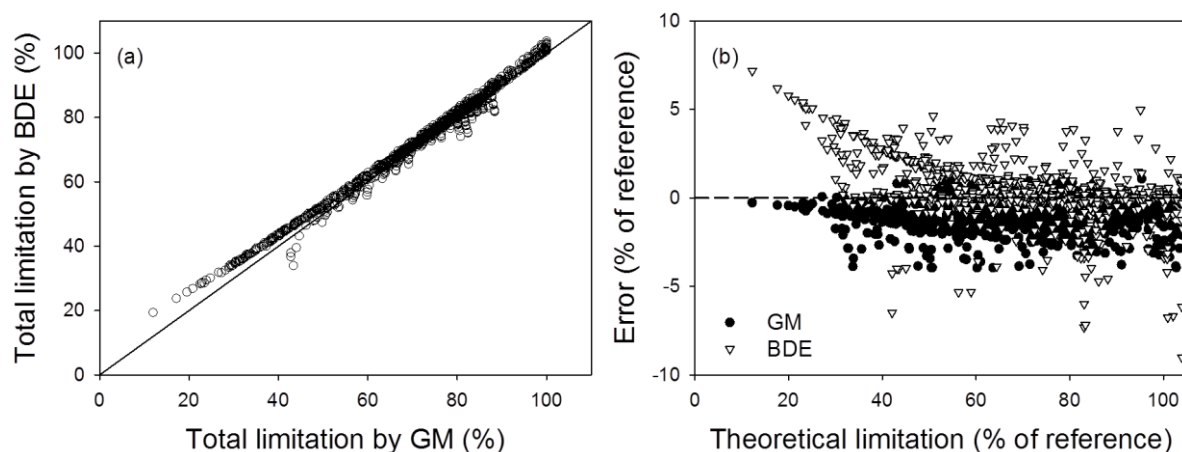


Figure 4-Note-3. (a) Comparison between total limitations calculated by partial differentiation method proposed by Grassi and Magnani (GM approach) and by numerical integration proposed by Buckley and Diaz-Espejo (BDE approach). The solid line represents the 1:1 line. (b) Dependencies of errors (differences between total limitation and theoretical limitation) on theoretical limitation. The dashed line represents the $y = 0$ line.

Differences in partitioning contributions of photosynthetic limitations

In the following, stomatal, mesophyll, biochemical and light limitations were noted as L_s , L_m , L_b and L_l , respectively. Additional subscripts, _{GM} and _{BDE}, indicate a limitation calculated by GM or

by BDE approach, respectively, e.g. $L_{s,GM}$ or $L_{s,BDE}$. Furthermore, Δ before a limitation indicates the difference between two approaches, e.g. $\Delta L_s = L_{s,BDE} - L_{s,GM}$. Furthermore, L_d and L_j indicate diffusional limitation ($L_d = L_s + L_m$) and limitation due to electron transport rate ($L_j = L_b + L_l$; most data points are A_j -limited in this dataset).

The main differences between GM and BDE approaches were the partitioning of contributions of different photosynthetic limitation. The range of $L_{s,GM}$ (between 0 and 28%) was different from the range of $L_{s,BDE}$ (between 5 and 14%, Fig. 4-Note-4a), although relationship between $L_{s,GM}$ and $L_{s,BDE}$ was found ($R^2 = 0.57$). The range of $L_{m,GM}$ (between 0 and 13%) was also wider than the range of $L_{m,BDE}$ (between 0 and 6%). When the total diffusional conductance (g_{tot}) was smaller, ΔL_d was farer from zero (Fig. 4-Note-4b). Similar relationships between ΔL_s and stomatal conductance and between ΔL_m and mesophyll conductance were found (data not shown). Strong correlations were found between $L_{b,GM}$ and $L_{b,BDE}$ and between $L_{l,GM}$ and $L_{l,BDE}$ ($R^2 = 0.85$ and 0.90 , respectively; Fig. 4-Note-4c). In average, $L_{b,GM}$ was 6.0% higher than $L_{b,BDE}$ but $L_{l,GM}$ was 7.3% lower than $L_{l,BDE}$. ΔL_b was negative correlated with ΔL_l (Fig. 4-Note-4d). Since both biochemical capacity and light absorption are related to L_j in the model and since there is a strong correlation between $L_{j,GM}$ and $L_{j,BDE}$ ($y = 0.75x + 15.30$, $R^2 = 0.95$, Fig. 4-Note-4e), it seems that BDE approach partitions the contribution of electron transport rate to photosynthetic limitation more into L_l and less into L_b than GM approach. This may be resulted from that, in GM approach, the relative changes of electron transport rate due to biochemical capacity and light interception (dJ_b/J and dJ_l/J) are approximated step-wisely by the differences between reference electron transport rate, electron transport rate at saturating light and actual electron transport rate (see Eqn 12a and 12b in Chen *et al.*, 2015), but not based on the partial differentiation of the equation in the model (see Eqn 8 in Chen *et al.*, 2015 or Eqn 5 in this manuscript). This indicates that GM approach may mathematically (according to Eqn 5 in this manuscript) overestimate L_b and underestimate L_l , especially when the light absorption and the biochemical capacity of a leaf are far from their references (Fig. 4-Note-4g and Fig. 4-Note-4h, respectively). The strong negative correlation between ΔL_d and ΔL_j ($y = -0.86x + 1.30$, $R^2 = 0.96$; Fig. 4-Note-4f) and the almost 1:1 relationship between total limitations calculated by both approaches indicates that GM and BDE approaches mainly differ from partitioning the contributions of photosynthetic limitations into diffusional processes or biochemical processes. For example, BED approach estimated lower contributions of diffusional and biochemical limitations (Fig. 4-Note-5a, 1-5b, 1-5c) but higher contribution of light limitation (Fig. 4-Note-5d). The differences between two approaches in estimating the effects of 25 mM NaCl on the contributions of photosynthetic limitations was smaller than 5% (Fig. 4-Note-6). In the lower canopy (leaves with lower leaf ranks in Fig. 4-Note-6), GM approach estimated a higher salinity effect on L_d but a lower salinity effect on L_b . In the upper canopy, the differences in salinity effect on photosynthetic limitations between two approaches were less than 8% and GM approach estimated a higher salinity effect on L_s and L_b but a lower salinity effect on L_l .

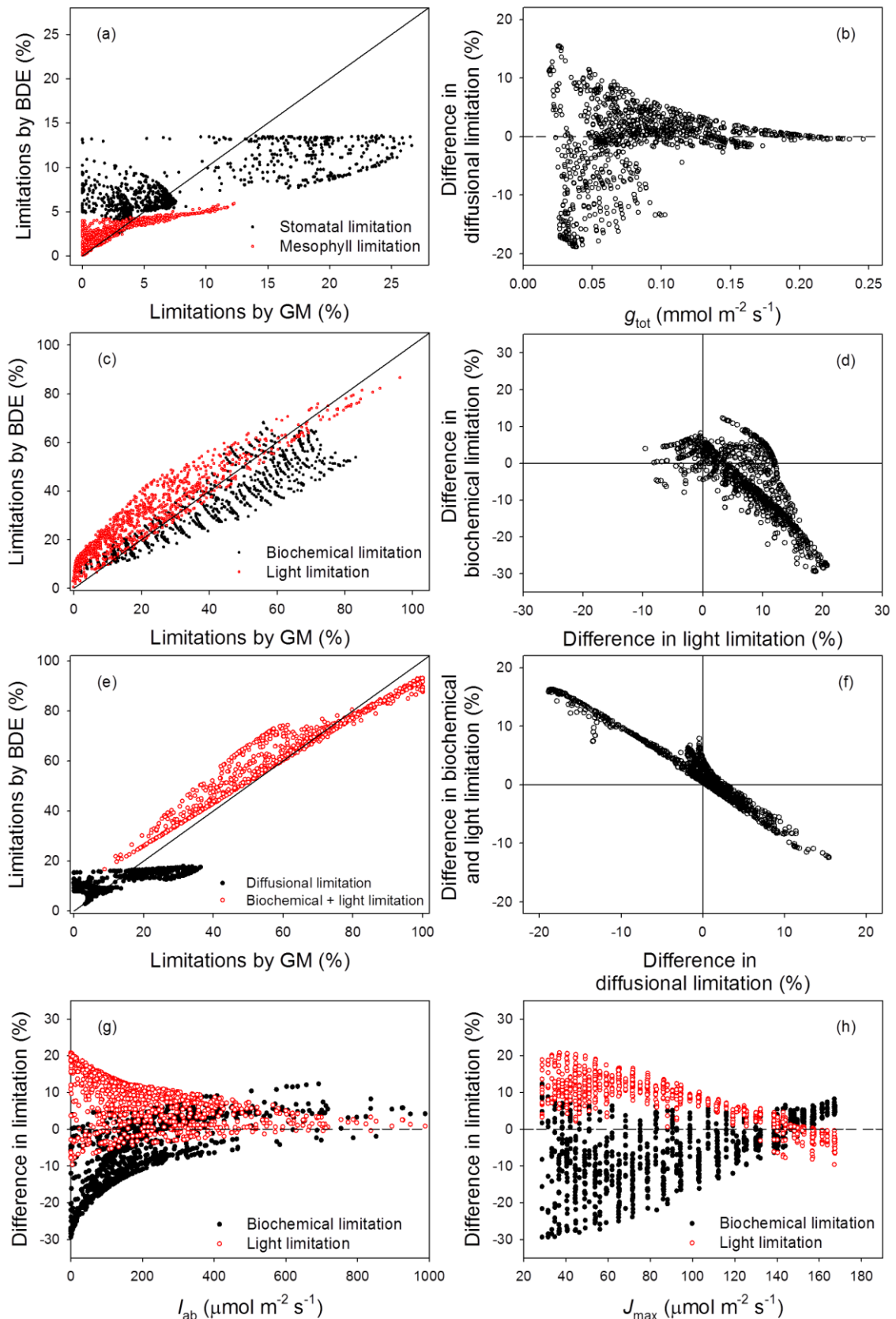


Figure 4-Note-4. Comparisons between stomatal (L_s), mesophyll (L_m), biochemical (L_b) and light (L_l) limitations calculated by partial differentiation method (GM approach) and by numerical integration method (BDE approach). (a) comparisons between L_s and L_m ; (b) relationship between total CO_2 conductance (g_{tot}) and differences in diffusional limitation ($L_d = L_s + L_m$) between BDE and GM approaches; (c) comparisons between L_b and L_l ; (d) relationship between differences in L_b and L_l between BDE and GM approaches; (e) comparisons between L_d and $L_b + L_l$; (f) relationship between differences in L_d and $L_b + L_l$ between BDE and GM approaches; (g) dependencies of differences in L_b and L_l to absorbed light (I_{ab}) and (h) dependencies of the differences in L_b and L_l to biochemical capacity (J_{max}).

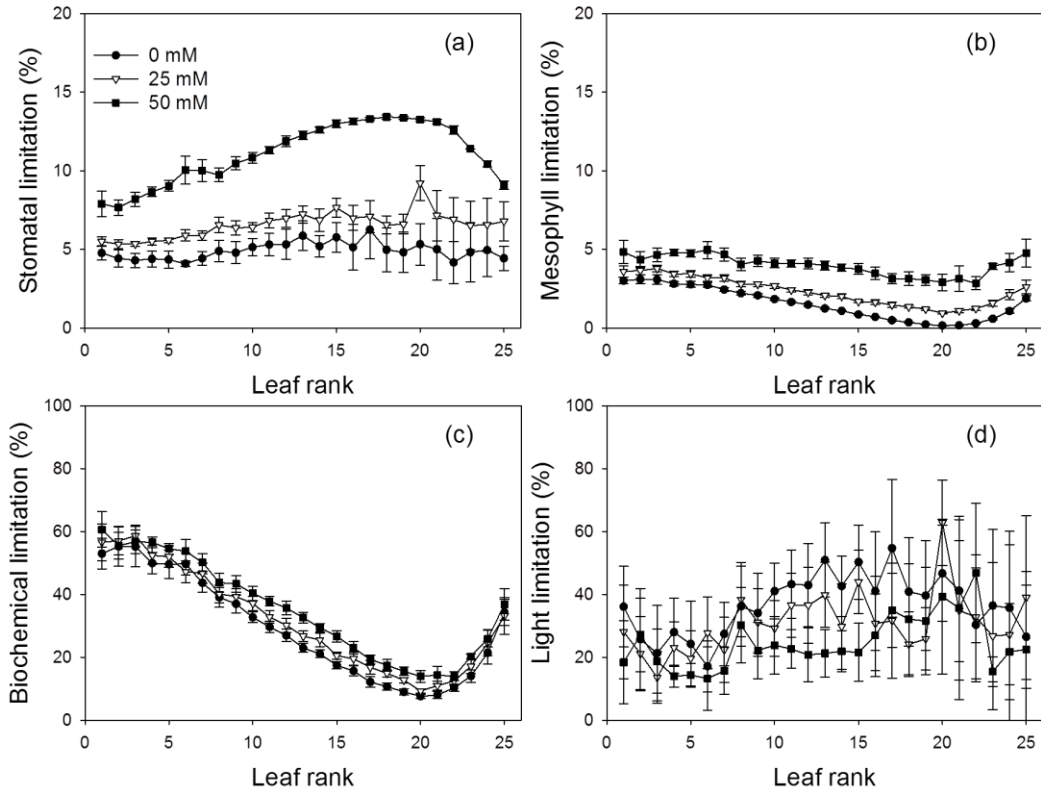


Figure 4-Note-5. Calculating (a) stomatal, (b) mesophyll, (c) biochemical and (d) light limitations by the numerical integration approach proposed by Buckley and Diaz-Espejo (2015), using the same dataset presented in Fig.4-4.

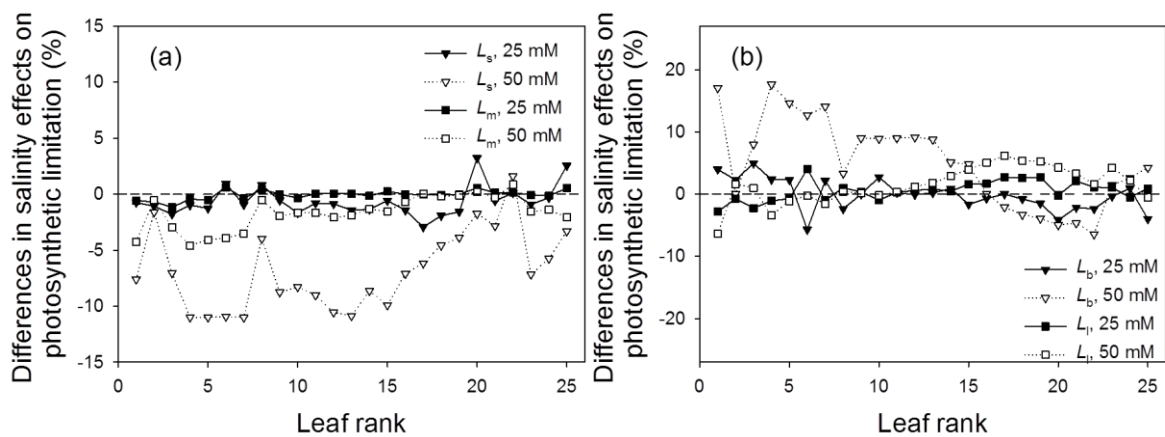


Figure 4-Note-6. Differences between BDE and GM approaches in estimating salinity effects on (a) stomatal limitation (L_s) and mesophyll limitation (L_m) and (b) biochemical limitation (L_b) and light limitation (L_l) under 25 and 50 mM NaCl in the nutrient solution. The salinity effect on a limitation was the increase of the limitation due to salinity stress, e.g. the effect of 25 mM NaCl on L_s was the L_s under 25 mM NaCl minus L_s under 0 mM NaCl. Therefore, a more positive value in the figure indicates that BDE approach estimates a higher salinity effect on that limitation.

Table 5-S1 Summary of experimental conditions.

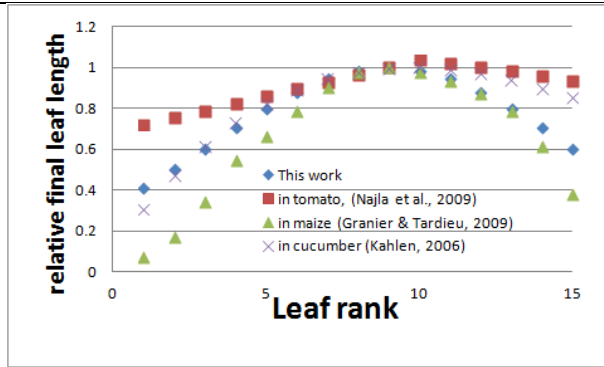
Expt.	Location	Set conditions			
		Day/night temperature (°C)	VPD (kPa)	PAR ($\mu\text{mol m}^{-2} \text{s}^{-1}$)	CO ₂ (ppm)
1	Growth chamber	17/13, 22/18, 26/22 & 30/26	0.8	300	380
2	Growth chamber	22/18	0.4, 0.8 & 1.2	300	380
3	Growth chamber	22/18	0.8	300, 500 & 700	380
4	Greenhouse	22/18	-	-	ambient
5	Greenhouse	22/18 & 32/28	-	-	ambient

Table 5-S2 Schedule for experiment cultivation

Experiment	Sowing	Transplanting to large rock wool cubes	Transplanting to growth chambers or greenhouses
1	5 Aug 2008	18 Aug 2008	22 Aug 2008
2	23 Oct 2008	5 Oct 2008	8 Oct 2008
3	23 Feb 2009	3 Mar 2009	9 Mar 2009
4	11 May 2009	20 May 2009	30 May 2009
5	22 Mar 2010	1 Apr 2010	14 Apr 2010

Table 5-S3. Values of all parameters used in the model and their comparable values reported in the literature. Numbers in brackets denote equation numbers.

Parameter (Eqn)	Our value	Unit	Value in the literature
T_{bl} (5-2a & b)	6.8	°C	5.9°C in tomato in Heuvelink (1995) 6-10°C in tomato in Calado and Portas (1987) 8°C in tomato in Najla <i>et al.</i> (2009)
$a_{El,max}$ (5-2a & b)	0.318	-	For $a_{El,max}$, $b_{El,max}$, $TS_{l,max}$ and h_l , no comparable parameters were found for tomato in the literature. However, Reymond <i>et al.</i> (2003) reported in maize that $a_{El,max}$ and $b_{El,max}$ range between 0.3 — 0.6 and -0.14 — -0.06, respectively. We do not find T_{opt} for tomato, but this parameter is between 25-30°C for most of plant species (Parent and Tardieu, 2012)
$b_{El,max}$ (5-2a & b)	-0.0291	-	
T_{opt} (5-2a & b)	28	°C	
$TS_{l,max}$ (5-3)	135	°Cd	
h_l (5-3)	82	-	
R_{max} (5-4)	9	-	R_{max} and h_r described the effect of leaf rank on leaf length. Here we compare the effect of leaf rank on final leaf length in different species. Points in the graph are derived from published data.
h_r (5-4)	6	-	



a_{Al} (5-5)	0.92	-	Schwarz and Kläring (2001) reported several sets of a_{Al} and g in tomato. a_{Al} was between 0.26-0.42 and g was between 2.03-2.70.
g (5-5)	2.4	-	
a_r (5-6a)	0.37	-	For a_r and b_r , no comparable parameters were found for tomato in the literature.
b_r (5-6a)	0.63	-	
a_θ (5-7)	114.6	-	Parameters in Eqn 5-7 and 5-8 describe the relationship between leaf length and leaf angle (θ). Najla <i>et al.</i> (2009) assumed that θ equal to 60° for all leaves, which is not realistic; Sarlikioti <i>et al.</i> (2011a) reported that θ ranges from 75° - 125° ; and de Visser <i>et al.</i> (2014) assumed that θ ranges from 60° - 90° . The simulated leaf angles in this work range between 45° - 100° (Fig. 5-4), which are in accordance with the data in the literature.
b_θ (5-7)	0.04	-	
a_{Cl} (5-8a)	200	$^\circ$	
b_{Cl} (5-8a)	2.6	$^\circ \text{ cm}^{-1}$	
a_{1Cl} (5-8b)	-161	$^\circ$	
b_{1Cl} (5-8b)	4.75	$^\circ \text{ cm}^{-1}$	
T_{bi} (5-9)	10	$^\circ\text{C}$	6-10 $^\circ\text{C}$ in tomato in Calado and Portas (1987) 8 $^\circ\text{C}$ in tomato in Najlia <i>et al.</i> (2009)
$a_{Ei,max}$ (5-9)	0.063	-	For $a_{Ei,max}$, $b_{Ei,max}$, $TS_{i,max}$ and h_i , no comparable parameters were found for tomato in the literature. Najla <i>et al.</i> (2009) simply described the growth of internode length increase 1.1 mm per $^\circ\text{Cd}$.
$b_{Ei,max}$ (5-9)	0.0000526	-	
$TS_{i,max}$ (5-10)	85	$^\circ\text{Cd}$	
h_i (5-10)	35	-	
a_{Di} (5-11)	1.33	cm	For a_{Di} and b_{Di} , no comparable parameters were found for tomato in the literature.
b_{Di} (5-11)	0.0011	cm $^\circ\text{Cd}^{-1}$	
μ (5-13)	0.87		0.89 in tomato in Maggio <i>et al.</i> , 2007 0.70-0.91 in tomato in Ågren and Franklin (2003)
Phy	144 \pm 10	$^\circ$	130 $^\circ$ in tomato in de Visser <i>et al.</i> (2014) 137.5 $^\circ$ in tomato in Tomato Anatomy 144 $^\circ$ in tomato in Najlia <i>et al.</i> (2009)
$TS_{1,sen}$	980	$^\circ\text{Cd}$	8-10 weeks in tomato in John <i>et al.</i> (1995). We recalculated $TS_{1,sen}$ according to the experimental condition in John <i>et al.</i> (1995) (22/18 $^\circ\text{C}$ day night temperature). $TS_{1,sen}$ ranges between 851-1064 $^\circ\text{Cd}$ in this experiment.

Ågren GI and Franklin O. 2003. Root: shoot ratios, optimization and nitrogen productivity. *Annals of Botany* **92**, 795-800.

Calado AM and Portas CM. 1987. Base-temperature and date of planting in processing tomatoes. *Acta Horticulturae* **200**, 185-188.

de Visser PHB, Buck-Sorlin GH and van der Heijden GWAM. 2014. Optimizing illumination in the greenhouse using a 3D model of tomato and a ray tracer. *Frontier in Plant Science* **5**, 48. doi:10.3389/fpls.2014.00048

Granier C and Tardieu. 2009. Multi-scale phenotyping of leaf expansion in response to environmental changes: the whole is more than the sum of parts. *Plant, Cell and Environment* **32**, 1175-1184.

Heuvelink E. 1995. Growth, development and yield of a tomato crop: periodic destructive measurements in a greenhouse. *Scientia Horticulturae* **61**, 77-99.

- John, I., Drake, R., Farrell, A., Cooper, W., Lee, P., Horton, P. and Grierson, D.** 1995. Delayed leaf senescence in ethylene-deficient ACC-oxidase antisense tomato plants: molecular and physiological analysis. *The Plant Journal*, **7**, 483–490. doi: 10.1046/j.1365-313X.1995.7030483.x
- Kahlen K.** 2006. 3D Architectural modelling of greenhouse cucumber (*Cucumis sativus* L.) using L-systems. *Acta Horticulturae* **718**, 51-59.
- Maggio A, Raimondi G, Martino A, Pascale S de.** 2007. Salt stress response in tomato beyond the salinity tolerance threshold. *Environmental and Experimental Botany* **59**, 276–282.
- Najla S, Vercambre G, Pages L, Grasselly D, Gautier H, Genard M.** 2009. Tomato plant architecture as affected by salinity: Descriptive analysis and integration in a 3-D simulation model. *Botany* **87**, 893–904.
- Parent B, Tardieu F.** 2012. Temperature responses of developmental processes have not been affected by breeding in different ecological areas for 17 crop species. *New Phytologist* **194**, 760–774.
- Reymond M, Muller B, Leonardi A, Charcosset A, Tardieu F.** 2003. Combining quantitative trait loci analysis and an ecophysiological model to analyze the genetic variability of the responses of maize leaf growth to temperature and water deficit. *Plant Physiology* **131**, 664–675.
- Sarlikioti V, Visser PHB de, Buck-Sorlin GH, Marcelis LFM.** 2011a. Exploring the spatial distribution of light interception and photosynthesis of canopies by means of a functional–structural plant model. *Annals of Botany* **107**, 875-883.
- Schwarz D and Kläring PH.** 2001. Allometry to estimate leaf area of tomato. *Journal of Plant Nutrition* **24**, 1291-1309, DOI: [10.1081/PLN-100106982](https://doi.org/10.1081/PLN-100106982)

Table. 5-S4 Influence of leaf curvature and leaf length:width ratio on light transmission through the simulated tomato canopy (Q_t/Q_0), light extinction coefficient (k), and on different days expressed in days after appearance of the first true leaf (DAFLA) at 22/18°C (LT, black bar) and 32/28°C (HT, grey bar) day/night temperature conditions. Numbers are means with standard error in parentheses.

Scenario	DAFLA	LT		HT	
		Q_t/Q_0	k	Q_t/Q_0	k
70% leaf curvature					
	28	0.66 (0.01)	0.75 (0.03)	0.70 (0.02)	0.64 (0.05)
	43	0.36 (0.02)	0.70 (0.04)	0.48 (0.02)	0.62 (0.04)
	56	0.28 (0.02)	0.59 (0.03)	0.40 (0.02)	0.56 (0.03)
	63	0.25 (0.02)	0.55 (0.03)	0.38 (0.01)	0.54 (0.02)
130% leaf curvature					
	28	0.70 (0.01)	0.64 (0.04)	0.71 (0.02)	0.62 (0.05)
	43	0.47 (0.02)	0.53 (0.03)	0.52 (0.02)	0.56 (0.04)
	56	0.39 (0.02)	0.44 (0.03)	0.44 (0.02)	0.50 (0.03)
	63	0.36 (0.01)	0.40 (0.02)	0.42 (0.02)	0.48 (0.02)
length:width = 0.5					
	28	0.71 (0.02)	0.60 (0.04)	0.75 (0.02)	0.52 (0.05)
	43	0.47 (0.02)	0.53 (0.03)	0.55 (0.02)	0.41 (0.02)
	56	0.38 (0.02)	0.45 (0.03)	0.46 (0.02)	0.36 (0.02)
	63	0.35 (0.02)	0.42 (0.02)	0.44 (0.02)	0.33 (0.01)
length:width = 2.0					
	28	0.65 (0.02)	0.75 (0.04)	0.68 (0.02)	0.70 (0.06)
	43	0.40 (0.03)	0.63 (0.05)	0.48 (0.03)	0.64 (0.05)
	56	0.31 (0.01)	0.55 (0.02)	0.38 (0.01)	0.59 (0.02)
	63	0.28 (0.02)	0.50 (0.02)	0.37 (0.02)	0.55 (0.03)

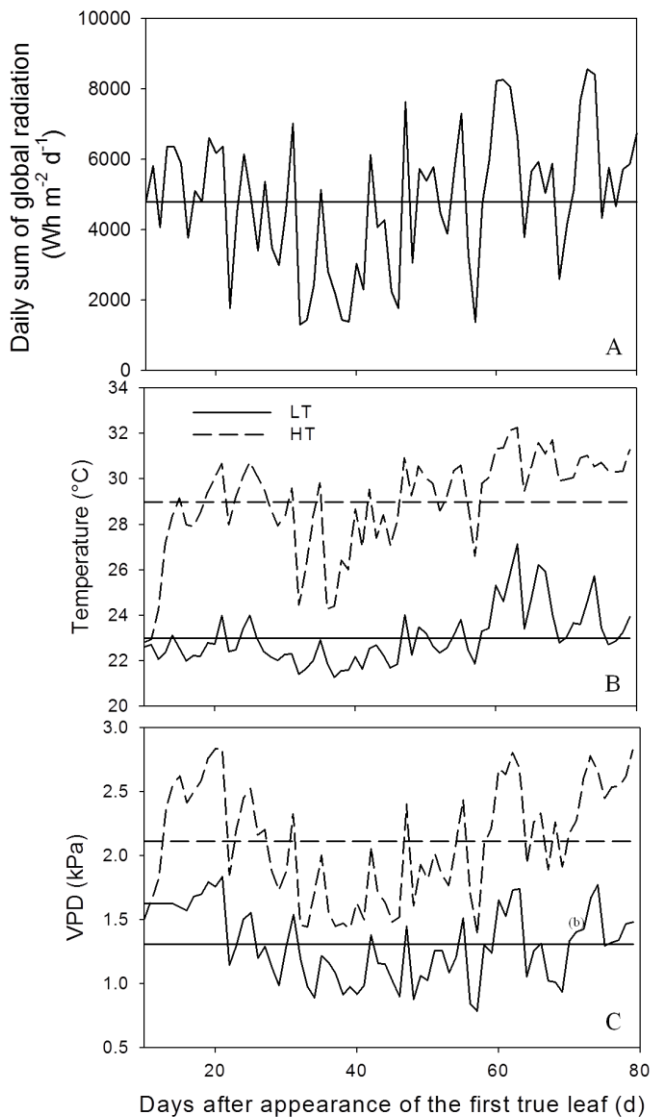


Fig. 5-S1. Fluctuation of daily global radiation (A), day temperature (B) and VPD (C) in Expt. 5. Horizontal lines represent the mean values. Solid and dashed lines represent data at 22/18°C (LT) and 32/28°C (HT) day/night temperature conditions.

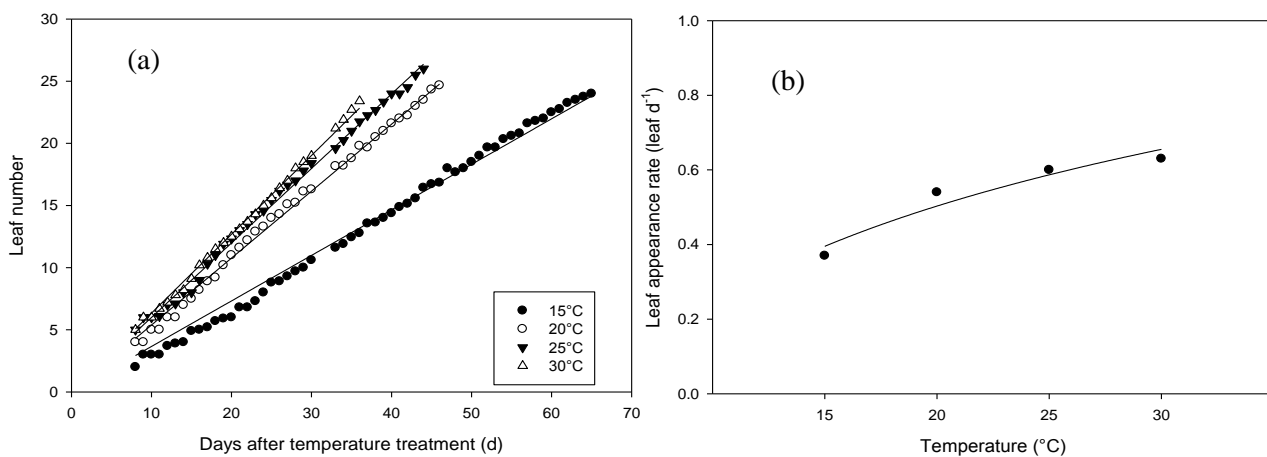


Fig. 5-S2. (a) Leaf number N_1 over time at different temperatures T (a). Symbols represent measured data (Expt. 1). Each point represents the mean value of six measurements. Lines resulted from linear regression analysis. At 15°C, $N_1 = 0.37 \cdot T$ with $R^2 = 0.99$; at 20°C, $N_1 = 0.54 \cdot T$ with $R^2 = 0.99$; at 25°C, $N_1 = 0.6 \cdot T$ with $R^2 = 0.99$ and at 30°C, $N_1 = 0.63 \cdot T$ with $R^2 = 0.99$. (b) Leaf appearance rate (LAR) in relation to temperature. Symbols represent the slopes from Fig 3a. $LAR = 0.37 \cdot \ln(T) - 0.63$, $R^2 = 0.96$.

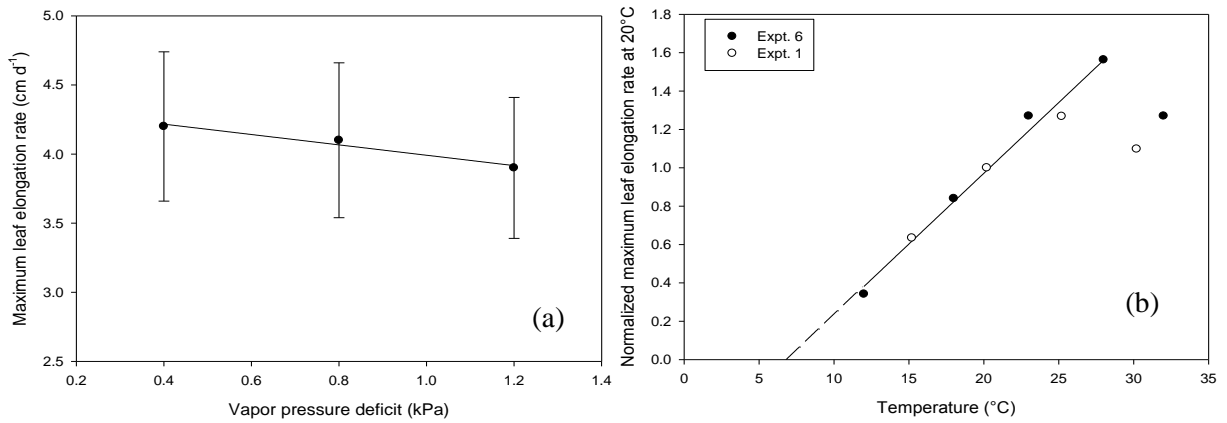


Fig. 5-S3. (a) Effect of vapor pressure deficit, VPD, on maximum leaf elongation rate, $E_{l,max}$, of the leaves at rank 8. Each point is the mean value of five measurements (Expt. 2). $E_{l,max} = (4.73 - 0.37 \cdot VPD)$ with $R^2 = 0.96$. Bars represent standard deviations. (b) Effect of temperature on maximum leaf elongation rate, $E_{l,max}$. Data of two experiments were normalized at 20°C. Open circles represent data of Expt. 1. Closed circles represent data of Expt. 6. The solid line is linear regression over a range of temperatures from 12°C to 28°C with $R^2=0.98$. The dashed line is an extrapolated line from the linear regression resulting in the base temperature for leaf growth of 6.8°C.

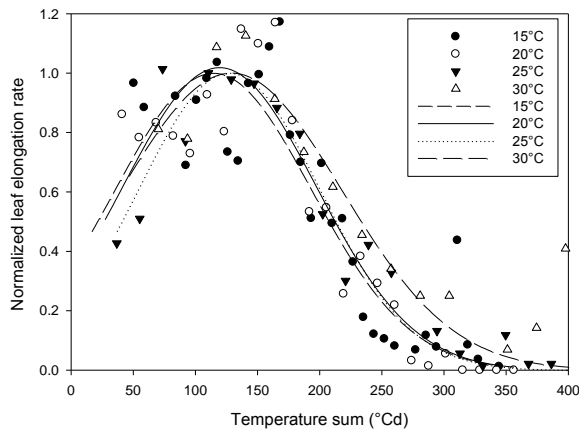


Fig. 5-S4. Time courses of normalized leaf elongation rate at different temperature regimes of the leaves at rank 8 (Expt. 1). Symbols represent measured data and lines are fitted curves.

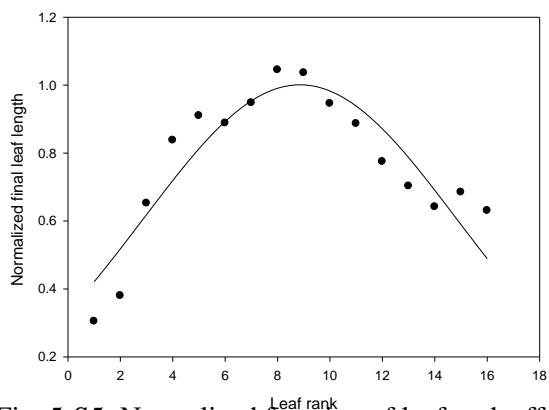


Fig. 5-S5. Normalized function of leaf rank effect on final leaf length. Data were derived from Expt. 1 at 20°C treatment ($n=3$). Line is fitted curve with the bell shaped function, $y = \exp(-0.5 \cdot ((rank-9)/5.97)^2)$ and $R^2=0.84$.

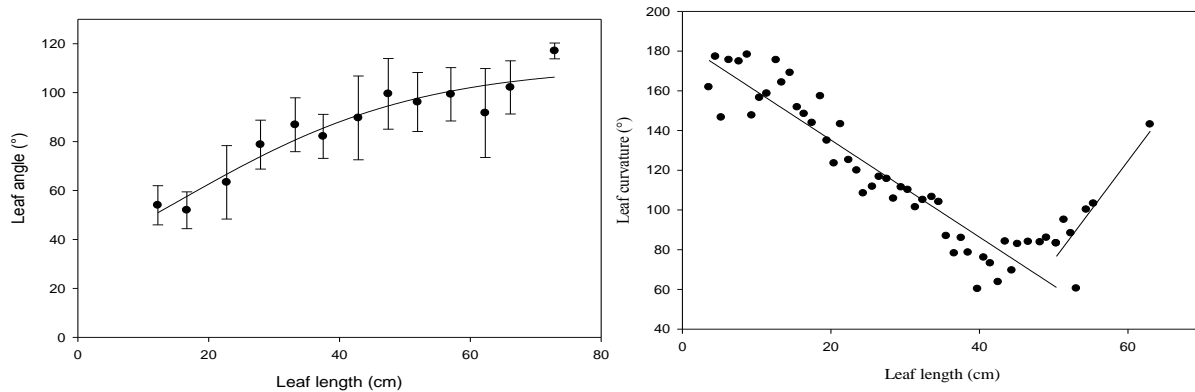


Fig. 5-S6. Leaf angle (a) and leaf curvature (b) with leaf length L_1 . Data were derived from digitizing data of Expt. 4 at different leaf ranks. The points are measured data ($n=10$). The lines are fitted curves with leaf angle, $ANG = 114.6(1-\exp(-0.04L_1))$, $R^2=0.95$ and leaf curvature, $CUR = 200-2.6L_1$, $R^2=0.67$ for $L_1 \leq 50$ and $CUR = -161 + 4.75L_1$, $R^2=0.95$ for $L_1 > 50$.

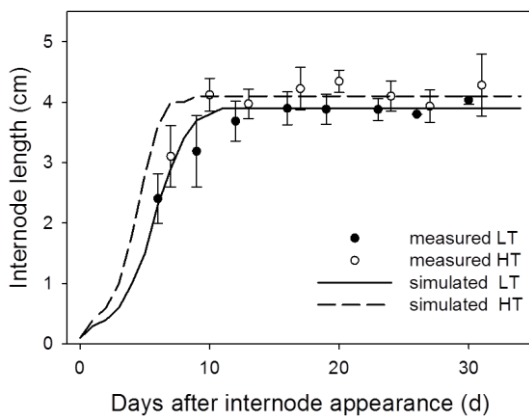


Fig. 5-S7. Measured (symbols) and simulated (lines) internode lengths at rank 8 at 22/18°C (LT, closed circle) and 32/28°C (HT, open circle) day/night temperature conditions (Expt. 5, $n = 4$). Bars are standard errors.

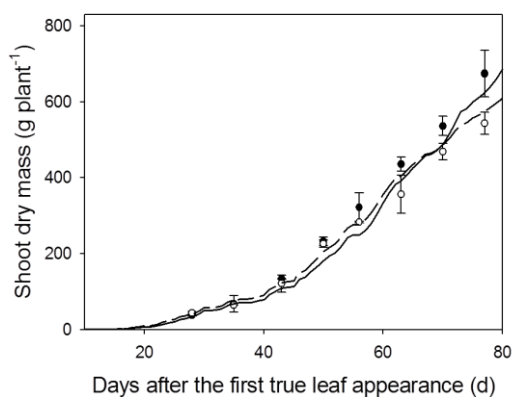


Fig. 5-S8. Comparison between simulated and measured shoot dry mass at 22/18°C (LT, closed circle) and 32/28°C (HT, open circle) day/night temperature conditions (Expt. 5, $n = 4$). Bars are standard errors. Lines represent the averages of simulated shoot dry mass without temperature effect on light use efficiency (the term $(1-\kappa(T(t)-T^*)^2)$ in Eqn 5-12) under LT (solid line) and HT conditions. For LT condition, RMSD, bias and accuracy were 44.94 g, 38.84 g and 85%, respectively. For HT conditions, RMSD, bias and accuracy were 17.39 g, -1.55 g and 93%, respectively.

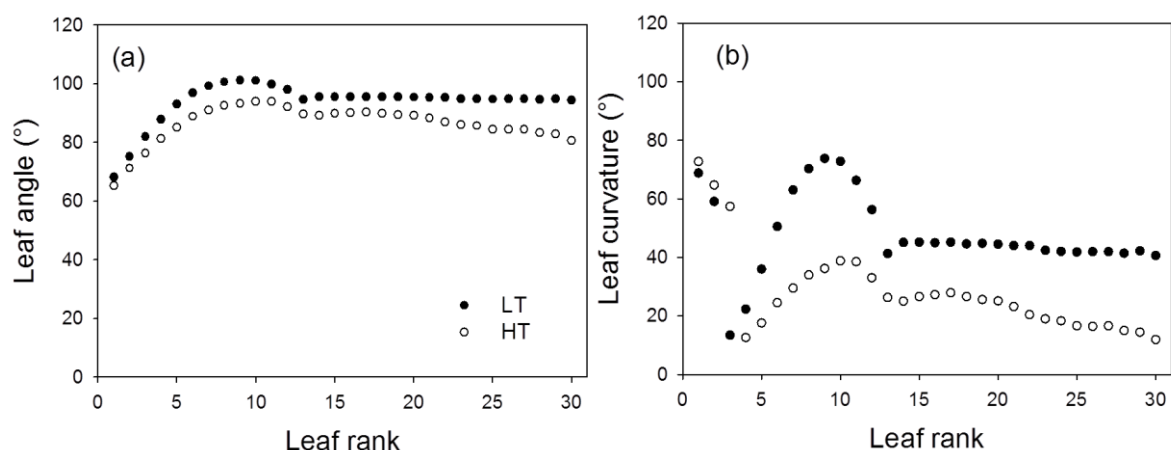


Fig. 5-S9. Leaf angle (a) and leaf curvature (b) along the leaf rank on day 77 after appearance of the first true leaf at 22/18°C (LT, close circles) and 32/28°C (HT, open circles) day/night temperature conditions.

Table 6-S1. Reported magnitudes of morphological changes in tomato under salinity stress

Morphological traits	Morphological change (per 10 mM NaCl in solution)				Reference
	Leaf number	Leaf area	Stem length	Leaf angle	
<i>Cultivar</i>					
Marmara	±0%	-7.4%	-4.0%	-	(Najla <i>et al.</i> , 2009)
Licata F1-COIS	-9.0%	-10.9%	-	-	(Maggio <i>et al.</i> , 2007)
Cois HC01	-5.6%	-7.5%	-	-	(Maggio <i>et al.</i> , 2004)
Rio Grande	-	-3.0%	-1.8%	-	(Zribi <i>et al.</i> , 2009)
Daniela	-1.7%	-3.7%	-3.3%	-	(Romero-Aranda <i>et al.</i> , 2001)
Moneymaker	-1.3%	-4.8%	-1.6%	-	(Romero-Aranda <i>et al.</i> , 2001)
Chaser	+3.7%	-9.5-17.1%	-	-	(Li and Stanghellini, 2001)
Patio	-2.5%	-	-3.8%	+9.2°	(Shibli <i>et al.</i> , 2007)
Roma	-2.3%	-	-3.4%	+12.4°	(Shibli <i>et al.</i> , 2007)
Various genotypes	-	-	-	0.7-2.4°	(Jones and El-Beltagy, 1989)

Table 6-S2 Effects of temperature (T) and salinity (S) in the root zone on final internode length (cm) at rank 8. Numbers are means with standard error in parentheses.

Temperature (°C)	Salt level in the nutrient solution (mM NaCl)			
	0	20	40	60
15	3.8(0.3)	3.8(0.4)	3.5(0.5)	3.3(0.6)
20	3.3(0.4)	3.3(0.2)	3.2(0.7)	2.9(0.4)
25	3.7(0.6)	3.5(0.6)	3.5(0.6)	3.5(0.7)
30	4.0(0.4)	3.9(0.3)	4.0(0.3)	3.8(0.3)
T	p=0.0001			
S	p=0.27			
T*S	p=0.98			

Table 6-S3 Effects of light (L) and salinity (S) in the root zone on final internode length (cm) at rank 8. Numbers are means with standard error in parentheses.

PAR ($\mu\text{mol m}^{-2} \text{s}^{-1}$)	Salt level in the nutrient solution (mM NaCl)			
	0	40	60	80
300	3.4(0.8)	2.9(1.2)	3.2(1.2)	3.6(1.3)
500	3.3(0.9)	3.3(0.8)	3.2(1.0)	3.0(0.6)
700	2.5(0.5)	2.4(0.8)	2.9(0.8)	2.9(0.6)
L	p=0.0008			
S	p=0.32			
L*S	p=0.33			

Table 6-S4 Effects of VPD and salinity (S) in the root zone on final internode length (cm) at rank 8. Numbers are means with standard error in parentheses.

VPD (kPa)	Salt level in the nutrient solution (mM NaCl)			
	0	40	60	80
0.4	2.6(0.3)	2.8(0.6)	3.6(1.0)	3.1(0.8)
0.8	3.1(0.8)	2.6(1.0)	3.5(0.8)	3.1(0.4)
1.2	2.7(0.6)	3.0(0.4)	2.8(0.9)	2.7(0.6)
VPD	p=0.42			
S	p=0.13			
VPD*S	p=0.41			

Table 6-S5 Summary of experimental conditions.

Expt	Location	Set conditions				
		Salinity (mM NaCl)	Day/night temperature ($^{\circ}\text{C}$)	VPD (kPa)	PAR ($\mu\text{mol m}^{-2} \text{s}^{-1}$)	CO ₂ (ppm)
1	Growth chamber	0, 20, 40, 60	17/13, 22/18, 26/22 & 30/26	0.8	300	380
2	Growth chamber	0, 40, 60, 80	22/18	0.4, 0.8 & 1.2	300	380
3	Growth chamber	0, 40, 60, 80	22/18	0.8	300, 500 & 700	380
4	Greenhouse	0, 40, 60, 80 ^A	22/18	1.1	-	ambient
5	Greenhouse	0, 40, 60, 80 ^B	22/18	1.39 ^C	-	ambient
			32/28	2.01 ^C	-	ambient

^A: seedlings were transplant to the greenhouse on 29 May and salt was applied in the solution on 2 Jun. 2009.

^B: seedlings were transplant to the greenhouse on 14 Apr. and salt was applied in the solution on 18 Apr. 2010, 12 DAFLA.

^C: average values in the greenhouses.

Table 6-S6 Sensitivity of shoot dry mass to internode length on day 77 after the first leaf appearance under 22/18°C (LT) and 32/28°C (HT) day/night temperature conditions. Numbers are means with standard error in parentheses.

Conditions	Relative internode length	Shoot dry mass (% of reference)		
		0mM NaCl	40 mM NaCl	80 mM NaCl
LT	0.7	88.1 (2.0)	85.8 (1.4)	86.7 (0.9)
	1.0	100.0 (2.5)	100.0 (1.4)	100.0 (1.0)
	1.3	109.2 (2.5)	110.5 (1.5)	107.3 (0.8)
HT	0.7	92.4 (1.2)	91.6 (0.7)	92.4 (0.4)
	1.0	100.0 (1.2)	100.0 (0.6)	100.0 (0.5)
	1.3	104.9 (1.1)	105.3 (0.6)	104.3 (0.3)

Table 6-S7 Reduction of light use efficiency (k_x/k_0) under x mM NaCl under 22/18°C (LT) and 32/28°C (HT) day/night temperature conditions

Day	k_{40}/k_0 (-)		k_{60}/k_0 (-)		k_{80}/k_0 (-)	
	LT	HT	LT	HT	LT	HT
29-35	1.17	1.07	0.96	0.93	0.80	0.81
36-43	1.10	1.06	0.88	0.91	0.69	0.78
44-50	1.05	1.02	0.85	0.86	0.68	0.73
51-56	1.07	1.02	0.86	0.85	0.66	0.72
57-63	0.97	0.93	0.78	0.79	0.64	0.67
64-70	1.05	1.05	0.73	0.89	0.66	0.75
71-77	0.93	0.96	0.75	0.83	0.61	0.71

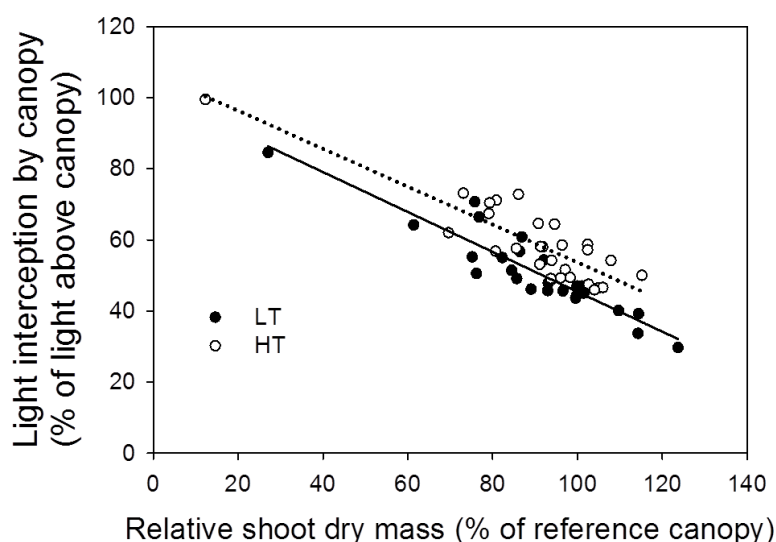


Fig. 6-S1. Relationship between relative shoot dry mass and light interception at 22/18°C (LT, closed symbols and solid line, $y = -0.56x + 101.52$, $R^2 = 0.85$) and 32/28°C (HT, open symbols and dotted line, $y = -0.53x + 106.97$, $R^2 = 0.76$) day/night temperature regimes (derived from Table 6-4).

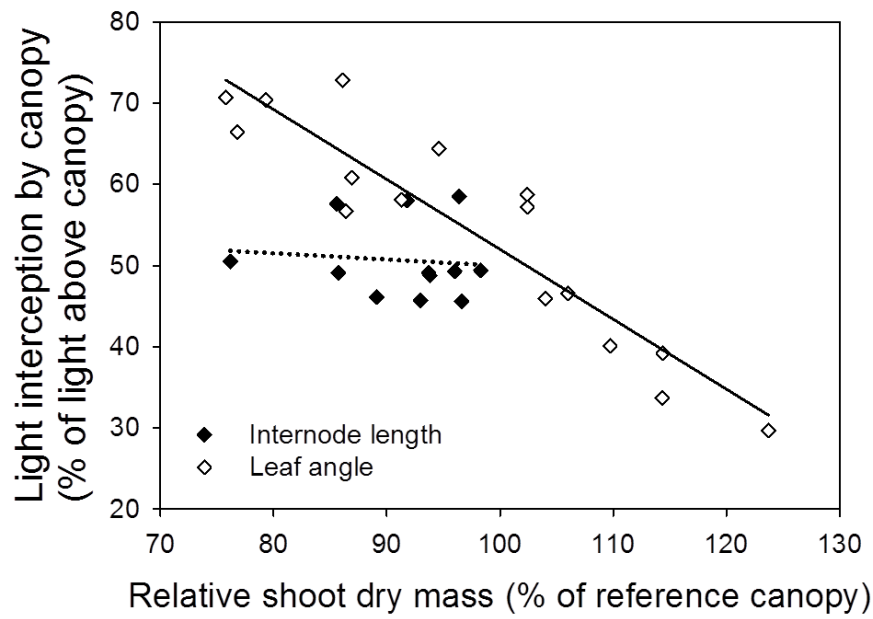


Fig. 6-S2. Relationship between relative shoot dry mass and light interception for internode length (closed symbols and dotted line, $y = -0.077x + 57.66$, $R^2 = 0.01$) and leaf angle (open symbols and solid line, $y = -0.86x + 138.1$, $R^2 = 0.85$) day/night temperature regimes (derived from Table 6-4).

Reference

- Al-Karaki GN.** 2000. Growth, water use efficiency, and sodium and potassium acquisition by tomato cultivars grown under salt stress. *Journal of Plant Nutrition* **23**: 1–8.
- Alton P, North P, Los S.** 2007. The impact of diffuse sunlight on canopy light-use efficiency, gross photosynthetic product and net ecosystem exchange in three forest biomes. *Global Change Biology* **13**: 776–787.
- Archontoulis SV, Yin X, Vos J, Danalatos NG, Struik PC.** 2012. Leaf photosynthesis and respiration of three bioenergy crops in relation to temperature and leaf nitrogen: how conserved are biochemical model parameters among crop species? *Journal of Experimental Botany* **63**: 895–911.
- Aschan G, Pfanz H.** 2003. Non-foliar photosynthesis – a strategy of additional carbon acquisition. *Flora* **198**: 81–97
- Bartelink HH.** 1997. Allometric relationships for biomass and leaf area of beech (*Fagus sylvatica* L). *Annals of Forest Science* **54**: 39–50.
- Ballaré CL.** 2009. Illuminated behavior: phytochrome as a key regulator of light foraging and plant anti-herbivore defence. *Plant, Cell and Environment* **32**: 713-725.
- Barillot R, Escobar-Gutiérrez AJ, Fournier C, Huynh P, Combes D.** 2014. Assessing the effects of architectural variations on light partitioning within virtual wheat–pea mixtures. *Ann. Bot.* **114**.
- Berthomieu P, Conéjéro G, Nublat A, et al.** 2003. Functional analysis of *AtHKT1* in *Arabidopsis* shows that Na⁺ recirculation by the phloem is crucial for salt tolerance. *EMBO J* **22**: 2004–2014.
- Bond BJ, Farnsworth BT, Coulombe RA, Winner WE.** 1999. Foliage physiology and biochemistry in response to light gradients in conifers with varying shade tolerance. *Oecologia* **120**: 183–192.
- Brodersen CR, Vogelmann TC.** 2010. Do changes in light direction affect absorption profiles in leaves? *Functional Plant Biology* **37**: 403–412.
- Brodersen CR, Vogelmann TC, Williams WE, Gorton HL.** 2008. A new paradigm in leaf-level photosynthesis: direct and diffuse lights are not equal. *Plant Cell and Environment* **31**: 159–164.
- Brodribb, TJ, Feild, TS, Jordan, GJ.** 2007. Leaf maximum photosynthetic rate and venation are linked by hydraulics. *Plant Physiology* **144**: 1890–1898.

- Buck-Sorlin G, Visser PH de, Henke M et al.** 2011. Towards a functional–structural plant model of cut-rose: simulation of light environment, light absorption, photosynthesis and interference with the plant structure. *Annals of Botany* **108**: 1121–1134.
- Buckley TN, Cescatti A, Farquhar G.** 2013. What does optimization theory actually predict about crown profiles of photosynthetic capacity when models incorporate greater realism? *Plant Cell Environ* **36**: 1547–1563.
- Buckley T., Diaz-Espejo A.** 2015. Partitioning changes in photosynthetic rate into contributions from different variables. *Plant, Cell & Environment*, **38**, 1200–1211.
- Caemmerer S von.** 2013. Steady-state models of photosynthesis. *Plant, Cell and Environment* **36**, 1617–1630.
- Caemmerer S von, Evans JR.** 2015. Temperature responses of mesophyll conductance differ greatly between species. *Plant Cell Environ* **38**: 629–637.
- Caldeira CF, Bosio M, Parent B, Jeanguenin L, Chaumont F, Tardieu F.** 2014. A hydraulic model is compatible with rapid changes in leaf elongation under fluctuating evaporative demand and soil water status. *Plant Physiol.* **164**: 1718–1730.
- Cano F, Sánchez-Gómez D, Rodríguez-Calcerrada J, Warren C, Gil L, Aranda I.** 2013. Effects of drought on mesophyll conductance and photosynthetic limitations at different tree canopy layers. *Plant Cell and Environment* **36**:1961-1980.
- Carmo-Silva AE, Salvucci ME.** 2012. The temperature response of CO₂ assimilation, photochemical activities and Rubisco activation in *Camelina sativa*, a potential bioenergy crop with limited capacity for acclimation to heat stress. *Planta* **236**: 1433–1445.
- Centritto M., Loreto F. and Chartzoulakis KS.** 2003. The use of low [CO₂] to estimate diffusional and non-diffusional limitations of photosynthetic capacity of salt-stressed olive saplings. *Plant, Cell and Environment* **26**, 585–594.
- Chaves M, Flexas J, Pinheiro C.** 2009. Photosynthesis under drought and salt stress: regulation mechanisms from whole plant to cell. *Annals of Botany* **103**, 551–560.
- Chen T-W, Henke M, Kahlen K, de Visser PHB, Buck-Sorlin G, Stützel H.** 2013. Revealing the relative importance of photosynthetic limitation in cucumber canopy. In: Lintunen A. eds. *Proceedings -FSPM2013 - 7th Workshop on Functional-Structural Plant Models*. Helsinki, 124-126.
- Chen TW, Nguyen TMN, Kahlen K, Stützel H.** 2014a. Quantification of the effects of architectural traits on dry mass production and light interception of tomato canopy

- under different temperature regimes using dynamic functional-structural plant model. *Journal of Experimental Botany* **65**: 6399–6410.
- Chen TW, Henke M, Visser PHB de et al.** 2014b. What is the most prominent factor limiting photosynthesis in different layers of a greenhouse cucumber canopy? *Annals of Botany*, **114**: 677-688.
- Chen, TW, Kahlen, K, Stützel, H.** 2015. Disentangling the contributions of osmotic and ionic effects of salinity on stomatal, mesophyll, biochemical and light limitations to photosynthesis. *Plant, Cell and Environment*: in press.
- Cieslak M, Lemieux C, Hanan J, Prusinkiewicz P.** 2008. Quasi-Monte Carlo simulation of the light environment of plants. *Functional Plant Biology* **35**, 837–849.
- Cieslak M, Seleznyowa A, Hanan J.** 2011. A functional–structural kiwifruit vine model integrating architecture, carbon dynamics and effects of the environment. *Annals of Botany* **107**, 747–764.
- Colmenero-Flores JM, Rosales MA.** 2014. Interaction between salt and heat stress: when two wrongs make a right. *Plant, Cell & Environment* **37**, 1042–1045.
- Condon AG, Richards R, Rebetzke G, Farquhar G.** 2004. Breeding for high water-use efficiency. *Journal of Experimental Botany* **55**, 2447–2460.
- Comstock, JP, Sperry, JS.** 2000. Theoretical considerations of optimal conduit length for water transport in vascular plants. *New Phytologist*: 195–218.
- Cuartero J, Fernández-Muñoz R.** 1998. Tomato and salinity. *Scientia Horticulturae* **78**, 83–125.
- Da Silva D, Han L, Faivre R, Costes E.** 2014. Influence of the variation of geometrical and topological traits on light interception efficiency of apple trees: sensitivity analysis and metamodelling for ideotype definition. *Ann. Bot.* **114**: 739–752.
- Davenport R, James R, Zakrisson-Plogander A, Tester M, Munns R.** 2005. Control of sodium transport in durum wheat. *Plant Physiol* **137**: 807–818.
- DeJong T, Da Silva D, Vos J, Escobar-Gutiérrez J.** 2011. Using functional – structural plant models to study, understand and integrate plant development and ecophysiology. *Annals of Botany* **108**, 987–989,
- Delfine S, Alvino A, Villani M, Loreto F.** 1999. Restrictions to carbon dioxide conductance and photosynthesis in spinach leaves recovering from salt stress. *Plant Physiology* **119**, 1101–1106.
- de Pury DG, Farquhar G.** 1997. Simple scaling of photosynthesis from leaves to canopies without the errors of big-leaf models. *Plant Cell & Environ* **20**: 537–557.

- de Visser PHB, Buck-Sorlin GH, van der Heijden GWAM. 2014** □ Optimizing illumination in the greenhouse using a 3D model of tomato and a ray tracer. *Frontiers in Plant Science* **5**: 48.
- Drew MC, Hole PS, Piccioni GA. 1990.** Inhibition by NaCl of net CO₂ fixation and yield of cucumber. *Journal of American Society of Horticultural Science* **115**, 472–477.
- Dubois JB, Fiscus EL, Booker FL, Flowers MD, Reid CD. 2007.** Optimizing the statistical estimation of the parameters of the Farquhar–von Caemmerer–Berry model of photosynthesis. *New Phytologist* **176**: 402–414.
- Duursma RA, Falster DS, Valladares F et al. 2012.** Light interception efficiency explained by two simple variables: a test using a diversity of small- to medium-sized woody plants. *New Phytologist* **193**, 397–408.
- Egea G, González-Real MM, Baille A, Nortes PA, Diaz-Espejo A. 2011.** Disentangling the contributions of ontogeny and water stress to photosynthetic limitations in almond trees. *Plant, Cell and Environment* **34**: 962–979.
- Espana ML, Baret F, Aries F, Chelle M, Andrieu B, Prevot L. 1999.** Modeling maize canopy 3D architecture Application to reflectance simulation. *Ecological Modelling* **122**, 25–43.
- Egea G, González-Real MM, Baille A, Nortes PA, Diaz-Espejo A. 2011.** Disentangling the contributions of ontogeny and water stress to photosynthetic limitations in almond trees. *Plant, Cell and Environment* **34**, 962–979.
- Enquist BJ, Brown JH, West GB. 1998.** Allometric scaling of plant energetics and population density. *Nature* **395**, 163–165.
- Evans JR. 2013.** Improving Photosynthesis. *Plant Physiology* **162**, 1780–1793.
- Evans JR, Caemmerer S von. 2013.** Temperature response of carbon isotope discrimination and mesophyll conductance in tobacco. *Plant, Cell & Environment* **36**, 745–756.
- Evers JB, Huth NI, Renton M. 2009.** Light extinction in spring wheat canopies in relation to crop configuration and solar angle. In: IEEE, ed. *Plant Growth Modeling, Simulation, Visualization and Applications (PMA)*. Beijing.
- Evers JB, Vos J, Yin X, Romero P, van der Putten PE, Struik PC. 2010.** Simulation of wheat growth and development based on organ-level photosynthesis and assimilate allocation. *Journal of Experimental Botany* **61**, 2203–2216.

- Fanwoua J.** 2007. *Modelling the Effect of High Temperature on the Development of Tomato*. Hannover.
- FAO.** 2005. Management of irrigation-induced salt-affected soils.
ftp://ftp.fao.org/agl/iptrid/salinity_brochure_en.pdf
- Farquhar G, Caemmerer S von, Berry J.** 1980. A biochemical model of photosynthetic CO₂ assimilation in leaves of C₃ species. *Planta* **149**: 78–90.
- Flexas J, Baron M, Bota J, et al.** 2009. Photosynthesis limitations during water stress acclimation and recovery in the drought-adapted *Vitis* hybrid Richter-110 (*V. berlandieri* x *V. rupestris*). *Journal of Experimental Botany* **60**: 2361–2377.
- Flexas J, Barbour MM, Brendel O et al.** 2012. Mesophyll diffusion conductance to CO₂: An unappreciated central player in photosynthesis. *Plant Science* **193-194**, 70–84.
- Flexas J, Diaz-Espejo A, Berry J et al.** 2007a. Analysis of leakage in IRGA's leaf chambers of open gas exchange systems: quantification and its effects in photosynthesis parameterization. *Journal of Experimental Botany* **58**, 1533–1543.
- Flexas J, Diaz-Espejo A, Galmés J, Kaldenhoff R, Merano H, Ribas-Carbo M.** 2007b. Rapid variations of mesophyll conductance in response to changes in CO₂ concentration around leaves. *Plant Cell Environ* **30**: 1284–1298.
- Flexas J, Loreto F, Cornic G, Sharkey T.** 2004. Diffusive and metabolic limitations to photosynthesis under drought and salinity in C₃ plants. *Plant Biology* **6**, 269–279.
- Flexas J, Niinemets Ü, Gallé A, et al.** 2013. Diffusional conductances to CO₂ as a target for increasing photosynthesis and photosynthetic water-use efficiency. *Photosynth Research* **117**: 45-59.
- Flower TJ.** 2004. Improving crop salt tolerance. *Journal of Experimental Botany*. **55**: 307-319.
- Ford ED, Cocke A, Horton L, Fellner M, Volkenburgh EV.** 2008. Estimation, variation and importance of leaf curvature in *Zea mays* hybrids. *Agricultural and Forest Meteorology* **148**, 1598–1610.
- Gago J, Coopman RE, Cabrera HM et al.** 2013. Photosynthesis limitations in three fern species. *Physiologia Plantarum* **149**, 599–611.
- Gent M, Seginer I.** 2012. A carbohydrate supply and demand model of vegetative growth: response to temperature and light. *Plant Cell and Environment* **35**, 1274–1286.
- Gibberd M, Turner N, Storey R.** 2002. Influence of saline irrigation on growth, ion accumulation and partitioning, and leaf gas exchange of carrot (*Daucus carota* L.). *Annals of Botany* **90**, 715–724.

- Granier C, Tardieu F.** 2009. Multi-scale phenotyping of leaf expansion in response to environmental changes: the whole is more than the sum of parts. *Plant, Cell and Environment* **32**, 1175–1184.
- Grassi G, Magnani F.** 2005. Stomatal, mesophyll conductance and biochemical limitations to photosynthesis as affected by drought and leaf ontogeny in ash and oak trees. *Plant Cell and Environment* **28**: 834–849.
- Grassi G, Ripullone F, Borghetti M, Raddi S, Magnani F.** 2009. Contribution of diffusional and non-diffusional limitations to midday depression of photosynthesis in *Arbutus unedo* L. *Trees* **23**: 1149–1161.
- Gunn S, Bailey SJ, Farrar JF.** 1999. Partitioning of dry mass and leaf area within plants of three species grown at elevated CO₂. *Functional Ecology* **13**, 3–11.
- Hammer GL, van Oosterom E, McLean G, et al.** 2010. Adapting APSIM to model the physiology and genetics of complex adaptive traits in field crops. *Journal of Experimental Botany* **61**: 2185–2202.
- Harley P, Loreto F, Di Marco G, Sharkey T.** 1992. Theoretical consideration of estimating the mesophyll conductance to CO₂ flux by analysis of the response of photosynthesis to CO₂. *Plant Physiology* **98**, 1429–1436.
- Harmens H, Stirling CM, Marshall C, Farrar JF.** 2000. Is partitioning of dry weight and leaf area within *Dactylis glomerata* affected by N and CO₂ enrichment? *Annals of Botany* **86**, 833–839.
- Harris BN, Sadras VO, Tester M.** 2010. A water-centred framework to assess the effects of salinity on the growth and yield of wheat and barley. *Plant and Soil* **336**, 377–389.
- Hasegawa P, Bressan R.** 2000. Plant cellular and molecular responses to high salinity. *Annual Review of Plant Physiology and Plant Molecular Biology* **51**, 463–499.
- Hassiotou F., Ludwig M., Renton M., Veneklaas E.J. & Evans J.R.** 2009. Influence of leaf dry mass per area, CO₂, and irradiance on mesophyll conductance in sclerophylls. *Journal of Experimental Botany* **60**, 2303–2314.
- Hemming S, Dueck T, Janse J, van Noort F.** 2008. The effect of diffuse light on crops. *Acta Horticulturae* **801**: 1293–1300.
- Heuvelink E.** 2005. *Tomatoes*. USA: CAB International.
- Hirose T.** 2005. Development of the Monsi–Saeki theory on canopy structure and function. *Annals of Botany* **95**, 483–494.

- Hirosaka K. 2014.** Optimal nitrogen distribution within a leaf canopy under direct and diffuse light. *Plant Cell Environ* **37**: 2077–2085.
- Hogewoning SW, Trouwborst G, Maljaars H, Poorter H, van Ieperen W, Harbinson J. 2010.** Blue light dose-responses of leaf photosynthesis, morphology, and chemical composition of *Cucumis sativus* grown under different combinations of red and blue light. *Journal of Experimental Botany* **61**, 3107–3117.
- Hovi T, Näkkilä J, Tahvonen R. 2004.** Interlighting improves production of year-round cucumber. *Scientia Horticulturae* **102**: 283–294.
- Hovi-Pekkanen T, Tahvonen R. 2008.** Effects of interlighting on yield and external fruit quality in year-round cultivated cucumber. *Scientia Horticulturae* **116**: 152–161.
- Hu Y, Fromm J, Schmidhalter U. 2005.** Effect of salinity on tissue architecture in expanding wheat leaves. *Planta* **220**, 838–848.
- Irving LJ, Robinson D. 2006.** A dynamic model of Rubisco turnover in cereal leaves. *New Phytologist* **169**: 493–504.
- James RA, Caemmerer S von, Condon AG, Zwart AB, Munns R. 2008.** Genetic variation in tolerance to the osmotic stress component of salinity stress in durum wheat. *Functional Plant Biology* **35**, 111.
- James RA, Munns R, Caemmerer S von, Trejo C, Miller C, Condon T. 2006.** Photosynthetic capacity is related to the cellular and subcellular partitioning of Na⁺, K⁺ and Cl⁻ in salt-affected barley and durum wheat. *Plant, Cell and Environment* **29**, 2185–2197.
- James RA, Rivelli AR, Munns R, Caemmerer S von. 2002.** Factors affecting CO₂ assimilation, leaf injury and growth in salt-stressed durum wheat. *Functional Plant Biology* **29**, 1393.
- John GP, Scoffoni C, Sack L. 2013.** Allometry of cells and tissues within leaves. *American Journal of Botany* **100**, 1936–1948.
- Jones HG. 1985.** Partitioning stomatal and non-stomatal limitations to photosynthesis. *Plant Cell and Environment* **8**: 95–104.
- Jones RA, El-Beltagy AS. 1989.** Epinasty promoted by salinity or ethylene is an indicator of salt-sensitivity in tomatoes. *Plant, Cell and Environment* **12**, 813–817.
- Jongschaap R, Dueck T, Marissen N. 2006.** Simulating seasonal patterns of increased greenhouse crop production by conversion of direct radiation into diffuse radiation *Acta Horticulturae* **718**: 315–322.

- Juszczuk IM, Flexas J, Szal B, Dąbrowska Z, Ribas-Carbo M, Rychter AM.** 2007. Effect of mitochondrial genome rearrangement on respiratory activity, photosynthesis, photorespiration and energy status of MSC16 cucumber (*Cucumis sativus*) mutant. *Physiologia Plantarum* **131**, 527–541.
- Kahlen K, Stützel H.** 2007. Estimation of geometric attributes and masses of individual cucumber organs using three-dimensional digitizing and allometric relationships. *Journal of America Society of Horticultural Science* **132**: 439–446.
- Kahlen K, Stützel H.** 2011. Modelling photo-modulated internode elongation in growing glasshouse cucumber canopies. *New Phytologist* **190**, 697–708.
- Kahlen K, Wiechers D, Stützel H.** 2008. Modelling leaf phototropism in a cucumber canopy. *Functional Plant Biology* **35**, 876.
- Kattge J, Knorr W.** 2007. Temperature acclimation in a biochemical model of photosynthesis: a reanalysis of data from 36 species. *Plant, Cell & Environment* **30**: 1176–1190.
- Keleş Y, Öncel I.** 2002: Response of antioxidative defence system to temperature and water stress combinations in wheat seedlings. *Plant Science* **163**: 783–790.
- Khaembah EN, Irving LJ, Thom ER, Faville MJ, Easton HS, Matthew C.** 2013. Leaf Rubisco turnover in a perennial ryegrass (*Lolium perenne* L.) mapping population: genetic variation, identification of associated QTL, and correlation with plant morphology and yield. *Journal of Experimental Botany* **64**: 1305–1316.
- Kirschbaum MUF.** 2011. Does enhanced photosynthesis enhance growth? Lessons learned from CO₂ enrichment studies. *Plant Physiol.* **155**: 117–124.
- Kniemeyer O.** 2008. Design and implementation of a graph grammar based language for functional–structural plant modelling. PhD thesis, BTU Cottbus, Germany. Available at <http://opus.kobv.de/btu/volltexte/2009/593/>
- Kobayashi K, Salam MS.** 2000. Comparing simulated and measured values using mean squared deviation and its components. *Agronomy Journal* **92**, 345–352.
- Körner C.** 2003. Carbon limitation in trees. *Journal of Ecology* **91**: 4–17.
- Körner C.** 2015. Nicht jede Limitierung ist ein Stress - Sprache verrät falsche Konzepte. *Biologie in Unserer Zeit* **45**: 68–69.
- Li YL, Stanghellini C.** 2001. Analysis of the effect of EC and potential transpiration on vegetative growth of tomato. *Scientia Horticulturae* **89**, 9–21.
- Lindenmayer A.** 1968. Mathematical models for cellular interactions in development I. Filaments with one-sided inputs. *Journal of Theoretical Biology* **18**, 280–299.

- Limosin J, Misson L, Lavoit A, Martin NK, Rambal S.** 2010. Do photosynthetic limitations of evergreen *Quercus ilex* leaves change with long-term increased drought severity? *Plant, Cell & Environment* **33**, 863–875.
- Lizaso JI, Batchelor WD, Westgate ME, Echarte L.** 2003. Enhancing the ability of CERES-Maize to compute light capture. *Agricultural Systems* **76**: 293–311.
- Lizaso JI, Boote KJ, Jones JW, et al.** 2011. CSM-IXIM: A new maize simulation model for dssat version 4.5. *Agronomy Journal*: 766–779.
- Loreto F, Centritto M, Chartzoulakis KS.** 2003. Photosynthetic limitations in olive cultivars with different sensitivity to salt stress. *Plant, Cell & Environment* **26**, 595–601.
- Loreto F, Harley P, Di Marco G, Sharkey T.** 1992. Estimation of mesophyll conductance to CO₂ flux by three different methods. *Plant Physiology* **98**: 1437–1443.
- Maggio A, Pascale S de, Angelino G, Ruggiero C, Barbieri G.** 2004. Physiological response of tomato to saline irrigation in long-term salinized soils. *European Journal of Agronomy* **21**, 149–159.
- Maggio A, Raimondi G, Martino A, Pascale S de.** 2007. Salt stress response in tomato beyond the salinity tolerance threshold. *Environmental and Experimental Botany* **59**, 276–282.
- Medlyn BE, Duursma RA, Eamus D, et al.** 2011. Reconciling the optimal and empirical approaches to modelling stomatal conductance. *Global Change Biology* **17**: 2134–2144.
- Mercado LM, Bellouin N, Sitch S, et al.** 2009. Impact of changes in diffuse radiation on the global land carbon sink. *Nature* **458**: 1014–1017. doi:10.1038/nature07949.
- Merilo E, Jõesaar I, Brosché M, Kollist H.** 2014. To open or to close: species-specific stomatal responses to simultaneously applied opposing environmental factors. *New Phytol* **202**: 499–508.
- Monsi M, Saeki T.** 1953. Über den Lichtfaktor in den Pflanzengesellschaften und seine Bedeutung für die Stoffproduktion. *Japanese Journal of Botany* **14**, 22–52.
- Monteith, J.** 1977. Climate and the efficiency of crop production in Britain. *Philos. Trans. R. Soc. Lond. Ser. B* **281**: 277–294.
- Mott KA, Buckley T.** 1998. Stomatal heterogeneity. *Journal of Experimental Botany* **49**, 407–417.
- Munns R.** 1993. Physiological processes limiting plant growth in saline soils: some dogmas and hypotheses. *Plant, Cell and Environment* **16**, 15–24.

- Munns R.** 2002. Comparative physiology of salt and water stress. *Plant, Cell and Environment* **25**, 239–250.
- Munns R, Tester M.** 2008. Mechanisms of salinity tolerance. *Annual Review of Plant Biology* **59**, 651–681.
- Murchie EH, Pinto M, Horton P.** 2009. Agriculture and the new challenges for photosynthesis research. *New Phytologist* **181**: 532–552.
- Najla S, Vercambre G, Pages L, Grasselly D, Gautier H, Genard M.** 2009. Tomato plant architecture as affected by salinity: Descriptive analysis and integration in a 3-D simulation model. *Botany* **87**, 893–904.
- Niinemets, Ü, Keenan, TF, Hallik, L.** 2015. A worldwide analysis of within-canopy variations in leaf structural, chemical and physiological traits across plant functional types. *New Phytologist* **205**: 973–993.
- Niklas KJ, Cobb ED, Spatz H.** 2009. Predicting the allometry of leaf surface area and dry mass. *American Journal of Botany* **96**, 531–536.
- Parent B, Tardieu F.** 2012. Temperature responses of developmental processes have not been affected by breeding in different ecological areas for 17 crop species. *New Phytologist* **194**, 760–774.
- Parent B, Tardieu F.** 2014. Can current crop models be used in the phenotyping era for predicting the genetic variability of yield of plants subjected to drought or high temperature? *Journal of Experimental Botany* **65**: 6179–6189.
- Peltoniemi MS, Duursma RA, Medlyn BE.** 2012. Co-optimal distribution of leaf nitrogen and hydraulic conductance in plant canopies. *Tree Physiology* **32**: 510–519.
- Pérez-López U, Robredo A, Lacuesta M, Mena-Petite A, Muñoz-Rueda A.** 2012. Elevated CO₂ reduces stomatal and metabolic limitations on photosynthesis caused by salinity in *Hordeum vulgare*. *Photosynthesis Research* **111**, 269–283.
- Poorter H, Anten N, Marcelis LFM.** 2013. Physiological mechanisms in plant growth models: do we need a supra-cellular systems biology approach? *Plant, Cell and Environment* **36**, 1673–1690.
- Poorter H, Niklas KJ, Reich PB, Oleksyn J, Poot P, Mommer L.** 2012. Biomass allocation to leaves, stems and roots: meta-analyses of interspecific variation and environmental control. *New Phytologist* **193**, 30–50.
- Prusinkiewicz P, Lindenmayer A.** 1990. *The algorithmic beauty of plants*. New York, USA: Springer.

- Qian, Y, Fu, J. 2005.** Response of creeping bentgrass to salinity and mowing management: carbohydrate availability and ion accumulation. *HortScience* **40**: 2170–2174.
- Qian T, Elings A, Dieleman J, Gort G, Marcelis L. 2012.** Estimation of photosynthesis parameters for a modified Farquhar–von Caemmerer–Berry model using simultaneous estimation method and nonlinear mixed effects model. *Environmental and Experimental Botany* **82**, 66–73.
- Rajendran K, Tester M, Roy SJ. 2009.** Quantifying the three main components of salinity tolerance in cereals. *Plant, Cell and Environment* **32**, 237–249.
- Rawson, H, Munns, R. 1984.** Leaf expansion in sunflower as influenced by salinity and short-term changes in carbon fixation. *Plant, Cell and Environment* **7**: 207–213.
- Reynolds M, Foulkes J, Furbank R, et al. 2012.** Achieving yield gains in wheat. *Plant Cell and Environment* **35**: 1799–1823.
- Reymond M, Muller B, Leonardi A, Charcosset A, Tardieu F. 2003.** Combining quantitative trait loci analysis and an ecophysiological model to analyze the genetic variability of the responses of maize leaf growth to temperature and water deficit. *Plant Physiology* **131**, 664–675.
- Rivero RM, Mestre TC, Mittler RO, Rubio F, Gracia-Sanchez F, Martinez V. 2014.** The combined effect of salinity and heat reveals a specific physiological, biochemical and molecular response in tomato plants. *Plant, Cell & Environment* **37**, 1059–1073.
- Romero-Aranda R, Soria T, Cuartero J. 2001.** Tomato plant-water uptake and plant-water
- Roy SJ, Tucker EJ, Tester M. 2011.** Genetic analysis of abiotic stress tolerance in crops. *Current Opinion in Plant Biology* **14**, 232–239.
- Roy, SJ, Negrão, S, Tester, M. 2014.** Salt resistant crop plants. *Current Opinion in Biotechnology* **26**: 115–124.
- Savvas, D, Pappa, V, Kotsiras, A, Gizas, G. 2005.** NaCl accumulation in a cucumber crop grown in a completely closed hydroponic system as influenced by NaCl concentration in irrigation water. *European Journal of Horticultural Science* **70**: 217–223.
- Sarlikioti V, Visser PHB de, Buck-Sorlin GH, Marcelis LFM. 2011a.** How plant architecture affects light absorption and photosynthesis in tomato: towards an ideotype for plant architecture using a functional–structural plant model. *Annals of Botany* **108**, 1065–1073.

- Sarlikioti V, Visser PHB de, Marcelis LFM.** 2011b. Exploring the spatial distribution of light interception and photosynthesis of canopies by means of a functional-structural plant model. *Annals of Botany* **107**: 875–883.
- Shabala S, Cuin TA.** 2008. Potassium transport and plant salt tolerance. *Physiologia Plantarum* **133**, 651–669.
- Shapira OR, Khadka S, Israeli Y, Shani UR, Schwartz A.** 2009. Functional anatomy controls ion distribution in banana leaves: significance of Na⁺ seclusion at the leaf margins. *Plant, Cell & Environment* **32**, 476–485.
- Sharkey T, Bernacchi C, Farquhar G, Singaas E.** 2007. Fitting photosynthetic carbon dioxide response curves for C₃ leaves. *Plant, Cell & Environment* **30**, 1035–1040.
- Shibli RA, Kushad M, Yousef GG, Lila MA.** 2007. Physiological and biochemical responses of tomato microshoots to induced salinity stress with associated ethylene accumulation. *Plant Growth Regulation* **51**, 159–169.
- Shu S, Guo S, Sun J, Yuan L.** 2012. Effects of salt stress on the structure and function of the photosynthetic apparatus in *Cucumis sativus* and its protection by exogenous putrescine. *Physiologia Plantarum* **146**, 285–296.
- Singaas E, Ort D, Delucia E.** 2003. Elevated CO₂ effects on mesophyll conductance and its consequences for interpreting photosynthetic physiology. *Plant, Cell and Environment* **27**: 41–50.
- Song Q, Zhang G, Zhu X.** 2013. Optimal crop canopy architecture to maximise canopy photosynthetic CO₂ uptake under elevated CO₂ - a theoretical study using a mechanistic model of canopy photosynthesis. *Functional Plant Biology* **40**, 108.
- Stępień, P, Klobus, G.** 2006. Water relations and photosynthesis in *Cucumis sativus* L. leaves under salt stress. *Biologia Plantarum* **50**: 610–616.
- Suzuki N, Rivero RM, Shulaev V, Blumwald E, Mittler R.** 2014. Abiotic and biotic stress combinations. *New Phytologist* **203**, 32–43.
- Takenaka A.** 1994. Effects of leaf blade narrowness and petiole length on the light capture efficiency of a shoot. *Ecological Research* **9**, 109–114.
- Tardieu F, Reymond M, Hamard P, Granier C, Muller B.** 2000. Spatial distributions of expansion rate cell division rate and cell size maize leaves: a. synthesis of the effects of soil water status evaporative demand and temperature. *Journal of Experimental Botany* **51**, 1505–1514.

- Tavakkoli E, Fatehi F, Coventry S, Rengasamy P, McDonald GK.** 2011. Additive effects of Na⁺ and Cl⁻ ions on barley growth under salinity stress. *Journal of Experimental Botany* **62**, 2189–2203.
- Tavakkoli E, Fatehi F, Rengasamy P, McDonald GK.** 2012. A comparison of hydroponic and soil-based screening methods to identify salt tolerance in the field in barley. *Journal of Experimental Botany* **63**, 3853–3868.
- Tavakkoli E, Rengasamy P, McDonald GK.** 2010. High concentrations of Na⁺ and Cl⁻ ions in soil solution have simultaneous detrimental effects on growth of faba bean under salinity stress. *Journal of Experimental Botany* **61**, 4449–4459.
- Tester M, Langridge P.** 2010. Breeding technologies to increase crop production in a changing world. *Science* **327**:818-822.
- Thornley J, Hand D, Wilson W.** 1992. Modelling light absorption and canopy net photosynthesis of glasshouse row crops and application to cucumber. *Journal of Experimental Botany* **43**: 383–391.
- Tosens T, Niinemets Ü, Vislap V, Eichelmann H, Díez P.** 2012. Developmental changes in mesophyll diffusion conductance and photosynthetic capacity under different light and water availabilities in *Populus tremula*: how structure constrains function. *Plant, Cell & Environment* **35**, 839–856.
- Trouwborst G, Hogewoning SW, Harbinson J, van Ieperen W.** 2011. Photosynthetic acclimation in relation to nitrogen allocation in cucumber leaves in response to changes in irradiance. *Physiologia Plantarum* **142**: 157–169.
- Turitzin, S, Drake, B.** 1981. The effect of a seasonal change in canopy structure on the photosynthetic efficiency of a salt marsh. *Oecologia* **48**: 79–84.
- van der Ploeg A, Heuvelink E.** 2005. Influence of sub-optimal temperature on tomato growth and yield: a review. *Journal of Horticultural Science and Biotechnology* **80**, 652-659.
- Vialet-Chabrand S, Dreyer E, Brendel O.** 2013. Performance of a new dynamic model for predicting diurnal time courses of stomatal conductance at the leaf level. *Plant Cell & Environ* **36**: 1529–1546.
- Vos J, Evers JB, Buck-Sorlin GH, Andrieu B, Chelle M, Visser PHB de.** 2010. Functional-structural plant modelling: a new versatile tool in crop science. *Journal of Experimental Botany* **61**, 2101–2115.
- Wang, D, Shannon, M, Grieve, C.** 2001. Salinity reduces radiation absorption and use efficiency in soybean. *Field Crops Research* **69**: 267–277.

- Wardlaw IF. 1990.** The control of carbon partitioning in plants. *New Phytologist* **116**: 341–381.
- Warren-Wilson J, Hand D, Hannah M. 1992.** Light interception and photosynthetic efficiency in some glasshouse crops. *Journal of Experimental Botany* **43**, 363–378.
- Weijsschede J, Berentsen R, de Kroon H, Huber H. 2008.** Variation in petiole and internode length affects plant performance in *Trifolium repens* under opposing selection regimes. *Evolutionary Ecology* **22**, 383–397.
- Wiechers D. 2011.** Influence of canopy structure on light interception and productivity of greenhouse cucumber. PhD thesis, Hannover, Germany: Leibniz Universität Hannover. Available at <http://www.gem.uni-hannover.de/publikationen.html>
- Wiechers D, Kahlen K, Hartmut Stützel. 2011a.** Dry matter partitioning models for the simulation of individual fruit growth in greenhouse cucumber canopies. *Annals of Botany* **108**: 1075–1084.
- Wiechers D, Kahlen K, Stützel H. 2011b.** Evaluation of a radiosity based light model for greenhouse cucumber canopies. *Agricultural and Forest Meteorology* **151**: 906–915.
- Wilson K, Baldocchi D, Hanson P. 2000.** Quantifying stomatal and non-stomatal limitations to carbon assimilation resulting from leaf aging and drought in mature deciduous tree species. *Tree Physiology* **20**: 787–797.
- Wohlfahrt G, Hammerle A, Haslwanter A, Bahn M, Tappeiner U, Cernusca A. 2008.** Disentangling leaf area and environmental effects on the response of the net ecosystem CO₂ exchange to diffuse radiation. *Geophysical Research Letters* **35**: L16805.
- Wolf O, Munns R, Tonnet M, Jeschke W. 1990.** Concentrations and transport of solutes in xylem and phloem along the leaf axis of NaCl-treated *Hordeum vulgare*. *Journal of Experimental Botany* **41**: 1133–1141.
- Wolf O, Munns R, Tonnet ML, Jeschke W. 1991.** The role of the stem in the partitioning of Na⁺ and K⁺ in salt-treated barley. *Journal of Experimental Botany* **42**: 697–704.
- Xu G, Fan X, Miller AJ. 2012.** Plant nitrogen assimilation and use efficiency. *Annual Review of Plant Biology* **63**, 153–182.
- Yamori W, Evans J, Caemmerer S von. 2010a.** Effects of growth and measurement light intensities on temperature dependence of CO₂ assimilation rate in tobacco leaves. *Plant, Cell & Environment* **33**, 332–343.

- Yamori W, Masumoto C, Fukayama H, Makino A. 2012.** Rubisco activase is a key regulator of non-steady-state photosynthesis at any leaf temperature and, to a lesser extent, of steady-state photosynthesis at high temperature. *The Plant Journal* **71**: 871–880.
- Yamori, W, Nagai, T, Makino, A. 2011.** The rate-limiting step for CO₂ assimilation at different temperatures is influenced by the leaf nitrogen content in several C₃ crop species. *Plant, Cell and Environment* **34**: 764–777.
- Yamori W, Noguchi K, Hikosaka K, Terashima I. 2009.** Phenotypic plasticity in photosynthetic temperature acclimation among crop species with different cold tolerances. *Plant Physiol.* **152**: 388–399.
- Yamori W, Noguchi K, Hikosaka K, Terashima I. 2010b.** Phenotypic plasticity in photosynthetic temperature acclimation among crop species with different cold tolerances. *Plant Physiology* **152**, 388–399.
- Yin X, Schapendonk AHCM, Kropff MJ, Oijen MV, Bindraban PS. 2000.** A generic equation for nitrogen-limited leaf area index and its application in crop growth models for predicting leaf senescence. *Annals of Botany* **85**, 579–585.
- Yin X, Sun Z, Struik PC, Gu J. 2011.** Evaluating a new method to estimate the rate of leaf respiration in the light by analysis of combined gas exchange and chlorophyll fluorescence measurements. *Journal of Experimental Botany* **62**, 3489–3499.
- Zhu X, Long SP, Ort DR. 2010.** Improving photosynthetic efficiency for greater yield. *Annual Review of Plant Biology* **61**, 235–261.
- Zhu X, Song Q, Ort DR. 2012.** Elements of a dynamic systems model of canopy photosynthesis. *Current Opinion in Plant Biology* **15**, 237–244.
- Zhu J, van der Werf W, Anten NPR, Vos J, Evers JB.** The contribution of phenotypic plasticity to complementary light capture in plant mixtures. *New Phytol*, in press.
- Zribi L, Fatma G, Fatma R, Salwa R, Hassan N, Néjib RM. 2009.** Application of chlorophyll fluorescence for the diagnosis of salt stress in tomato “*Solanum lycopersicum* (variety Rio Grande)”. *Scientia Horticulturae* **120**, 367–372.

Acknowledgement

I may not finish this work without the supports from my parents, Tsun-Li Chen (陳遵禮) and Tao-Chih Mu (穆道芝). They are always supportive and have never judged my life style. I also thank Martin Fleischhacker, who had come along with me in the past years and is always a good friend to talk with. Their company enabled me to concentrate on my scientific works.

I am glad to meet my supervisors, PD Dr. Katrin Kahlen and Prof. Dr. Hartmut Stützel. I have to thank them for giving me the freedom to develop my research interests. Katrin brings me to the world of functional-structural plant models, inspires me to find out the cross-talk between different disciplines by her works and is the person with whom I can share my scientific findings. She lets me know why and how science is interesting. Hartmut likes to challenge my idea and to ask critical questions about my work. He also pushes me to think from different perspectives and to move one step further. He lets me know what is important in science. I also appreciate that they give me the freedom to develop my research interests.

I have to acknowledge several international colleagues in plant science. I would not have achieved so much without their insights and suggestions. First of all, I would like to thank Dr. Daniel Tholen (Universität für Bodenkultur, Vienna, Austrian) for sharing his knowledge about photosynthesis with me. Michael Henke (Georg-August-Universität Göttingen, Germany), Pieter de Vissers (Wageningen UR, the Netherlands) and Gerhard Buck-Sorlin (IRHS Angers, France), are acknowledged for their collaboration in the chapter 2. I would also like to thank Prof. Dr. Ching-Lung Lee, Prof. Dr. Ling-Long Kuo-Huang, Prof. Dr. Su-Hwa Chen and Prof. Dr. Wendy Wen-Ju Yang for encouraging me to pursue my PhD in Germany and sharing their experiences about living in Germany.

I have also many thanks to my colleagues in Hannover: to Ilona Napp for her excellent helps throughout the all experiments that I have conducted in the institute, to Marie-Luise Lehmann for her great carefulness in doing all chemical analyses, to Dr. Andreas Fricke, Dr. Dirk Wiecher and Dr. Karsten Zutz for the discussions in the weekly lab meeting, to our secretary, Heike Bank, for administrative works, to Magnus Adler, Anni Romey, Christoph Knacke and Ulrich Hering for solving computational and technical problems and to Dr. Dagmar Kunze, Uwe Spillebeen, Rüdiger Wagner, Benjamin Vahrmeyer, Katharina Meyer and Elke Neitzel-Rode for their contributions on creating comfortable working surroundings and atmosphere.

I also thank the Taiwan Ministry of Education which granted me the *Studying Abroad Scholarship* in 2011-2012 (SAS1001151DE007), die Deutsche Forschungsgemeinschaft which supported my research project and Landgard Stiftung and TASPO Stiftung which granted me the *Grow-Award 2013*.

Curriculum vitae

Personal information

Name: Tsu-Wei Chen
Date of birth: 18.10.1983
Place of birth: Taipei
Nationality: Taiwan (Republic of China)

Education

Sep. 1999 - Jun. 2002 Chien-Kuo Senior High School (Taiwan, Taipei)
Sep. 2002 - Jun. 2007 National Taiwan University (Taiwan).
Bachelor of Science in horticulture
Sep. 2003 - Jun. 2007 National Taiwan University (Taiwan).
Bachelor of Science in life science (biology)
Okt. 2009 - Sep. 2011 Leibniz Universität Hannover.
Master of Science in horticulture.
Topic of master thesis: *Pattern of Na⁺ Accumulation in Cucumber under Salinity Stress*
Since Nov. 2011 PhD candidate in Institute of Horticultural Production Systems, Leibniz Universität Hannover.

Awards

2011-2013 Study Abroad Scholarship from Taiwan Ministry of Education
2013 Grow Award from Landgard Foundation and TASPO Foundation

Research experiences

Feb-Mar 2014 Research stay in Laboratory of Plant Ecology, Ghent University
(group leader: Kathy Steppe)
Mar 2015 - Review editor in *Frontiers in Plant Science*

Publications

Reviewed articles

Chen T-W, Kahlen K, Stützel H. (2015): [Disentangling the contributions of osmotic and ionic effects of salinity on stomatal, mesophyll, biochemical and light limitations to photosynthesis](#). *Plant, Cell & Environment* (in press). DOI: 10.1111/pce.12504

Chen T-W, Nguyen TMN, Kahlen K, Stützel H. (2014): [Quantification of the effects of architectural traits on dry mass production and light interception of tomato canopy under different temperature regimes using a dynamic functional-structural plant model](#). *Journal of Experimental Botany* **65**: 6399-6410.

Chen T-W, Henke M, de Visser PHB, Buck-Sorlin G, Kahlen K, Wiechers D, Stützel H. (2014): [What is the most prominent factor limiting photosynthesis? – A model study to quantify photosynthetic limitations in different layers of a cucumber canopy](#). *Annals of Botany* **114**: 677-688.

Conference papers

Chen T-W, Tholen D, Kahlen K, Stützel H. (2014): Comparison of maximum chlorophyll fluorescence yield and photosynthetic parameters derived by single multiphase flash and single rectangular flash. *Society of Experimental Biology*, Manchester, UK.

Chen T-W, Kahlen K, Stützel H. (2014): Modelling the effects of temperature, CO₂ enrichment and water stress on photosynthetic limitations – a new approach to upscale from leaf to canopy level *Mitteilung der Gesellschaft für Pflanzenbauwissenschaften* 26. Wien, Austria

Stützel H, **Chen T-W** (2014): Plant canopy under drought stress – structures, functions genes and models. *13th ESA Congress*. Debrecen, Hungary. 25-30.

Chen T-W, Kahlen K, Stützel H. (2014): Quantifying photosynthetic limitations from leaf to canopy level. *13th ESA Congress*. Debrecen, Hungary. 243-244.

Chen T-W, Kahlen K, Stützel H. (2013): Applying quantitative limitation analysis of photosynthesis in crop production research. *Mitteilung der Gesellschaft für Pflanzenbauwissenschaften* 25, Göttingen, 162-163.

Chen T-W, Henke M, de Visser PHB, Buck-Sorlin G, Stützel H. (2013): [Revealing the relative importance of photosynthetic limitations in cucumber canopy](#). In Lintunen A. FSPM2013 - *7th Workshop on Functional-Structural Plant Models*. Helsinki, 124-126.

Chen T-W, Kahlen K, Stützel H. (2013): [Up-scaling salt effects in cucumber: trade-off between photosynthesis and toxic ion accumulation](#). In Lintunen A. FSPM2013 - *7th Workshop on Functional-Structural Plant Models*. Helsinki, 131-133.

Kahlen K, **Chen T-W**, Zinkernagel J, Stützel H. (2013): [Modelling temperature-modulated internode elongation in greenhouse grown cucumber canopies](#). In Lintunen A. FSPM2013 - 7th Workshop on Functional-Structural Plant Models. Helsinki, 168-170.

Kahlen K, **Chen T-W**, Wiechers D, Stützel H. (2012): [Architectural modelling in horticulture - quo vadis?](#), *Acta Horticulturae* 957: 207-214

Chen T-W, Kahlen K, Stützel H. (2012): [Determining photosynthetic limitations under saturated and non-saturated light conditions](#), Kang M, Dumont Y, Guo Y, eds. Plant growth modeling, simulation, visualization and applications, Proceedings – PMA'12. IEEE Computer Society Conference Publishing Services, 93-95

Chen T-W, Sprengel M, Kahlen K, Stützel H. (2011): [Using Digitized Data for Dynamic Functional-Structural Plant Model](#), *BHGL-Schriftenreihe* 28., Deutsche Gartenbauwissenschaftliche Gesellschaft, Hannover, 106

Chen T-W, Kahlen K, Stützel H. (2011): [A Simple Model of Sodium Accumulation in Cucumber Leaves under Salinity Stress](#), Programme and Abstract Book, *Society of Experimental Biology*, Glasgow, UK. 226

Chen T-W, Kahlen K, Stützel H. (2010): [Up-scaling salt stress effects in cucumber: a model approach](#), In DeJong T, Da Silva D. FSPM2010 - 6th Workshop on Functional-Structural Plant Models. Davis: University of California. 283